Synaptic Specializations Mediated by Synaptotagmin Isoforms

Synaptic specializations mediated by Synaptotagmin isoforms

A dissertation presented

by

Josef Turecek

to

The Division of Medical Sciences

in partial fulfillment of the requirements

for the degree of

Doctor of Philosophy

in the subject of

Neurobiology

Harvard University

Cambridge, Massachusetts

March 2019

Dissertation Advisor: Professor Wade Regehr Josef Turecek

Synaptic specializations mediated by Synaptotagmin isoforms

The timing of neurotransmitter release in response to presynaptic firing varies widely across synapses in the brain. The release of synaptic vesicles can be synchronous and occur within milliseconds of an action potential, or asynchronous and persist for tens of milliseconds. Release can also undergo short-term facilitation in which it is enhanced by two closely timed action potentials. The molecular properties of synapses that determine the relative timing of synaptic vesicle release have remained poorly understood. We have found that Synaptotagmin 7 (Syt7) plays a major role in multiple aspects of synaptic transmission. Syt7 mediates short-term facilitation at almost all synapses where it is present, including seven different synapses tested here. Loss of Syt7 also eliminated facilitation that was activated by trains of stimuli at Purkinje cell and vestibular synapses, revealing an interplay between short-term facilitation and depression that maintains constant synaptic strength. Changes in the initial probability of release were not detectable in Syt7 KOs at three different synapses, and removal of Syt7 did not reduce the rate of recovery from depression in cerebellar Purkinje cell synapses. Facilitation could be rescued in Syt7 KOs by presynaptic expression of Syt7, but not Ca^{2+}-insensitive Syt7. At cerebellar parallel fibers we found that Syt7 can mediate both facilitation and asynchronous release, but there are additional mechanisms of facilitation and asynchronous release in the absence of Syt7. In contrast to facilitation, the presence or absence of Syt7 does not determine whether asynchronous release occurs. Syt7 was most strongly expressed at Purkinje cell synapses in the cerebellar nuclei, even though no asynchronous release could be detected. Inhibitory synapses in the inferior olive are exclusively asynchronous, and we found that release synchrony is instead determined by the absence of Synaptotagmin 1 and 2. Syt7 plays a role in shaping the kinetics of asynchronous release in the inferior olive, but does not control the magnitude of asynchronous release. Our findings suggest that Syt7 could be a Ca sensor for facilitation that is

prominent at many synapses, and that it may also play a role in asynchronous release in combination with other additional mechanisms.

Table of Contents

Abstract ..... **iii**

Table of Contents ..... **v**

Acknowledgements ..... **vi**

Chapter 1: Introduction **1**

Chapter 2: Synaptic specializations support frequency-independent Purkinje cell output from the cerebellar cortex **15**

Chapter 3: Synaptotagmin 7 confers frequency invariance onto specialized depressing synapses **65**

Chapter 4: Synaptotagmin 7 mediates both facilitation and asynchronous release at granule cell synapses **101**

Chapter 5: Neuronal regulation of fast Synaptotagmin isoforms controls the relative contribution of synchronous and asynchronous release **134**

Chapter 6: Conclusion **173**

Appendix A, The calcium sensor Synaptotagmin 7 is required for synaptic facilitation **178**

Appendix B, The role of CaV2.1 channel facilitation in synaptic facilitation **205**

References **234**

Acknowledgments

I would like to thank my advisor Wade Regehr for his rigorous training and guidance. I also thank current and former members of the Regehr lab for supplying the lab with humor: Kimberly McDaniels, Skyler Jackman, Laurence Witter, Stephanie Rudolph, Jay Wang, Chris Chen, Chris Weyrer, Chong Guo, Kyung Han, Tomas Osorno, Mehak Khan, Monica Thanawala, and Diasynou Fioravante.

I thank members of my dissertation advisory committee: Pascal Kaeser, Chinfei Chen, and Bruce Bean for taking the time to provide me with feedback and suggestions. I also thank Rachel Wilson for her career and personal advice. I thank Karen Harmin for keeping a watchful eye over my graduate education.

I would like to thank my parents, Frank and Olga Turecek for their endless support, and for providing me with the opportunity to obtain a world-class education. Finally, I would like to thank Keiko Weir for her close friendship, support, wisdom, and love.

Chapter 1

Introduction

The presynaptic terminal

Neurotransmitter is typically released from presynaptic terminals by highly specialized machinery. Transmitter is stored in synaptic vesicles that undergo fusion in the presence of calcium. Fusion of the vesicle with the presynaptic membrane releases its internal contents, allowing neurotransmitter to enter the synaptic cleft and be detected post-synaptically by neurotransmitter receptors. Fusion usually occurs at a release site where fusion machinery is concentrated and synaptic vesicles are docked and primed to be released.

Synchronous and asynchronous release

Several forms of release can occur, and they are distinguished by their timing relative to presynaptic action potentials. When an action potential invades the presynaptic bouton, synchronous release is evoked within a millisecond, closely time-locked to presynaptic spiking (Katz and Miledi, 1965, Sabatini and Regehr, 1996, Borst and Sakmann, 1996). In contrast, asynchronous release is delayed and loosely time-locked to the presynaptic action potential, occurring for tens to hundreds of milliseconds after spiking (Atluri and Regehr, 1998, Lu and Trussell, 2000, Hefft and Jonas, 2005, Iremonger and Bains, 2007, Daw et al., 2009, Best and Regehr, 2009, Peters et al., 2010). Release can also occur in the absence of presynaptic activity in the form of spontaneous release. For individual release sites the rate of spontaneous release is very low and may serve to maintain synapses rather than contributing to the rapid processing of information (but see Carter and Regehr, 2002).

Different forms of release are evoked more effectively by different patterns of activity. Synchronous release is often maximally evoked by single stimuli or infrequent presynaptic firing. In contrast, asynchronous release is always weakly evoked by single stimuli and instead builds with repeated stimulation, especially if the frequency of stimulation is high (Atluri and Regehr, 1998, Lu and Trussell, 2000, Hefft and Jonas, 2005, Iremonger and Bains, 2007, Daw et al., 2009, Best and Regehr, 2009, Peters et al., 2010). Thus, the contribution of asynchronous release is only prominent when presynaptic firing is elevated, or during brief bursts of presynaptic activity.

The contributions of synchronous, asynchronous and spontaneous release at different synapses in the brain can vary widely. Release at almost all synapses is predominantly synchronous, but some synapses have especially fast synchronized release. At the mature Calyx of Held, synchronous release occurs for less than a millisecond after firing (Borst and Sakmann, 1996). Inhibitory (GABAergic) synapses can also be very rapid. For example, the release of GABA at cerebellar Purkinje cell synapses is restricted to two milliseconds following a spike (Person and Raman, 2012b). Release at these synapses is tightly controlled, and there is no evidence of asynchronous release in mature animals, even after prolonged stimulation. Thus, release at these synapses is rapid and entirely synchronized. Asynchronous release is less common in the brain, but can be prominent at several synapses in adults. Mixed synchronous and asynchronous release has been demonstrated in cerebellar parallel fibers (Atluri and Regehr, 1998), excitatory inputs to the paraventricular nucleus of the hypothalamus (Iremonger and Bains, 2007), and from cholecystokinin-positive GABAergic interneurons onto multiple targets in the hippocampus (Daw et al., 2009; Hefft and Jonas, 2005). Mixed release may also occur from vagal afferents in the nucleus of the solitary tract (Peters et al., 2010), and among GABAergic dorsal horn interneurons of the spinal cord (Labrakakis et al., 2009), although these synapses have been less well characterized. Finally, at least one synapse in the mature brain is exclusively asynchronous. The release of GABA in the inferior olive occurs over the course of one hundred milliseconds in response to a single stimulus (Best and Regehr, 2009). Thus, the kinetics of GABA release can span approximately two orders of magnitude depending on which synapse it is being released from.

The functions of synchronous and asynchronous release are closely related to their definitions. Fast synchronized transmitter release is ideally suited when information must be transmitted rapidly and temporal structure of presynaptic firing must be preserved. Asynchronous release is better suited for providing slow, prolonged or tonic signals in which the precise pattern of presynaptic firing is of less importance, or is preferably ignored (Hefft and Jonas, 2005, Best and Regehr, 2009). It has been suggested that asynchronous release at excitatory synapses can prolong post-synaptic firing and amplify bursts of presynaptic activity (Iremonger and Bains, 2007). Asynchronous release may also be effective at

activating high-affinity metabotropic receptors that are more sensitive to small and slow neurotransmitter signals. In contrast, fast synchronized release is required for tight control of spike timing of post-synaptic cells.

Mechanisms of synchronous and asynchronous release

All evoked release is driven by presynaptic calcium, but synchronous and asynchronous release are driven by different components of presynaptic calcium. Following an action potential, Ca enters the presynaptic bouton and generates a large local Ca signal near Ca channels at μM concentrations. Ca is then rapidly bound by Ca-buffering protein and Ca-bound buffer diffuses throughout the terminal, generating a small and more diffuse residual Ca signal that is in the hundreds of nM range (Katz and Miledi, 1965, Sabatini and Regehr, 1996, Borst and Sakmann, 1996).

The proteins involved in synchronous release have been identified and are conserved across synapses. Fusion of the vesicle requires SNARE and S/M proteins. SNARE proteins on the membrane (typically SNAP-25 and syntaxin) and vesicles (typically Synaptobrevin 2) form a tight complex and bring the membranes close together to fuse. S/M proteins such as Munc18-1 are also required for fusion and have multiple interactions with SNARE proteins and membranes. S/M proteins are likely involved in the formation of SNARE complexes (Weber et al., 1998, Li et al., 2007, Hua and Scheller, 2001, Verhage et al., 2000, Dulubova et al., 1999, Dulubova et al., 2007, Sudhof and Rothman, 2009).

Synchronous release is triggered by Synaptotagmin isoforms Syt1,2 or 9 that are present on the vesicle membrane and have rapid kinetics and low Ca affinity. Thus, these Syts detect large local Ca signals and trigger synchronous release, whereas other Syt isoforms do not (Xu et al., 2007). Fast Syts are composed of a transmembrane domain, a linker region, and two C2 domains. The detection of Ca by fast Syts causes vesicle fusion but it is unclear how fusion is triggered (Jahn and Fasshauer, 2012). Syts bind phospholipids and it has been proposed that phospholipid binding with the plasma membrane and SNAREs can bring the vesicular and plasma membrane close together to lower the energy barrier for fusion (Martens et al., 2007, Lee et al., 2010, Stein et al., 2007, Hui et al., 2009). Another possibility is that fast Syts clamp SNARE complexes, preventing zippering of the complex and inducing fusion. Ca

binding to Syts triggers the release of the clamping by Syt itself, or alternatively relieves the clamping of SNARE complexes by complexin (Kaeser-Woo et al., 2012, Chicka et al., 2008, Yang et al., 2010).

The triggering of vesicle release depends critically on the binding of fast Syts and Ca, and is therefore sensitive to the spatial relationship of Ca entry and Syts. As Ca is rapidly bound by buffers and diffused, sites of vesicle release are spatially organized such that Ca sensors are in close proximity to Ca sources (Llinas et al., 1992, Meinrenken et al., 2002). As a result of the rapid kinetics of fast Syt isoforms and the spatial arrangement of synapses, release depends on the fourth or fifth power of Ca. Thus, the relationship between release and Ca is steeply non-linear. At some synapses Ca signals are rapid and spatially restricted to within 100 nm of Ca channels, and in these cases synaptic vesicles are believed to be closely coupled with Ca channels (Eggermann et al., 2011). In other synapses, multiple Ca channels act cooperatively to generate Ca signals in a larger area and vesicles are not as closely associated with channels (Mintz et al., 1995, Vyleta and Jonas, 2014).

The mechanisms of asynchronous release are less well understood than synchronous release. Whereas synchronous release relies on fast local Ca signals near Ca channels, asynchronous release has been shown to be dependent on residual Ca signals (Atluri and Regehr, 1998, Hefft and Jonas, 2005, Iremonger and Bains, 2007). At every synapse where asynchronous release occurs, asynchronous release is eliminated by the attenuation of residual Ca signals using the slow buffer EGTA. In some cases, it has been shown that introduction of EGTA into presynaptic terminals can nearly eliminate asynchronous release without altering synchronous release. Experiments in which fast Syts are eliminated reveal a prominent component of asynchronous release, and many properties of asynchronous release have been most studied in the absence of fast Syts. Whereas synchronous release is steeply dependent on Ca by a power law, it has been shown that the extent of asynchronous release is linearly dependent on Ca (Kochubey and Schneggenburger, 2011, Sun et al., 2007).

The dependence of asynchronous release on residual Ca has led to several mechanistic hypotheses. It has been proposed that asynchronous release is mediated by loose coupling between Ca channels and synaptic vesicles (Eggermann et al., 2011). Large distances between Ca sources and fast Syts would be

expected to introduce delays and stochasticity to release, and would therefore be consistent with the sensitivity of asynchronous release to residual Ca. However, the elimination of fast Syt isoforms results in prominent asynchronous release, suggesting that other mechanisms are at least capable of generating asynchronous release (Kochubey and Schneggenburger, 2011, Sun et al., 2007). It remains unknown whether fast Syts contribute to asynchronous release under normal conditions.

The prominence of asynchronous release in the absence of fast Syts has led to the hypothesis that asynchronous release could be mediated by distinct Ca sensors that would have slower kinetics than the triggers of synchronous release. Sensors for asynchronous release would also be required to have a higher affinity to detect weak residual Ca signals. The prominence of asynchronous release remaining when fast Syt isoforms are eliminated is consistent with the existence of additional Ca sensors that drive asynchronous release.

Short-term plasticity and use-dependent release

Many neurons have patterns of continuous activity rather than single low frequency action potentials. Both synchronous and asynchronous release undergo use-dependent changes when multiple stimuli or trains of action potentials occur (Zucker and Regehr, 2002a). As stated above, asynchronous release is always more prominent with repeated high-frequency stimulation. However, synchronous release can undergo two forms of short-term plasticity that occur on the order of tens to hundreds of milliseconds and become more prominent with higher stimulation frequency. Short-term depression is a use-dependent decrease in synaptic strength, whereas short-term facilitation is a use-dependent increase in synaptic strength. Short-term plasticity varies widely among synapses. For example, climbing fiber synapses on the Purkinje cells in the cerebellum depress, releasing most of their neurotransmitter in response to a single action potential. Release on subsequent stimuli within several hundred milliseconds is typically very weak. In contrast, parallel fibers synapse onto the same post-synaptic target but facilitate, releasing very little for low frequency stimuli, and instead release much more during bursts of parallel fiber activity (Dittman et al., 2000).

The use-dependence of transmitter release introduces a new dimension when considering the function of synaptic transmission at different synapses. The properties of release can shape the way synapses filter information. Synapses can therefore be tailored to suit the needs of circuit elements (Jackman and Regehr, 2017). At synapses with prominent short-term facilitation, single spikes evoke little, and the bulk of release is instead evoked by elevated high-frequency activity. Thus, short-term facilitation is effective at transmitting high-frequency firing or bursts, and poorly conveys single infrequent action potentials. Short-term depression results in effective transmission of low-frequency firing, but poorly conveys high-frequencies. Such filtering is particularly prominent in sensory systems, where only changes in sensory stimuli are effectively conveyed because short-term depression curtails vesicle release during sustained stimulation.

Mechanisms of short-term plasticity

Short-term facilitation and depression have been proposed to have distinct mechanisms. Short-term depression at many synapses is well-described by the depletion of synaptic vesicles. If many synaptic vesicles are initially released, and there is insufficient time to fully replenish the supply of releasable vesicles, there are fewer available to be released on subsequent stimuli, resulting in reduced synaptic strength (Zucker and Regehr, 2002a).

Additional mechanisms that are either presynaptic or postsynaptic can also contribute to short-term depression. Synchronous release is critically dependent on Ca, and it has been proposed that use-dependent decreases in calcium entry could contribute to short-term depression (Kawaguchi and Sakaba, 2015, Forsythe et al., 1998). Ca signals at some synapses do not undergo use-dependent changes (Brenowitz and Regehr, 2007), but it remains to be determined whether local calcium signals that drive release are more dynamic.

Reductions in calcium entry can occur not from the properties of Ca channels, but also as a result of other ionic conductances. It has been shown that the properties of different axons and boutons can vary widely and that in some cases action potentials can propagate with high fidelity through axons, but fail to invade presynaptic boutons (Kawaguchi and Sakaba, 2015). The failure of action potential invasion

within a subset of boutons becomes more likely at high frequencies, causing a failure to release and a decrease in synaptic strength. This mechanism has been demonstrated in cultured synapses where it is possible to obtain whole-cell recordings from large presynaptic terminals (Kawaguchi and Sakaba, 2015), but it remains to be demonstrated at native synapses. At several synapses action potentials reliably propagate into the terminal compartment suggesting that action potentials do not fail to invade presynaptic boutons (Ritzau-Jost et al., 2014, Borst et al., 1995, Brenowitz and Regehr, 2007, Rancz et al., 2007).

Short-term depression can also occur post-synaptically through changes in the properties of post-synaptic receptors. It is known that AMPA receptors can desensitize, decreasing synaptic strength with multiple stimuli even when vesicular release remains constant, and post-synaptic receptors can be saturated by neurotransmitter to reduce the effects of short-term changes in presynaptic release (Chen et al., 2002, Trussell et al., 1993, Xu-Friedman and Regehr, 2003, Foster and Regehr, 2004, Foster et al., 2002, Chanda and Xu-Friedman, 2010, Wadiche and Jahr, 2001).

Short-term facilitation is more difficult to explain than short-term depression. Whereas depression can arise from even the most simplified model of a synapse that undergoes vesicle depletion, facilitation requires additional mechanisms to be considered. Unlike short-term depression, short-term facilitation is sensitive to residual Ca. Thus, mechanisms of short-term facilitation rely on small (hundreds of nM) and slow (tens to hundreds of milliseconds) Ca signals.

It has been proposed that facilitation is caused by use-dependent changes in Ca entry. Ca channels can be inactivated in a use-dependent manner, but it has also been shown that $Ca_V2.1$ channels that drive vesicle release can be facilitated to increase calcium entry with repetitive use. Access to presynaptic compartments has made it difficult to measure presynaptic calcium entry to directly test this hypothesis. Work at the Calyx of Held, where presynaptic Ca currents can be measured, has yielded mixed results. Early studies showed that Ca currents mediated by $Ca_V2.1$ channels can facilitate in response to action potential-like voltage steps and could account for the facilitation evoked by voltage step stimuli (Borst and Sakmann, 1998). However, the voltage steps were substantially longer than the presynaptic action

potential (1 ms long voltage step vs. 0.44 ms AP width). Later work showed that action potential waveforms evoke smaller calcium current facilitation, and provided a less substantial contribution to the facilitation of release (Muller et al., 2008). Thus, the contribution of Ca current facilitation to synaptic facilitation is unclear and requires additional experiments.

Use-dependent changes in Ca entry need not arise from Ca channels themselves, but could also be driven by changes in the presynaptic action potential waveform. At hippocampal mossy fiber boutons, it was shown that the action potential broadens with multiple stimuli and can drive increases in Ca entry (Geiger and Jonas, 2000). Many synapses that have short-term facilitation do not have use-dependent changes in action potential waveform, but it cannot be excluded that action potential broadening occurs in distal compartments that are undetected by recordings made in the cell body. The contribution of action potential broadening in short-term facilitation at many synapses is therefore unclear.

Another mechanism that has been proposed to account for facilitation is the saturation of endogenous Ca buffers (Blatow et al., 2003). When Ca enters the presynaptic bouton, it is bound by Ca binding proteins that act as Ca buffers. Whether Ca is detected by fast Syt isoforms will depend on the distance between Ca channels and synaptic vesicles, and the kinetics and abundance of Ca buffers in the cell. When the concentration of buffers is high, it can reduce the probability of triggering vesicle fusion. It has been suggested that when Ca influx is sufficiently high, Ca buffers can be overwhelmed after a single stimulus, such that on subsequent stimuli more free Ca is available to trigger release. It is unclear to what extent buffer saturation plays a role at native synapses because it is difficult to assess both the buffer capacity and the magnitude of Ca influx of distal compartments. However, at many synapses Ca buffering capacity is very high and is unlikely to be saturated by single stimuli. Thus, for synapses that are known to have high buffer capacity, the saturation of endogenous Ca buffering is unlikely to play a major role in short-term facilitation.

Vesicle release during prolonged activity

Synaptic vesicle release and short-term plasticity are often studied with single or pairs of stimuli, but activity patterns *in vivo* are much more complicated. Many neurons in the brain are constantly active without long quiescent periods, whereas synapses are often studied in quiescent cultures or slice preparations in which activity is intentionally suppressed. Release in response to a single stimulus is the product of the number of vesicles in the readily releasable pool (RRP) and the initial probability of release for each synaptic vesicle (P_R). With multiple stimuli, the number of variables controlling release increases, and they can become more difficult to isolate experimentally. Vesicles are replenished between stimuli, and the rate of replenishment (R) must be taken into account. It has also been shown that the properties of synapses likely change when they are activated. Changes in P_R, RRP size and R have all been proposed to change in response to Ca signals generated by activity (Thanawala and Regehr, 2013, Del Castillo and Katz, 1954, Dittman and Regehr, 1998). Each one of these properties has been proposed to be driven by Ca-sensing proteins that have not been identified. It can become difficult to determine the relative contributions of each parameter because they cannot be directly measured, and cannot be measured during trains of stimuli. Measuring synaptic parameters can be confounded during prolonged stimulation by an increased susceptibility to transmitter accumulation, spillover, activation of metabotropic receptors and post-synaptic receptor desensitization. Despite these pitfalls, determining how presynaptic parameters interact and their underlying mechanisms during prolonged firing has been of great interest because they are processes that are more likely to be activated during naturalistic firing patterns. Identifying the sensors involved in use-dependent changes at synapses could also help explain the role of short-term plasticity in information processing within circuits.

The role of Synaptotagmin 7 in synaptic transmission

Synaptotagmin 7 (Syt7) is a strong candidate to play a role in synaptic transmission. Its structure is similar to other Ca-sensing Syt isoforms, containing a transmembrane region and a linker to two C2 domains that bind phospholipids in a Ca-dependent manner. Syt7 is an attractive candidate for facilitation and asynchronous release because of its high calcium sensitivity when bound to phospholipids compared

to other Syt isoforms. Both C2A and C2B domains of Syt7 show a K_d of 1.5-2.5 μM Ca under co-sedimentation with liposomes, whereas the K_d of Syt1 C2A and C2B domains are 10-20 μM, respectively (Sugita et al., 2002). The intrinsic Ca affinity for C2 domains of most other Syts is approximately an order of magnitude lower, suggesting that the presence of phospholipids may provide additional coordination sites for Ca bound to C2 domains.

The linker connecting the transmembrane region and C2 domains is alternatively spliced, but the degree of splicing varies greatly between species: mice have three splice variants, whereas rats may have eight, and humans may have five (Sugita et al., 2001, Fukuda et al., 2002). The most common splice variant contains 403 amino-acids and is found in all three species, and is the smallest splice variant that contains C2 domains. In rats, short protein fragments likely lacking C2 domains have been detected in tissue samples, but their existence *in vivo* has not been confirmed. Splice variants may be expressed differently in various brain regions. In rats, the cerebellum lacks one of two large splice variants found in hippocampus and cortex (Sugita et al., 2001). However, the functional differences between splice variants remain unknown.

Many other features of Syt7 remain unknown. It has been suggested that Syt7 is localized to the plasma membrane in neurons because subcellular fractionation of rat brain tissue has revealed that it is enriched in plasma membrane and absent in synaptic vesicle membrane fractions (Sugita et al., 2002). Syt7 co-localizes with dense core vesicle proteins (Fukuda et al., 2004), but may also be present on other organelles because immunohistochemistry of Syt7 labels the internal contents of neuronal cell bodies.

Syt7 has been proposed to have multiple non-synaptic functions, including a role in the release of dense core vesicles. Deletion of Syt7 reduces the slow release of dense core vesicles in adrenal chromaffin cells (Schonn et al., 2008), reduces glucagon release in pancreatic α-cells, and insulin release from pancreatic β-cells (Gustavsson et al., 2008, Gustavsson et al., 2009). Dense core vesicles in these endocrine cells have been speculated to be similar to neuropeptide-containing dense core vesicles found in neurons, but it is unclear how these results translate to synaptic vesicles because the kinetics of dense core vesicle release is orders of magnitude slower than for synaptic vesicles. Additionally, unlike synaptic

vesicles, both Syt1 and Syt7 have been localized to dense core vesicles (Fukuda et al., 2004). Thus, the role of Syt7 may be very different for the release of synaptic vesicles.

Syt7 is also involved in the regulation of lysosomal exocytosis. It has been suggested that lysosomal exocytosis requires Syt7 and that it may consequently be involved in membrane repair (Rao et al., 2004, Chakrabarti et al., 2003, Martinez et al., 2000, Flannery et al., 2010). In fibroblast-collagen matrices of Syt7 KO mice, release of tissue damage markers and lysosomal enzymes are reduced, suggesting that impaired lysosomal exocytosis results in membrane repair problems, and Syt7 mice display inflammatory myopathy and muscle weakness (Chakrabarti et al., 2003). However, the requirement of Syt7 in lysosomal exocytosis is controversial. Functional studies using total internal reflection microscopy have shown that lysosome exocytosis in fibroblasts persists in Syt7 KO mice (Jaiswal et al., 2004). In these experiments, lysosomes from wildtype cells show only partial fusion, whereas lysosomes from Syt7 KO mice not only fuse, but appear to fuse fully. These results have not been reconciled, and the exact role of Syt7 in lysosomal exocytosis remains unclear.

Syt7 has been implicated in several aspects of synaptic transmission and has been closely studied by several labs. Syt7 was first implicated in asynchronous release at the zebrafish neuromuscular junction (NMJ), where synchronous acetylcholine release is prominent, but transitions into completely asynchronous release after several seconds of high-frequency firing (Wen et al., 2010). In zebrafish injected with morpholino targeted to Syt2 alone, release at the NMJ is completely desynchronized, whereas knockdown of Syt7 alone strongly reduces asynchronous release. It has also been shown that lentiviral knockdown of Syt7 reduces asynchronous release in hippocampal cultures of Syt1 KO mice (Bacaj et al., 2013). Importantly, the work in culture showed that rescue with a Ca-insensitive mutant of Syt7 failed to rescue asynchronous release. The results suggest that synchronous and asynchronous release are controlled by two distinct mechanisms, and that Syt7 could act as a calcium sensor for asynchronous release.

Other recent work has also implicated Syt7 in asynchronous release, but suggests a very different role. Cultured hippocampal autapses in which SNAP-25 is knocked out and replaced with virally-

expressed SNAP-23 show a loss of synchronous release and prominent asynchronous release (Weber et al., 2014). When Syt7 was also knocked out in this system, the total amount of asynchronous release remained unchanged. In contrast, the kinetics of asynchronous release were much slower when Syt7 was eliminated. It is unclear whether these effects are dependent on Ca-binding to Syt7, and whether there is any relationship between the role of Syt7 in SNAP-25 KO cultures and the role of Syt7 in WT synapses.

Syt7 has also been implicated in calcium-dependent recovery from depression (Liu et al., 2014). It has been proposed that a Ca-sensing protein accelerates vesicle replenishment at some synapses (Dittman and Regehr, 1998, Sakaba and Neher, 2001). It was recently found that in cultured cortical neurons of Syt7 KOs, trains of stimuli resulted in stronger depression of synchronized release (Liu et al., 2014). The stronger depression was attributed to slowing of vesicle replenishment because recovery of evoked release following trains had slower kinetics: in wildtype animals recovery is mediated by fast and slow components, whereas in Syt7 KOs the fast component is strongly attenuated. The fast component of recovery could not be rescued when a Ca-insensitive mutant of Syt7 was expressed, suggesting that Syt7 is a Ca sensor for vesicle replenishment. The authors found that Syt7 interacts with calmodulin, and suggested that Syt7 could act through calmodulin. This hypothesis is consistent with a role of calmodulin in recovery from depression at the Calyx of Held (Sakaba and Neher, 2001).

An interesting aspect of the work on Syt7 is that different groups have observed different results. In cortical cultures prolonged trains of stimuli resulted in more profound short-term depression in Syt7 KOs (Liu et al., 2014). However, at the zebrafish NMJ, synchronous release was unaltered, and no changes in short-term depression were reported (Wen et al., 2010). Similarly, no changes were reported in short-term plasticity in hippocampal cultures, or at the drosophila NMJ. Conversely, work in cortical cultures reported no differences in asynchronous release (Liu et al., 2014), although the authors did not perform experiments in the background of Syt1 KOs, and it is unclear whether there is any detectable asynchronous release in wildtype cortical culture systems. Among studies examining asynchronous release, two have found that reductions in Syt7 can decrease the magnitude of asynchronous release without changing release kinetics (Bacaj et al., 2013, Wen et al., 2010), but another has found that loss of

Syt7 alters kinetics without substantially changing the total amount of release (Weber et al., 2014). These differences may be attributed to the widely different species and types of synapses that have been studied: mixed hippocampal vs. cortical cultures vs. autaptic cultures vs. zebrafish NMJ. It may also reflect the different forms of asynchronous release that have been studied: asynchronous release after prolonged trains, delayed release left in the absence of Syt1, and slow release in the presence of Syt1 but when SNAP25 is replaced with SNAP23. Thus, it remains to be determined whether Syt7 is involved in asynchronous release or recovery from depression in an exclusive way and whether Syt7 can have different functional consequences at different types of synapses or under different conditions.

Chapter 2

Synaptic specializations support frequency-independent Purkinje cell output from the cerebellar cortex

Josef Turecek, Skyler L. Jackman, Wade G. Regehr

Cell reports, *17*(12), 3256-3268.

Author contributions JT & WGR designed research, JT & SLJ performed research, JT analyzed data, JT & WGR wrote the paper.

Abstract

The output of the cerebellar cortex is conveyed to the deep cerebellar nuclei (DCN) by Purkinje cells (PCs). Here we characterize the properties of the PC-DCN synapse in juvenile and adult mice and find that prolonged high-frequency stimulation leads to steady-state responses that become increasingly frequency-independent within the physiological firing range of PCs in older animals, resulting in a linear relationship between charge transfer and activation frequency. We use a low affinity antagonist to show that $GABA_A$ receptor saturation occurs at this synapse, but it does not underlie frequency invariant transmission. We propose that PC-DCN synapses have two components of release: one prominent early in trains, and another specialized to maintain transmission during prolonged activation. Short-term facilitation offsets partial vesicle depletion to produce frequency-independent transmission.

Introduction

Although the cerebellum has been associated primarily with controlling motor function, growing evidence suggests that the cerebellum plays important roles in social and cognitive behaviors (Van Overwalle et al., 2014, Wang et al., 2014, Reeber et al., 2013). To understand how the cerebellum participates in behaviors it is crucial to determine how cerebellar outputs regulate activity in other brain regions. Purkinje cells (PC), the sole outputs of the cerebellar cortex, make powerful inhibitory synapses onto target neurons in the deep cerebellar nuclei (DCN). By modulating DCN activity, PCs ultimately influence downstream targets throughout the brain, including the brainstem and thalamic structures (Teune et al., 2000, Chen et al., 2014, Dum and Strick, 2003).

In order to understand how PC activity regulates the firing of neurons in the DCN it is important to clarify the properties of PC-DCN synapses under physiological conditions, and preferably to do so in mature animals. However, because of technical challenges, previous work focused primarily on young animals (Telgkamp and Raman, 2002, Telgkamp et al., 2004, Kawaguchi and Sakaba, 2015). Moreover, those and other studies activated PC-DCN synapses with relatively brief stimulus bursts (Pedroarena and Schwarz, 2003, Telgkamp et al., 2004, Telgkamp and Raman, 2002, Han et al., 2014), whereas PCs typically fire constantly at high frequencies *in vivo* (Zhou et al., 2014). Thus, characterizing PC-DCN synapses during prolonged periods of high frequency activation could more accurately reflect the properties of synaptic transmission *in vivo*.

The properties of PC-DCN synapses remain a matter of debate. Studies in young animals (P13-P15) indicate that PC-DCN synapses depress in a frequency dependent manner, with depression increasing at higher stimulus frequencies (Telgkamp and Raman, 2002). In young animals the properties of PC synapses are strongly influenced by the spillover and pooling of GABA released from the many release sites on PC boutons (Telgkamp and Raman, 2002, Telgkamp et al., 2004, Pugh and Raman, 2005). Recently, the observation that action potentials sometimes fail to invade PC presynaptic boutons, particularly at high firing frequencies, led to the alternative hypothesis that action potential failures account for the more pronounced depression for high frequency firing (Kawaguchi and Sakaba, 2015).

This finding is significant because it suggests that a substantial fraction of action potentials propagate down the length of PC axons only to fail to invade presynaptic terminals. However, in older animals, some aspects of synaptic transmission are frequency-independent (Jackman et al., 2014, Person and Raman, 2012a). This suggests that the properties of depression and the mechanisms that underlie depression may change during development.

Here, we investigate the properties of the PC-DCN synapse under near-physiological conditions using prolonged high frequency activation. We find that although steady-state responses are frequency dependent in young animals, in juveniles and adults these synapses depress to similar steady-state levels across a wide range of frequencies. As a result, charge transfer is linearly related to the range of average PC firing frequencies observed at rest *in vivo* (10-100 Hz). This suggests that depression arising from frequency-dependent spike invasion does not contribute significantly to depression under our experimental conditions. The linear frequency dependence of charge transfer is an unusual synaptic property that has also been observed at glutamatergic afferents in vestibular nuclei (McElvain et al., 2015, Bagnall et al., 2008). We find that at the PC-DCN synapse linear charge transfer appears to arise from a number of synaptic specializations, including an unexpected component of short-term facilitation that is normally masked by depression. Together, these specializations allow the PC-DCN synapse to linearly encode PC firing.

Results

Purkinje cell synapses onto neurons in the DCN were studied by activating PC axons with an extracellular electrode placed in the white matter between the cerebellar cortex and the DCN (**Figure 2.1A**). The resulting inhibitory post-synaptic currents (IPSCs) were recorded from putative glutamatergic projection neurons that can be visually identified by their large cell bodies (Uusisaari et al., 2007).

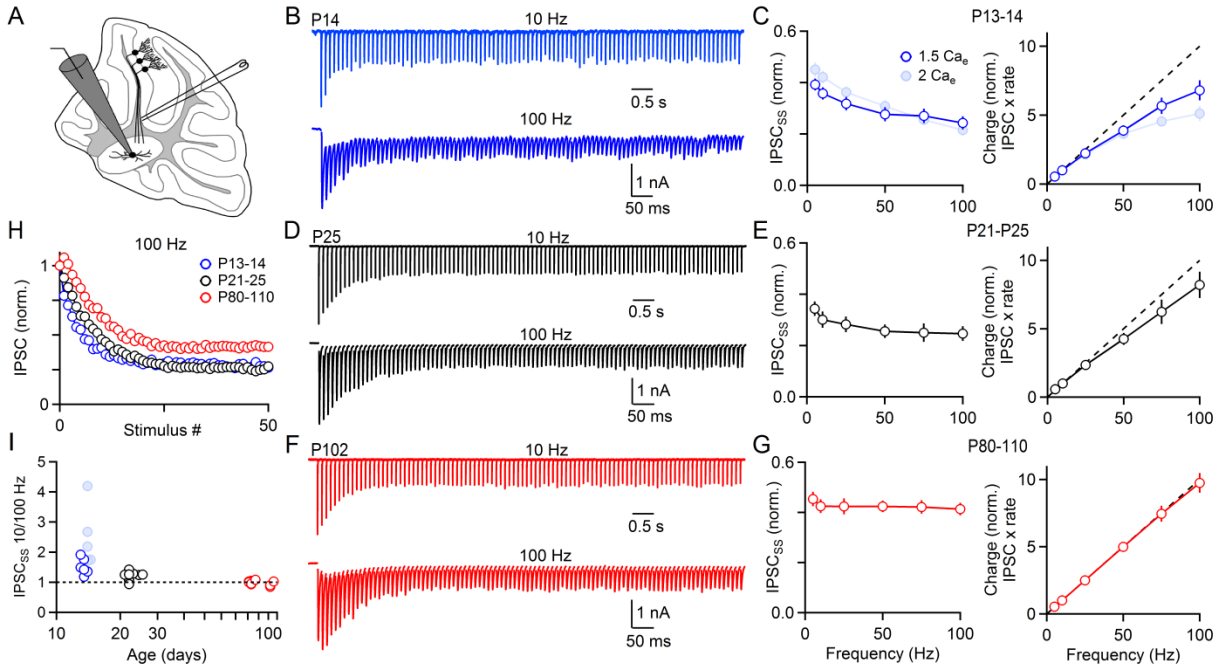

Figure 2.1 Charge transfer at PC-DCN synapses is linearly dependent on presynaptic firing frequency in juveniles and adults.

A. Schematic of sagittal cerebellar slice preparation and recording configuration.

B. Average IPSCs at P14 evoked by 100 stimuli at the indicated frequencies for the same cell in 1.5 mM external calcium (Cae).

C. (left) Summary of normalized steady-state IPSC amplitude as a function of stimulus frequency in P13-14 animals in 1.5 mM Cae (n = 6) and 2 mM Cae (n = 7). (right) Charge transfer due to incremental evoked IPSCs (product of IPSCSS and stimulation frequency, normalized to 10 Hz) as a function of stimulus frequency.

D. As in B but for a P25 animal.

E. As in C but for P21-25 animals (n = 8).

F. Same as in B but for a P102 animal.

G. As in C but for P80-P110 animals (n = 7).

H. Amplitudes of IPSCs as a function of stimulus frequency for 100 Hz stimulation.

Figure 2.1 (Continued)

I. Ratio of steady-state responses to 10 Hz trains to those of 100 Hz trains as a function of age. Each point is one cell. All experiments were performed in 1.5 mM Ca_e other than those indicated for P13-14 animals and summarized in C and I. All data points are presented as means ± SEM unless otherwise noted.

Synaptic properties are strongly regulated during development; thus, in order to relate synaptic properties to behavior it is important to determine the properties of mature synapses in juveniles and adults under physiological conditions. Previously, PC synapses onto neurons in the DCN had been characterized in very young animals and in elevated external calcium (Ca_e, 2 mM) (**Figure 2.1**, **C** left, light blue). We confirmed that under these experimental conditions there is a strong frequency dependence of steady-state synaptic strength at PC-DCN synapses. These differences were reduced in more physiological Ca_e, (1.5 mM) (**Figure 2.1B, C** left). In juvenile animals (P21-30), transmission during trains reached steady-state and became less frequency-dependent. Steady-state IPSC amplitudes during 10 Hz stimulation was comparable to that of 100 Hz (**Figure 2.1D, E** left). These differences were absent in adults (P80-110, **Figure 2.1F, G, H** left). Plots of the steady-state IPSC amplitude as a function of stimulus frequency indicates that steady-state transmission becomes more frequency-invariant with age. Whereas in very young animals there is a steep dependence between steady-state transmission and frequency (**Figure 2.1C** left), adult PC-DCN synapses remain constant within the 10 to 100 Hz firing range (**Figure 2.1G** left). The ratio of steady-state IPSC sizes evoked by 10 and 100 Hz trains ($IPSC_{SS10/100}$), which provides a measure of the frequency-invariance of transmission, shows that transmission becomes more frequency-invariant with age (**Figure 2.1I**), ($IPSC_{SS10/100}$ = 2.34 ± 0.34 at P12-15 in 2 Ca_e, 1.52 ± 0.10 at P12-15 in 1.5 Ca_e, 1.21 ± 0.05 at P21-30, 0.98 ± 0.02 at P80-110), and in adults this ratio is not significantly different than 1 ($p<0.05$, one-sample t-test for P80-100). The steady-state IPSC size for individual cells reflected these averages (**Figure 2.2**).

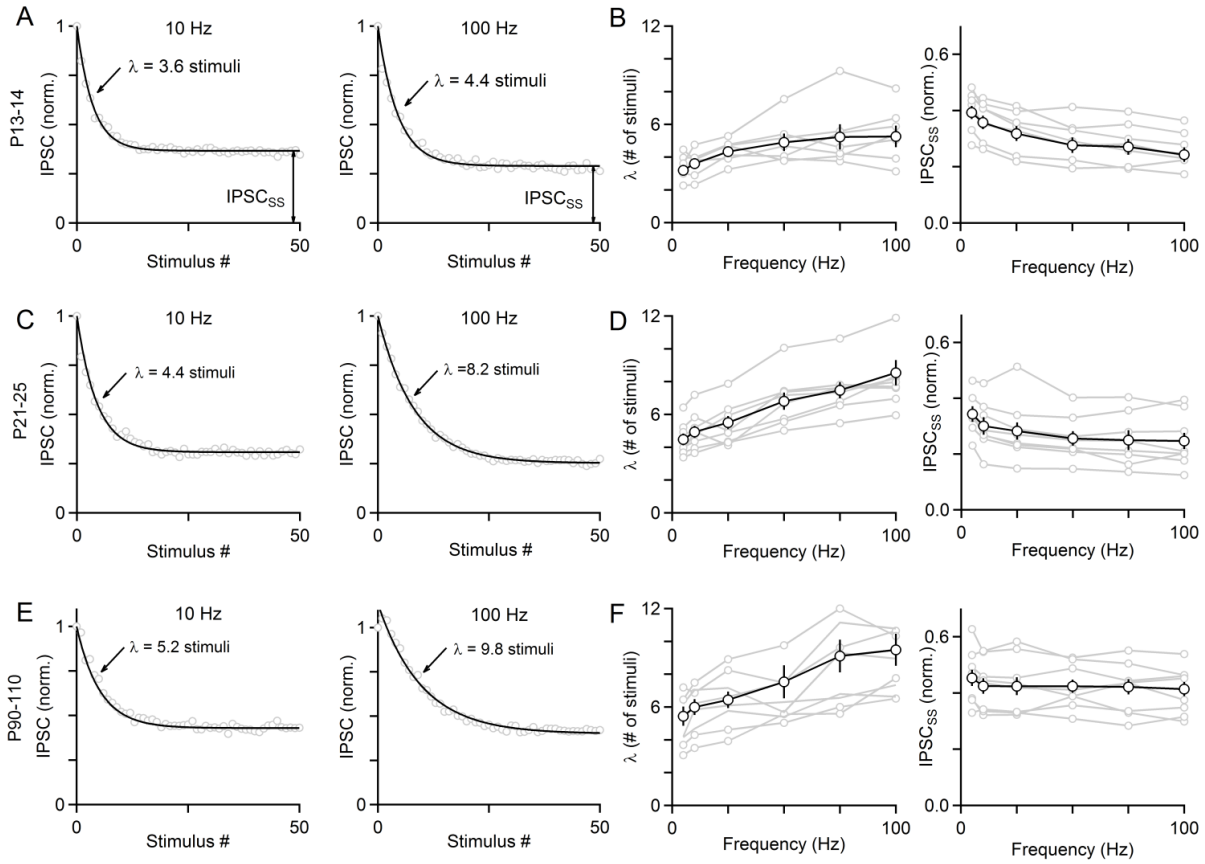

Figure 2.2: Linear charge transfer occurs in individual large DCN neurons

(A) Average IPSC amplitudes evoked by 10 Hz (left) or 100 Hz (right) trains with exponential fit in P13-15 animals in 1.5 Ca_e.

(B) Plot of steady-state IPSC amplitudes (left) and decay constant λ as a function of stimulus frequency for all cells in P13-15 animals.

(C) Same as in A but for P21-25 animals.

(D) Same as in B but for P21-25 animals.

(E) Same as in A, C but for P80-110 animals.

(F) Same as in B, D but for P80-110 animals. All data are presented as means ± SEM.

The degree of frequency invariance was significantly different between age groups: $IPSC_{SS10/100}$ = 1.52 ± 0.10 at P12-15 in 1.5 Ca_e vs 1.21 ± 0.05 at P21-30, $p < 0.05$; and for $IPSC_{SS10/100}$ = 1.21 ± 0.05 at P21-30 vs 0.98 ± 0.02 at P80-110, $p < 0.001$, student's t-test.

This frequency-invariance of steady-state transmission is an unusual and unexpected property. For most depressing synapses, increased firing frequency leads to more pronounced depression (Galarreta and Hestrin, 1998, Cook et al., 2003, Brenowitz et al., 1998, Abbott et al., 1997), with the exception of vestibular afferents in vestibular nuclei (McElvain et al., 2015, Bagnall et al., 2008) and possibly auditory inputs in the chick brainstem (Macleod et al. 2007). At the PC-DCN synapse in very young animals, depression is frequency-dependent and it has been proposed that this is due to the failure or attenuation of action potentials upon invasion of presynaptic boutons at high frequency (Kawaguchi and Sakaba, 2015). Here we find that at near physiological temperatures in juvenile and adult mice, there is no such frequency dependence to the extent of depression, suggesting that action potentials reliably invade presynaptic boutons within the resting physiological firing range at mature PC-DCN synapses.

Since steady-state IPSC amplitudes at PC-DCN synapses remain invariant of stimulation frequency, we determined how stimulation frequency relates to the charge transfer due to incremental IPSC amplitude, calculated as the product of steady-state IPSC size and stimulation rate. To compare values across cells, we plotted the average charge transfer normalized to 10 Hz as a function of frequency. In very young animals, there was a non-linear relationship between charge transfer and stimulation frequency that was somewhat more pronounced (**Figure 2.1C**, right). During high-frequency stimulation, stronger depression reduced the total charge transfer relative to low-frequency stimulation. In juveniles and adults charge transfer became progressively more linear (**Figure 2.1E, G**, right), such that in adults a tenfold increase in stimulation frequency correspondingly resulted in a tenfold increase in charge transfer. As steady-state transmission is approximately frequency invariant in juveniles and adults, and since experiments are more difficult in adults, we focused on juvenile PC-DCN synapses.

There are a number of factors that must be considered in order to understand how PC-DCN synapses provide frequency-independent depression over such a large range of stimulus frequencies. Recovery from depression is a major determinant of steady-state responses during stimulus trains. At some synapses recovery from depression is calcium dependent, and accelerates when higher firing rates lead to more calcium influx (Sakaba and Neher, 2001, Dittman and Regehr, 1998, Wang and Kaczmarek,

1998, Stevens and Wesseling, 1998, Yang and Xu-Friedman, 2009). This could allow synapses to adjust recovery from depression in a frequency-dependent manner to better maintain transmission when challenged with sustained high-frequency activation. Thus, it is possible that the recovery rate accelerates as the stimulus frequency increases. If recovery at PC-DCN synapses is accelerated during high-frequency stimulation, it could counteract stronger depression to produce net steady-state transmission that appears invariant of frequency.

We therefore quantified recovery from depression by activating PC-DCN synapses with trains of 100 stimuli at either 100 Hz or 20 Hz, and applying test pulses at different time intervals following these trains (**Figure 2.3A**). The time course of recovery from depression following a 100 Hz stimulus train is well approximated by a single exponential with a time constant τ_R = 7.5 ± 0.6 s (**Figure 2.3B**). Even at short times after the train a rapid phase of recovery was not apparent (**Figure 2.3B**, right). This contrasts with other synapses where similar experiments revealed a rapid component of recovery that could be effective at allowing synapses to maintain transmission during long-lasting high frequency activation. Recovery from depression was not significantly different following 100 stimuli at 20 Hz (**Figure 2.3C**, τ_R = 7.0 ± 1.1 s, p = 0.73 student's t-test). This suggests that a frequency-dependent acceleration in recovery from depression does not play a role in the linearity of PC-DCN synapses.

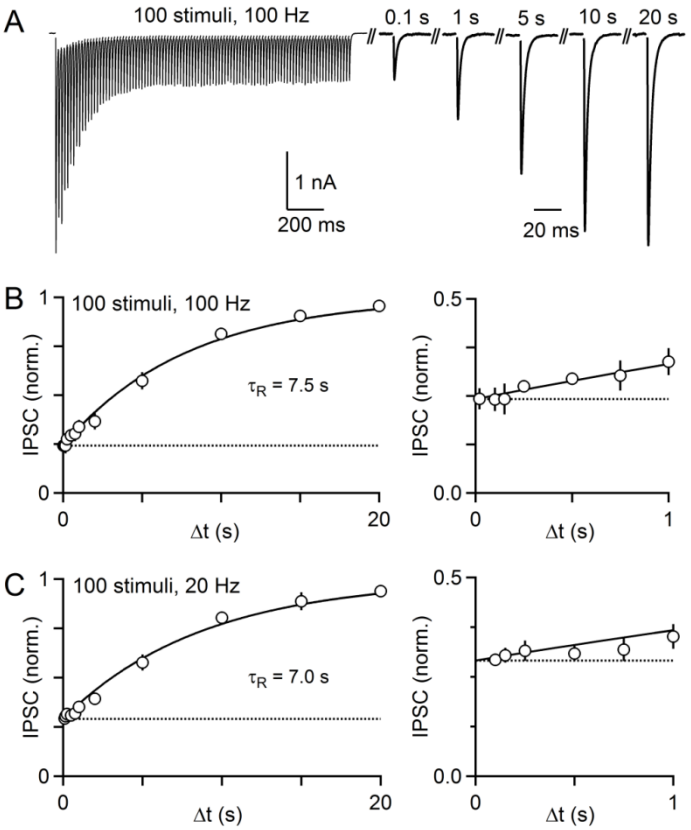

Figure 2.3: Recovery from depression following a stimulus train is slow and independent of the train frequency in P21-30 animals.

(A) IPSCs evoked by a 100 Hz stimulus train followed by IPSCs after a delay of 0.1 s to 20 s. Traces are averages of 6-8 trials.

(B) Recovery of IPSC amplitude following 100 Hz stimulation is approximated with a single exponential fit constrained to go to 1 ($R^2 = 0.994$). The average steady-state IPSC amplitude is indicated by dashed line. Expanded axes at right shows recovery time points within the first second after the train (n = 8 cells).

(C) As in (B) but for 20 Hz stimulation (n = 7 cells). $R^2 = 0.992$ for the exponential fit. All data are presented as means ± SEM unless otherwise noted.

The responses to high-frequency stimulation and slow recovery from depression provide important constraints on models that could describe the properties of the PC-DCN synapse. We determined whether the observed properties of the PC-DCN synapse could be described by a simple depletion model, which has been used to describe release at a number of depressing synapses (Ruiz et al., 2011, Neher and Sakaba, 2008, Thanawala and Regehr, 2013, Thanawala and Regehr, 2016a). This model consists of a uniform pool of vesicles with three parameters: N, the number of vesicles in the readily releasable pool at rest, P, the release probability, and the time constant of vesicle replenishment τ_R (**Figure 2.4A**). The parameter τ_R was determined from the time course of recovery from depression (**Figure 2.3B**; see Thanawala and Regehr, 2013, 2016, methods) and P was unconstrained. Experimental data for 100 Hz trains was fit with an exponential to the initial rate of decay of the IPSC amplitude (**Figure 2.4B**, λ) and the steady-state IPSC level (**Figure 2.4B**; $IPSC_{SS}$, $IPSC_i = IPSC_{SS} + (1\text{-}IPSC_{SS})\, e^{-i/\lambda}$). According to the model λ and $IPSC_{SS}$ are both dependent on P (**Figure 2.4C-E**). Steady-state IPSCs comparable to what we observe are only present when $P < 0.005$ (**Figure 2.4E**), but when P is very low it takes hundreds of stimuli to reach steady-state (**Figure 2.4D**). These findings suggest that PC-DCN synapses cannot be accounted for by a depletion model for a single uniform pool of vesicles.

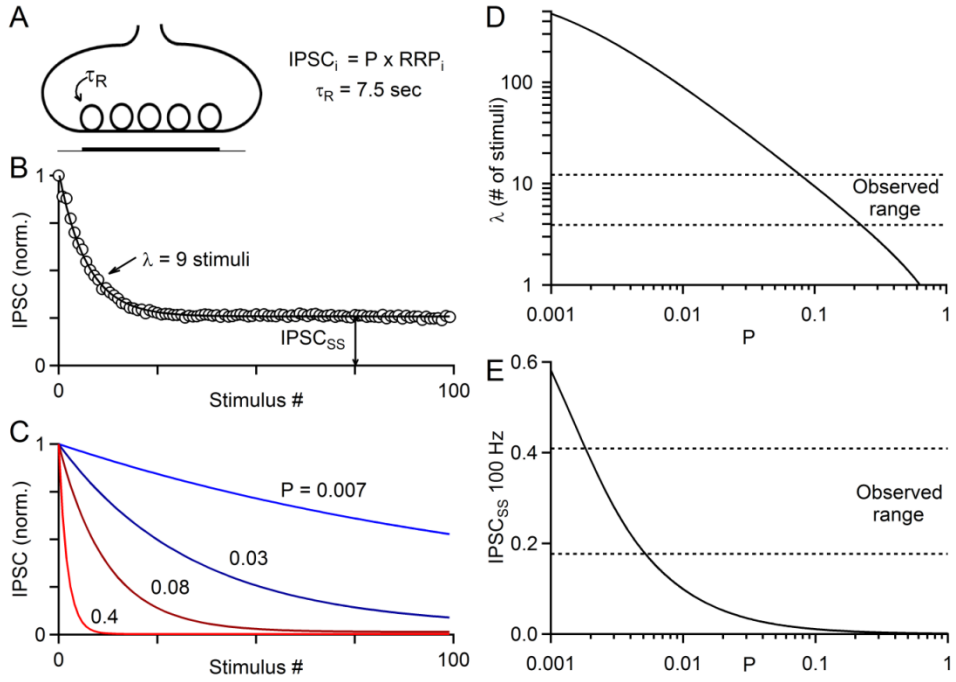

Figure 2.4: PC-DCN synapses in P21-30 animals cannot be described by a single pool depletion model

(A) Schematic representation of a single pool model with a readily releasable pool (RRP) of vesicles with uniform properties. During the first stimulus, the fraction of the RRP released is determined by the release probability (P). Between stimuli, replenishment of the RRP is dependent on extent of depletion and on the recovery time constant (τ_R, see methods).

(B) Experimental data of IPSC amplitudes evoked by 100 Hz stimulation as a function of stimulus number were well approximated by an exponential decay. Data are presented as means ± SEM, error bars are occluded by markers (n = 8 cells).

(C) IPSC amplitudes determined from a single pool model for 100 Hz trains using experimentally measured τ_R (7.5 s, Figure 2.3B) and the indicated values of P.

(D) Decay constant λ in terms of number of stimuli according to a single pool depletion model for a range of P. Dashed lines indicated the range of experimentally observed responses.

(E) Steady-state IPSC size produced by the model across all values of P. Dashed lines indicated the range of experimentally observed responses.

Synapses often have multiple forms of use-dependent plasticity, and it is possible that they combine to produce linear charge transfer. Short-term facilitation is one form of synaptic enhancement that increases synaptic responses in a frequency-dependent manner, and could thus counteract depression. Such an interaction between facilitation and depression has been proposed to contribute to responses at synapses in the chick auditory brainstem (MacLeod et al., 2007). We therefore assessed the possibility that facilitation might also be present in addition to depression. Lowering Ca_e decreased synaptic strength to 11.7 ± 1.5% (n=11) of control values (**Figure 2.5**) and revealed that PC-DCN synapses undergo short-term facilitation that is masked by depression under normal conditions. Trains of 100 Hz stimulation evoked prominent facilitation in 0.5 mM Ca_e (**Figure 2.6**). On average, facilitation peaked within the first few stimuli, reaching 170 ± 10% of the initial IPSC amplitude at 100 Hz (**Figure 2.6B**). The magnitude of facilitation scaled with stimulation frequency (**Figure 2.6C**), and could be revealed with modest changes in Ca_e (**Figure 2.5**).

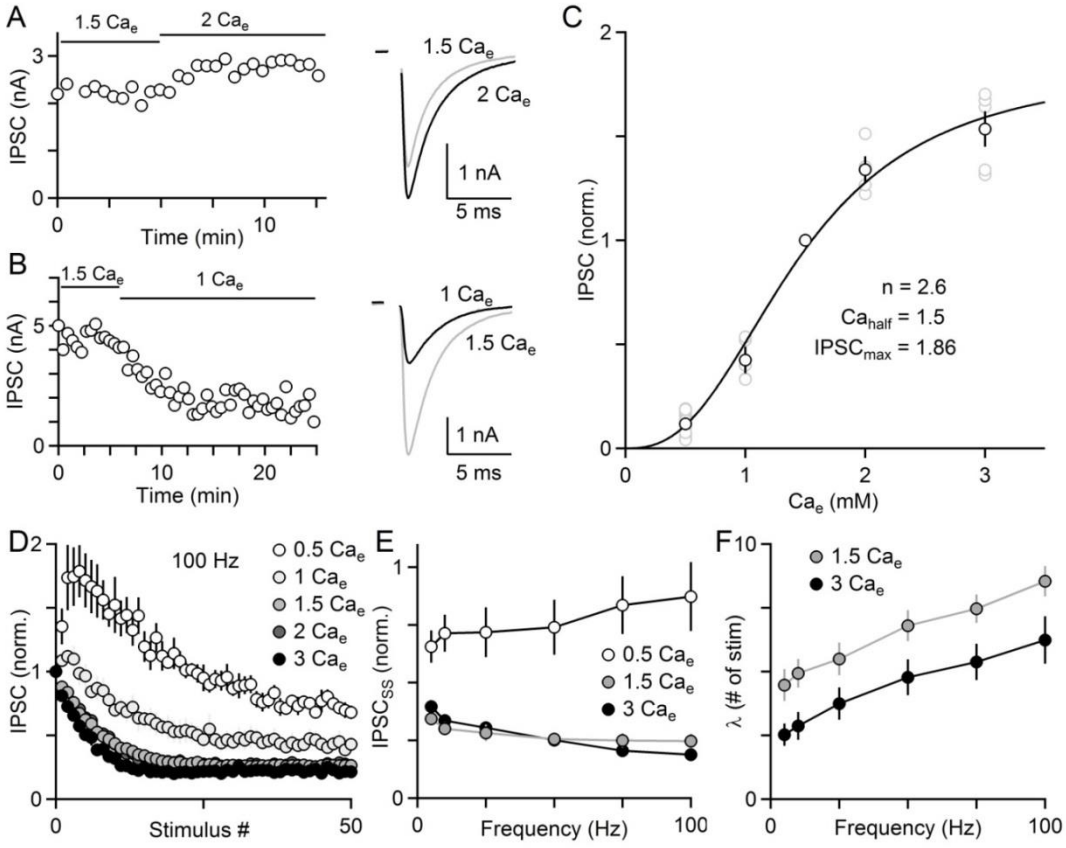

Figure 2.5: The calcium dependence of release at the PC-DCN synapse is non-linear.

Experiments were performed to determine how the strength of the PC-DCN synapse depends on external calcium (Ca_e). IPSC amplitude was initially measured in 1.5 mM Ca_e and then Ca_e was changed and the effect on the IPSC was determined.

(A) Example experiment in which Ca_e was increased to 2 mM Ca_e with average IPSCs shown at right taken at baseline (0-5 min) and in 2 Ca_e (9-13 min).

(B) Another example experiment in which Ca_e was lowered to 1 mM with averaged traces shown at right taken at baseline (0-5 min) and in 2 Ca_e (18-22 min).

(C) IPSC amplitude as a function of Ca_e normalized to the IPSC amplitude in 1.5 mM Ca_e. Ca_e was washed in for each cell from a baseline of 1.5 mM Ca_e, with total divalent concentrations held at 2.5 mM except in in 3 Ca_e, Mg_e was 0.1 mM. A fit to the Hill equation:

Figure 2.5 (Continued)

$IPSC_{max}/(1+[(Ca_e)_{1/2}/Ca_e]^n)$ constrained to go through (0,0) is shown, with $(Ca_e)_{1/2}$ = 1.5 mM, n = 2.6 and $IPSC_{max}$ = 1.86.

(D) Average IPSCs evoked by 100 Hz stimulus trains in the presence of different Ca_e (n = 4-8 cells per condition).

(E) The amplitude of the average steady-state IPSC amplitude normalized to the initial IPSC amplitude is shown at various frequencies for 0.5, 1.5 and 3 mM Ca_e.

(F) The average decay constant of depression is shown at various frequencies for 1.5 and 3 mM Ca_e. All data are presented as means ± SEM.

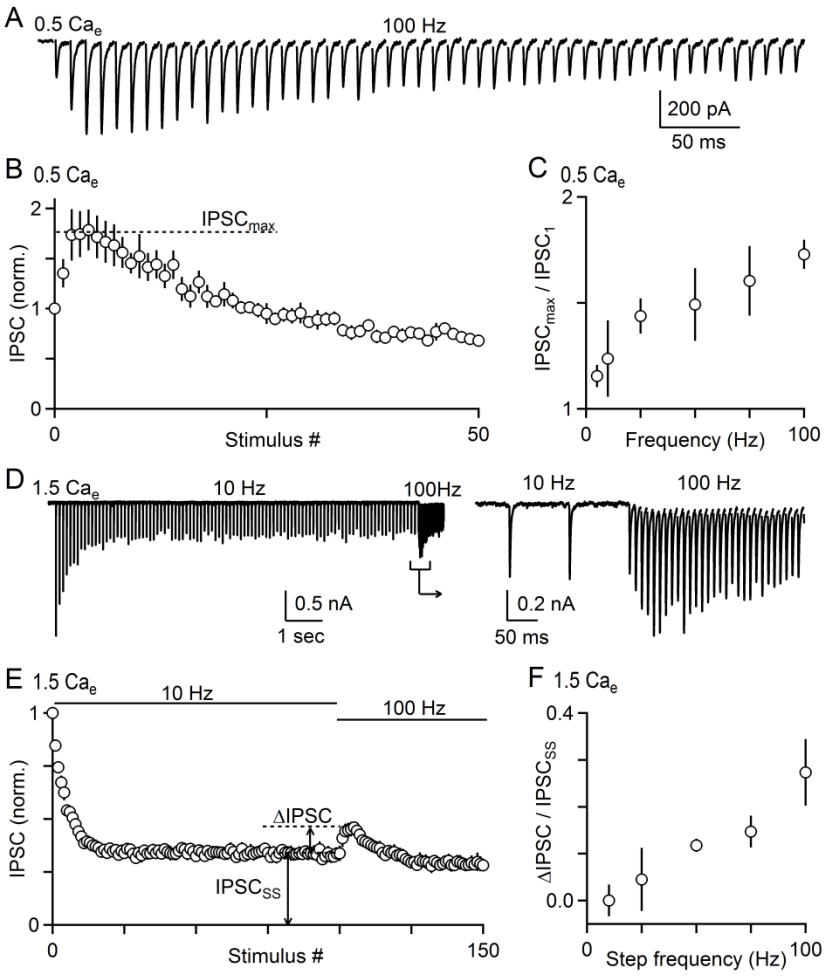

Figure 2.6: Short-term synaptic facilitation is present at the PC-DCN synapse in P21-30 animals.

(A-C) Stimulus trains were used to evoke synaptic responses in 0.5 mM external calcium (Ca_e).

(A) IPSCs evoked by 100 Hz stimulation.

(B) Summary of average IPSC amplitudes evoked by 100 Hz trains (n = 6 cells).

(C) Facilitation ($IPSC_{max}$) as a function of stimulation frequency (n = 6 cells).

(D-F) In experiments conducted at 1.5 mM Ca_e, the DCN inputs were stimulated 100 times at 10 Hz, followed by 50 stimuli at another frequency.

(D) IPSCs evoked by 10 Hz stimulation followed by 100 Hz stimulation. Expanded panel at right shows IPSCs just before and after the change in frequency.

Figure 2.6 (Continued)

(E) Average IPSC size for protocol shown in (D) with the percent change in IPSC size (ΔIPSC/IPSC$_{SS}$) measured as indicated (n = 6 cells).

(F) Change in IPSC size stepping from 10 Hz to various frequencies. A conditioning train of 10 Hz was applied to reach steady-state, followed by a step increase to 10-100 Hz (n = 6 cells). All data are presented as means ± SEM.

Even though depression can mask facilitation in physiological calcium (1.5 mM Ca_e), it is possible to reveal facilitation with appropriate stimulus protocols (Muller et al., 2010, Lu and Trussell, 2016). A 10 Hz train was initially applied to depress the synapse and reach steady-state, and this was followed by a step increase to 100 Hz. Stepping from low to high-frequency stimulation during steady-state revealed a transient increase in IPSC amplitude (**Figure 2.6D, E**). Although it appears that facilitation is transient, it is more likely that facilitation increases P to a steady state value during prolonged stimulation, but that vesicle depletion builds during sustained activation and eventually reduces the extent of synaptic enhancement (see modeling below). We quantified the percent change in IPSC size after steps from 10 Hz to higher frequencies and found that the increase in IPSC size was frequency-dependent (**Figure 2.6F**). These findings suggest that facilitation occurs in physiological conditions in a similar manner to that observed in 0.5 mM Ca_e. Thus it is possible that the PC-DCN synapse achieves frequency-independent transmission by balancing depression with facilitation.

The saturation and desensitization of postsynaptic receptors can also influence short-term synaptic plasticity during stimulus trains (Chen et al., 2002, Trussell et al., 1993, Xu-Friedman and Regehr, 2003, Foster and Regehr, 2004, Foster et al., 2002, Chanda and Xu-Friedman, 2010, Wadiche and Jahr, 2001). We relieved receptor saturation and desensitization with a low-affinity competitive receptor antagonist. This approach has been used extensively to study excitatory synapses, but has not been as widely used to study inhibitory synapses (Sakaba, 2008). We used the low-affinity competitive $GABA_AR$ antagonist TPMPA (K_d = 300 μM) (Jones et al., 2001, Ragozzino et al., 1996) and compared responses to those obtained in the presence of a low concentration of high-affinity $GABA_AR$ antagonist SR-95531 (K_d = 0.15 μM). SR-95531 is not expected to influence saturation or desensitization because of its slow unbinding rate.

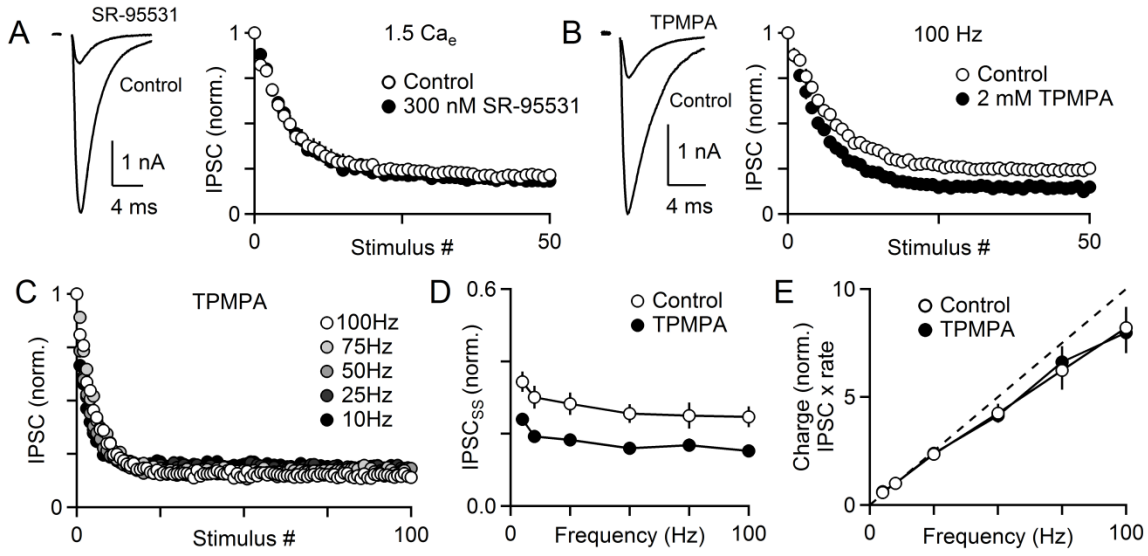

Figure 2.7. Relief of receptor saturation and desensitization does not alter linear charge transfer in P21-30 animals.

(A) IPSCs before and after washin of the high affinity $GABA_A$ receptor antagonist SR-95531 (300 nM) in a single cell. Graph at right shows average IPSC amplitudes as a function of stimulus number for a 100 Hz train in the absence (open symbols) and presence of SR-95531 (filled symbols, n = 6 cells).

(B) Similar to (A), but using the low affinity $GABA_A$ receptor antagonist TPMPA (2 mM, n = 5 cells)

(C) Average IPSC size evoked by trains of the indicated frequencies in the presence of 2 mM TPMPA (n = 7 cells).

(D) Summary of normalized steady-state IPSC amplitude as a function of stimulus frequency in control conditions (as in **Figure 2.1**, n = 8 cells) and in the presence of 2 mM TPMPA (n = 7 cells).

(E) Average charge transfer as a function of stimulus frequency, normalized to 10 Hz. All data are presented as means ± SEM, error bars are occluded in some cases by markers.

The differential effects of these $GABA_AR$ antagonists suggest that receptor saturation affects plasticity during stimulus trains at PC-DCN synapses. Low concentrations of SR-95531 (300 nM) and high concentrations of TPMPA (2 mM) reduced IPSC amplitudes to a similar extent (reduced to 26 ± 5 vs. 29 ± 6% of control in SR-95531 and TPMPA respectively, p = 0.71, student's t-test), but had very different effects on short-term plasticity. Depression became significantly more pronounced in TPMPA (**Figure 2.7B,** $IPSC_{SS}$ Ctrl = 0.24 ± 0.02, $IPSC_{SS}$ TPMPA = 0.12 ± 0.01, p<0.01, paired student's t-test), but was not significantly affected in SR-95531 (**Figure 2.7A,** $IPSC_{SS}$ Ctrl = 0.21 ± 0.02, $IPSC_{SS}$ SR-95531 = 0.19 ± 0.02, p = 0.21 paired student's t-test). This is consistent with saturation limiting the magnitude of IPSCs to a greater extent for responses early in the train that evoke more GABA release. In contrast, TPMPA had no effect on short-term plasticity in low Ca_e conditions in which GABA release is reduced and therefore receptor saturation should be minimal (**Figure 2.8**).

We determined whether PC-DCN synapses maintained linear charge transfer when receptor saturation was attenuated. Across the range of physiological frequencies, steady-state IPSCs were similar (**Figure 2.7C**), and the steady-state IPSC amplitude remained relatively constant in both the presence and absence of TPMPA (**Figure 2.7D, 2.9,** $IPSC_{SS10/100}$ control = 1.31 ± 0.07, TPMPA = 1.27 ± 0.06, p = 0.61 student's t-test). There was a similarly linear relationship between charge transfer and stimulation frequency with or without TPMPA (**Figure 2.7E**). This indicates that receptor saturation is not required for the nearly linear relationship between PC firing frequency and charge transfer.

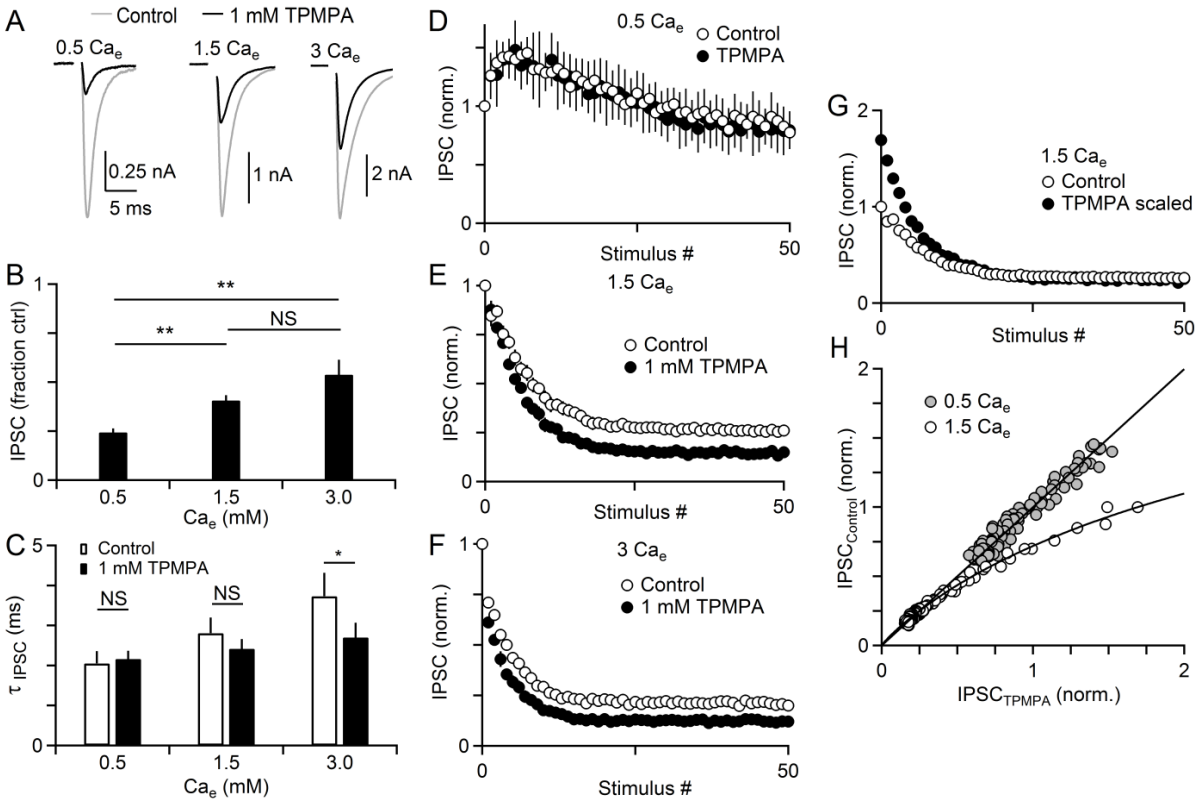

Figure 2.8: Influence of TPMPA on single stimuli and trains for a range of Ca_e

(A) IPSCs before and after washin of 1 mM TPMPA in 0.5 (*left*), 1.5 (*middle*), and 3 (*right*) Ca_e.

(B) Summary of the IPSC blockade by 1 mM TPMPA in different Ca_e. The Ca_e dependence of the extent of IPSC blockade is consistent with multivesicular release and high receptor $GABA_AR$ occupancy being more prominent in high Ca_e (Fraction of control in 0.5 Ca_e = 0.24 ± 0.02; 1.5 Ca_e = 0.47 ± =0.03; 3 Ca_e = 0.54 ± 0.07, n = 3-6 cells per condition).

(C) Summary of the IPSC decay time constant in different Ca_e with or without 1 mM TPMPA (τ_{IPSC} in 0.5 Ca_e = 2.1 ± 0.3 ms control vs 2.2 ± 0.2 ms TPMPA, p = 0.49; in 1.5 Ca_e = 2.6 ± 0.4 ms control vs 2.4 ± 0.3 ms TPMPA, p = 0.18; in 3 Ca_e = 3.7 ± 0.5 ms control vs 2.7 ± 0.3 ms TPMPA, $p < 0.05$, paired student's t-test.)

(D) Summary of average IPSC amplitude for 100 Hz stimulation before (*open symbols*) and after (*closed symbols*) washin of TPMPA in 0.5 Ca_e. Responses are normalized to the amplitude of

Figure 2.8 (Continued)

the first IPSC (n = 5 cells, $IPSC_{40\text{-}50}$ in 0.5 Ca_e = 0.80 ± 0.06 control vs. 0.76 ± 0.07 TPMPA, p = 0.23, paired student's t-test).

(E) Same as in (D) but in 1.5 Ca_e (n = 6 cells, $IPSC_{40\text{-}50}$ in 1.5 Ca_e = 0.24 ± 0.02 control vs 0.14 ± 0.02 TPMPA, $p < 0.01$, paired student's t-test).

(F) Same as in (E) but in 3.0 Ca_e (n = 3 cells, $IPSC_{40\text{-}50}$ in 3 Ca_e = 0.21 ± 0.02 control vs 0.12 ± 0.03 TPMPA, $p < 0.001$, paired student's t-test).

(G) Data shown in (E), but responses in TPMPA are scaled to the steady-state amplitude in control conditions to illustrate the effects of receptor saturation.

(H) Plot of IPSCs in control vs. TPMPA from (D) and (E) fit with a line or Hill equation, respectively. Responses in TPMPA are scaled to the steady-state amplitude in control conditions. All data are presented as means ± SEM. ** indicates $p < 0.01$, and * $p < 0.05$, student's t-test

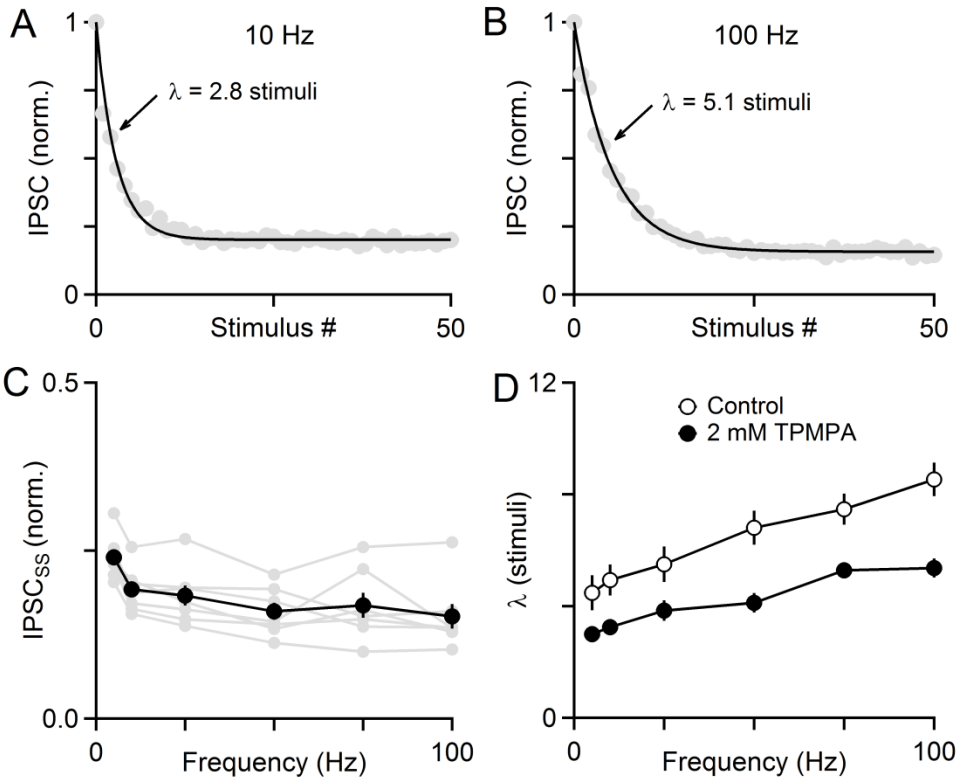

Figure 2.9: Linear charge transfer occurs in all large DCN neurons in the presence of TPMPA

(A) Average IPSC amplitude evoked by 10 Hz train with exponential fit in 2 mM TPMPA.

(B) Same as in A but 100 Hz.

(C) Plot of steady-state IPSC amplitudes as a function of stimulus frequency for all cells in 2 mM TPMPA.

(D) Plot of average decay constant of depression as a function of stimulus frequency in control and 2 mM TPMPA. All data are presented as means ± SEM except (C).

These experiments establish key aspects of the PC-DCN synapse that can be used to constrain the mechanism by which the PC-DCN synapse conveys linear charge transfer. This includes (1) the responses to 10-100 Hz stimulus trains, (2) recovery from depression curves following stimulus trains, and (3) facilitating responses to step change in stimulus frequencies. We found that a simple single pool depletion model cannot describe the PC-DCN synapse (**Figure 2.5**), even with the incorporation of facilitation (not shown).

We also evaluated a model developed by Raman and her colleagues to describe the PC-DCN synapse in young animals (Telgkamp et al., 2004) (**Figure 2.10, 2.11G, H**). This model is based on the close proximity of active zones and associated PSDs at this synapse that allows GABA release from different active zones to pool and saturate or partially saturate $GABA_A$ receptors. We applied this model to describe older PC-DCN synapses and found that it could account for the effects of TPMPA (**Figure 2.11G, H**) but on its own could not account for the near frequency-invariance of transmission (**Figure 2.10**).

The failure of single pool models to describe the PC-DCN synapse prompted us to consider other possibilities, beginning with a model that was developed to describe synapses between vestibular afferents and neurons in the medial vestibular nucleus, one of the only other synapses known to have frequency independent transmission (Bagnall et al., 2008). According to this model, each release site contains two releasable vesicles but release is limited to a single vesicle per release site per stimulus. Consequently, vesicles are always available for release, and depression is determined by frequency-independent decreases in release probability (McElvain et al., 2015). Since PC-DCN synapses facilitate, and the magnitude of facilitation is frequency dependent, it does not conform to the model of the vestibular synapse.

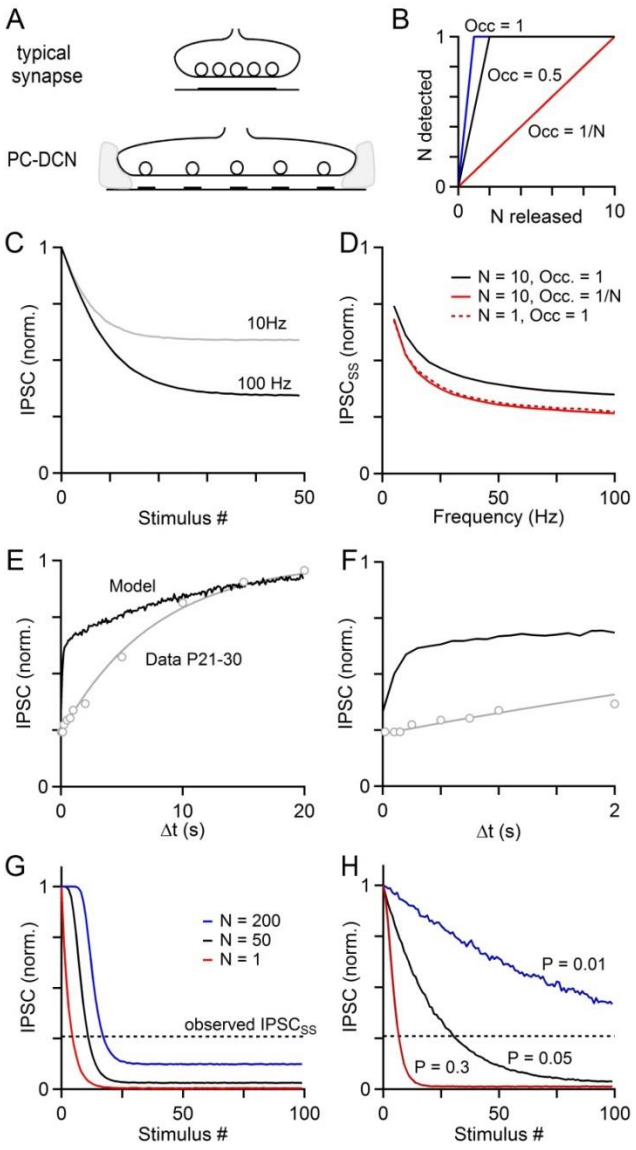

Figure 2.10: **A model based on receptor saturation cannot describe frequency-invariance in P21-30 animals.**

We evaluated a model developed by Raman and her colleagues to describe the PC-DCN synapse in young animals (Telgkamp et al., 2004). At most synapses each bouton has a single active zone that is associated with a post synaptic density (PSD), and many vesicles (N) are associated with each active zone. At the PC-DCN synapse the ultrastructure differs in that each bouton has multiple active zones, each with its own PSD. For both types of synapses the probability of release from the bouton is high [P_{bouton} =1-(1-$P_{vesicle}$)^N, for N docked vesicles with a probability of release $P_{vesicle}$], while vesicle depletion is reduced

Figure 2.10 (Continued)

(Telgkamp et al., 2004, Xu-Friedman and Regehr, 2004). For synaptic boutons with a single active zone associated with a single PSD, N is the number of docked vesicles, but in the PC-DCN model of Telgkamp et al. 2004, N is the number of active zones and it is assumed that there is a single docked vesicle per active zone. It is thought that a vesicle released from any active zone can activate many receptors in all of the PSDs associated with the bouton because PSDs are close to each other and GABA uptake does not occur between PSDs (Telgkamp et al., 2004, Ribak et al., 1996). In the model, release from a single site activates all PSDs, but the post-synaptic receptor occupancy (Occ) can be varied. If receptor occupancy is high, fusion of a single vesicle activates many of the postsynaptic receptors in the corresponding PSD and there is a sublinear relationship between the number of vesicles that fuse and the postsynaptic response, as seen at other synapses (Chanda and Xu-Friedman, 2010; Foster et al. 2005; Wadiche and Jahr, 2001). If receptor occupancy is low, a single vesicle spills over to activate all post-synaptic sites but the postsynaptic response at each site is small; under these circumstances, the model is functionally equivalent to a single-pool depletion model with one PSD per active zone (N = 1, Occ = 1). We explored the behavior of the Telgkamp et al. 2004 model to determine whether it could account for the synaptic properties we observe in older animals. This model assumes that there are 10 active zones per bouton and assumes that the fusion of 1 or more vesicles saturates all postsynaptic receptors at all PSDs associated with a bouton. We also used a model containing 20 active zones and the assumption that 2 or more vesicles saturate all receptors, which produced nearly identical results, as in Telgkamp et al. 2004.

(A) A model bouton at a typical synapse contains N docked vesicles apposed to a single PSD, whereas modeled boutons of PC-DCN synapses contain N individual release sites, each with their own PSD. Release from a single site reaches multiple PSDs because reuptake occurs exclusively at the periphery of the bouton.

Figure 2.10 (Continued)

(B) Plot of post-synaptic response as a function of number of released vesicles at PC-DCN synapses modeled by Telgkamp et al. 2004.

(C) Simulated trains of 10 and 100 Hz stimulation using a saturation model developed by Telgkamp et al. 2004 containing 10 sites per bouton and $P_{vesicle}$ of 0.1.

(D) Modeled steady-state IPSCs as a function of stimulation frequency with release from a single site resulting in 100% post-synaptic receptor occupancy, minimal receptor occupancy (Occ = 1/N) or with only one release site per bouton (N = 1).

(E) Recovery from depression following 20 or 100 Hz trains in the saturation model developed by Telgkamp et al. 2004 compared to experimentally observed recovery in P21-30 PC-DCN synapses. Data are presented as means ± SEM.

(F) Recovery from depression as shown in (E), but at short interstimulus intervals.

(G) Model 100 Hz trains using recovery from depression experimentally observed in P21-30 animals with varying N release sites per bouton.

(H) Same as in (G), but varying $P_{vesicle}$ with 10 release sites per bouton.

This model accounts for the strong frequency dependence of steady-state responses observed in young animals (**Figure 2.10C, D** *black trace*)(Telgkamp et al., 2004). The model relies on receptor saturation, and when saturation is eliminated by reducing receptor occupancy (a linear relationship between number of vesicles that fuse and the postsynaptic response, Occ = 1/10), as in the presence of TPMPA, normalized steady-state responses decreases while preserving the frequency dependence (**Figure 2.10D,** *red trace*). This situation is indistinguishable from the case where each bouton has a single vesicle docked at a single active zone (**Figure 2.10D,** *dashed line*). We also examined recovery from depression following train stimulation and found that recovery from depression following 20 Hz stimulation for the model did not match the time course of recovery we observed in older animals (**Figure 2.10E, F**). This is

Figure 2.10 (Continued)

consistent with differences in the properties of recovery from depression in young (Telgkamp and Raman, 2002) and juvenile animals.

We adapted this model to try to describe the PC-DCN synapse in older animals (**Figure 2.10G, H**). When we matched the recovery from depression to that observed in older animals, we were unable to simultaneously match the decay of the IPSC amplitude at the onset of stimulation and the steady-state amplitudes. This is shown for an occupancy of 1 for $P_{vesicle}$= 0.26 and a range of active zones per bouton (**Figure 2.10G**). This was also true when we explored a range of $P_{vesicle}$ values with N = 10 active zones per bouton (**Figure 2.10H**).

There is increasing evidence that at some synapses release may be mediated by multiple pools of vesicles (Hallermann et al., 2003, Sakaba and Neher, 2001, Lu and Trussell, 2016, Mennerick and Matthews, 1996). We therefore considered a model that includes two distinct vesicle pools with different parameters. We varied the parameters of a two-pool model across a wide range of values to determine if it was possible to reproduce the properties of the PC-DCN synapse. We found that a two-pool model with parameters in **Table 2.1** provided the best approximation of the data. This is illustrated for 10 Hz and 100 Hz trains (**Figure 2.12**). One pool (red) accounts for approximately 30% of the total readily releasable pool, has a relatively high release probability ($P_1 = 0.26$), and recovers slowly ($\tau_{R1} = 12$ s). A second pool (blue) has a low initial release probability ($P_{2\ initial} = 0.023$) that increases due to facilitation during high frequency stimulation ($P_{2\ final} = 0.058$ at 100 Hz), and rapid recovery from depression ($\tau_{R2} = 0.28$ s). Based on our experimental findings we used a linear relationship between stimulation frequency and facilitation (**Figure 2.9C, 2.9E**).

Table 2.1: Two-pool model parameters

Parameter	*Value*
N_1	0.3
N_2	0.7
P_1	0.26
P_2	0.023
τ_{R1}	12 s
τ_{R2}	0.28 s
F_1	0
F_2	0.035
τ_{F2}	0.125 s

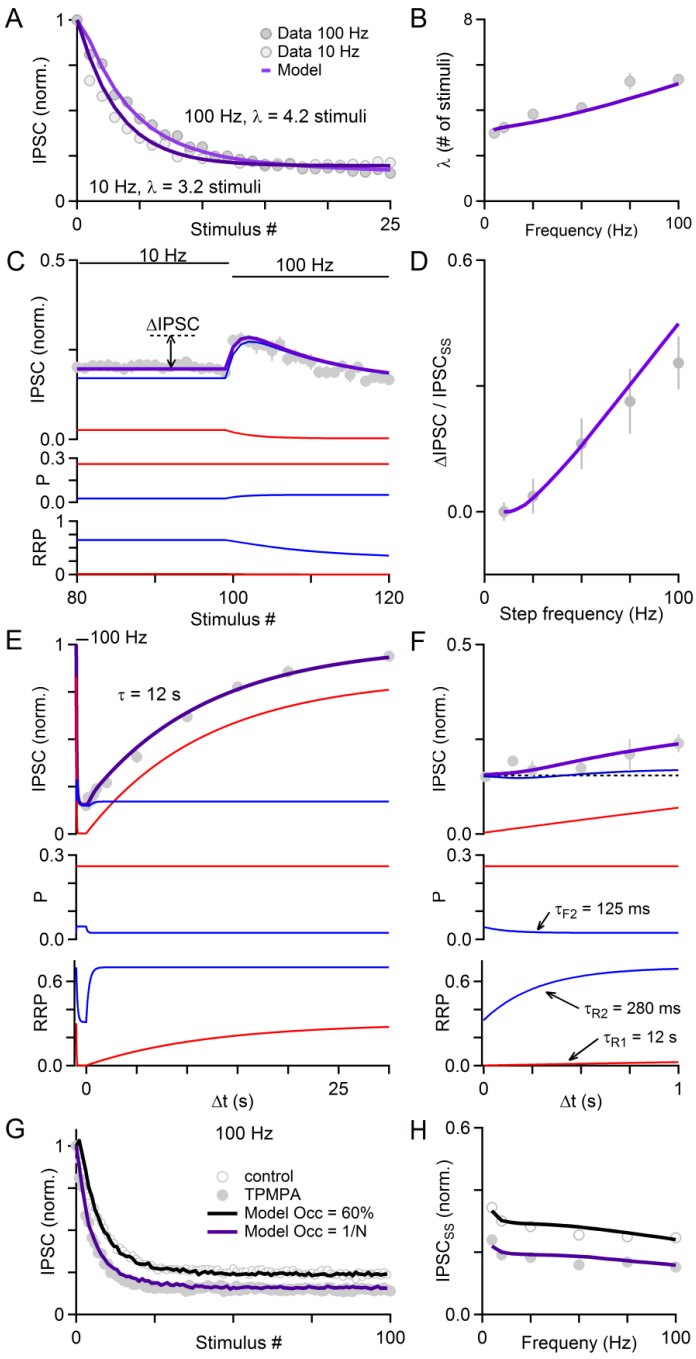

Figure 2.11: Constraining model parameters with synaptic responses measured in the presence of 2 mM TPMPA to relieve $GABA_A$ receptor saturation in P21-30 animals.

(A) Average normalized IPSCs in response to 10 and 100 Hz trains (symbols, n = 7 cells) overlaid with model responses.

Figure 2.11 (Continued)

(B) Plot of decay constant of depression as a function of frequency (filled symbols, n = 7 cells) overlaid with model predictions.

(C) IPSCs in response to a conditioning train of 10 Hz, stepped to 100 Hz with experimental data and modeled vesicle pools. Contributions of the depleting (red line) and sustaining pools (blue line) are shown along with the total response (*thick line*), which is the sum of these components.

(D) Summary of IPSC size in response to frequency steps from a 10 Hz conditioning train as shown in (C) for experimentally observed and model data (n = 5 cells). Contributions of the depleting (red line) and sustaining pools (blue line) are shown.

(E) Recovery following 100 Hz stimulation for experimentally observed and model data (n = 5 cells). Note that recovery from depression is slower in the presence of TPMPA compared to control conditions; this is expected from relieving the effects of receptor saturation as shown previously (Foster et al. 2002).

(F) Expanded axis of (E) showing recovery within the first second following the train.

(G) Average normalized IPSCs evoked by 100 Hz stimulation in 2 mM TPMPA (filled markers) and in control conditions (empty markers). Purple trace is a model by Telgkamp et al. 2004 consisting of individual boutons modified to contain two vesicle pools as in (A-F) and black trace is the model with saturation of post-synaptic receptors. An occupancy of 1/N (purple trace) corresponds to a linear relationship between the number of vesicles that fuse and the postsynaptic response, whereas for an occupancy of 0.6 (black trace) postsynaptic receptors are saturated by the release of 2 or more vesicles from the bouton.

(H) Plot of steady-state IPSC size for models and data shown in (G). All data are presented as means ± SEM.

The contribution of each pool can be illustrated by the responses to 10 Hz (**Figure 2.12A**) and 100 Hz (**Figure 2.12B**) stimulus trains. The depleting pool (red) accounts for most of the IPSC early in the stimulus trains, but it is depleted at steady-state for both 10 Hz and 100 Hz stimulation (**Figure 2.12A, B**, *red*). Consequently the depleting pool makes little contribution to the steady-state response. It is the sustaining pool that accounts for most of the steady-state synaptic response (**Figure 2.12A, B**, *blue*). For 10 Hz stimulation the sustaining pool exhibits little depletion because the initial P_2 is low, and recovery from depression is rapid. At 10 Hz, the facilitation is so low that P_2 remains roughly constant. For 100 Hz stimulation the sustaining pool also accounts for most of the steady-state responses, which is approximately the same amplitude as for 10 Hz stimulation, but it does so in a very different manner. For 100 Hz stimulation recovery from depression is not sufficiently rapid to replenish the sustaining pool and partial depletion reduces the steady-state size of the sustaining pool. Facilitation increases the steady-state probability of release, releasing additional vesicles to offset this partial depletion. Thus, it is the sustaining pool that maintains nearly frequency-independent steady-state responses (**Figure 2.12A-C**) and is responsible for the approximately linear charge transfer (**Figure 2.12D**).

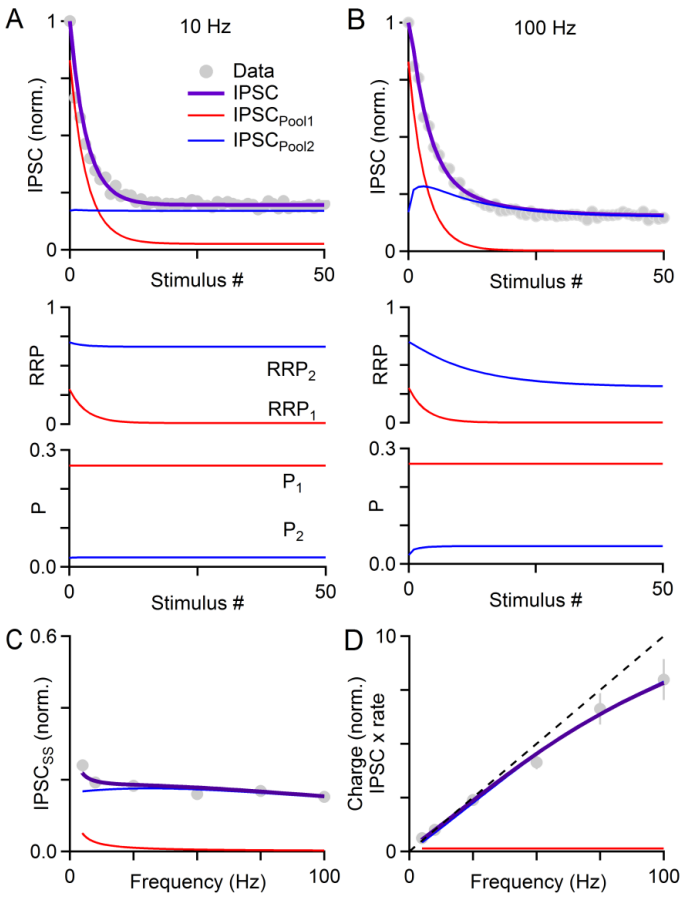

Figure 2.12: A two-pool model and facilitation are sufficient to explain the frequency-independence of PC-DCN synapses in P21-30 animals.

(A) Average IPSCs (top) in response to a 10 Hz train for experimental data in 2 mM TPMPA and two modeled vesicle pools (combined in purple). Readily releasable pool size (RRP, middle) and release probability (P, bottom) of each pool during the train.

(B) Same as (A), but with 100 Hz trains.

(C) Average steady-state IPSC size observed from data in 2 mM TPMPA (n = 7 cells) and predicted by models.

(D) Plot of charge transfer as a function of stimulation frequency for experimental data and models. Charge was calculated as the product of steady-state IPSC size and stimulation frequency and normalized to charge at 10 Hz. All data are presented as means ± SEM, error bars are occluded in some cases by markers.

The parameters for the two-pool model were constrained by many aspects of our experimental results in the presence of TPMPA. For example, the IPSC amplitude decayed more slowly as the stimulus frequency increased (**Figure 2.11A, B**). This is not readily explained by a single pool model, which predicts that the decay of IPSC amplitude (λ) is determined by the initial probability of release. The frequency dependence of λ is, however, readily accounted for by the two-pool model (**Figure 2.11A, B**). It naturally arises as a consequence of facilitation, which allows the sustaining pool to facilitate and prolong λ during 100 Hz stimulation but contribute very little to λ during 10 Hz stimulation (**Figure 2.12A, B**).

Model parameters were also constrained by experiments where the stimulus frequency was rapidly changed (**Figure 2.6**). Steps from 10-100 Hz were modeled and compared to experimental data (**Figure 2.11C, D**). The two-pool model accounted for the transient increase in IPSC amplitude. According to the model, the depleting pool is strongly depleted by prolonged 10 Hz stimulation and does not contribute to the transient increase in IPSC amplitude. In contrast, stepping from low to high frequency stimulation increased the probability of release of the sustaining pool. The increase in IPSC strength is transient even though P_2 remains elevated for the duration of high frequency stimulation, due to the depletion of the RRP.

Lastly, the recovery of the IPSC amplitude following high frequency stimulation constrained our model. The model had to account for the experimental observation that recovery from depression is well approximated by a single exponential of 12 seconds in 2 mM TPMPA (**Figure 2.11E, F**) and there is no sign of a rapidly recovering component corresponding to the sustaining pool. For 10 Hz stimulation this is expected because there is very little depletion of the quickly-replenished sustaining pool. But for 100 Hz stimulation, where depletion of the sustaining pool is more prominent, a fast component of recovery from depression would be expected. The reason such a fast component of recovery from depression is not observed is illustrated by modeling recovery following a 100 Hz train (**Figure 2.11E, F**). Although there is a rapid component of recovery from depression for the sustaining pool, this is offset by facilitation so that a rapid decrease in P_2 offsets a rapid recovery in the number of vesicles in the sustaining pool.

Although it is possible that other models could also describe our experimental findings, the two-pool model accounts for all of our experimental observations. First, it highlights the importance of having a pool with a low initial probability of release that helps to maintain transmission during sustained high-frequency activation. Second, this pool with a low initial probability of release must recover rapidly to sustain transmission during prolonged high-frequency activation. Finally, facilitation, which is more prominent at high frequencies, offsets more prominent depletion that occurs during sustained high-frequency activation, and is essential to achieving frequency-independent steady-state transmission. Although in our model the pool with the high initial probability of release does not facilitate, this is not an essential feature. It is possible that this pool is also capable of facilitation, but that when the initial probability of release is high the extent of facilitation is small and obscured by depression.

We went on to determine how PC-DCN synapses operate during physiological activity patterns recorded from an awake mouse that underwent delay eyeblink conditioning (Ohmae and Medina, 2015). Mice were trained with a 500 ms conditioning light stimulus (CS) that was accompanied by an air puff to the eye 220 ms after the onset of stimulation. PC responses were then recorded in response to the CS alone in 16 trails. The average firing rate transiently decreased from ~100 Hz to ~25 Hz, and in individual trials prolonged pauses were often followed by brief bursts (**Figure 2.13A**). We stimulated PC axons using the firing patterns obtained from individual trials (**Figure 2.13A,** bottom) and measured responses in DCN neurons. The IPSC size was remarkably constant, even after a 140 ms pause and during bursts of activity (**Figure 2.13B**). IPSC amplitudes averaged for all conditioning trains (10 ms bins) were nearly constant despite large PC firing rate modulation (**Figure 2.13C**). Consequently, the charge transfer was proportional to the firing rate (**Figure 2.13C**, bottom vs. **Figure 2.13A**, top). A plot of IPSC amplitudes as a function of the time following the preceding stimulus also showed that the instantaneous firing frequency (inverse interstimulus interval) did not alter IPSC amplitude (**Figure 2.13D**), similar to results found in vivo at the mature Calyx and endbulb of Held (Lorteije et al., 2009, Kuenzel et al., 2011b). As a result, there was a linear relationship between the charge transfer and instantaneous firing frequency (**Figure 2.13E**);

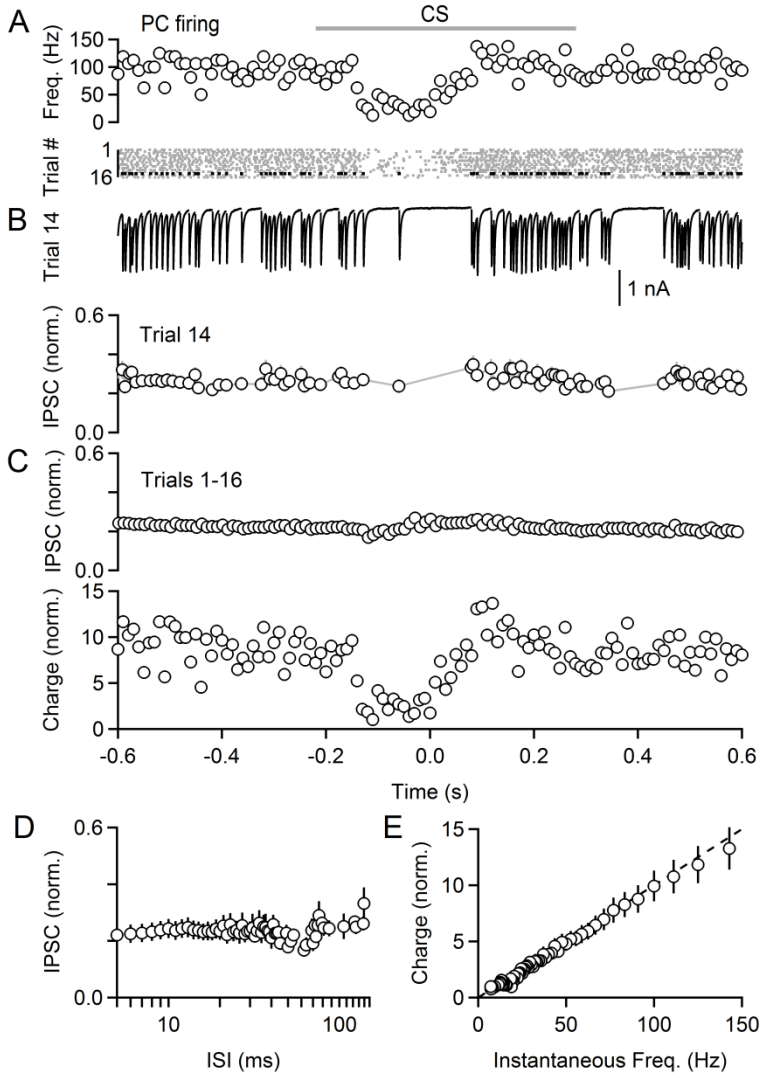

Figure 2.13: Input of a single PC to the DCN during conditioned eyeblink trains in P21-30 animals.

(A) Average firing rate (top) and individual trials (bottom) of a PC in an awake mouse that underwent delay eyeblink conditioning from Ohmae & Medina, 2015. In these trials the conditioning light stimulus alone was applied without a periocular airpuff that was present at t = 0 in acquisition trials.

(B) Top: IPSCs in a DCN neuron evoked by stimulating trial 14 followed a 50 Hz train of 25 stimuli to allow the synapse to reach steady state (not shown). Bottom*:* Average IPSC size for the stimulation pattern shown above (n = 4 cells). Responses are normalized to initial IPSC amplitude following a prolonged silent period.

Figure 2.13 (Continued)

(C) Top*:* Average IPSC size for the 16 PC trials shown in (A, bottom), in 10 ms bins. Bottom*:* Average charge transfer (product of IPSC size (C, top) shown above and PC firing rate in (A, top)). Responses are normalized to the charge transfer for 10 Hz stimulation.

(D) Average IPSC size from all trials for each interstimulus interval (ISI).

(E) Total charge transfer as a function of instantaneous firing frequency (product of IPSC size and inverse of interstimulus intervals shown in (D)). All data are presented as means ± SEM, error bars occluded in some cases by markers.

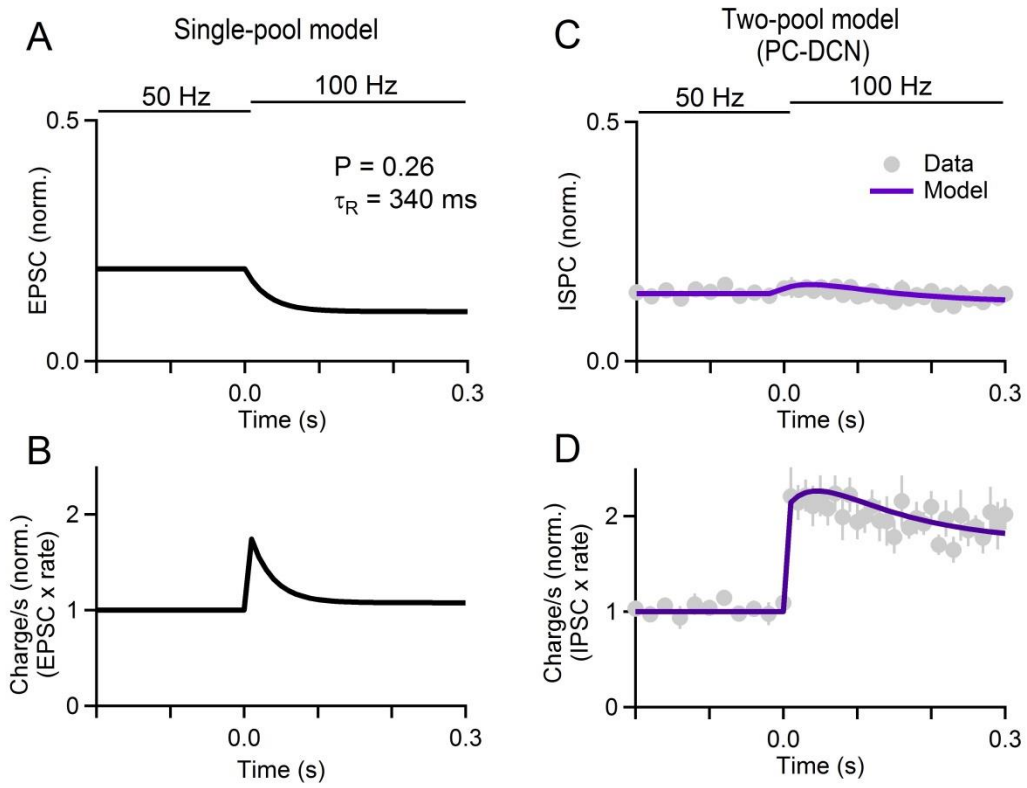

Figure 2.14: **Synaptic specializations of different depressing synapses**

(A) Average EPSCs in response to a 50 Hz conditioning train, followed by a step to 100 Hz stimulation for a single pool depletion model synapse with indicated parameters.

(B) Normalized charge transfer calculated from the stimulation protocol shown in (A).

(C) IPSC sizes in response to the same stimulation shown in (A) but using two-pool model of the PC-DCN synapse, overlaying data collected in the presence of 2 mM TPMPA in P21-30 animals (n = 7).

(D) Normalized charge transfer calculated for two-pool model and data shown in C. All data are presented as means ± SEM.

The linear relationship between charge transfer and stimulation frequency is in contrast to many depressing synapses that can efficiently encode changes in presynaptic activity (Abbott et al., 1997) rather than the absolute rate of presynaptic firing. These differences are well illustrated by step changes in frequency, which reveal very different profiles of charge transfer between typical depressing synapses and PC-DCN synapses (**Figure 2.14**). Thus, even though PC-DCN synapses depress like many other synapses, they are specialized to serve a very different role.

Discussion

Our main finding is that steady-state responses of PC-DCN synapses are invariant for a broad range of PC firing frequencies, which leads to a linear relationship between firing frequency and charge transfer. We show that this unusual synaptic property arises from a number of specializations, including a component of release that facilitates and that is well-suited to maintaining transmission during prolonged high-frequency activation.

Release at the PC-DCN synapse is linear

The properties of the PC-DCN synapse we observe are unusual in that in the 10-100 Hz stimulation range steady-state transmission is frequency-independent, and charge transfer is linearly related to PC firing frequency. This property is a feature of relatively mature PCs, as depression in young animals is dependent on stimulation frequency (Telgkamp and Raman, 2002, Kawaguchi and Sakaba, 2015). It appears that the failure of spike invasion of presynaptic boutons present in cultured synapses does not contribute significantly to depression in older animals because we do not see the strong frequency-dependent depression that is a hallmark of such a mechanism. This mechanism is also inconsistent with our observation that release is enhanced when stepping from low to high frequencies.

Frequency independent release has been observed at only a few other synapses, including vestibular synapses (Bagnall et al., 2008, McElvain et al., 2015) and possibly in the chick auditory brainstem (MacLeod et al., 2007). At most depressing synapses the extent of depression becomes more pronounced as the stimulus frequency is increased, and as a result the frequency-dependence of charge transfer is sublinear.

Important properties of the PC-DCN synapse

We find that the properties of the PC-DCN synapse arise from a number of specializations. One surprising feature is that recovery from depression is slow (τ_R 7.5 s), which appears to be incompatible with maintaining transmission during sustained high-frequency stimulation. Many synapses that sustain transmission during prolonged high-frequency activation have a fast component of recovery (Lipstein et al., 2013, Yang and Xu-Friedman, 2009). However, at PC-DCN synapses the similarity of recovery from depression following 20 Hz and 100 Hz trains indicated that recovery from depression is not accelerated at high frequencies.

Even though depression dominates the PC-DCN synapse under physiological conditions, facilitation is also present and makes important contributions. Responses to a step increase from 10 Hz to 100 Hz stimulation established that facilitation and depression coexist under physiological conditions. Our experimental results and model indicate that facilitation plays an important role in determining the properties of the PC-DCN synapse, and most importantly helps to boost steady-state responses evoked by high-frequency stimulation and thereby contribute to the frequency independence of steady-state responses.

We found that $GABA_AR$ saturation occurs at the PC-DCN synapse and strongly influences synaptic responses. Our findings using the low-affinity $GABA_AR$ antagonist TPMPA provides functional support for previous work showing that short-term depression is shaped by the saturation of postsynaptic receptors at PC-DCN synapses (Telgkamp et al., 2004). Our findings in P21-30 animals suggest that saturation at PC-DCN synapses is most prominent at the onset of stimulation following a quiescent period, when depletion is not prominent and GABA release is maximal. $GABA_AR$ saturation is not prominent at steady-state, when depletion limits GABA release. This is consistent with our finding that steady-state synaptic strength remained linear even when $GABA_AR$ saturation was prevented by TPMPA. $GABA_AR$ saturation limits the size of IPSCs evoked at the start of a stimulus train, which increases the relative size of the steady-state response compared to the initial IPSC amplitude. Frequency-dependent responses in young animals (P13-16) can be sufficiently explained by a model bouton containing many

release sites in which GABA release results in spillover and saturation of multiple release sites (Telgkamp et al., 2004, Pugh and Raman, 2005). In older animals, we found that these models could explain the effects of TPMPA (**Figure 2.11G, H**), but were unable to explain nearly frequency-invariant responses.

Two-pool model of PC-DCN synapses

The PC-DCN synapse cannot be described by a simple depletion model consisting of a single pool of vesicles, even though such a model describes depression at many other synapses (Ruiz et al., 2011, Neher and Sakaba, 2008, Thanawala and Regehr, 2013, Thanawala and Regehr, 2016a, Dittman et al., 2000). We found that a model with two pools of vesicles could account for transmission at this synapse. It was straightforward to describe the depleting pool using a depletion model with a uniform probability of release and slow recovery that was determined experimentally. The sustaining pool was more challenging to explain. The observation that responses facilitated when increasing stimulus frequencies from 10 Hz to 100 Hz suggested that this component facilitated. The observation that facilitation was short-lived suggested that this sustaining pool underwent depletion at high frequencies. This model also reconciled the apparent lack of a rapid component of recovery and the ability of the PC-DCN synapse to maintain transmission during high-frequency stimulation. This appears to be a consequence of a transient decrease in P due to deactivation of facilitation, that masks rapid recovery from depression of the sustaining pool. The importance of facilitation in offsetting depression at high frequencies is reminiscent of the synapses made by the auditory nerve in nucleus angularis of chicks (MacLeod et al., 2007). This two-component model even accounted for important details of transmission, such as the prolongation of the decay of IPSC amplitude for high-frequency stimulation. When we combined the two-pool model with existing models of PC-DCN synapses to explain the effects of receptor saturation (Telghamp et al. 2004), we were able to additionally account for the effects of TPMPA (**Figure 2.11G, H**), suggesting the two-pool model is consistent with the known ultrastructure of the synapse.

The two components of release have very different roles in transmission. The depleting component accounts for most of the synaptic current for low frequency stimulation or at the onset of high-frequency stimulus trains, whereas the sustaining component accounts for most of the steady-state synaptic currents

evoked by moderate to high-frequency stimulation. This suggests that studying persistently active synapses such as the PC-DCN synapse using prolonged high-frequency stimulation may provide insight into the forms of transmission that are likely much more important under physiological conditions.

The model we have introduced is the simplest model we could devise to account for our experimental findings, but it is possible that other models describe the PC-DCN synapse. We do not exclude more complex models, and the mechanisms involved in achieving frequency-independent release may be more complicated than in our simplified model. We ignore heterogeneity (Dobrunz and Stevens, 1997), assume that the model parameters are discrete values rather than distributions (Neher, 2015), and do not consider presynaptic calcium dynamics (Sakaba and Neher, 2001, Dittman and Regehr, 1998).

Multiple or heterogeneous pools of vesicles may more generally allow synapses to achieve a wide variety of synaptic phenotypes to efficiently suit the needs of a particular system. Multiple types of vesicle pools have been described and modeled at other synapses (Wu and Borst, 1999, Neher and Sakaba, 2001, Lu and Trussell, 2016, Wen et al., 2016, Trommershauser et al., 2003), although it is often unclear how these pools function under physiological conditions. For other synapses where depression cannot be described by a depletion model, it is possible that these synapses function using multiple or heterogeneous vesicle pools.

Functional implications of frequency-independent transmission at PC-DCN synapses

PC-DCN synapses can reliably encode the presynaptic firing of their parent PCs, but how populations of PCs control the firing of DCN neurons remains uncertain. PCs influence the activity of DCN neurons either through rate coding or by regulating the degree of synchrony of PCs (Heck et al., 2013) and it is possible that PC regulation of DCN neurons is specialized to reflect different types of computations performed in different regions. Rate coding predicts that increases in the firing rate of PCs suppress firing in DCN neurons (Walter and Khodakhah, 2009). Consistent with this model, it as has been observed that DCN firing varies inversely with PC firing during eyeblink conditioning (Jirenhed et al., 2007, Hesslow and Ivarsson, 1994, Heiney et al., 2014). Rate coding has generally been an attractive hypothesis because PC firing rates can be directly proportional to a wide range of external events

(Armstrong and Edgley, 1984b, Thach, 1970, Medina and Lisberger, 2009, De Zeeuw et al., 1995, Chen et al., 2016). We find that the PC-DCN synapse differs from many other synapses, in that frequency-independent transmission leads to linear charge transfer that could encode the absolute rate of PC firing more efficiently than typical depressing synapses. PC-DCN synapses may therefore be specialized to reliably convey the absolute rate of sustained PC firing during behaviors.

It has also been shown that the synchronized firing of multiple presynaptic PCs can time-lock the activity of DCN neurons to its inputs, whereas desynchronized PCs inhibit DCN firing (Person and Raman, 2012a, Gauck and Jaeger, 2000). Consistent with this hypothesis, the firing across populations of PC and DCN cells are not inversely related during many behaviors (McDevitt et al., 1987, Armstrong and Edgley, 1984a). Although synchronized PC firing is not widely observed, synchronized firing by adjacent PCs has been observed *in vivo* (de Solages et al., 2008). It has been proposed that PC collaterals could allow PCs to synchronize activity in narrow parasagittal bands (de Solages et al., 2008, Witter et al., 2016), making it difficult to detect synchronized PC activity. Frequency-dependent depression, as would occur at most types of synapses, would be expected to diminish strength of PC inputs, and thereby limit the efficacy of PCs to time lock DCN neurons at high frequencies. The frequency-independence of IPSC amplitude described here would avoid such a degradation of performance by preserving inhibition at high frequencies. Thus, frequency-independent synaptic strength has advantages for the PC-DCN synapse regardless of whether PCs regulate DCN firing with a rate code or by the degree of PC synchrony.

Experimental Procedures

Slice preparation: C57/BL6 mice (P21-30, other than as indicated in Figure 1) of both sexes were anesthetized with ketamine / xylazine / acepromazine and transcardially perfused with solution containing in mM: 110 Choline Cl, 2.5 KCl, 1.25 NaH_2PO_4, 25 $NaHCO_3$, 25 glucose, 0.5 $CaCl_2$, 7 $MgCl_2$, 3.1 Na Pyruvate, 11.6 Na Ascorbate, 0.002 (R)-CPP, 0.005 NBQX, oxygenated with 95% O2 / 5% CO_2, kept at 35°C. The hindbrain was removed and a cut was made down the midline of the cerebellum and brainstem. Each half of the hindbrain was glued to the slicing chamber, cut face down. Sagittal slices (250 μm) were

made using a Leica 1200S vibratome in choline ACSF maintained at 35°C. Slices were then transferred to a holding chamber with solution containing in mM: 127 NaCl, 2.5 KCl, 1.25 NaH_2PO_4, 25 $NaHCO_3$, 25 glucose, 1.5 $CaCl_2$, 1 $MgCl_2$ and allowed to recover at 35°C for at least 20 minutes before cooling to room temperature. All procedures involving animals were approved by the Harvard Medical Area Standing Committee on Animals.

Electrophysiology: Whole-cell voltage clamp recordings were obtained from large (>15 μm diameter, >100 pF) neurons in all three subnuclei of the DCN. Large cells in these nuclei have been reported to consist primarily of glutamatergic projection neurons (Bagnall et al., 2009, Uusisaari et al., 2007). We confirmed this in a subset of experiments using mice in which cells expressing the vesicular glutamate transporter VGLUT2 were labeled with TdTomato (Slc17a6-IRES-Cre;Ai14, not shown). Borosilicate electrodes (1-2 MΩ) were filled with internal solution consisting in mM of: 110 CsCl, 10 HEPES, 10 TEA-Cl, 1 $MgCl_2$, 4 $CaCl_2$, 5 EGTA, 20 Cs-BAPTA, 2 QX314, 0.2 D600, pH to 7.3 using CsOH. High concentrations of BAPTA were used to prevent long-term plasticity (Zhang and Linden, 2006, Pugh and Raman, 2006, Ouardouz and Sastry, 2000). Series resistance (1-6 MΩ) was compensated up to 80% and experiments were discarded if series resistance changed by 20%. Only the capacitance roughly equivalent to the cell body was compensated (5 pF). Cells were held at -30 or -40 mV for all experiments shown and liquid junction potentials left unsubtracted. All experiments were performed at 34-35°C in the presence of 5 μM NBQX to block AMPARs, 2.5 μM (R)-CPP to block NMDARs, 1 μM strychnine to block glycine receptors, and 1 μM CGP 55845 to block $GABA_B$Rs, with a flow rate of 3-5 ml/min.

A subset of experiments in P23-27 animals were performed with a low Cl^- internal consisting in mM of 150 K-gluconate, 3 KCl, 10 HEPES, 0.5 EGTA, 3 MgATP, 0.5 NaGTP, 5 tris-Phosphocreatine, 5 Na_2Phosphocreatine, pH to 7.2 using KOH. It was difficult to obtain high quality voltage clamp with this internal solution at a holding potential of -40 mV because active conductances were often observed. When cells were held at 0 mV with this K-based low Cl^- internal solution steady-state synaptic currents across a wide range of frequencies were similar to those observed for Cs-based high Cl^- internal used for

all other experiments. Although there was a minor difference in steady-state IPSC sizes, (0.31 ± 0.02 K-gluconate, n = 5, vs 0.25 ± 0.03 CsCl, n = 8, at 100 Hz), the degree of frequency-invariance was similar (ratio of steady-state IPSC sizes evoked by 10 and 100 Hz were 1.29 ± 0.06 gluconate vs. 1.21 ± 0.05 CsCl). We also observed similar decay constants of 100 Hz trains trains (λ = 8.29 ± 0.52 in K-gluconate vs λ = 8.53 ± 0.55 in CsCl). IPSC kinetics during 100 Hz trains were also similar (decay time constant τ_{IPSC50} = 1.88 ± 0.16 ms for K-gluconate and τ_{IPSC1} = 2.40 ± 0.10 ms and τ_{IPSC50} = 1.78 ± 0.06 ms for CsCl vs τ_{IPSC1} = 2.37 ± 0.06 ms).

Previous studies have reported that synaptic responses at the PC-DCN synapses exhibit sex differences in some synaptic properties (Mercer et al., 2016). We therefore compared synaptic properties in males and females. In general, the number of experiments for either sex for a given experiment was quite small, so the statistical power of this comparison was limited. We performed a large number of experiments with 100 Hz trains, which allowed a quantitative comparison of the responses. The IPSC decay time of the first and the fiftieth stimuli were, respectively, 2.47 ± 0.13 ms and 1.81 ± 0.07 for males (n = 29) and 2.27 ± 0.11 ms and 1.69 ± 0.09 for females (n = 15). The steady-state phasic currents for 100 Hz trains were 0.242 ± 0.012 for males and 0.255 ± 0.014 for females. A previous study found that mGluR1/5 receptors can contribute a tonic current during stimulus trains (Mercer et al., 2016), but no large residual currents were evoked in the presence of 5 μM gabazine (data not shown), indicating that under our experimental conditions mGluR1/5 receptors do not contribute to responses during high frequency stimulation.

For experiments using the low-affinity $GABA_AR$ antagonist TPMPA, the total circulation volume of ACSF was reduced to 10 mL to achieve high concentrations of TPMPA. TPMPA can act as a low-affinity agonist of $GABA_BRs$ (Ragozzino et al., 1996), but we found this was prevented by the presence of the $GABA_BR$ antagonist CGP 55845 (data not shown).

Analysis: Recordings were collected using a Multiclamp 700B (Molecular Devices), sampled at 20 kHz and filtered at 4 kHz. All data were collected in Igor Pro (Wavemetrics) and analyzed using custom-

written scripts in Matlab (Mathworks). Stimulus artifacts were blanked for clarity for all figures. All data are presented as means ± SEM unless otherwise indicated.

IPSC amplitudes during trains were measured from averaged traces as the peak evoked current, with a baseline measured 2 ms before stimulus onset. During high frequency trains, IPSCs did not fully decay before subsequent stimuli. Baselines in this case were measured by extrapolating a single exponential fit from the previous IPSC. The steady-state was measured as the average IPSC size of the 50^{th} to the 70^{th} stimuli. For experiments in which IPSCs were small due to low Ca_e or the wash in of the low-affinity $GABA_A$ receptor antagonist TPMPA, 5 μM SR-95531 was washed in at the end of the experiment and the resulting trace was subtracted to remove stimulus artifacts. In cases when this could not be done, averaged traces of stimulus artifacts that failed to evoke an IPSC were instead used for subtraction. Charge transfer was calculated as the product of steady-state IPSC size and stimulation frequency, and was then normalized to the charge transfer of 10 Hz stimulation.

For physiological trains shown in **Figure 2.13**, raw spike train times from Ohmae & Medina 2015 were used to drive stimulation. The 16 PC firing trials shown in the raster of **Figure 2.13A** were used in the order presented. For each PC firing trial, a 50 Hz train of 25 stimuli preceded the PC firing train, and this was repeated 5 times. Responses to individual PC firing trials were then averaged to obtain an average trace for each PC trial for one cell. The IPSC amplitude was then averaged across cells. To compare to PC firing, IPSC amplitudes across all PC firing trials were binned (10 ms) and averaged. Charge in **Figure 2.13C** was calculated by multiplying the PC firing rate and binned averaged IPSC amplitudes, then normalized to the charge transfer of 100 ms interstimulus intervals. In **Figure 2.13D** IPSC amplitudes for each interstimulus interval across trials were averaged. These IPSC amplitudes were then multiplied by the instantaneous stimulation rate (inverse of interstimulus intervals), and normalized to the charge at 100 ms interstimulus intervals (10 Hz), yielding the charge shown in **Figure 2.13E**.

Single pool model: The model shown in **Figure 2.5** has been introduced previously (Thanawala and Regehr, 2016a, Thanawala and Regehr, 2013). The single pool model contains two free parameters: P, the uniform

release probability for all vesicles, and the time constant of vesicle replenishment τ_R, which was later constrained by data shown in **Figure 2.4** (N, the number of release sites was normalized to 1). The outputs of the model are IPSC amplitudes as a function of stimulus number *i* for a constant stimulation frequency ($IPSC_i$). Simulations were performed for many combinations of parameters with N set to 1 and P varied logarithmically from 0.001 to 1 with τ_R set to 7.5 s.

For analyzing IPSC trains, each IPSC train for a single set of parameters was normalized by the initial IPSC in the train, constraining N for the single pool model to 1. A single exponential fit was then applied to each train, and the resulting decay time constant and Y-offset were used as measures of the decay of depression (λ) and steady-state IPSC size ($IPSC_{SS}$), respectively.

In order to incorporate facilitation for more advanced models, we introduced an additional parameter F. On the ith stimulus, a constant value F was added to P with an exponential onset of two stimuli, which was determined experimentally (**Figure 2.7**). The magnitude of facilitation was linearly related to frequency, with maximal facilitation at 100 Hz.

Two-pool model: The two pool model contained two single pool models that were added together, resulting in seven parameters: N_1/N_2, P_1, P_2, τ_{R1}, τ_{R2} and F_2, and τ_{F2}. These parameters were constrained by experiments performed in the presence of TPMPA. τ_{R1} was the recovery time constant of 12 seconds in TPMPA (**Figure 2.11**), and due to this slow recovery the effects of facilitation in pool 1 was always negligible and therefore as a simplification pool 1 was assumed not to facilitate. We assumed a linear relationship between short-term facilitation and stimulus frequency based on experimentally observed facilitation in 0.5 and 1.5 mM Ca_e. The amplitude of facilitation (F_2) was determined from the facilitation observed in frequency jump experiments (**Figure 2.6**). τ_{F2}, the decay of facilitation following trains (**Figure 2.11E, F**) was a free parameter. Simulations were systematically performed for many combinations of parameters to constrain the free parameters (N_1/N_2, P_1, P_2, τ_{R2}, τ_{F2}). Simulations were initially compared to responses evoked by100 Hz trains, then to trains evoked by 10 Hz to 100 Hz stimulation, and then F_2 and τ_{R2} were adjusted to reproduce the 10-100 Hz step protocol shown in **Figure 2.11**. Experiments shown in **Figure 2.10** and **Figure 2.11** were used to constrain all parameters.

Saturation & spillover models: The model of Telgkamp et al. 2004 was used to consider the effects of spillover and receptor saturation (**Figure 2.8**). Briefly, this model simulates N individual release sites per bouton with a uniform probability of release ($P_{vesicle}$). Release from any site results in activation of all post-synaptic sites with some occupancy of post-synaptic receptors (Occ). The post-synaptic response of the bouton is calculated as the product of receptor occupancy and the number of released vesicles with a maximal post-synaptic response of the bouton set to 1. For the saturating case, a single vesicle reaches all post-synaptic sites with occupancy of 1. In the non-saturating case, a single vesicle reaches all post-synaptic sites with occupancy of 1/N, resulting in a linear relationship between the number of vesicles released and the postsynaptic response. After each iteration, vesicles were replenished with two equally weighted time-constants as in Telgkamp et al. 2004 τ_{fast} = 150 ms at 100 Hz and τ_{fast} = 600 ms at 10 Hz; τ_{slow} = 15 s). Because these parameters assumed different replenishment rates at 10 and 100 Hz, the fast component of replenishment at intermediate frequencies was varied linearly between 10 and 100 Hz. For **Figure 2.10G**, we used model parameters that were better constrained by our experimental data from juvenile (P21-30) animals.

In order to determine the role of saturation in a two-pool model in **Figure 2.10G-H**, two versions of the Telgkamp et al. 2004 model were run, each representing a different pool of vesicles with properties shown in **Table 2.1**; all boutons contained 10 release sites. The two groups of boutons were then averaged together at the ratio of the two pools. The pools were separated into groups of boutons for convenience, and similar results were obtained if pools were mixed within boutons. To model the data in the presence of low-affinity antagonist, the occupancy of both pools was set to 1/N, which is functionally equivalent to the two-pool model described above except that it simulates individual release sites. The occupancy was then varied in order to fit data observed in control conditions. Simulations modeling boutons were averaged across 1,000 boutons. All simulations were run in Matlab.

Chapter 3

Synaptotagmin 7 confers frequency invariance onto specialized depressing synapses

Josef Turecek, Skyler L. Jackman, Wade G. Regehr

Nature, *551*(7681).

Contributions

J.T., S.J. and W.R. designed experiments. J.T. and S.J. performed electrophysiology. J.T. performed stereotaxic surgeries, immunohistochemistry and simulations. J.T. S.J. and W.R. wrote the manuscript.

Abstract

At most synapses in the brain, short-term plasticity dynamically modulates synaptic strength. Rapid frequency-dependent changes in synaptic strength play critical roles in sensory adaptation, gain control and many other neural computations (Abbott et al., 1997, Abbott and Regehr, 2004). However, some auditory, vestibular and cerebellar synapses maintain constant strength over a wide range of firing frequencies(MacLeod et al., 2007, Bagnall et al., 2008, Turecek et al., 2016b), and as a result efficiently encode firing rates. Despite its apparent simplicity, frequency-invariant transmission is difficult to achieve because of inherent synaptic nonlinearities (Zucker and Regehr, 2002a). Here we study frequency-invariant transmission at Purkinje cell to deep cerebellar nuclear (PC to DCN) synapses and vestibular synapses. Prolonged activation of these synapses leads to initial depression, which is followed by steady-state responses that are frequency invariant for their physiological activity range. We find that Synaptotagmin 7 (Syt7), a recently identified calcium sensor for short-term facilitation (Jackman et al., 2016), is present at both synapses. It was unclear why a sensor for facilitation would be present at these and other depressing synapses. We find that at PC and vestibular synapses, Syt7 supports a hidden component of facilitation that can be unmasked in wildtype animals but is absent in Syt7 knockout animals. In wildtype mice, facilitation increases with firing frequency and counteracts depression to produce frequency-invariant transmission. In Syt7 knockout mice, PC and vestibular synapses exhibit conventional use-dependent depression, weakening to a greater extent as the firing frequency is increased. Presynaptic rescue of Syt7 expression restores both facilitation and frequency-invariant transmission. Our

results identify a function for Syt7 at synapses that exhibit overall depression, and demonstrate that facilitation plays an unexpected and important role in producing frequency-invariant transmission.

Results

A primary challenge to maintaining constant synaptic strength is that during high frequency presynaptic activation there is little time to replenish vesicles, and synaptic strength decreases as vesicle depletion becomes more severe (**Figure 3.1a,b**). Consequently, many synapses depress to a greater extent as activation frequencies increase (Cook et al., 2003, Galarreta and Hestrin, 1998, Brenowitz et al., 1998). This property can be used computationally as a dynamic gain control mechanism(Abbott et al., 1997). Despite the challenges posed by vesicle depletion, some synapses faithfully transmit across a wide range of activation frequencies (MacLeod et al., 2007, Bagnall et al., 2008, Turecek et al., 2016b) (**Figure 3.1c-f**). In the vestibular system, such frequency-invariant transmission effectively conveys the absolute firing rate of vestibular afferents, and contributes to the linearity of occulomotor reflexes (Bagnall et al., 2008). Several mechanisms have been proposed to explain how synapses could maintain frequency-invariant transmission (McElvain et al., 2015, MacLeod et al., 2007, Turecek et al., 2016b), but the molecular tools to address these models directly have remained elusive. Here we test the hypothesis that facilitation, a short-lived increase in the probability of release (P_R), counteracts vesicle depletion to produce frequency-invariant transmission (**Figure 3.1d**). We take advantage of the recent finding that genetic knockout of the slow Synaptotagmin isoform Syt7 selectively eliminates facilitation at some synapses (Jackman et al., 2016).

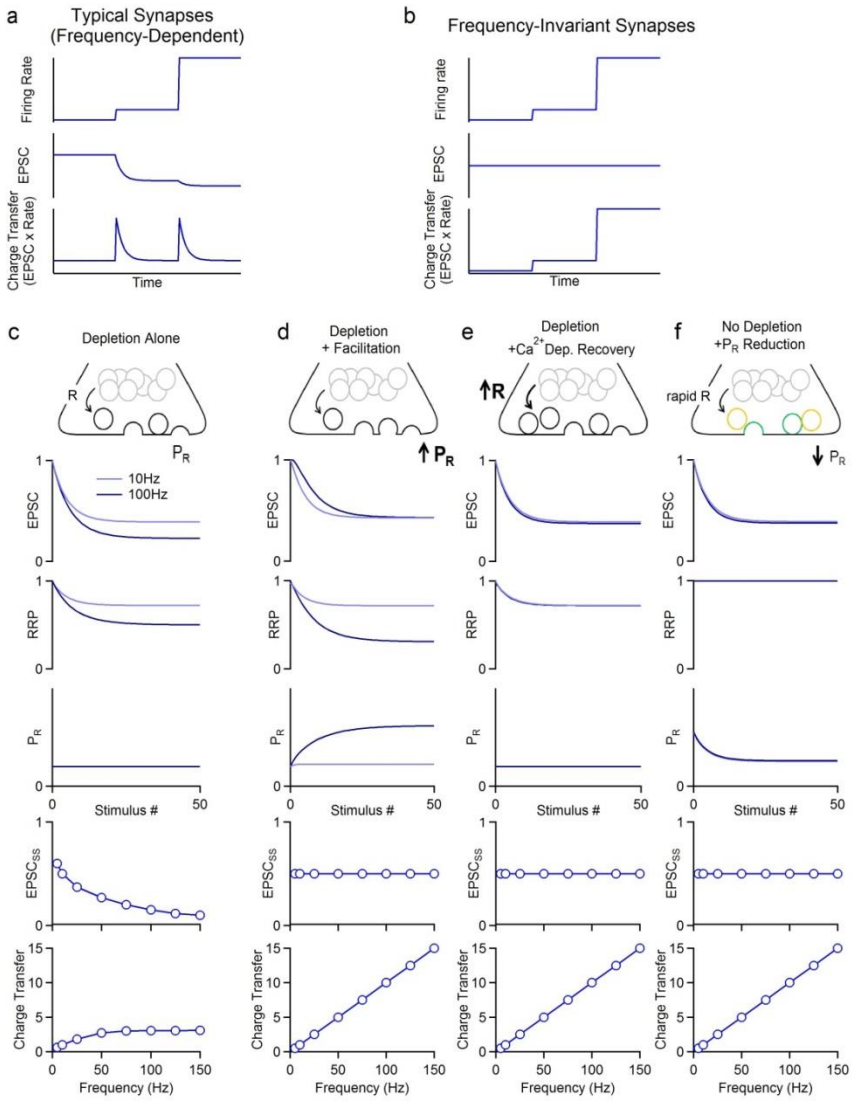

Figure 3.1: Functions and possible mechanisms of frequency-invariant synapses.

Short-term plasticity at synapses can be tuned to perform different computations.

a, Many synapses in the brain undergo short-term depression that is use-dependent: elevations in presynaptic firing rate (top) result in more profound depression of post-synaptic currents (EPSCs, middle). The charge transfer that ultimately drives post-synaptic firing rapidly increases with presynaptic firing, but short-term depression of the synapse reduces charge transfer back to a similar steady-state. Thus, short-term depression is suited to convey temporal information about changes in presynaptic firing.

b, Some synapses maintain constant synapse strength across firing frequencies (top, middle). Charge transfer at these synapses therefore can reliably reflect the absolute rate of presynaptic firing.

Figure 3.1 (Continued)

c, Typical depressing synapses can be well-approximated by intrinsic synaptic properties alone. Synapses have a limited number of vesicles in the readily releasable pool (RRP). High frequency presynaptic activity depletes the RRP until it can be replenished at some rate (R). Less recovery occurs as the interval between stimuli is reduced, thereby leading to an increase in depletion during high frequency stimulation.

d-f, Other synaptic features must operate in order to generate frequency-invariant synapses, and several possibilities have been proposed.

d, One way of making transmission frequency-invariant would be to balance depletion with facilitation(Turecek et al., 2016b, MacLeod et al., 2007) (Extended Data Figure 9). Activating a mechanism of short-term facilitation with high-frequency stimulation increases P_R, releasing more vesicles from the RRP. The increase in release results in steady-state transmission that is consistent across the physiological firing range.

e, Another way of generating a frequency-invariant synapse is to have a rapid, calcium-dependent increase in R(Sakaba and Neher, 2001, Dittman and Regehr, 1998, Stevens and Wesseling, 1998, Wang and Kaczmarek, 1998, Yang and Xu-Friedman, 2009). When the presynaptic frequency is elevated, presynaptic calcium and the rate of replenishment are increased to maintain the same RRP size regardless of activation frequency. However, this cannot explain the frequency invariance of PC and vestibular synapses, where recovery from depression is insensitive to stimulation frequency in juvenile animals(Turecek et al., 2016b, McElvain et al., 2010).

f, A model proposed by McElvain et al.(McElvain et al., 2010) proposes that each release site can hold two vesicles, but only one can be released per stimulus (green: releasable, orange: non-releasable). Vesicle replenishment to each release site is very rapid, and release is limited by decrease in P_R. Decreases in P_R are independent of stimulation frequency. The high replenishment rate and additional vesicle per release site results in very little vesicle depletion, and responses are instead shaped by decreases in P_R that are constant across frequencies. Another possibility is that a synapse could have very low P_R to limit vesicle depletion at each release site, but still maintain synaptic strength by having a very

Figure 3.1 (Continued)

large number of release sites (not shown). However, such a mechanism would require an extremely large number of release sites, and is inconsistent with the depression present at PC and vestibular synapses. Finally, post-synaptic mechanisms of short-term plasticity, such as receptor saturation and desensitization, could also contribute to frequency-invariant transmission (not shown). These mechanisms are unlikely to contribute to frequency-invariance at PC and vestibular synapses because frequency-independent transmission is unaltered when saturation and desensitization are minimized by competitive low-affinity postsynaptic receptor antagonists(Bagnall et al., 2008, Turecek et al., 2016b).

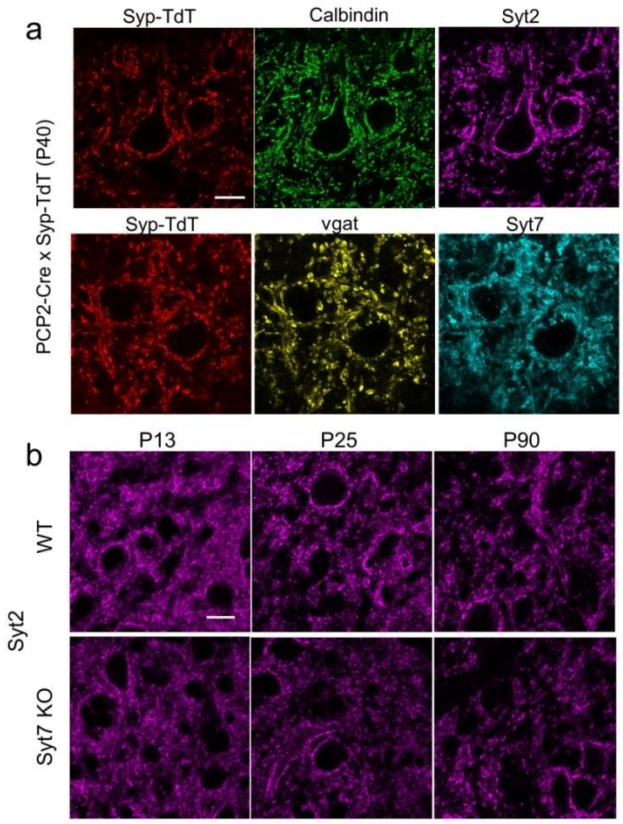

Figure 3.2: Expression and localization of synaptic proteins to PC synapses in the DCN.

To determine whether Syt7 was present in PC synapses in the DCN, we compared immunohistochemical labeling in mice expressing synaptophysin-TdTomato (Syp-TdT) specifically in PCs (PCP2-Cre x Syp-TdT).

a, Syp-TdT could be observed in boutons surrounding neurons in the DCN (upper left). Immunolabeling of Calbindin could be seen in both PC boutons labeled with Syp-TdT, and throughout the length of PC axons traversing the DCN (upper middle). Syt2 was also highly expressed in PC boutons, with most Syt2 puncta co-localizing with Syp-TdT (upper right). We found that the vast majority of inhibitory synapses labeled by VGAT were syp-TdT positive, suggesting that most inhibitory input to the DCN arises from PCs (lower middle). Syt7 was also prominent in PC boutons labeled by Syp-TdT, but with less punctate expression compared to Syt2 or VGAT. Scale bar, 15 μm.

b, The expression of Syt2 was stable across development, and showed no prominent differences in intensity between wildtypes and Syt7 knockouts. Scale bar, 20 μm.

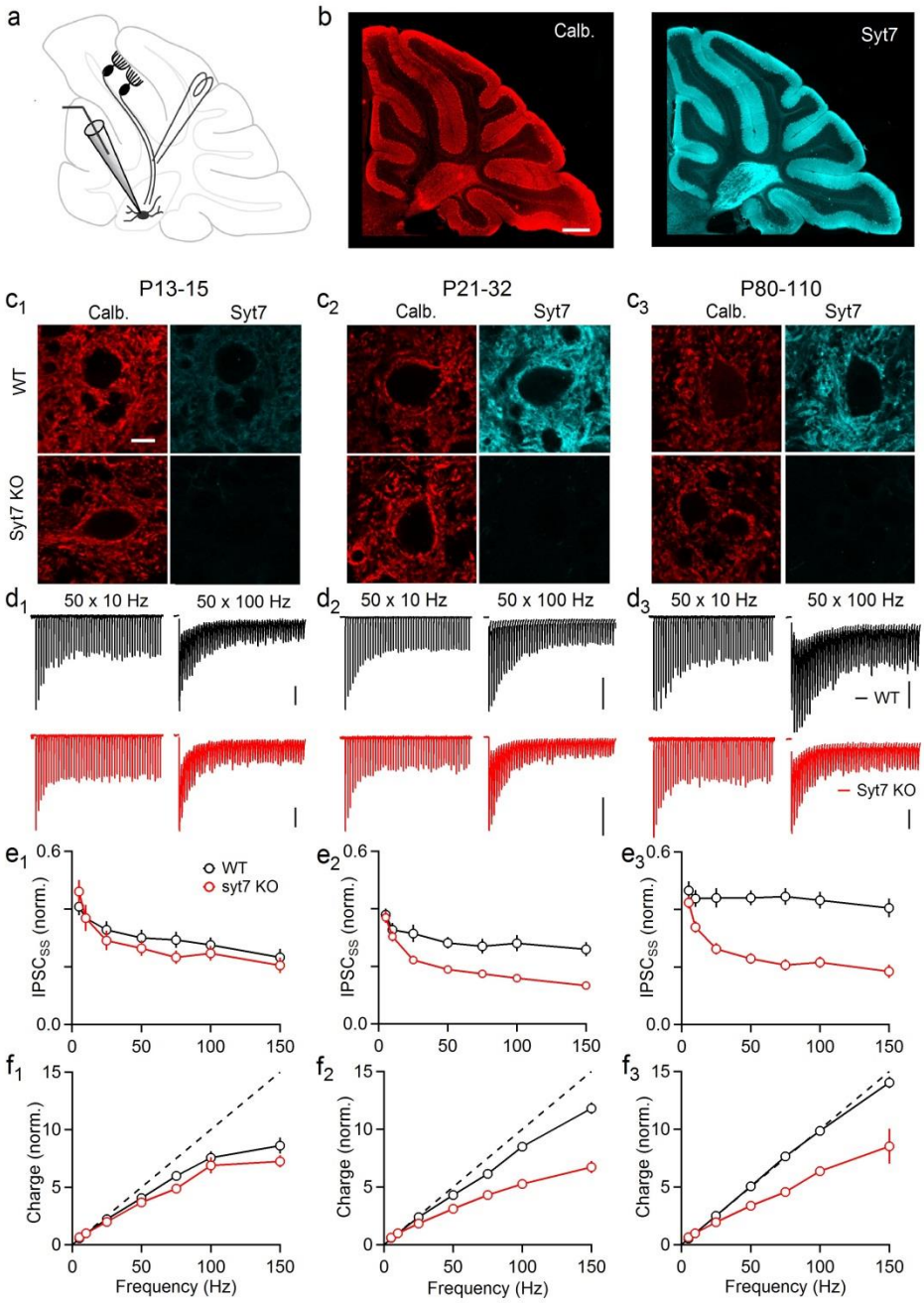

Figure 3.3: Syt7 is required for frequency-invariant transmission at PC to DCN synapses. **a**, PC axons were stimulated and responses were recorded from DCN projection neurons.

b, Sagittal cerebellum from a P25 wildtype mouse immunolabeled for Calbindin and Syt7. Scalebar, 0.5 mm.

Figure 3.3 (Continued)

c, High-power images of the DCN immunolabeled for Calbindin and Syt7 shown for young (**c_1**, P13-15), juvenile (**c_2**, P21-32), and adult (**c_3**, P80-110) wildtype and Syt7 knockouts. Scalebar, 10 μm**.**

d, Representative IPSCs for wildtype (black) and Syt7 knockouts (red). Vertical scalebars, 1 nA. **e**, Normalized steady-state amplitudes ($IPSC_{SS}$) as a function of stimulation frequency for young (**e_1**), juveniles (**e_2**) and adults (**e_3**).

f, Charge transfer calculated as the product of $IPSC_{SS}$ amplitude and stimulation frequency for young (**f_1**), juveniles (**f_2**) and adults (**f_3**). Data are mean ± s.e.m.

We began by studying synapses made by Purkinje cells (PCs), the sole output of the cerebellar cortex that fire spontaneously at 10 to 120 Hz in vivo (Zhou et al., 2014). PCs form GABAergic synapses in the deep cerebellar nuclei (DCN, **Figure 3.3a**), and express Syt7 (**Figure 3.3**). The presence of Syt7 was intriguing because unlike many synapses with prominent Syt7 expression, PC to DCN synapses depress. We found that Syt7 expression at PC to DCN synapses is age dependent, which is not the case for the PC marker Calbindin and Syt2 (**Figure 3.2**). The onset of Syt7 expression is correlated with the development of frequency-invariant transmission at PC to DCN synapses (**Figure 3.3c-f** and **Figure 3.4-3.5**). In young animals Syt7 expression is low, and steady-state transmission is frequency-dependent in both wildtype and Syt7 knockouts (**Figure 3.3c$_1$-e$_1$**). Syt7 expression increases in juvenile wildtype animals, and transmission becomes more frequency-invariant with age. However, in juvenile Syt7 knockouts frequency-invariant transmission does not develop (**Figure 3.3c$_2$-e$_2$**). The differences between wildtypes and knockouts become more pronounced in adults (**Figure 3.3c$_3$-e$_3$**). As a consequence, synaptic charge transfer, the product of IPSC amplitude and activation frequency, becomes more linear during development in wildtype animals, but remains sublinear in Syt7 knockouts (**Figure 3.3f)**. These findings indicate that Syt7 is required for frequency-invariant transmission at PC to DCN synapses.

To determine what caused the loss off frequency-invariant transmission in Syt7 knockouts, we examined recovery from depression, the initial release probability (P_R), and facilitation. It has been shown that Syt7 mediates rapid calcium-dependent recovery from depression in cultured hippocampal synapses (Liu et al., 2014). One possibility is that Syt7 contributes to frequency-independent transmission by accelerating recovery from depression during high-frequency activity (**Figure 3.1e**). Recovery from depression would then be faster in wildtype animals than in Syt7 knockout animals, but this was not the case (**Figure 3.6**). Syt7 also mediates asynchronous release during high-frequency stimulation at some synapses (Wen et al., 2010, Luo and Sudhof, 2017), but asynchronous release is not prominent at PC to DCN synapses (**Figure 3.7**).

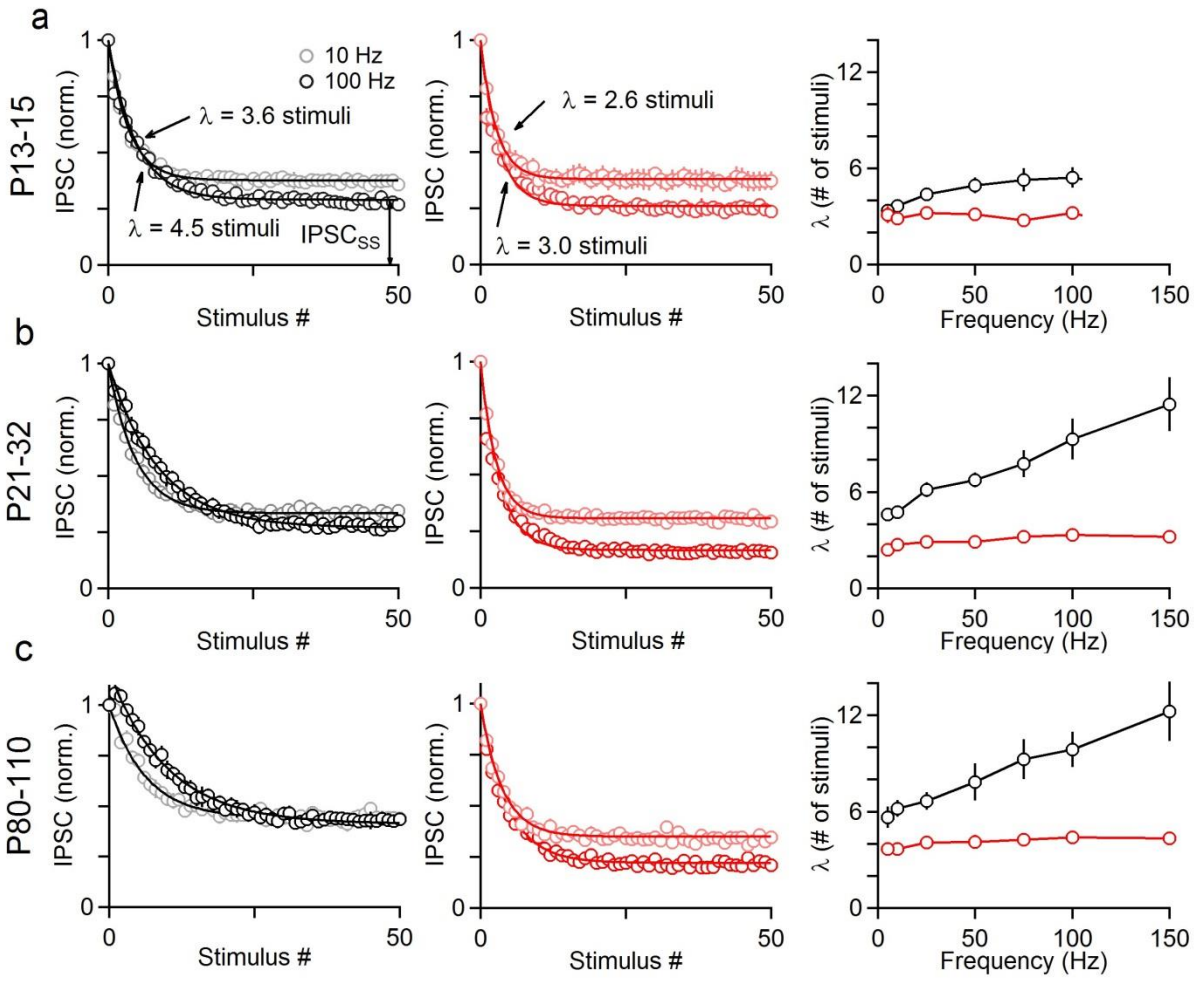

Figure 3.4: Alterations in short-term depression at PC to DCN synapses in Syt7 knockout mice are consistent with the predicted consequences of eliminating facilitation. High frequency stimulation of the PC to DCN synapse leads to depressing IPSCs that can be approximated by the equation IPSC = $IPSC_{SS} + (1- IPSC_{SS})e^{-S/\lambda}$, where S is the stimulus number, $IPSC_{SS}$ is the steady-state IPSC amplitude, and λ is exponential decay constant.

a, Average normalized IPSC amplitude for 10 and 100 Hz trains and fits in P13-15 wildtype (left) and Syt7 knockout (middle) mice. λ is plotted as a function of stimulation frequency (right).

b, Same as in (**a**), but for P21-32 animals.

c, Same as (**a**), but for P80-110 animals. According to a model of the PC to DCN synapse depression and facilitation are both present, but depletion of the readily releasable pool dominates and leads to depression

Figure 3.4 (Continued)

during high frequency stimulation(Turecek et al., 2016b). In wildtype animals λ is prolonged in a frequency-dependent manner, and it has been hypothesized that this arises from short-term facilitation that is more prominent as the stimulus frequency is increased. In young animals when Syt7 expression is low (Figure 1c), λ is weakly modulated by stimulation frequency. The prolongation of λ is more prominent in juveniles and adults. In the absence of Syt7, λ is not frequency dependent at any age. These observations are consistent with an age-dependent increase in Syt7 expression in wildtype animals leading to an age-dependent increase in facilitation, which in turn leads to age-dependent increases in the frequency dependence of λ. Data are mean ± s.e.m.

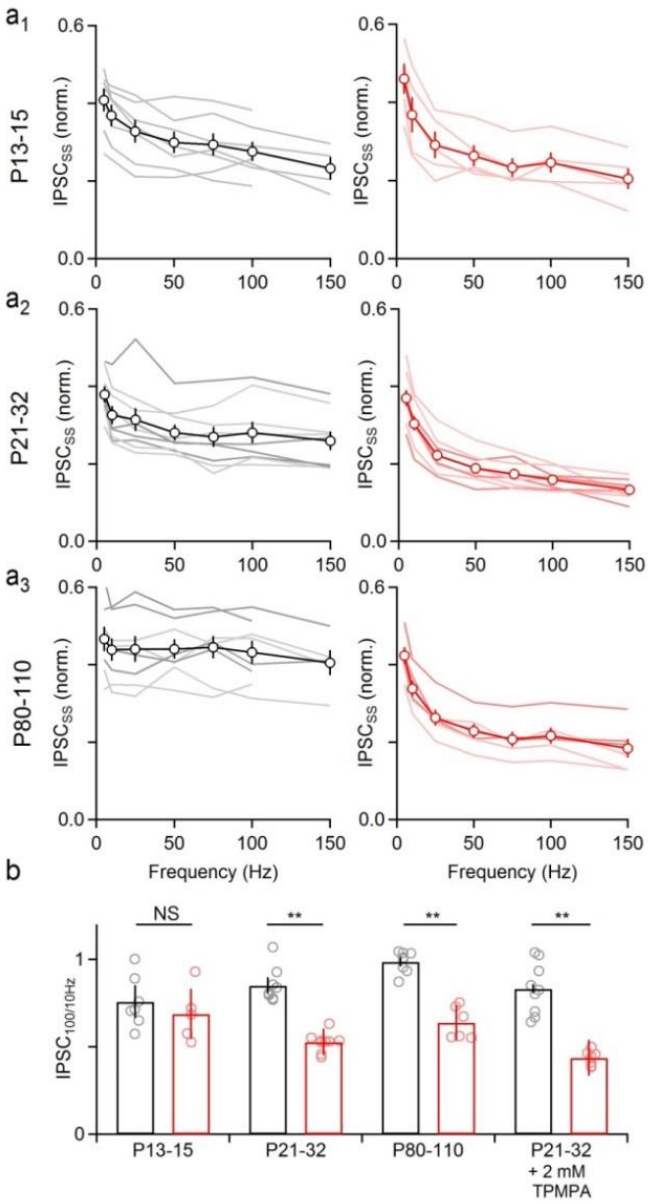

Figure 3.5: The frequency dependence of synaptic strength is consistent for different cells for a given age and genotype.

a_{1-3}, The steady-state IPSC amplitude as a function of frequency for each cell analyzed (thin lines) and averages (markers) for each genotype and age. Normalized steady-state IPSC amplitude across frequencies are plotted for wildtypes (left) and Syt7 knockouts (right) for P13-15 (**a_1**), P21-32 (**a_2**), and P80-110 (**a_3**) animals.

Figure 3.5 (Continued)

b, Ratio of the steady-state IPSC amplitudes at 100 Hz divided by steady-state amplitudes at 10 Hz is summarized for different ages of wildtype and Syt7 knockouts, and in P21-32 animals in the presence of the low-affinity $GABA_AR$ antagonist TPMPA (2 mM, far right). Data from young animals is consistent with previous reports(Telgkamp and Raman, 2002, Telgkamp et al., 2004, Turecek et al., 2016b). **$p < 0.01$, unpaired two-tailed Student's t-test. Data are mean ± s.e.m.

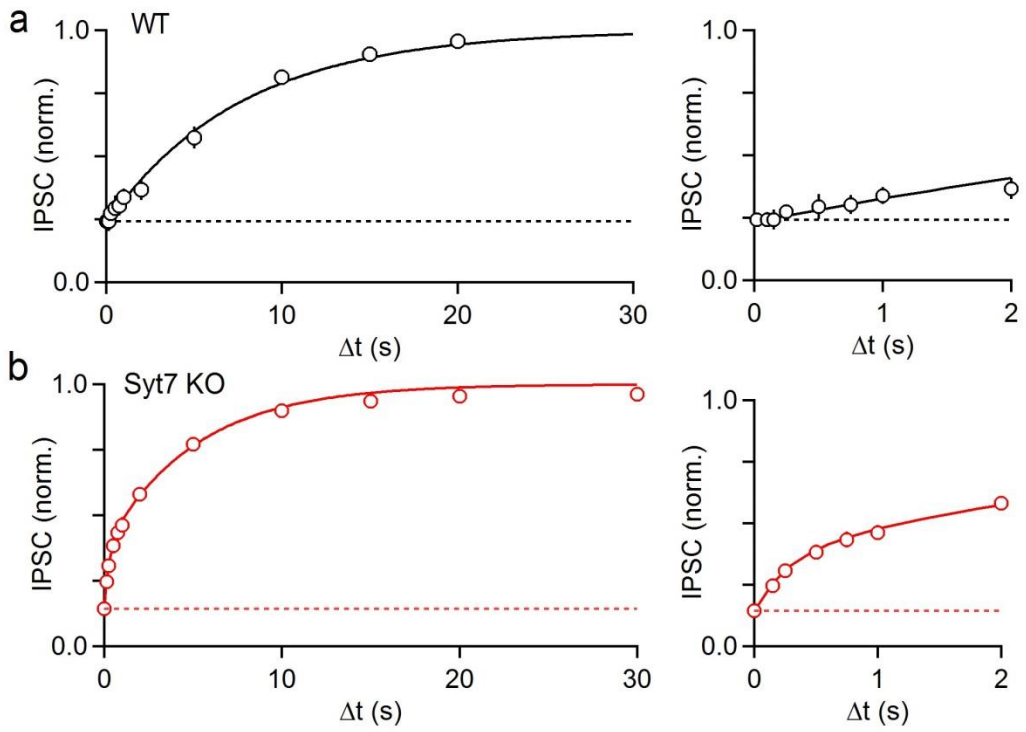

Figure 3.6: Altered recovery from depression in Syt7 knockout mice cannot account for the loss of frequency invariance at the PC to DCN synapse in Syt7 knockout mice (P21-32).

It has been shown previously that the loss of Syt7 in hippocampal cultures slows recovery from depression(Liu et al., 2014). If recovery from depression was slower in Syt7 knockouts, it could partially explain the reduction of sustained transmission at high frequencies. We therefore examined recovery from depression at PC to DCN synapses. One hundred stimuli at 100 Hz was followed by a single stimulus after an interval. This was repeated for many trials and a range of time intervals. Experiments were performed in wildtype (**a**) and Syt7 knockout (**b**) animals.

a, PC to DCN synapses recovered slowly with a single exponential of 7.7 s (left).

b, In Syt7 knockout mice recovery could not be approximated by a single exponential but was well approximated by a double exponential with time constants of 280 ms and 5.1 s. These findings indicate that a slowed recovery from depression does not occur in Syt7 knockout animals and thus does not contribute to the reduced steady-state responses in Syt7 knockout animals. The rapid time constant of recovery from depression that is apparent in Syt7 knockout animals is consistent with the prediction of a

Figure 3.6 (Continued)

model of the PC to DCN synapse in which the decay of facilitation obscures this rapid phase of recovery in wildtype animals (Turecek et al., 2016b) (Figure 3.13). The role of Syt7 in recovery from depression at the PC to DCN synapse differs from cultured hippocampal synapses where calcium dependent recovery from depression relies on Syt7, and recovery from depression is slowed in the absence of Syt7(Liu et al., 2014). Data are mean ± s.e.m.

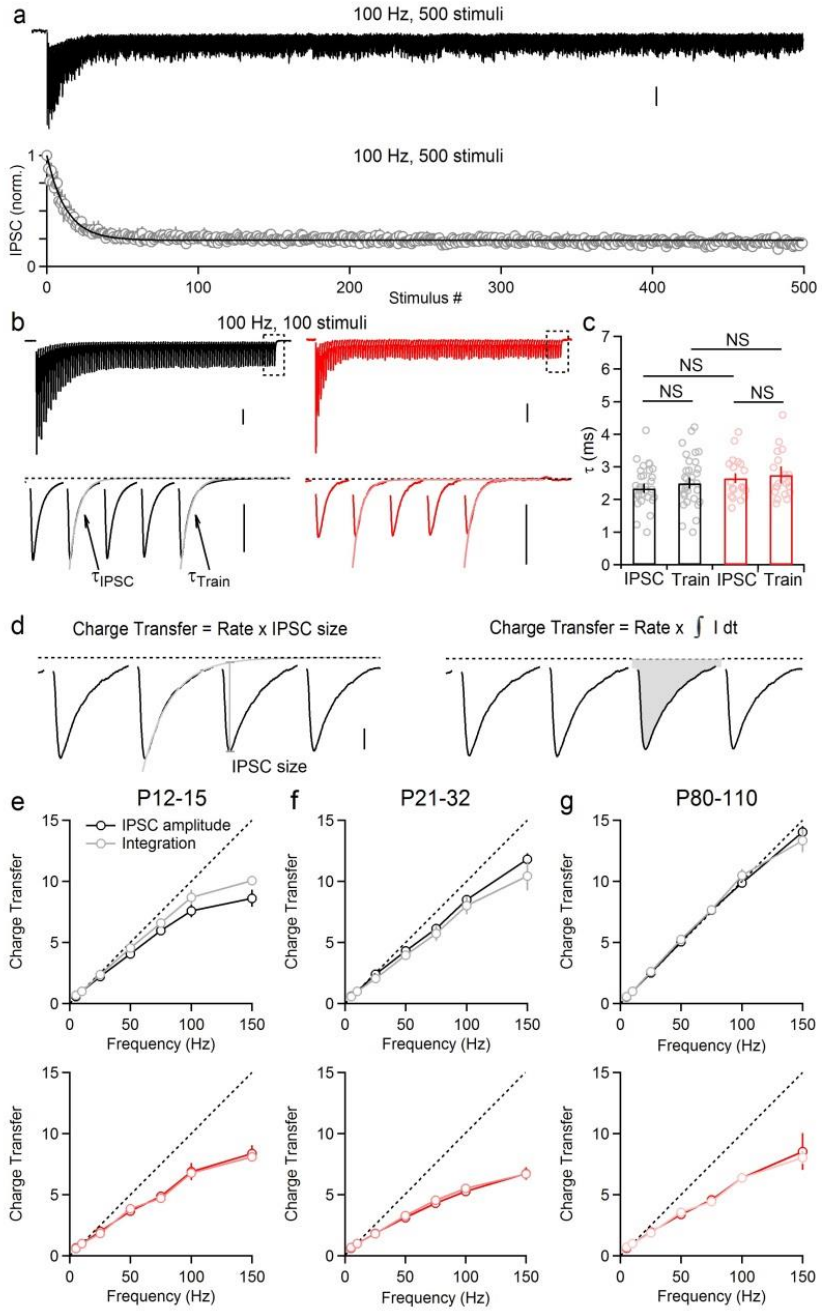

Figure 3.7: Release from PCs to DCN neurons is sustained, fast and synchronous. a, PCs fire at high rates spontaneously in vivo. We therefore examined whether the PC to DCN synapse could sustain transmission for prolonged high frequency activation.

Figure 3.7 (Continued)

a, Example of prolonged stimulation of PC axons (500 stimuli, 100 Hz), average of 4 trials (top), and average across cells (bottom) and fit with the equation IPSC = $IPSC_{SS}$+(1-$IPSC_{SS}$)e-$^{S/\lambda}$ as in Extended Data Figure 3. Vertical scale bar, 1 nA.

b-g, At some synapses asynchronous release becomes more prominent with prolonged high-frequency stimulation (Luo and Sudhof, 2017, Atluri and Regehr, 1998, Wen et al., 2010, Hefft and Jonas, 2005). At these synapses, fast synchronous release can be seen riding on top of a slowly-decaying current that is in part mediated by asynchronous release. We therefore examined whether asynchronous release contributes to transmission during trains at this synapse.

b, An example train of 100 stimuli at 100 Hz from a wildtype (black) and Syt7 knockout (red). We measured the average decay time constant of IPSCs during the train (average IPSC #50-99, τ_{IPSC}), and for the last IPSC in the train (τ_{Train}). IPSCs were well fit by a single exponential decay with similar τ's. This indicates that asynchronous release is not prominent at this synapse. Vertical scale bars, 0.5 nA, dashed line indicates baseline before the train.

c, Average decay time for IPSCs during the train, and for the last IPSC in the train to decay back to baseline measured before the onset of stimulation. No significant differences were found between WT τ_{IPSC} vs WT τ_{train} ($p = 0.36$), KO τ_{IPSC} vs KO τ_{train} ($p = 0.71$), WT τ_{IPSC} vs KO τ_{IPSC} ($p = 0.23$), WT τ_{train} vs KO τ_{train} ($p = 0.48$), unpaired two-tailed student's t-test.

d, Charge transfer was measured in two different ways to isolate different components of release. The average incremental IPSC amplitude was multiplied by the stimulation rate (left), or traces were integrated and multiplied by stimulation rate (right).

The average charge transfer as a function of stimulation frequency, calculated either by IPSC amplitude, or by integration, for **e,** young (P12-15), **f**, juvenile (P21-32), and **g**, adult (P80-110) wildtype and Syt7 knockouts is shown. Data are mean ± s.e.m.

We also tested the hypothesis that P_R is elevated in Syt7 knockout mice. If P_R were increased, stronger depletion could more effectively mask facilitation and lead to a loss of frequency-invariant transmission (Zucker and Regehr, 2002a). It is expected that an increase in P_R would increase the size of PC inputs, but we found no significant difference in single fiber size between wildtype and Syt7 knockouts (**Figure 3.8**). We lowered external calcium (Ca_e) to decrease P_R and reduced the masking effects of vesicle depletion, and found that at PC to DCN synapses facilitation was prominent in wildtypes, but weak or absent in Syt7 knockouts (**Figure 3.9a**). If the loss of frequency-independent transmission is a consequence of an increase in P_R, then reducing P_R by lowering Ca_e should lead to frequency-invariant transmission in Syt7 knockout animals. However, when Ca_e was lowered from 1.5 mM (control) to 1 or 0.5 mM to reduce IPSC amplitudes to 42% and 12% of control respectively (Turecek et al., 2016b), transmission in Syt7 knockout mice remained frequency-dependent (**Figure 3.9b-c**). These results indicate that the loss of frequency invariance in Syt7 knockout animals is not a consequence of an increase in initial P_R.

We next looked for evidence of facilitation in physiological Ca_e (1.5 mM). Facilitation was measured by first stimulating at 10 Hz to induce baseline depletion, followed by steps to 100 Hz (Turecek et al., 2016b, Muller et al., 2010). In wildtype animals, frequency steps revealed a transient enhancement whose magnitude was correlated with the development of frequency-invariant transmission. (**Figure 3.9d$_{1\text{-}3}$**). These results are consistent with facilitation leading to sustained increases in P_R that is transiently revealed until it is masked by vesicle depletion. In Syt7 knockout animals, facilitation was not observed at any age, and increases in stimulus frequency depressed IPSCs. Thus, Syt7-dependent facilitation is prominent when transmission is frequency independent (juveniles and adult wildtypes), and is weak when transmission is frequency dependent (young wildtype and Syt7 knockouts of all ages).
To determine whether impaired frequency-invariant transmission was due specifically to presynaptic loss of Syt7 (Wu et al., 2017) we performed rescue experiments in global Syt7 knockout animals. We used AAVs to express ChR2-YFP alone, or to bicistronically express both Syt7 and ChR2-YFP presynaptically(Jackman et al., 2016) (**Figure 3.10a**). However, it is not possible to obtain expression in

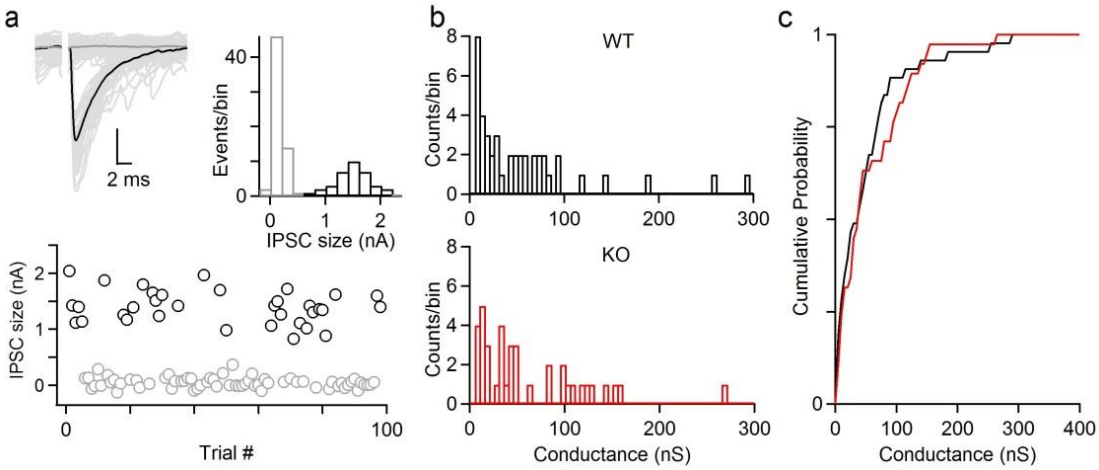

Figure 3.8: Single fiber conductances are not elevated in Syt7 knockout mice (P21-32). Single PC axons provide powerful inhibition on their post-synaptic targets in the DCN, and can be identified by their all-or-nothing nature. If the loss of Syt7 caused elevations in P_R, it would be expected to increase the strength of unitary fiber inputs. Experiments were done using minimal stimulation to determine the amplitudes of single PC to DCN inputs.

a, The stimulus was adjusted so that at a constant intensity synaptic inputs were activated approximately half the time in a stochastic manner. This is shown for 100 superimposed traces (left), along with average of failures (thick grey) and average of successes (thick black), for the amplitude histogram for the events recorded in that cell (middle), and for the IPSC amplitude as a function of trial number (bottom). Vertical scale bar, 0.5 nA.

b, Amplitude histogram of single fiber conductances for wildtype (black) and Syt7 knockouts (red).

c, Cumulative amplitude histograms of single fiber conductances. No significant difference was found between wildtype and Syt7 knockouts. p = 0.43, Kolmogorov-Smirnov test.

all PCs, and it is impractical to optically stimulate axons at high frequencies for prolonged trains(Jackman et al., 2014). We therefore used optical stimulation to identify ChR2-expressing fibers that could be isolated electrically (**Figure 3.10b, c**). These axons were then electrically stimulated at high frequency. We found that in Syt7 knockouts facilitation was absent in axons expressing ChR2 alone, but was prominent in fibers expressing ChR2 and Syt7 (**Figure 3.10d**). Steady-state transmission was nearly constant when Syt7 was expressed, but remained frequency-dependent when only ChR2 was present (**Figure 3.10e, f**). Consequently, charge transfer in Syt7-expressing PC axons was linear, but remained sub-linear when only ChR2 was expressed (**Figure 3.10g-h**). Viral expression of Syt7 allowed PCs in Syt7 knockouts to become as frequency invariant as wildtype animals (Figure 3.10h), indicating that presynaptic Syt7 mediates frequency-invariant transmission.

Having established that Syt7 is required for frequency invariance in PC synapses, we asked whether Syt7 plays a similar role at vestibular synapses. Afferents from the vestibular ganglion project to the magnocellular medial vestibular nucleus (MVNm, **Figure 3.11a**). Syt7 is expressed in the neuropil of the MVNm where vestibular afferents form glutamatergic synapses (**Figure 3.11b**). Although previous studies did not report facilitation at this synapse (McElvain et al., 2015), we found that vestibular synapses facilitate in low Ca_e in wildtype animals, but not in Syt7 knockouts (**Figure 3.11c**). In physiological Ca_e, step changes in stimulation frequency produced transient enhancement in wildtypes but not in Syt7 knockouts (**Figure 3.11d**). These responses suggest that at vestibular synapses Syt7-mediated facilitation is also present, but is masked by depletion. We also found that steady-state transmission was frequency-invariant and charge transfer was linear in wildtypes, but not in Syt7 knockouts (**Figure 3.11e-g, Figure 3.12**).

Here we show that Syt7 mediates a hidden component of facilitation that counteracts partial vesicle depletion to produce linear charge transfer. Synaptic properties in wildtype and Syt7 knockouts conform to a model in which the loss of frequency-invariance in Syt7 knockouts is accounted for by the absence of facilitation (Turecek et al., 2016b) (**Figure 3.13**). Linear charge transfer and Syt7 expression at PC synapses emerge during development, but for technical reasons most synapses have only been

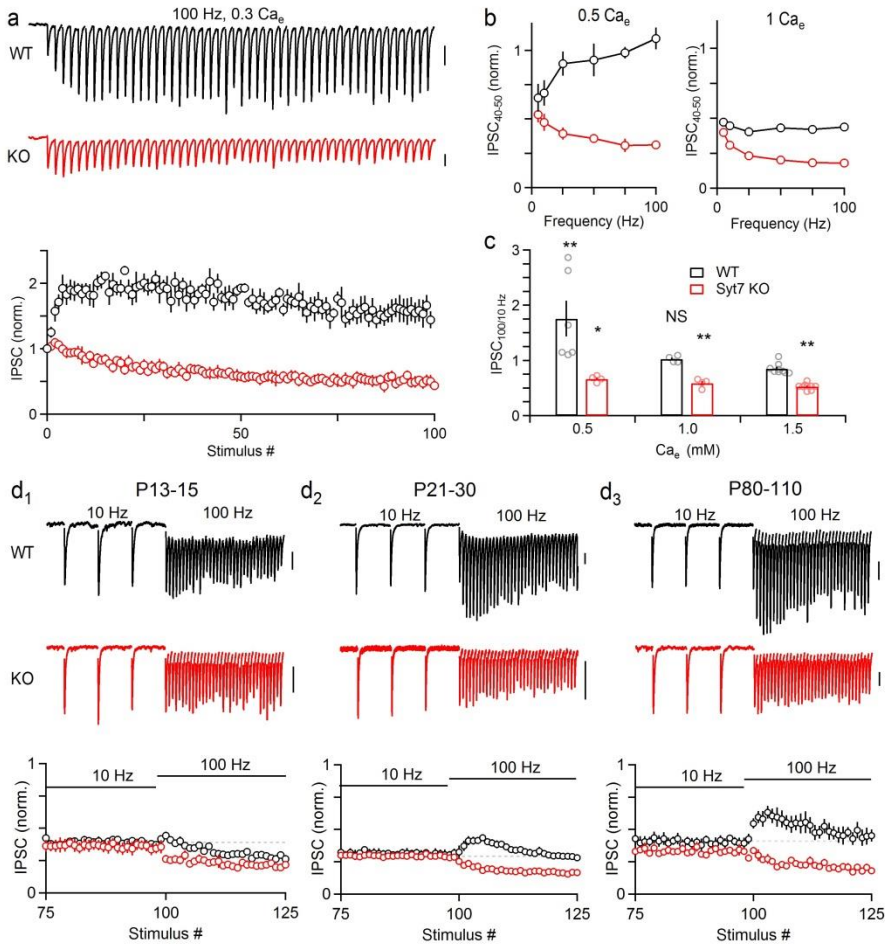

Figure 3.9: Syt7 is required for a hidden form of facilitation at PC to DCN synapses.

a, Experiments were conducted in P21-32 mice in low Ca_e (0.3 mM) to reduce the initial probability of release. Responses are shown for representative experiments (top) and summarized across experiments (bottom).

b, Average of 40-50th IPSC as a function of stimulation frequency.

c, Ratio of $IPSC_{SS}$ from 100 and 10 Hz stimulation in different Ca_e.

d_{1-3}, PC synapses were stimulated in 1.5 mM Ca_e at 10 Hz to reach steady-state, followed by 100 Hz stimulation in young (**d_1**) juvenile (**d_2**) and adult (**d_3**) animals. Example responses (top) and summaries (bottom) are shown. Vertical scale bars, 0.25 nA. *$p < 0.05$, **$p < 0.01$, one-way ANOVA with Tukey's post-hoc test. Data are mean ± s.e.m.

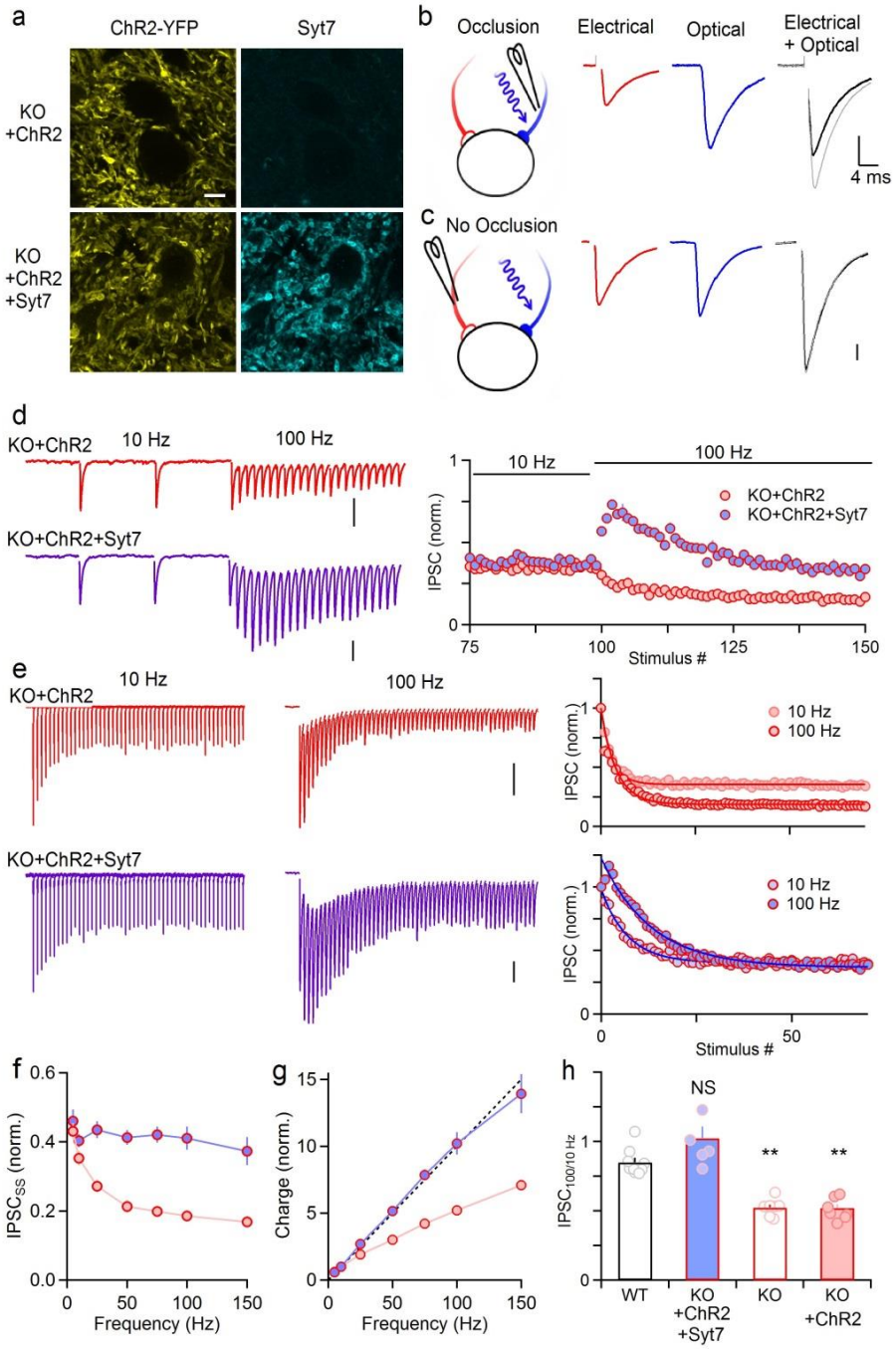

Figure 3.10: Presynaptic expression of Syt7 restores facilitation and frequency-invariant transmission at PC to DCN synapses in Syt7 knockouts.

Figure 3.10 (Continued)

a, ChR2-YFP fluorescence and Syt7 immunolabeling in the DCN of Syt7 knockouts following AAV-driven expression of either ChR2-YFP alone (a, top) or ChR2-YFP and Syt7 (a, bottom) in PCs. Scalebar, 10 μm.

b, c, The ability of IPSCs evoked electrically and optically to occlude each other was used to identify labeled fibers.

b, If PC fibers express ChR2, the algebraic sum of electrical (red) and optical (blue) stimulation (gray) exceeds responses evoked by simultaneous optical/electrical stimulation (black).

c, If electrically stimulated axons did not express ChR2, the sum of optical and electrical responses (gray) matched responses evoked by simultaneous optical and electrical stimulation (black).

d, PC axons expressing ChR2 alone (red) or ChR2+Syt7 (purple) were electrically stimulated at 10 Hz and then 100 Hz e.

e-g, PC inputs were stimulated at 5-150 Hz for ChR2 alone (red) or ChR2+ Syt7 (purple).

e, Responses evoked by trains. Vertical scale bars, 1 nA.

f, Average steady-state responses vs. stimulation frequency.

g, Charge transfer as a function of stimulation frequency.

h, Summary of ratios of $IPSC_{SS}$ amplitudes at 100 Hz and 10 Hz. $^{**}p < 0.01$, one-way ANOVA with Tukey's post-hoc test. Data are mean ± s.e.m.

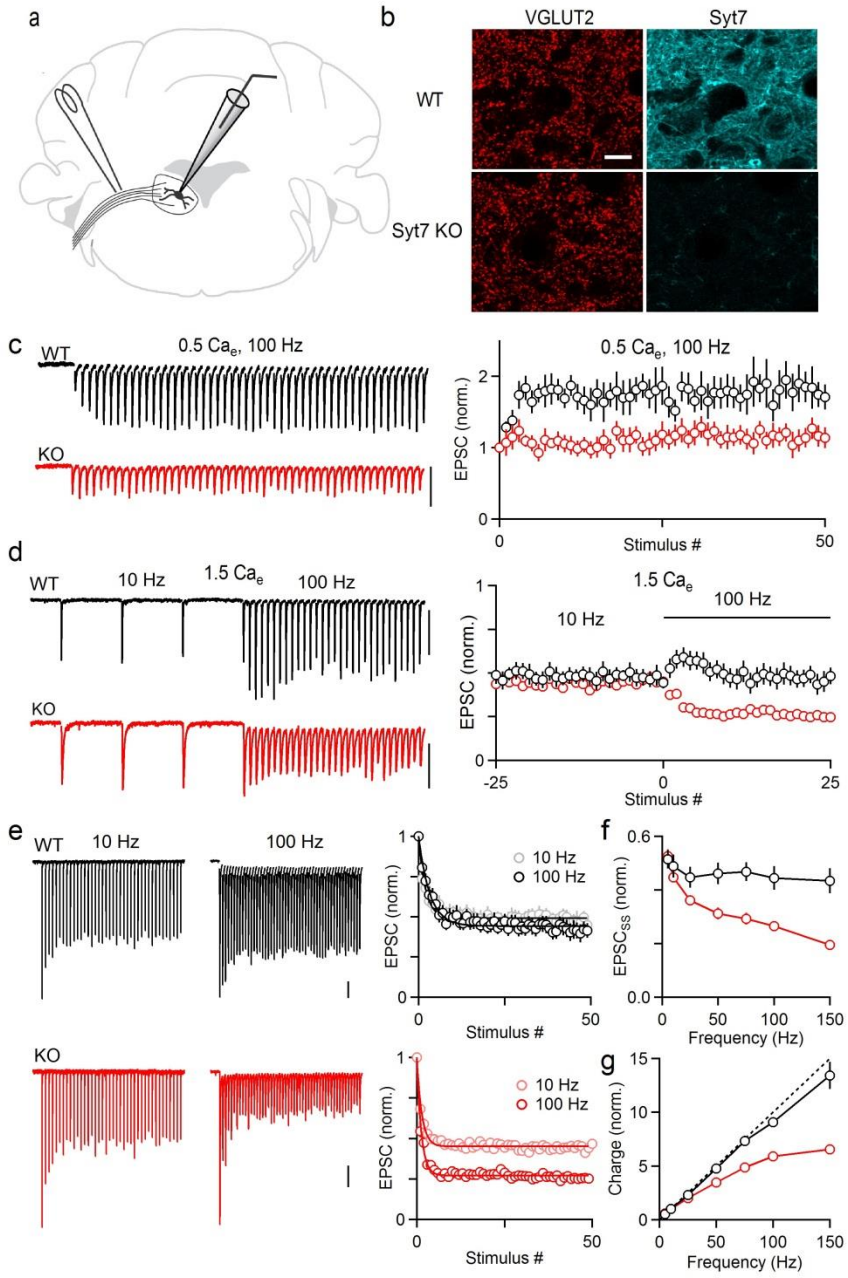

Figure 3.11: Syt7 is also required for frequency-invariant transmission at vestibular synapses.

a, Schematic showing stimulus electrode placement to activate vestibular afferents while recording from MVNm neurons.

b, Immunofluorescence of VGLUT2 (left) and Syt7 (right) surrounding MVNm cells in P25 mice.

c, Responses evoked by stimulating vestibular afferents in 0.5 mM Ca_e.

Figure 3.11 (Continued)

d, Vestibular inputs were stimulated at 10 Hz, followed by 100 Hz in 1.5 mM Ca_e.

e-g, Vestibular inputs were stimulated with 5-150 Hz trains in 1.5 mM Ca_e for wildtype and Syt7 knockout mice.

e, Responses evoked by trains are shown.

f, Average steady-state responses vs. stimulation frequency.

g, Charge transfer as a function of stimulation frequency. Vertical scale bars, 0.1 nA. Data are mean ± s.e.m..

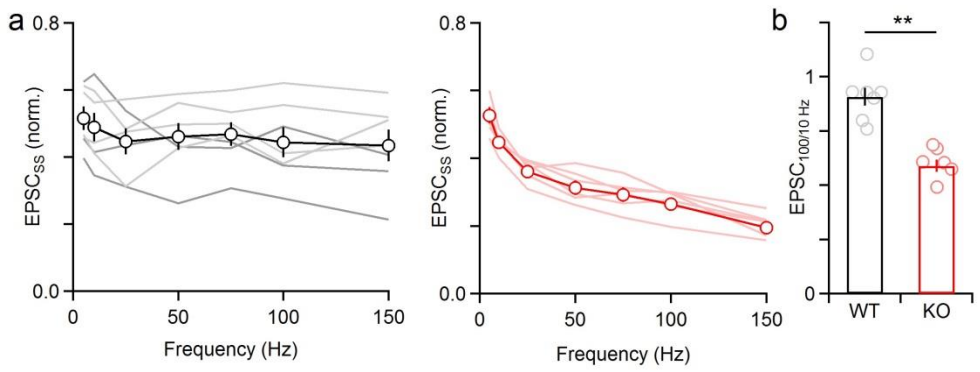

Figure 3.12: The frequency invariance of synaptic strength is consistent in the MVNm.

a, The steady-state EPSC size as a function of stimulation frequency for each cell analyzed (thin lines) and averages (markers) for wildtype (left, black) and Syt7 knockouts (red, right).

b, Ratio of the steady-state EPSC amplitudes at 100 Hz divided by steady-state amplitudes at 10 Hz is summarized for vestibular synapses in wildtype and Syt7 knockouts. **$p < 0.01$, unpaired two-tailed Student's t-test. Data are mean ± s.e.m.

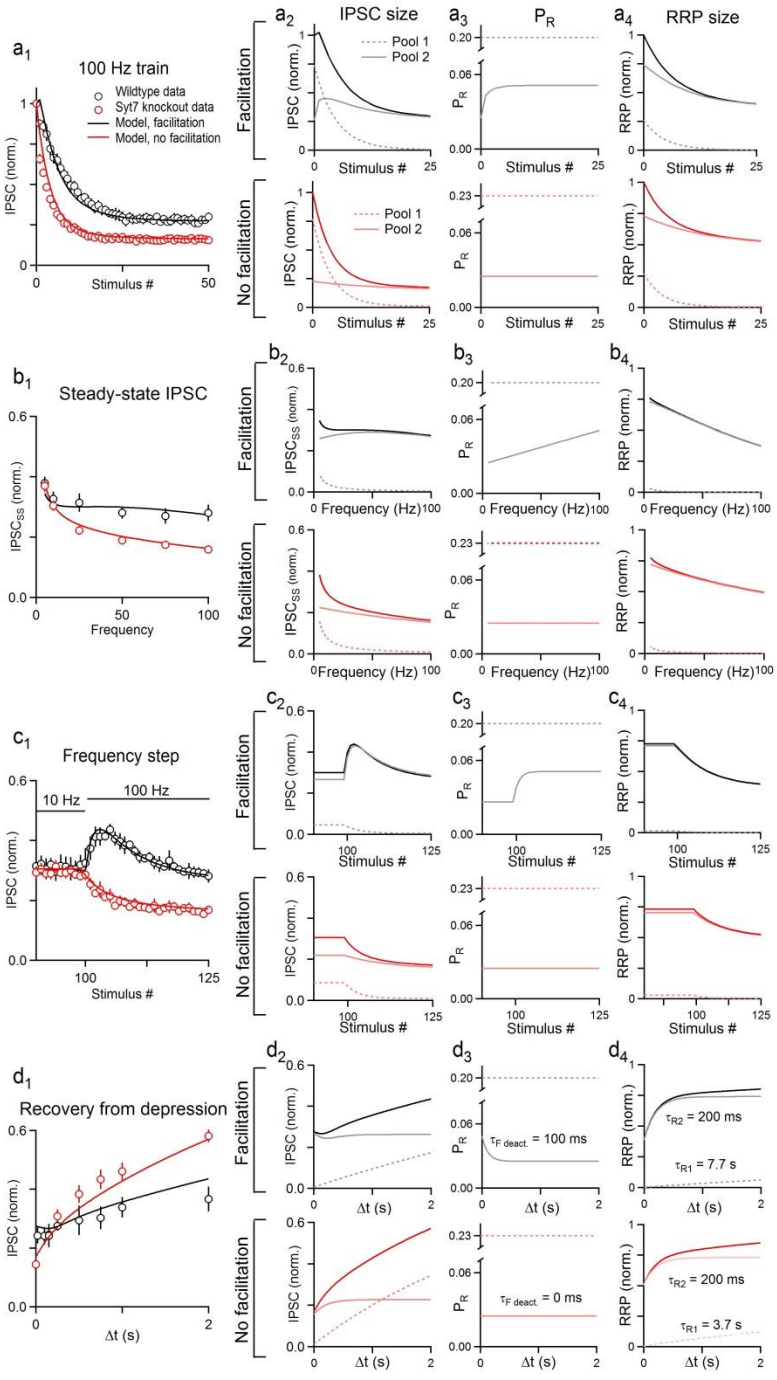

Figure 3.13: A model of the PC to DCN synapses indicates that eliminating facilitation can explain the loss of frequency-invariant transmission and other synaptic changes observed in Syt7 knockout animals.

We extended a previously described model of PC to DCN synapses to explore transmission in Syt7 knockout animals(Turecek et al., 2016b). The model consists of two pools of vesicles: Pool 1 vesicles

Figure 3.13 (Continued)

have a high release probability and are replenished slowly. Pool 2 vesicles have a low initial release probability that increases with facilitation (in wildtype animals only), and replenish rapidly. The existence of multiple vesicle pools has been proposed at several types of synapses(Lu and Trussell, 2016, Trommershauser et al., 2003, Thanawala and Regehr, 2016b). The model was constrained by many experiments and in the simplest configuration could account for all experimental observations(Turecek et al., 2016b). The model is compared to data in wildtype and Syt7 knockouts (**a_1-d_1**). The contribution of each pool and its properties (IPSC size **a-d_2**, release probability P_R **a-d_3**, and readily releasable pool size RRP **a-d_4**) are also shown for each experiment. **a,** During high frequency stimulation in wildtype animals (**$a_{1\text{-}2}$,** black), Pool 1 primarily contributes to depression seen during the onset of stimulation, but is strongly depleted during sustained firing (**a_2**, dashed gray). Pool 2 facilitates and maintains release at steady-state (**$a_{2\text{-}3}$,** solid gray). We modeled Syt7 knockout animals by removing facilitation (**a_3,** red). When facilitation was eliminated, steady-state transmission was reduced during high frequency stimulation because fewer vesicles were released from Pool 2 (**a_4,** light red). **b,** In the model of wildtype synapses, the magnitude of facilitation increased with stimulation frequency (**b_3**, gray), allowing more of the readily releasable pool of Pool 2 (RRP2) to be released at high frequencies, resulting in similar IPSC amplitude across frequencies (**$b_{1\text{-}2}$**, black). When facilitation was removed (**b_3,** red), transmission was no longer frequency invariant, because fewer vesicles were released at high frequencies (**$b_{1,4}$,** red). **c**, When the frequency of stimulation was stepped from 10 to 100 Hz, a transient enhancement was observed in wildtype animals (**c_1**, black markers). In the model, this transient enhancement is mediated by facilitation of Pool 2 (**c_3,** gray). Facilitation is weakly activated by 10 Hz stimulation, but increases when stepping to 100 Hz stimulation. As more vesicles are released, RRP2 is partially depleted and the IPSC amplitude depresses, ultimately reaching steady-state levels that are similar to those reached during 10 Hz stimulation. When facilitation is removed, no transient enhancement occurs, and the IPSC amplitude simply depresses (**$c_{1\text{-}2}$,** red). **d**, The model is also able to explain recovery from depression. In wildtype animals, a single slow recovery is observed (**d_1**, black markers) because the decay of facilitation obscures

Figure 3.13 (Continued)

the rapid recovery of RRP2 ($\mathbf{d_{3\text{-}4}}$, τ_{Fdeact}). When facilitation is removed, this rapid component of recovery is unmasked ($\mathbf{d_{1\text{-}2}}$, red). The known role of Syt7 in facilitation, and the fact that the many alterations in synaptic responses in Syt7 knockout animals are explained by eliminating facilitation in this model, support the importance of Syt7-mediated facilitation in frequency invariant transmission.

studied in young animals (Borst, 2010). The prevalence of frequency-invariant transmission in adults is unknown but indirect measurements *in vivo* suggest it may be widespread (Arenz et al., 2008, Kuenzel et al., 2011a). Moreover, Syt7 is developmentally regulated(Sugita et al., 2001, Bakken et al., 2016) and widely expressed in the adult brain, often in cells that make depressing synapses(Sugita et al., 2001, Lein et al., 2007). The kinetics of Syt7 make it well suited to operate within the physiological firing range of PCs and vestibular afferents (Zhou et al., 2014, Jackman and Regehr, 2017, Bagnall et al., 2008, Brandt et al., 2012). While our results show linear charge transfer is mediated by Syt7 at PC and vestibular synapses, other synapses may use different mechanisms (**Figure 3.1**).

At frequency-invariant synapses, the amount of neurotransmitter release scales linearly with the firing frequency, and can thus faithfully encode presynaptic spike rates. Sensorimotor processing in the vestibular system and intensity discrimination in the auditory system have been proposed to operate through a linear rate code (Robinson, 1981, Bagnall et al., 2008)(Sullivan and Konishi, 1984, MacLeod et al., 2007). Understanding the mechanisms involved in frequency-invariant transmission will enable genetic manipulations that could yield fundamental insights into how synaptic computations contribute to circuit function and behavior.

Methods

Animals and viruses. All mice were handled in accordance with NIH guidelines and protocols approved by Harvard Medical Area Standing Committee on Animals. Syt7 knockout mice(Chakrabarti et al., 2003) (Jackson Laboratory) and wild-type littermates of either sex were used. Statistical tests were not used to predetermine sample size. In Figure 3-4, Extended Data Figure 2, 7, 8, all experiments were performed blind to genotype and virus identity. In Figures 1-2, Extended Data Figure 3-6, experiments were initially performed blind but abandoned after initial rounds of experiments because genotypes could easily be identified from physiology alone. AAV2/1-hSyn-hChR2(H134R)-EYFP was obtained from the University of Pennsylvania Vector Core. AAV2/1-hSyn-hChR2(H134R)-EYFP-2A-Syt7 was obtained from the Boston Children's Virus Core. Plasmid sequences are available upon request.

Stereotaxic surgeries were performed on P16-18 Syt7 knockout mice anesthetized with ketamine/xylazine (100/10 mg/kg) supplemented with isoflurane (1-4%). Viruses were injected through glass capillary needles using a Nanoject II (Drummond) mounted on a stereotaxic (Kopf). Three injections were made in the right cerebellar cortex, 1.0, 1.5, 2.0 mm lateral, 1 mm posterior from lambda, 0.2-0.3 mm depth. 300-500 nL of virus suspension was delivered to each site at a rate of 100 nL/minute, and the needle was retracted 5-10 minutes following injection. Analgesic (buprenorphine 0.05 mg/kg) was administered subcutaneously for 48 hours post-surgery.

Slice preparation. Acute slices were prepared in mice of both sexes (P21-32 unless otherwise indicated). Mice were sacrificed 12-14 days following AAV injections. Animals were anesthetized with ketamine/xylazine (100/10 mg/kg) and transcardially perfused with solution composed of in mM: 110 Choline Cl, 2.5 KCl, 1.25 NaH_2PO_4, 25 $NaHCO_3$, 25 glucose, 0.5 $CaCl_2$, 7 $MgCl_2$, 3.1 Na Pyruvate, 11.6 Na Ascorbate, 0.002 (R)-CPP, 0.005 NBQX, oxygenated with 95% O2 / 5% CO_2, kept at 35°C. For DCN recordings, a cut was made down the midline of the hindbrain, and the cut face of each side was glued to the slicing chamber to generate sagittal slices. For the vestibular nuclei, a cut was made down the midbrain between the cerebellum and cortex and glued to the slicing chamber to generate coronal slices. 250 μm thick sections were made on a Leica 1200S vibratome and were then transferred to a holding chamber with ACSF containing in mM: 127 NaCl, 2.5 KCl, 1.25 NaH_2PO_4, 25 $NaHCO_3$, 25 glucose, 1.5 $CaCl_2$, 1 $MgCl_2$, and allowed to recover at 35°C for at least 20 minutes before cooling to room temperature.

Electrophysiology. All experiments were performed at 34-35°C with a flow rate of 3-5 ml/min. Recording ACSF had the same composition as incubation ACSF unless otherwise stated. Recordings were made primarily in the dentate and interposed nuclei of the DCN. Large diameter (>15 μm) neurons were selected for recording as previously described (Turecek et al., 2016b). For DCN recordings, borosilicate electrodes (1-2 MΩ) were filled with internal solution consisting in mM of: 110 CsCl, 10 HEPES, 10 TEA-Cl, 1 $MgCl_2$, 4 $CaCl_2$, 5 EGTA, 20 Cs-BAPTA, 2 QX314, 0.2 D600, pH to 7.3. Cells

were held at -30 to -40 mV in the presence of 5 μM NBQX to block AMPARs, 2.5 μM (R)-CPP to block NMDARs, 1 μM strychnine to block glycine receptors, and 1 μM CGP 55845 to block $GABA_B$Rs. A glass monopolar stimulus electrode (2-3 MΩ) filled with ACSF was placed in the white matter surrounding the DCN to activate PC axons.

To study vestibular afferents, recordings were made from cells in the magnocellular medial vestibular nucleus. Recordings electrodes (1.5-2 MΩ) were filled with in mM: 150 Cs-gluconate, 3 CsCl, 10 HEPES, 0.5 EGTA, 3 MgATP, 0.5 NaGTP, 5 Tris-phosphocreatine-Tris and 5 Na-phosphocreatine; pH to 7.2. Cells were held at -60 mV in the presence of 100 μM picrotoxin or 5 μM SR-95531 to block $GABA_A$Rs, 2.5 μM (R)-CPP to block NMDARs, 1 μM strychnine to block glycine receptors, and 1 μM CGP 55845 to block $GABA_B$Rs. A concentric bipolar electrode was placed in the expansion of the vestibulocochlear nerve as it reaches the dorsal brainstem, adjacent to the lateral vestibular nucleus. To prevent the possibility of poor fiber recruitment or entraining local circuit elements, trains with EPSCs composed of multi-phasic rise or decay phases were excluded from analysis. For trains in low Ca_e EPSCs became very small. In some cases, 5 μM NBQX was washed in at the end of experiments and traces in the presence of NBQX were subtracted in order to remove stimulus artifacts.

Trains of 100 stimuli (5-150 Hz, randomized), followed by 100 stimuli at 100 Hz, were applied every 20-30 s for vestibular and PC synapses. For 500 stimulus trains at 100 Hz, trials were collected every 60 s. Extracellular stimulation of axons became unreliable after 500 stimuli. For all recordings, only the capacitance roughly equivalent to the cell body was compensated (5 pF), and series resistance (1-6 MΩ) was compensated up to 80%. Experiments were discarded if series resistance changed by 30%. Experiments were discarded if fibers could not be consistently recruited, as assessed by major discrete changes observed in PSC amplitude during trains, or if the PSC amplitude never reached steady state during trains. Liquid junction potentials were left unsubtracted. In low Ca_e experiments, total divalents were kept constant by elevating external Mg. Experiments using the low affinity $GABA_A$R antagonist TPMPA were performed as previously described(Turecek et al., 2016b).

Analysis. Recordings were collected using a Multiclamp 700B (Molecular Devices) in Igor Pro (Wavemetrics) sampled at 20 kHz and filtered at 4 kHz. All data was analyzed using custom-written scripts in Matlab (Mathworks). Stimulus artifacts were blanked for clarity. IPSC amplitudes during trains were measured from averaged traces of 3-10 trials as the peak evoked current, with a baseline measured 2 ms before stimulus onset. During high frequency trains, IPSCs did not fully decay before subsequent stimuli. Baselines in this case were measured by extrapolating a single exponential fit from the previous IPSC (as shown in Extended Data Figure 6). Trains from rest typically reached steady-state after 10-20 stimuli, and the steady-state was measured as the average IPSC size of the 40^{th} to the 60^{th} stimuli. Charge transfer was calculated as the product of steady-state IPSC size and stimulation frequency, and normalized to the charge transfer of 10 Hz stimulation. All data are presented as means ± s.e.m. unless otherwise indicated. In some cases error bars are occluded by markers. Statistical significance was assessed using unpaired two-tailed Student's t-test or one-way ANOVA with Tukey's post-hoc test unless otherwise noted. A subset of the data from wildtype Syt7 litter mate animals (~50%) in Figure 1 and Figure $2d_2$ was presented previously (Turecek et al., 2016b).

Optogenetics. It was impossible to reliably stimulate PC axons with prolonged trains at high frequency (>50 Hz) using optical stimulation alone (ChR2-H134R or Chronos). We therefore used ChR2 to identify labeled fibers that were then stimulated electrically. In this approach, optical stimulation of axons expressing ChR2 could occlude electrical stimulation of the same fibers, presumably because of the refractory period of the action potential. In contrast, if electrically stimulated fibers did not express ChR2, electrically-evoked responses could not be occluded by optical stimulation, and combined stimulation was equivalent to the linear sum of optical and electrical activation alone. PC boutons expressing ChR2 were stimulated by pulses of 473 nm light (0.5-1 ms, 160 mW/mm^2) from an LED (Thorlabs) through a 60x objective producing an 80 µm diameter spot of light over the cell body. A stimulus electrode was placed in the white matter and converging PC axons were located as in other experiments. Randomized trials of single optical, electrical, or closely-timed (0-2 ms) paired optical/electrical stimuli were applied every 5 s.

When >70% of the electrically evoked component could be occluded by optical stimulation, and could be consistently recruited, those fibers were then activated using high-frequency electrical stimulation. Following electrical trains, occlusion trials were performed again to confirm that the same set of fibers was stimulated throughout all trials. At the end of experiments, a low concentration of SR-95531 (300-800 nM) was washed in and occlusion trials were again repeated to ensure occlusion was not the result of poor voltage clamp. In a subset of experiments light pulses were also delivered over the stimulus electrode instead of the cell body, producing similar results.

Immunohistochemistry. Mice of both sexes (P21-32 unless otherwise indicated) were anesthetized with ketamine/xylazine (100/10 mg/kg) and transcardially perfused with PBS followed by 4% paraformaldehyde (PFA) in PBS. To determine the expression of Syt7, Syt2, Calbindin and VGAT specifically in PCs, we also perfused one mouse (P43) in which PC synapses are labeled with TdTomato (Pcp2-Cre(Jdhu) x Synaptophysin-TdTomato, Figure 3.4). Brains were removed and post-fixed in PFA overnight. Sagittal sections of the cerebellum or coronal sections of the brainstem (50 μm) were then permeabilized (0.2% triton X-100 in PBS) for 10 min and blocked for 1 hr (4% Normal Goat Serum in 0.1 % triton X-100) at room temperature. Slices were then incubated overnight at 4°C with primary antibodies (Mouse anti-Syt7 targeting the C2A domain, UC Davis/NIH NeuroMab Facility, clone N275/14, RRID: AB_11030371, 1 μg/mL, 1:100; Rabbit anti-Calbindin D28K, Millipore Ab1778, 1:200; Mouse anti-Syt2, Zirc znp-1, 1:200; Guinea-pig anti-VGAT, Synaptic Systems 131004, 1 μg/mL, 1:500; Guinea-pig anti-VGLUT2, Synaptic Systems 135404, 1 μg/mL, 1:1200). To prevent background when co-staining with VGLUT2 and Syt7, Syt7 primary antibodies were applied alone overnight at 4°C, then VGLUT2 primary antibodies alone for 2 hrs at room temperature. Following primaries, slices were incubated with secondary antibodies for 2 hrs at room temperature (anti-Rabbit-AlexaFluor488, Abcam ab150077; anti-Guinea-pig-AlexaFluor488, Abcam ab150185; anti-Mouse-AlexaFluor647, Abcam ab150115). For experiments comparing ages or genotypes, all tissue was stained and processed in parallel. Z-Stacks of each sample were collected using an Olympus Fluoview1000 confocal microscope

using the same settings across ages and genotypes, and processed identically in ImageJ. For each genotype and age, identical anatomical locations and tissue depth were selected for presentation.

Modeling. In a previous study we modeled the PC to DCN synapse(Turecek et al., 2016b). Models used previously to explain data in young animals(Telgkamp et al., 2004) were reproduced, but could not fit data in P21-32 animals(Turecek et al., 2016b). Several other types of models were also attempted but failed to accurately account for data observed in juvenile wildtype animals. We found that a two pool model fit all experimental observations(Turecek et al., 2016b) . We extended this model to Syt7 knockout animals (Extended Figure 9). In this model there are 2 pools of vesicles, consisting of, respectively, N1 and N2 vesicles, initial probability of release P1 and P2 and time constants of recovery τ_{R1}, and τ_{R2} . P1 stays constant whereas P2 increases as a result of facilitation, F2, which has the frequency dependence that was determined experimentally. All of these parameters were constrained by extensive experimental studies for wildtype animals(Turecek et al., 2016b). Once parameters for wildtype data were determined, F2 was set to 0 to model Syt7 knockout animals. Minor adjustments (<10% change) were made to some parameters to fit the data more accurately, with the exception of τ_{R1} which was reduced by 55% to conform to the observed recovery from depression in Syt7 knockouts (Extended Data Figure 5). This change in τ_{R1} had a negligible effect on steady-state IPSC amplitudes because Pool 1 still depletes rapidly. Parameters for modeling wildtypes were: N1/N2 = 0.35; P1 = 0.20; τ_{R1} = 7.7 s; P2 = 0.025; τ_{R2} = 0.2 s; F2 = 0.04; τ_{Fdeact} = 0.1 s. Parameters for modeling Syt7 knockouts were: N1/N2 = 0.36; P1 = 0.23; τ_{R1} = 3.5 s; P2 = 0.025; τ_{R2} = 0.2 s; F2 = 0.

Chapter 4

Synaptotagmin 7 Mediates Both Facilitation and Asynchronous Release at Granule Cell Synapses

Josef Turecek & Wade G. Regehr

Journal of Neuroscience, *38*(13), 3240-3251.

Author Contributions. J.T. and W.R. designed experiments. J.T. performed experiments and analyzed data. J.T. and W.R. wrote the paper.

Abstract:

When an action potential invades a presynaptic terminal it evokes large, brief Ca^{2+} signals that trigger vesicle fusion within milliseconds that is followed by a small residual Ca^{2+} (Ca_{res}) signal. At many synapses Ca_{res} produces synaptic facilitation that lasts up to hundreds of milliseconds and, although less common, Ca_{res} can also evoke asynchronous release (AR) that persists for tens of milliseconds. The properties of facilitation and AR are very different, which suggests that they are mediated by distinct mechanisms. However, recently it has been shown that the slow calcium sensor Synaptotagmin 7 (Syt7) mediates facilitation at many synapses where AR does not occur, and conversely Syt7 can mediate AR without mediating facilitation. Here we study cerebellar granule cell synapses onto stellate cells and Purkinje cells in mice of both sexes in order to assess the role of Syt7 in these phenomena at the same synapse. This is of particular interest at granule cell synapses where AR is much more calcium-dependent and shorter-lived than facilitation. We find that Syt7 can mediate these two processes despite their divergent properties. In Syt7 knockout animals, facilitation and AR are smaller and shorter lived than in wildtype animals, even though the initial probability of release and Ca_{res} signals are unchanged. Although there are short-lived Syt7-independent mechanisms that mediate facilitation and AR in Syt7 KO animals, we find that at granule cell synapses AR and facilitation are both mediated primarily by Syt7.

Introduction

Activation of presynaptic cells opens voltage gated Ca^{2+} channels within presynaptic boutons leading to large, fast, highly localized Ca^{2+} signals that trigger rapid vesicle fusion. Ca^{2+} then binds to Ca^{2+}-binding proteins and diffuses, thereby collapsing spatial gradients and giving rise to a small residual Ca^{2+} (Ca_{res}) signal that persists for tens of milliseconds and controls neurotransmitter release in multiple ways. Ca_{res} can elevate the probability of release (P_R) to produce synaptic facilitation of synchronous release for hundreds of milliseconds. Facilitation is present at synapses throughout the brain, and is most prominent at synapses with low initial P_R. Ca_{res} can also trigger asynchronous release (AR) that lasts for tens of milliseconds following single stimuli (Atluri and Regehr, 1998, Iremonger and Bains, 2007). AR is not apparent at most synapses, but when observed it is most prominent following bursts of presynaptic activity or during sustained activation (Hefft and Jonas, 2005, Peters et al., 2010, Iremonger and Bains, 2007, Labrakakis et al., 2009, Best and Regehr, 2009, Atluri and Regehr, 1998, Lu and Trussell, 2000).

It has been hypothesized that facilitation and AR involve specialized Ca^{2+} sensors, and that the same sensor might mediate both phenomena (Jackman and Regehr, 2017, Zucker and Regehr, 2002a, Rahamimoff and Yaari, 1973). However, many synapses facilitate in the absence of AR, whereas some synapses with AR do not facilitate (Hefft and Jonas, 2005, Labrakakis et al., 2009, Peters et al., 2010). Further, when both phenomena are present at the same synapses, their timecourse and Ca^{2+}-dependence can be different (Atluri and Regehr, 1998), but see (Molgo and Van der Kloot, 1991). These observations made it seem unlikely that the same Ca^{2+} sensor mediates both AR and facilitation.

Despite the differences between the two processes, recent studies indicate that Synaptotagmin 7 (Syt7) can contribute to either facilitation or AR (Jackman et al., 2014, Turecek et al., 2017, Bacaj et al., 2013, Luo et al., 2015, Luo and Sudhof, 2017, Wen et al., 2010). The properties of Syt7 make it a strong candidate for both processes because it is the Synaptotagmin isoform with the highest affinity for Ca^{2+} and the slowest kinetics (Sugita et al., 2002, Brandt et al., 2012), and it is widely expressed (Mittelsteadt et al., 2009). Syt7 was initially implicated in AR at the zebrafish neuromuscular junction, where sustained presynaptic activation led to Syt7-dependent AR (Wen et al., 2010). Initial studies of cultured mammalian

synapses found that eliminating Syt7 did not alter synaptic responses (Maximov et al., 2008), but it was subsequently found that in the absence of Syt1 AR is prominent and Syt7-dependent (Bacaj et al., 2013). At the young calyx of Held, sustained high-frequency stimulation led to slow currents that were attributed to AR, and that were strongly reduced in Syt7 KOs (Luo and Sudhof, 2017). However, facilitation is absent or very weak at synapses where Syt7 has been implicated in AR. In contrast, at 3 types of hippocampal synapses and thalamocortical synapses, paired-pulse facilitation is prominent in wildtypes, but eliminated in Syt7 KOs (Jackman et al., 2016). At Purkinje cell synapses and vestibular synapses, Syt7-mediated facilitation is present but it is masked by depression (Turecek et al., 2017). At synapses where Syt7 has been implicated in facilitation, AR is not apparent. Thus, Syt7 mediates facilitation without producing AR at some synapses, but mediates AR without generating facilitation at others.

Here we determine the role of Syt7 in transmission at synapses made by cerebellar granule cells (grCs) onto stellate cells (SCs) and Purkinje cells (PCs). These synapses are of particular interest because they have large facilitation, AR is prominent after single stimuli, and AR is shorter-lived and more Ca^{2+}-dependent than facilitation (Atluri and Regehr, 1998). We find that Syt7 elimination strongly attenuates both AR and facilitation and decreases their duration, indicating that both processes are mediated primarily by Syt7. We also conclude that additional mechanisms mediate the rapid AR and facilitation remaining in Syt7 KO mice.

Methods

Animals: Syt7 KO mice and wildtype littermates (Chakrabarti et al., 2003) of either sex were used. All mice were handled in accordance with NIH guidelines and protocols approved by Harvard Medical Area Standing Committee on Animals. Experiments and analysis shown in Figure 4.1,4.3 and 4.5 were performed blind. Experiments in Figures 4.2, 4.4, 4.6-4.8 were initially performed blind but blinding was abandoned because the genotype could be reliably determined from physiology alone.

Slice preparation: P16-23 animals of both sexes were anesthetized with ketamine / xylazine and transcardially perfused with solution containing in mM: 110 Choline Cl, 2.5 KCl, 1.25 NaH_2PO_4, 25 $NaHCO_3$, 25 glucose, 0.5 $CaCl_2$, 7 $MgCl_2$, 3.1 Na Pyruvate, 11.6 Na Ascorbate, 0.002 (R)-CPP, 0.005 NBQX, oxygenated with 95% O2 / 5% CO_2, kept at 4°C. The cerebellum was removed and horizontal / transverse slices (250 μm) were made using a Leica 1200S vibratome in choline ACSF maintained at 4°C. Slices were then transferred to a holding chamber with solution containing in mM: 127 NaCl, 2.5 KCl, 1.25 NaH_2PO_4, 25 $NaHCO_3$, 25 glucose, 2 $CaCl_2$, 1 $MgCl_2$ and allowed to recover at 35°C for at least 30 minutes before cooling to room temperature.

Electrophysiology: Experiments in Figures 4.2-4.7 were performed at room temperature and experiments in Figure 4.8 were performed at 35°C. Unless otherwise stated, the composition of ACSF used for recording was the same as for slice incubation. Whole-cell voltage clamp recordings were made from PCs, or molecular layer interneurons in the outer third of the molecular layer (SCs) in vermal lobules V and VI. Borosillicate electrodes (1-1.5 MΩ for PCs, 1.5-2.5 MΩ for stellate cells) were filled with in mM: 35 CsF, 100 CsCl, 10 EGTA, 10 HEPES, pH 7.3 with CsOH. A recording electrode (1.5-2.5 MΩ) filled with ACSF was placed several hundred μm away in the molecular layer to stimulate parallel fibers (0.2 ms pulses, 5-40 μA). For PCs, the tip of the stimulation electrode was placed within 10-50 μm of the PC layer to activate parallel fibers synapses close to the PC body. For SCs, the electrode was placed in alignment with the SC body and at a depth to prevent activation of off-beam fibers (Carter and Regehr, 2000). For all experiments measuring facilitation, the average initial EPSC amplitude was kept

between 100-250 pA to minimize the activation of off-beam fibers and to maintain voltage clamp. PCs were held at -60 mV, with series resistance (1-10 MΩ) compensated up to 80% and whole-cell capacitance compensated only for the cell body (5 pF). SCs were held at -70 mV and series resistance and whole-cell capacitance were left uncompensated. Experiments were performed in the presence of bicuculine (20 μM) or SR-95531 (5 μM) to block $GABA_A$Rs. Experiments measuring mEPSCs were performed in SCs in the presence of 0.5 μM TTX and performed in slices unperturbed by stimulation electrodes.

In paired recordings between grCs and PCs, cell-attached recordings were obtained from grCs using electrodes filled with in mM: 135 K-gluconate, 20 KCl, 2 $MgCl_2$, 10 HEPES, 0.1 EGTA pH to 7.3 using KOH. When searching for grCs, brief infrequent (0.1 Hz) pulses of positive pressure were applied in the grC layer. Regions of the grC layer in which puffs elicited synaptic currents were then targeted for single-cell recordings. grCs were at least 150 μm away from the recorded PC in order to avoid ascending branch synapses which are reported to have different properties than parallel fiber synapses (Sims and Hartell, 2005). grCs were held in cell-attached mode with a holding potential of -60 mV and 3-5 ms voltage steps of 50-200 mV were pulsed to elicit action currents as previously described (Schmidt et al., 2013). For grC to PC pairs, PCs were recorded using leaded glass electrodes (1-1.5 MΩ) filled with, in mM: 110 Cs_2SO_4, 10 HEPES, 10 EGTA, 4 $CaCl_2$, 1.5 $MgCl_2$, 5.5 $MgSO_4$, 4 Na2-ATP, 0.1 D600, and 5 QX-314, pH to 7.3 with CsOH. For these experiments, PCs were held at -70 mV and series resistance and whole-cell capacitance were left uncompensated

For experiments measuring the effect of EGTA-AM, 20 μM EGTA-AM was washed into the bath for 15 minutes. Data was collected from multiple cells within the same slice following washin. Thus, data shown in Figure 4.7 are from some cells in which recordings were maintained before, during and after washins, as well as cells in which recordings were made following washin. Experiments measuring AR in Sr^{2+} were performed as previously described (Xu-Friedman and Regehr, 2000). Briefly, control ACSF contained in mM, 2 $CaCl_2$ and 1 $MgCl_2$, which was then replaced with ACSF containing 2 EGTA, 4 $SrCl_2$ and 1 $MgCl_2$. EGTA binds Ca^{2+} with high affinity (K_d of ~100 nM), Sr^{2+} with moderate affinity (K_d ~30

μM) and Mg^{2+} with low affinity (K_d ~15 mM), resulting in estimated free divalent levels of 2 Sr^{2+}, 1 Mg^{2+}, and very low free Ca^{2+}. All data shown in Figure 4.6 are washins.

Ca^{2+} transients were measured from either Mg-Green AM or Fura-2 AM (240 μM) loaded into parallel fibers as previously described (Brenowitz and Regehr, 2014, Regehr and Tank, 1991, Regehr and Atluri, 1995, Atluri and Regehr, 1996a). Briefly, indicator was loaded into a pipette (8-15 μm diameter) which was lowered into the molecular layer under positive pressure for three minutes. Fast green (1%) was included to allow visualization under bright field. A suction pipette (15-20 μm diameter) was positioned near the outflow of the labeling pipette to confine the area of indicator loading. Slices were imaged using a 60x objective and custom-built photodiode at least one hour following loading, with imaging sites > 300 μm from the loading site. A stimulus electrode was placed > 400 μm from the imaging site to excite parallel fibers. Mg-Green and Fura-2 were excited by a tungsten and xenon lamp, respectively.

Sr^{2+}levels were determined as described previously (Xu-Friedman and Regehr, 1999, Xu-Friedman and Regehr, 2000). Briefly, fluorescence transients in Sr^{2+}were normalized to transients in Ca^{2+} at the same imaging site and converted to relative concentrations by adjusting for the binding affinity of Mg-Green for Ca^{2+}versus Sr^{2+}(multiplying Sr^{2+} transients by 5.5 = $K_{D\text{-}Sr}/K_{D\text{-}Ca}$).

Analysis: Recordings were collected using a Multiclamp 700B (Molecular Devices) sampled at 20 kHz and filtered at 2 kHz. All data was collected in Igor Pro (Wavemetrics). All analysis was performed using custom-written scripts in Matlab (Mathworks). Paired pulse facilitation was measured from averages of at least 10 trials per interstimulus interval. For short interstimulus intervals in PCs, EPSCs were elicited during the decay of the initial EPSC. In these cases, the initial EPSC from long duration interstimulus intervals was subtracted. All data in figures are summarized as mean ± SEM across individual cells. In some cases error bars are occluded by markers. Number of experiments are presented in figure legends as number of cells, except for Ca^{2+} imaging experiments where the number of slices are indicated. In text, fit coefficients are provided ± SD, and all other values are summarized as mean ± SEM.

To quantify AR, events were detected for each trial. Histograms of asynchronous release vs. time were generated by summing the events across all trials, and dividing by the number of trials. The peak amplitude of the synchronous component (within 9 ms following stimulation) was used as a measure of the number of synapses stimulated. Histograms of asynchronous release vs. time for each cell were therefore divided by the peak amplitude of the synchronous EPSC, measured from the averaged trace of all trials for that cell.

In paired recordings, only trials in which action potentials were evoked in the grC were included for analysis. The amplitude of the evoked current in PCs for each trial was measured as the average of 2 ms around the peak current following stimulation. At least 120 acceptable trials were collected per cell, and up to 600 trials were collected for cells with low P_R. Trials in which spontaneous release obscured the detection of post-synaptic events were discarded. A double Gaussian fit was applied to histograms of EPSC amplitudes for each cell and used to estimate the number of successes and failures. For all cells, release events were also detected manually by visual inspection, which resulted in good agreement with Gaussian fits. In rare cases, histograms of evoked responses contained two peaks, and were discarded. In order to determine PPR, all trials were averaged and the PPR was measured from the averaged trace as the peak amplitude of the second EPSC divided by the peak amplitude of the first. The potency was determined by averaging all trials in which there was a successful release event on the first stimulus and measuring the peak amplitude of the first EPSC.

Experimental Design and Statistical Analysis: Facilitation curves and AR were averaged across cells and fit with a single exponential and offset of the form: PPR = ($c + Ae^{-(t-t0)/\tau}$) or release = ($c + Ae^{-(t-t0)/\tau}$). For facilitation curves, the offset was set to 1, and t_0 was the smallest interstimulus interval (10 ms for 25°C, 5 ms for 35°C). For AR, t_0 was taken as the time when individual events could first be detected following synchronous release (9 ms following stimulation for experiments at 25°C, 5 ms for experiments at 35°C). In all cases data were well-fit by single exponentials (R^2>0.95). Once single exponential fits were obtained, permutation tests were used to determine whether fit coefficients between wildtype and Syt7 KO were significantly different (Quinn and Keough, 2002). Wildtype and Syt7 KO

data were randomly assigned to two groups and the averages were fit with the above equations. The residuals, or the differences between the fit coefficients between the two groups ($A_1 - A_2$; $\tau_1 - \tau_2$), were collected. This process was repeated 10,000 times to generate a distribution of residuals. The difference between observed, unpermutated, wildtype and Syt7 KO data was then compared to the generated distribution. A p-value was obtained as the number of generated residuals greater than the observed difference, with $p < 0.01$ considered significant.

For imaging experiments, results were compared using two-tailed unpaired student's t-tests. For paired grC to PC recordings, the distributions of P_R, PPR, and potency were compared between wildtypes and Syt7 KOs using a two-sample Kolmogorov-Smirnov test. The distributions of mEPSC amplitudes and mEPSC frequencies were compared between wildtypes and Syt7 KOs using two-sample Kolmogorov-Smirnov tests.

Immunohistochemistry: P21 female mice were anesthetized with ketamine/xylazine (100/10 mg/kg) and perfused transcardially with phosphate buffered saline (PBS) followed by 4% paraformaldehyde (PFA) in PBS. The brain was removed and kept in PFA overnight. Transverse sections of the cerebellum (50 μm) were permeabilized using 0.2% triton X-100 in PBS for 10 min and blocked with 4% Normal Goat Serum in 0.1 % triton X-100 for 1 hour at room temperature. Slices were incubated overnight at 4°C with primary Syt7 antibodies (Mouse anti-Syt7 targeting the C2A domain, UC Davis/NIH NeuroMab Facility, clone N275/14, RRID: AB_11030371, 1 μg/mL, 1:100). Following overnight incubation with Syt7 antibodies VGLUT1 primary antibodies (Guinea-pig anti-VGLUT1, Synaptic Systems 135304, 1 μg/mL, 1:1600) were applied alone for 2 hrs at room temperature in order to reduce background. Slices were then incubated with secondary antibodies for 2 hrs at room temperature (anti-Guinea-pig-AlexaFluor488, Abcam ab150185; anti-Mouse-AlexaFluor647, Abcam ab150115). All tissue was stained and processed in parallel. Z-Stacks of lobule VI along the vermis were collected using an Olympus Fluoview1000 confocal microscope. Images were collected using the same settings, and processed identically in ImageJ.

Results

Syt7 is present in the molecular layer of the cerebellum

We used immunohistochemistry to determine whether Syt7 is expressed in parallel fibers of the cerebellum. In transverse sections of the cerebellum, grCs give rise to parallel fibers that traverse the slice while PC and SC dendrites are oriented orthogonally into the slice (**Figure 4.1A**). Due to the preservation of parallel fibers, this orientation was used for both anatomy and physiology experiments. grCs form glutamatergic synapses onto both PCs and SCs in the molecular layer of the cerebellum and express VGLUT1. In wildtype animals Syt7 labeling was prominent in the molecular layer where VGLUT1-expressing grC synapses are enriched (**Figure 4.1B, C**). Syt7 labeling was weak in KO animals, whereas the expression of VGLUT1 in grC synapses was comparable.

Facilitation and asynchronous release are strongly attenuated in Syt7 KO animals

We examined synaptic facilitation by stimulating with pairs of stimuli separated by different interstimulus intervals. The resulting synaptic currents evoked for different interstimulus intervals are shown for the grC to PC synapse for wildtype animals (**Figure 4.2A, top**) and for Syt7 KO animals (**Figure 4.2A, middle**) and the average paired pulse facilitation curves for many cells are shown (**Figure 4.2A, bottom**). The facilitation curves were fit to the equation ($1 + Ae^{-(t-t0)/\tau}$) where A is the amplitude of facilitation and τ is the time constant of facilitation. The magnitude and time constant of facilitation were reduced, respectively, from 2.12 ± 0.04 to 1.02 ± 0.06 and from 85 ± 5 ms to 46 ± 7 ms in Syt7 KO mice. Similar experiments were performed at the grC to SC synapse (**Figure 4.2B**), and the magnitude and time constant of facilitation were reduced, respectively, from 1.52 ± 0.07 to 0.67 ± 0.08 and from 132 ± 20 ms to 35 ± 10 ms in Syt7 KO mice. The decreases in amplitudes and time constants of facilitation were statistically significant ($p<0.01$, permutation test, see methods). These results indicate that Syt7 mediates most of the facilitation at these synapses, but there is also a Syt7-independent mechanism that mediates shorter-lived facilitation in Syt7 KO mice.

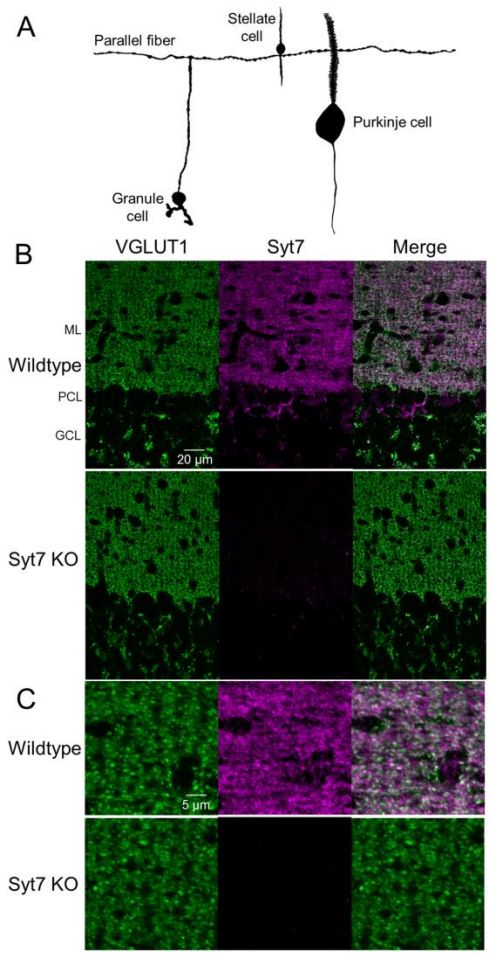

Figure 4.1. Immunohistochemical localization of Synaptotagmin-7 in the cerebellar cortex.

A. Parallel fibers originate from granule cells and extend laterally in transverse sections, forming synapses onto stellate and Purkinje cells in the cerebellar cortex (vermal lobule VI). The stellate cell and Purkinje cell dendrites are oriented perpendicular to the surface of the slice.

B. Transverse sections of cerebellar cortex immunolabelled for the presynaptic marker VGLUT1 (green) and Syt7 (magenta) in a wildtype (top) and Syt7 KO (bottom). ML: molecular layer; PCL: Purkinje cell layer; GCL: granule cell layer.

C. Expanded view of the molecular layer for the images in B.

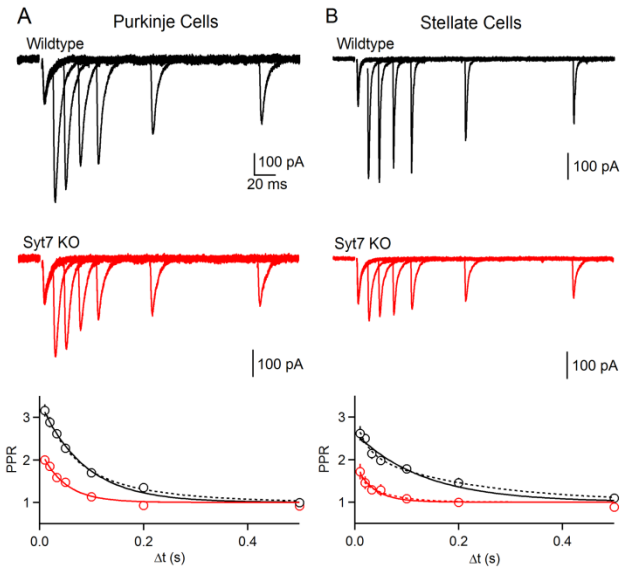

Figure 4.2. Facilitation is strongly attenuated in Syt7 KO animals at synapses made by granule cells onto Purkinje cells and stellate cells.

Paired-pulse facilitation in wildtype and Syt7 KO mice.

A. Representative paired-pulse facilitation at the grC to PC synapse in wildtype (top) and Syt7 KO (middle). Paired pulse ratio (PPR) as a function of interstimulus interval (Δt) is summarized (bottom) for wildtype (n = 9) and Syt7 KOs (n = 10). Fits to single (solid) and double (dashed) exponential fits are shown.

B. Same as in A, but at grC to SC synapses for wildtype (n = 6) and Syt7 KO (n = 7). Data are mean ± SEM. For some points error bars are occluded by markers.

The observation that PPR decays more rapidly in Syt7 KO animals than in wildtype animals raises the question as to whether facilitation is normally mediated by 2 processes with different time courses in wildtype animals:

$$PPR = 1 + A_{fast}e^{-(t-t0)/\tau_{fast}} + A_{slow}e^{-(t-t0)/\tau_{slow}}, \qquad (1)$$

and for Syt7 KO animals the slow component is selectively eliminated and facilitation is mediated only by the fast component,

$$PPR = 1 + A_{fast}e^{-(t-t0)/\tau_{fast}}. \qquad (2)$$

A fit to equation 1 for the average PPR in grC to PC synapses in wildtype animals yielded constants $\{A_{fast}, \tau_{fast}, A_{fast}, \tau_{slow}\}$ of {1.12, 47 ms, 1.04, 147 ms}, and a for a fit to equation 2 for PPR in Syt7 KO animals $\{A_{fast}, t_{fast}\}$ are {1.02, 47 ms}. The similarity of A_{fast} and τ_{fast} for wildtype and Syt7 KO would seem to suggest that PPR is a consequence of a fast and a slow component in wildtype animals, and that the slow component is eliminated selectively in Syt7 KO animals. However, the double exponential fit is essentially indistinguishable from the single exponential fit (Figure 4.2A) and both are good fits to the data (R^2 >0.95) making it unclear whether a double exponential fit is more appropriate. Moreover, the 4 free parameters of the double exponential fits cannot be precisely estimated because there are only 7 points. Thus, we conclude that the faster decay of facilitation in Syt7 KO animals is compatible with either an acceleration of a single exponential decay, or with the selective elimination of a slow component of facilitation.

Synaptic facilitation can be reduced either as a direct effect on the mechanism of facilitation, or indirectly by increasing the probability of release (P_R). Previous studies indicated that the initial P_R is not altered at the CA3 to CA1 synapse in Syt7 KO animals (Jackman et al., 2016). At that synapse P_R was assessed with input/output curves and with the use-dependent block of NMDARs by MK801. These approaches are more difficult to apply at grC synapses. Input/output curves are highly sensitive to slice orientation for grC parallel fibers, and use-dependent blockade by MK-801 is impractical because at this age PCs do not express NMDARs and the NMDAR component in SCs is extremely small. Most grCs

form a single contact onto SCs and PCs, allowing a measure of release from single putative release sites. Given the extremely low connection probability between grCs and SCs, we therefore determined if initial P_R was altered by determining the properties of single grC to PC connections (**Figure 4.3**). We stimulated single grCs using brief voltage steps in a cell-attached configuration that also allowed us to detect the presynaptic action potential. We targeted grCs at least 150 μm lateral from the PC (**Figure 4.3A**), which provide parallel fiber inputs to PCs that consist of single contacts. grC stimulation generated artifacts in the PC that were followed by synaptic currents in some trials, and by failures in others (**Figure 4.3B, C**). Successes and failures were evident as two distinct distributions in the histogram of the response amplitudes (**Figure 4.3C**), and the fraction of trials in which release was detected was used as a measure of P_R. There was considerable variability in the magnitude of P_R, but there was no significant difference between the initial P_R between wildtype and Syt7 KOs (**Figure 4.3G**, *left*, wildtype: 0.44 ± 0.06, n = 19; Syt7 KO: 0.48 ± 0.05 n = 17; p = 0.80, K-S test). There was also no difference in the potency, or the amplitude of successful events, between wildtypes and Syt7 KOs (wildtype: 16.9 ± 2.8 pA, n=19; Syt7 KO: 14.4 ± 2.4 pA, n=17; p = 0.32, K-S test). This suggests that differences in facilitation are not a secondary consequence of alterations in the initial P_R at grC to PC synapses.

We also examined facilitation at synapses between individual grCs and PCs in order to provide additional insight into the mechanism of facilitation. Average synaptic responses evoked by pairs of stimuli are shown for synapses with a low initial P_R (**Figure 4.3D**) and high P_R (**Figure 4.3E**) for both wildtype and Syt7 KO animals. For wildtype animals, facilitation was variable but was generally larger at synapses with low initial P_R, as illustrated by plotting PPR as a function of P_R and fitting to a line, with $PPR=(1+2.65)-2.41*P_R$ (**Figure 4.3F**, left; $R^2 = 0.34$). The more prominent facilitation at low initial P_R synapses is consistent with more severe vesicle depletion at high P_R synapses (Zucker & Regehr, 2002). Facilitation in Syt7 KO animals is also variable and dependent on P_R, but it is less steeply dependent upon P_R than for wildtype animals, with $PPR=(1+1.39)-0.97*P_R$ (**Figure 4.3F**, right; $R^2 = 0.16$). Facilitation (PPR-1) was significantly reduced in Syt7 KOs (**Figure 4.3G**, *right*, wildtype: 1.58 ± 0.23, n=19; Syt7 KO: 0.93 ± 0.12, n=17; p<0.01 K-S test).

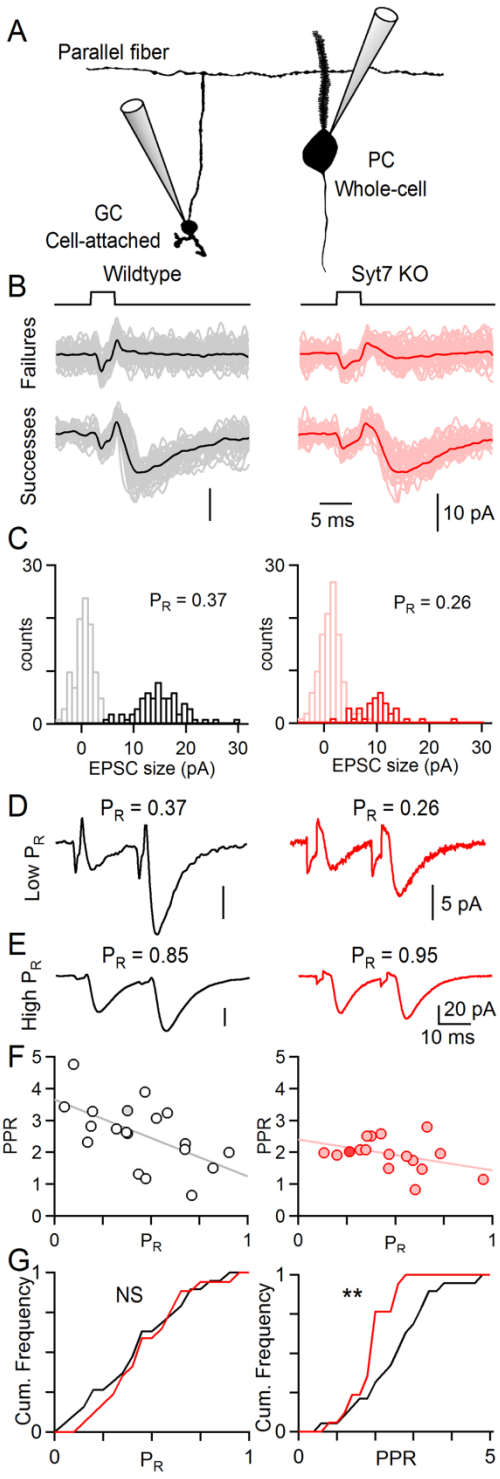

Figure 4.3. The probability of release at single granule cell to Purkinje cell synapses is unaltered in Syt7 KO animals. Cell-attached recordings were used to stimulate single grCs and PC responses were measured.

Figure 4.3 (Continued)

A. Experimental configuration. A single grC was stimulated in cell-attached mode and whole-cell responses were recorded in PCs at least 150 μm away in the transverse plane.

B. Synaptic currents evoked by a voltage step to a grC cell body (upper) were recorded in PCs. Averaged synaptic responses of failed and successful release events for wildtype (left) and Syt7 KOs (right). Voltage steps applied to grCs generated a small stimulus artifact preceding synaptic currents.

C. Histogram of response amplitudes for pairs shown in B. P_R was calculated as the fraction successes.

D. Averaged synaptic currents evoked by two stimuli (20 ms) for cells from wildtype and Syt7 KO animals shown in B, C.

E. Example of averaged synaptic currents at grC to PC pairs that had high initial P_R.

F. All grC to PC pairs plotted by PPR vs. P_R for wildtypes (left, n = 19) and Syt7 KOs (right, n = 17) with linear fits. Filled markers indicate cells shown in B-D.

G. Cumulative histograms of P_R (left) and PPR (right) for all paired recordings.

Facilitation at individual synapses showed the same trend as the facilitation evoked by extracellular stimulation of many parallel fibers (**Figure 4.2**, 2.12 for wildtype animals and 1.02 for Syt7 KO animals for an interstimulus interval of 20 ms), but facilitation for individual sites was slightly smaller than extracellular stimulation. This may reflect the contribution of individual synapses that have a very low initial P_R (<0.1). In paired recordings, such synapses are expected to be difficult to identify, and have large facilitation, particularly in wildtype animals. We found several such synapses in which postsynaptic currents could be detected only by evoking a brief burst in a grC, but events following the first stimulus were too infrequent to be quantified to measure P_R. As P_R could not be measured, these cells were not included in the analysis. It is therefore expected that difficulty in detecting very low P_R synapses could have increased average P_R and reduced the average PPR of paired recordings.

We also examined the role of Syt7 in AR by comparing AR in wildtype and Syt7 KO animals. Previous studies have shown that the properties of AR at grC to SC and grC to PC synapses are similar (Atluri and Regehr, 1998, Xu-Friedman and Regehr, 2000, Xu-Friedman and Regehr, 1999), but that it is much easier to quantify AR in SCs because quantal events are large, rapid and readily detected and there is much less noise and spontaneous activity compared to PCs. We therefore studied asynchronous release at grC to SC synapses. AR at this synapse consists of a prominent fast component and a much smaller slow component (Atluri & Regehr 1998). Here we focus on the fast component of AR. In wildtype animals a single stimulus evoked an average EPSC with rapid kinetics (**Figure 4.4A**). When individual trials were examined on an expanded vertical axis individual quantal events were apparent (**Figure 4.4B**) that could be detected and quantified (**Figure 4.4C**). The high release rates associated with synchronous release made it impractical to detect quantal events closely time-locked to stimulation (grey region in **Figure 4.4B, C**). The AR in wildtype animals (**Figure 4.4D**) had a time constant of 6.2 ± 0.4 ms. In Syt7 KO animals, the average EPSC (**Figure 4.4A**) was qualitatively similar to that observed in wildtype animals. However, as shown in individual trials (**Figure 4.4B, C**) AR was strongly attenuated in Syt7 KOs. A summary of AR in KOs indicates that compared to wildtype animals the magnitude of AR is reduced to approximately 44% ($p<0.01$, permutation test) and the time constant of decay following a

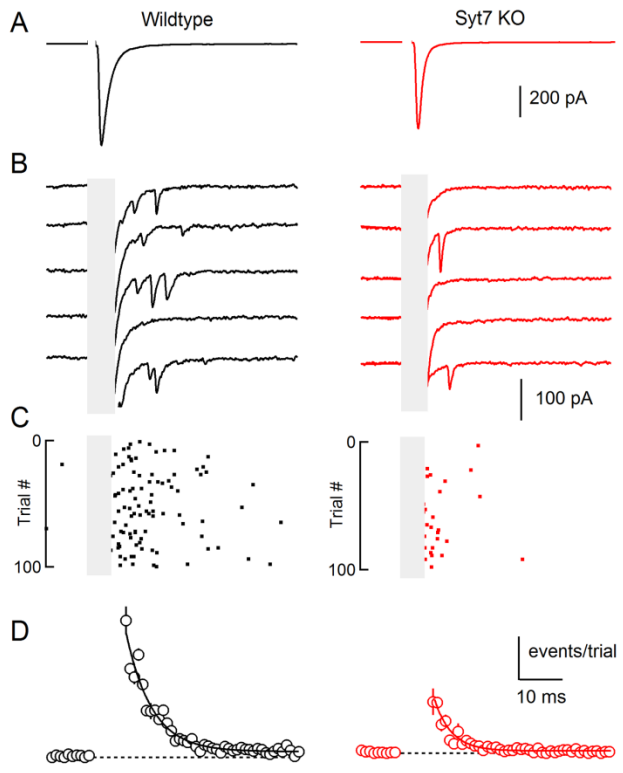

Figure 4.4. Asynchronous release at the granule cell to stellate cell synapse is mediated primarily by Syt7.

A. Extracellular activation of grC parallel fibers with single stimuli evoked synaptic responses in SCs: the average EPSC (100 trials) showed a large prominent synchronous component in both wildtypes (left) and Syt7 KOs (right).

B. Asynchronous quantal events were apparent in individual trials (stimulus artifact and synchronous EPSC has been blanked).

C. Raster plot of quantal events for all trials for cells shown in A and B.

D. The time course and amplitude of quantal events evoked by single stimuli summarized across cells for wildtypes (n = 17, left) and Syt7 KOs (right, n = 10). Data are mean ± SEM. For some points error bars are occluded by markers.

single stimulus significantly decreased from 6.2 ± 0.1 ms for wildtype animals to 4.0 ± 0.1 ms for Syt7 KO animals ($p<0.01$, permutation test). On average the total number of asynchronous events was reduced to 31% in Syt7 KOs. The reduction in asynchronous events could not be accounted for by changes in quantal size because we found no differences in mEPSC amplitude in SCs, which receive their glutamatergic inputs exclusively from parallel fibers (Wildtype: 66.9 ± 2.2 pA, n = 18; Syt7 KO: 61.8 ± 3.4 pA, n = 8; K-S test, p = 0.49). We also did not observe differences in mEPSC frequency (Wildtype: 0.43 ± 0.12 Hz, n = 18; Syt7 KO: 0.30 ± 0.05 Hz, n = 8; K-S test, p = 0.35). Thus, just as for synaptic facilitation, AR at the grC to SC synapse is primarily mediated by Syt7.

Presynaptic Ca^{2+} signaling in granule cells is unaltered in Syt7 KO animals

Facilitation and AR at the grC to PC and SC synapses is Ca^{2+} dependent (Atluri and Regehr, 1996a), and it is possible that changes in presynaptic Ca^{2+} could alter facilitation and AR in Syt7 KO animals. We compared presynaptic Ca^{2+} signals in wildtype and Syt7 KO animals by using the low affinity fluorescent Ca^{2+} indicator Mg green (**Figure 4.5A**), as has been used extensively to characterize presynaptic Ca^{2+} signals in cerebellar parallel fibers (Dittman and Regehr, 1997, Regehr and Tank, 1991, Sabatini and Regehr, 1995, Safo and Regehr, 2005, Xu-Friedman and Regehr, 1999). This approach relies on labeling many parallel fibers with a small amount of indicator and recording Ca^{2+}-dependent fluorescence transients from many presynaptic boutons. This has been a useful approach to characterize presynaptic Ca^{2+} entry because low levels of indicator can be used to avoid significant perturbation of presynaptic Ca^{2+} signals (Dittman and Regehr, 1997, Sabatini and Regehr, 1995, Safo and Regehr, 2005). We have also previously shown that low affinity Ca^{2+} indicators provide a good measure of the time course of presynaptic Ca^{2+} signals (Regehr and Atluri, 1995, Kreitzer et al., 2000). We found that the time courses of Ca^{2+} signals evoked by single stimuli were similar in wildtype and Syt7 KO animals (wildtype: $t_{□□□}$ = 18.1 ± 1.4 ms, n = 6; Syt7 KO: $t_{□□□}$ = 16.4 ± 0.4 ms, n = 6; unpaired two-tailed Student's t-test, t(10) = 1.12, p = 0.29). We used trains of 5 stimuli at 50 Hz to determine whether there could be changes in Ca^{2+} signals between stimuli (**Figure 4.5B**), but found that ratio of the first and second stimuli were

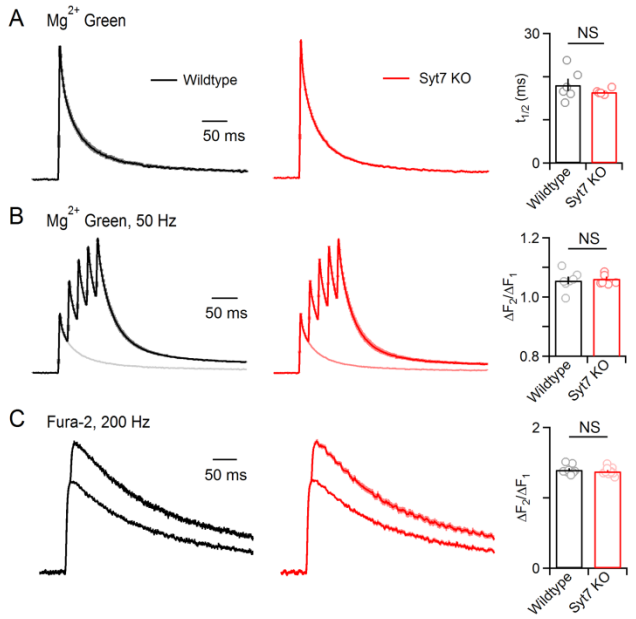

Figure 4.5. Presynaptic Ca^{2+} signaling is unaltered in Syt7 KO animals.

A. Parallel fibers were loaded with the low affinity Ca^{2+} indicator Mg-Green-AM (K_d = 7 µM for Ca^{2+}), and stimulated. Ca^{2+}-dependent presynaptic fluorescence changes are shown for average wildtype (black) and Syt7 KO animal (red). The half decay time was measured and summarized (right; Wildtype n = 6, Syt7 KO n = 6).

B. Same as in A, but for brief stimulus trains (5 stimuli at 50 Hz). Averages are shown for wildtype and Syt7 KOs (left) with single stimuli overlaid. The ratio between the amplitude of the first and second transient in the train are summarized (right; Wildtype n = 7, Syt7 KO n = 6).

Parallel fibers were labeled with the high affinity Ca^{2+} indicator Fura-2-AM (K_d = 0.2 µM) and responses were evoked by 1 and 2 stimuli. Averages are shown for a wildtype (black) and Syt7 KO (red). The ratio of the amplitudes of the responses evoked by 2 stimuli and one stimulus provides a measure of the magnitude of presynaptic Ca^{2+} entry, and is summarized (right; Wildtype n = 9, Syt7 KO n = 10). Traces are normalized to peak values evoked by a single stimulus. Data are mean ± SEM.

similar in wildtype and Syt7 KO animals (wildtype: $\tau F2/\tau F1 = 1.06 \pm 0.01$, n = 7; Syt7 KO: $\tau F2/\tau F1 = 1.06 \pm 0.1$, n = 6; unpaired two-tailed Student's t-test, t(10) = -0.43, p = 0.68).

It difficult to use low affinity Ca^{2+} indicators to quantify the magnitude of presynaptic Ca^{2+} signals because fluorescence changes are proportional to both the number of activated fibers, and to the size of the presynaptic Ca^{2+} signal in each fiber (Regehr and Atluri, 1995). However, high affinity Ca^{2+} indicators such as fura-2 can be used to estimate the amplitude of presynaptic Ca^{2+} entry (**Figure 4.5C**). This approach relies on the observation that Ca^{2+} entry for each of two closely spaced stimuli is similar (Regehr and Atluri, 1995, Kreitzer et al., 2000), but the second stimulus produces a smaller increase in fura-2 fluorescence (Sabatini and Regehr, 1995, Chen and Regehr, 1997). This is because the first stimulus produces such large Ca^{2+} signals that most of the fura-2 binds Ca^{2+}, and there is a less unbound fura-2 present for the second stimulus. If the presynaptic Ca^{2+} entry evoked by a single pulse is increased, then less fura-2 is available to respond to the second stimulus and $\Delta F_2/\Delta F_1$ decreases (Sabatini and Regehr, 1995). We found, however, that $\Delta F_2/\Delta F_1$ was not different in wildtype and Syt7 KO animals (wildtype: $\tau_{F2/F1} = 1.40 \pm 0.02$, n = 9; Syt7 KO: $\tau F2/F1 = 1.38 \pm 0.02$, n = 10; unpaired two-tailed Student's t-test, t(17) = 0.77, p = 0.45). We also used a related approach and measured the maximal change in fluorescence (F_{max}) and determined $\Delta F_1/\Delta F_{max}$, which provides another measure of the magnitude of presynaptic Ca^{2+} signals (Maravall et al., 2000). There was also no significant change in $\Delta F_1/\Delta F_{max}$ (wildtype: $\tau F1/F_{max} = 0.32 \pm 0.02$, n = 9; Syt7 KO: $\tau F1/F_{max} = 0.32 \pm 0.01$, n = 10; unpaired two-tailed Student's t-test, t(17) = -0.05 p = 0.96). Thus, we conclude that differences in facilitation and AR in Syt7 KO animals and wildtype animals are not a consequence of alterations in presynaptic Ca^{2+} signaling.

The Sr^{2+} dependence of asynchronous release

AR is often studied by replacing extracellular Ca^{2+} with Sr^{2+}, which increases the amplitude and time course of AR while attenuating the amplitude of synchronous release (Goda and Stevens, 1994, Bekkers, 2003, Calakos et al., 2004, Dodge et al., 1969, Searl and Silinsky, 2002, Shin et al., 2003, Yang

and Xu-Friedman, 2010, Zengel and Magleby, 1980, Zhao et al., 2006, Babai et al., 2014). We therefore examined the properties of AR in wildtype and Syt7 KO animals in the presence of Sr^{2+}. Prior to determining the properties of AR in the presence of Sr^{2+} we measured presynaptic Sr^{2+} signals in wildtype and Syt7 KO animals using an established approach ((Xu-Friedman and Regehr, 1999, Xu-Friedman and Regehr, 2000), see methods). Presynaptic Sr^{2+} signals are larger and longer lasting than presynaptic Ca^{2+} signals in wildtype animals (**Figure 4.6A**), which is a consequence of less effective presynaptic buffering and extrusion of Sr^{2+} relative to Ca^{2+} (Xu-Friedman and Regehr, 1999, Xu-Friedman and Regehr, 2000). Presynaptic Sr^{2+} signals were the same in wildtype and Syt7 KO animals (**Figure 4.6A**), indicating that any differences in AR occurs downstream of Sr^{2+} signaling. Changing from external Ca^{2+} to Sr^{2+} reversibly attenuated the synchronous EPSC amplitude, and increased the magnitude and duration of AR in both wildtype and Syt7 KO animals (**Figure 4.6B**). AR was more prominent in the presence of Sr^{2+} than in the presence of Ca^{2+} (**Figure 4.6C-E**). A comparison of the AR evoked in the presence of Sr^{2+} in wildtype and Syt7 KO animals revealed an approximately 2- to 3-fold reduction in AR in Syt7 KO mice (**Figure 4.6F** right, *squares,* **Table 4.1**). These findings establish that just as for AR mediated by Ca^{2+}, most AR mediated by Sr^{2+} relies on Syt7, but a component of AR remains even when Syt7 is eliminated.

The dependence of facilitation on residual Ca^{2+}

It has previously been shown that the slow Ca^{2+} chelator EGTA can be used to accelerate the decay of residual Ca^{2+} in grC presynaptic boutons (Atluri and Regehr, 1996a). This in turn decreased the amplitude and accelerated the decay of facilitation and AR, and established that these phenomena depend upon residual Ca^{2+}. Facilitation was not completely eliminated by even the highest concentration of EGTA-AM used. This suggested that this component of facilitation might be driven by high local Ca^{2+} rather than residual Ca^{2+}, or that it involved a different mechanism. We therefore assessed whether the remaining facilitation in Syt7 KO mice is also sensitive to EGTA using bath application of EGTA-AM in wildtype and Syt7 KO animals. We used a concentration of EGTA-AM (20 μM) that accelerates the decay but does not affect the peak of Ca^{2+} transients in parallel fibers (Atluri and Regehr, 1996a). In

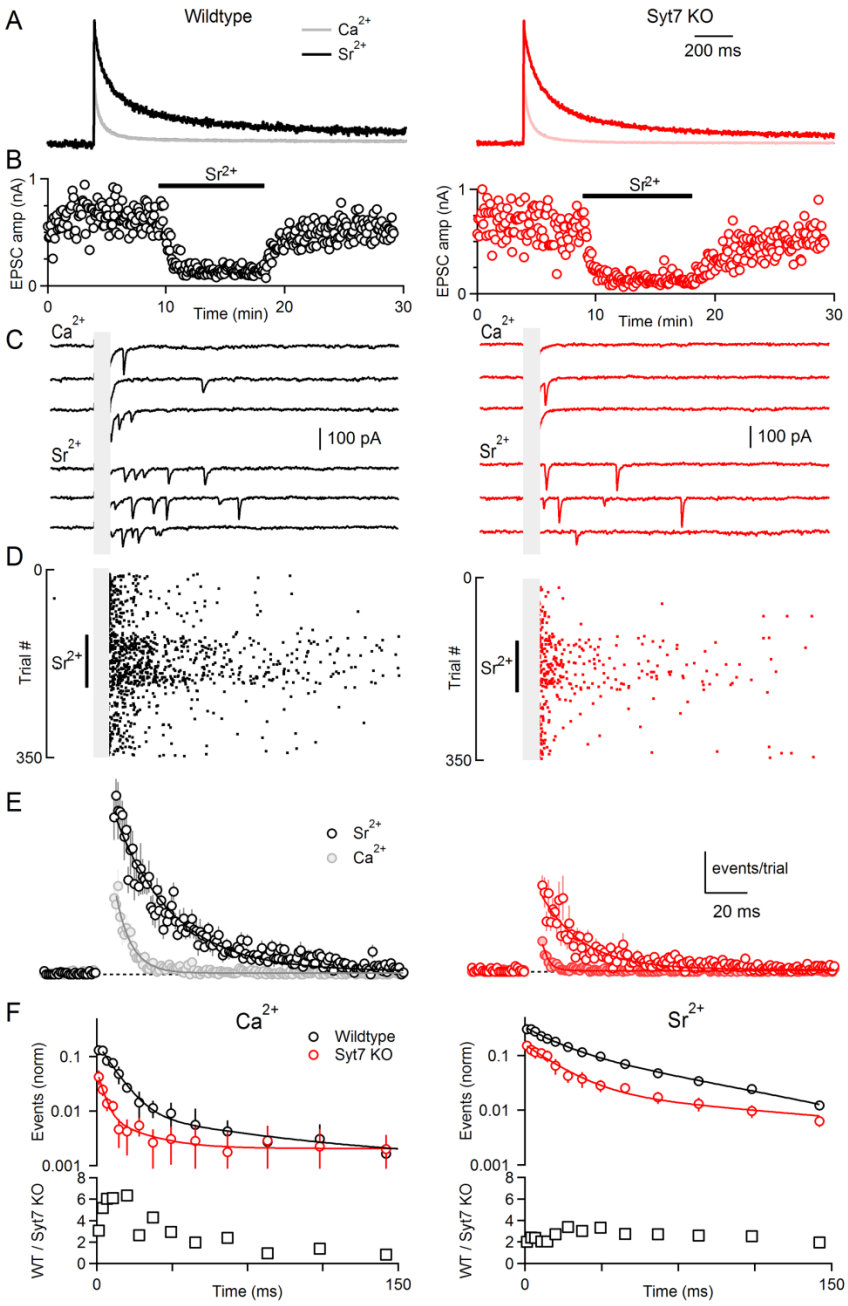

Figure 4.6. The Sr^{2+} dependence of asynchronous release in wildtype **and Syt7 KO animals.**

A. Presynaptic divalent levels were measured in the presence of extracellular Ca^{2+} and extracellular Sr^{2+} using Mg-Green in wildtype and Syt7 KO animals as described in the methods.

B. Synaptic currents were evoked by single stimuli in the presence of external Ca^{2+} and Sr^{2+} and peak EPSC amplitudes are shown as a function of time for representative cells.

C. Example traces from cells shown in B in the presence of Ca^{2+} and Sr^{2+}.

Figure 4.6 (Continued)

D. Raster of quantal events shown during the application and washout of Sr^{2+} for example cells shown in B-C.

E. Summary of delayed events evoked by single stimuli in the presence of Ca^{2+} and Sr^{2+} for wildtype (n = 7) and Syt7 KO mice (n = 7).

F. Left: The frequency of quantal events in the presence of Ca^{2+} is shown as a function of time for wildtype (upper graph, black) and Syt7 KO animals (upper graph, red) in a semi-logarithmic plot with logarithmic binning. A point-by-point ratio of the rate of events of wildtype to Syt7 KO animals is plotted in the lower graph. Right: similar analysis but for events in the presence of Sr^{2+}. Data are mean ± SEM. For some points error bars are occluded by markers.

Table 4.1: Fit parameters for average paired-pulse facilitation and asynchronous release

Figure	Expt.	Cell type	Conditions	Genotype	*A*	τ (ms)	*c*
4.2	PPR	PC	2 Ca, 25°C	Wildtype	2.12 ± 0.04	85 ± 5	1
4.2	PPR	PC	2 Ca, 25°C	Syt7 KO	1.02 ±0.06	46 ± 7	1
4.2	PPR	SC	2 Ca, 25°C	Wildtype	1.52 ± 0.07	132 ± 20	1
4.2	PPR	SC	2 Ca, 25°C	Syt7 KO	0.67 ± 0.08	35 ± 10	1
4.4	AR	SC	2 Ca, 25°C	Wildtype	0.122 ± 0.005	6 ± 1	0.005 ± 0.002
4.4	AR	SC	2 Ca, 25°C	Syt7 KO	0.054 ± 0.003	4 ± 1	0.002 ± 0.001
4.6	AR	SC	2 Sr, 25°C+Sr	Wildtype	0.272 ± 0.003	28 ± 1	0.006 ± 0.001
4.6	AR	SC	2 Sr, 25°C+Sr	Syt7 KO	0.131 ± 0.003	20 ± 1	0.004 ± 0.003
4.7	PPR	PC	2 Ca, 25°C +EGTA	Wildtype	1.21 ± 0.08	49 ± 9	1
4.7	PPR	PC	2 Ca, 25°C +EGTA	Syt7 KO	0.51 ± 0.09	22 ± 9	1
4.8B	PPR	PC	1.5 Ca, 35°C	Wildtype	1.78 ± 0.06	64 ± 6	1
4.8B	PPR	PC	1.5 Ca, 35°C	Syt7 KO	0.866 ± 0.033	17 ± 2	1
4.8F	AR	SC	1.5 Ca, 35°C	Wildtype	0.090 ± 0.002	4 ± 1	0.001 ± 0.001
4.8F	AR	SC	1.5 Ca, 35°C	Syt7 KO	0.033 ± 0.001	3 ± 1	0.002 ± 0.001

wildtypes we found after exposure to EGTA-AM the magnitude of facilitation was reduced to 57% of control (Control: A = 2.12 ± 0.04; EGTA: A = 1.21 ± 0.08; $p<0.01$, permutation test) and time constant of decay was reduced to 57% of control (Control: $\tau = 85 \pm 5$ ms; EGTA: $\tau = 49 \pm 9$ ms; $p<0.01$, permutation test) (**Figure 4.7A, B**). In Syt7 KOs EGTA-AM reduced the magnitude of facilitation to 50% of control (Control: A = 1.02 ± 0.06; EGTA: A = 0.51 ± 0.09; $p<0.01$, permutation test) and the time constant of decay to 48% of control (Control: $\tau = 46 \pm 7$ ms; EGTA: $\tau = 22 \pm 9$ ms; $p<0.01$, permutation test) (**Figure 4.7C, D**). These findings suggest that the component of facilitation that remains in Syt7 KO animals has approximately the same Ca^{2+} dependence as the facilitation present in wildtype animals. We did not examine the effect of EGTA on AR in Syt7 KO animals because AR is exceedingly small and the decay is very rapid.

Facilitation and asynchronous release in physiological conditions

Our studies thus far have been performed at room temperature in the presence of 2 mM external Ca^{2+}, which are the conditions of most previous studies of facilitation and AR at these synapses. It is known that presynaptic waveform, presynaptic Ca^{2+}signaling, and neurotransmitter release are highly dependent on temperature and external Ca^{2+} levels. This raises the possibility that the contribution of Syt7 to synaptic transmission, AR and facilitation could be different under physiological conditions. We therefore extended our studies to more physiological conditions (35°C, and 1.5 mM external Ca^{2+}). Under these conditions in wildtype animals, facilitation at the grC to PC synapse was prominent and decayed slightly faster than at room temperature ($\tau = 63$ ms). In Syt7 KO animals the amplitude of facilitation was significantly smaller (wildtype: A = 1.78 ± 0.06; Syt7 KO: A = 0.87 ± 0.03, $p<0.01$, permutation test) and faster (wildtype: $\tau = 64 \pm 6$ ms; Syt7 KO: $\tau = 17 \pm 2$ ms; $p<0.01$, permutation test) (**Figure 4.8A, B**). The accelerated decay of facilitation in Syt7 KO animals is particularly obvious under these experimental conditions. A fit to equation 1 for PPR in wildtype animals yielded constants $\{A_{fast}, \tau_{fast}, A_{fast}, \tau_{slow}\}$ of {0.44, 15 ms, 1.40, 85 ms}, and a for a fit to equation 2 for PPR in Syt7 KO animals $\{A_{fast}, t_{fast}\}$ are {0.87, 17 ms}. It is difficult to precisely estimate the parameters of the double exponential fit, and as for

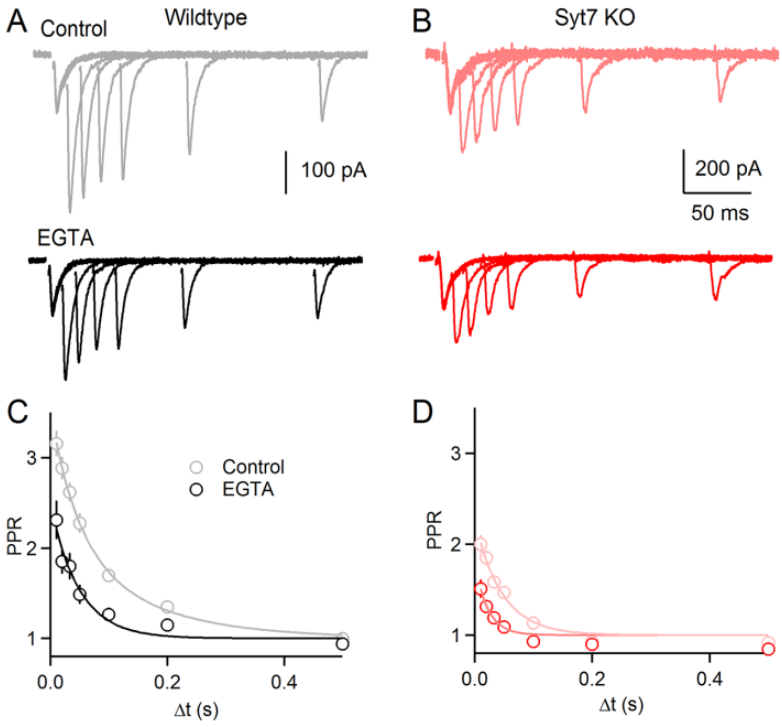

Figure 4.7. Facilitation in wildtype and Syt7 KO animals is dependent on residual Ca^{2+}.

A. Paired pulse facilitation for a representative PC shown before (control, gray) and after bath application of EGTA-AM (20 µM for 15 minutes, bottom, black).

B. Same as in A, but for a Syt7 KO.

C. Summary of the effect of EGTA on paired pulse facilitation in wildtype grC to PC synapses (control: n = 17; EGTA: n = 8).

D. Same as in C, but for Syt7 KOs (control: n = 11; EGTA: n = 9). Data are mean ± SEM. For some points error bars are occluded by markers.

room temperature experiments the faster decay of facilitation in Syt7 KO animals is compatible with either an acceleration of a single exponential decay or with the selective elimination of a slow component of facilitation.

We also studied AR under these experimental conditions at the grC to SC synapse. In wildtype animals, AR was less prominent and decayed more rapidly than in room temperature experiments (**Figure 4.8C-F**). As at room temperature and 2 mM external Ca^{2+}, AR was dominated by a rapid component that could be well described by a single exponential fit. Under near physiological conditions, AR was reduced to 30% in Syt7 KOs ($p<0.01$, permutation test). Differences in time course of AR were not statistically significant (wildtype: $\tau = 3.8 \pm 0.1$ ms; Syt7 KO: $\tau = 2.8 \pm 0.1$ ms; $p = 0.50$, permutation test), although there was a trend towards an accelerated decay. These studies indicate that the qualitative contribution of Syt7 to AR and facilitation are the same at 35°C in 1.5 mM external Ca^{2+} as at 24°C in 2 mM external Ca^{2+}. We find, however, that under physiological conditions AR is less prominent, and the Syt7-independent component of facilitation is very short-lived.

Discussion

Our primary finding is that Syt7 can mediate both AR and facilitation at the same synapses, even though AR is much shorter-lived and much more Ca^{2+} dependent than facilitation. Although most facilitation and AR at grC synapses is reliant on Syt7, they are also partially mediated by a Syt7-independent mechanism.

Syt7 mediates both facilitation and asynchronous release

Previous studies suggested that Ca_{res} produces both facilitation and AR, but it was not known whether the same Ca^{2+} sensor mediates both phenomena (Van der Kloot and Molgo, 1993, Zucker and Lara-Estrella, 1983), The observations that AR decays much more rapidly than facilitation, and that reducing extracellular Ca^{2+} strongly attenuates AR but increases facilitation, suggested that the mechanisms underlying these phenomena must differ (Atluri and Regehr, 1998). Nonetheless, here we show that despite these differences, Syt7 mediates both phenomena at the same synapses.

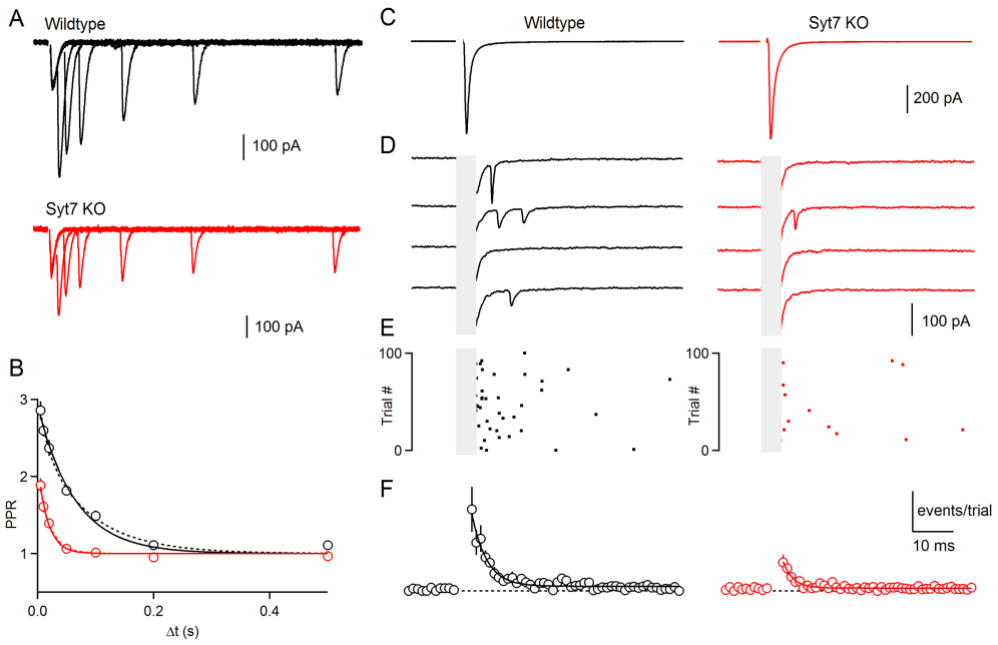

Figure 4.8. Facilitation and asynchronous release under physiological conditions in wildtype and Syt7 KO animals. Experiments were performed at 35°C in 1.5 mM external Ca^{2+}.

A. Paired-pulse facilitation in representative PCs for wildtype and Syt7 KO animals.

B. Summarized paired-pulse facilitation curves for wildtypes (n = 5) and Syt7 KOs (n = 5). Single (solid) and double (dashed) exponential fits are shown.

Asynchronous release was examined in wildtype and Syt7 KO animals (C-F)

C. Average evoked current by single stimuli in a representative wildtype SC.

D. Single stimuli evoked delayed events during single trials for cells shown in C. Synchronous component of the EPSC and stimulus artifact are blanked.

E. Raster plot of quantal events.

F. The time course and amplitude of quantal events evoked by single stimuli summarized across cells in wildtype (n = 9) and Syt7 KOs (n = 8). Data are mean ± SEM. For some points error bars are occluded by markers.

A recent model can qualitatively account for some aspects of the role of Syt7 in these two phenomena (Jackman and Regehr, 2017). According to this model, Syt1 and Syt7 bind to phospholipids in the presence of Ca^{2+}, reducing the energy barrier for vesicle fusion. For low frequency stimulation high local Ca^{2+} drives rapid synchronous release mediated entirely by Syt1 and does not activate Syt7 due to its high affinity and slow kinetics. Syt7 is instead activated after several milliseconds and this activation persists for tens of milliseconds. If both Syt1 and Syt7 are activated, as occurs for closely spaced stimuli, they lead to a slightly larger reduction in the energy barrier than for Syt1 alone, which leads to facilitation. AR could be produced by modest Syt1 activation for many milliseconds after an action potential acting in concert with Syt7 to produce AR.

This scheme provides a framework that accounts qualitatively for the roles of Syt7 in AR and facilitation, but it is highly speculative. Moreover, there are many unknown features that could also contribute to how Syt7 mediates facilitation and AR at different synapses. The precise location of Syt7 is important, but is not known. Syt7 is thought to be present on plasma membranes (Sugita et al., 2001), but its location relative to docked vesicles is unknown, and whether it might also be present at low levels in vesicles is difficult to rule out. The absolute level of Syt7 expression could also affect its function, and it is possible that AR and facilitation are differentially sensitive to Syt7 levels. Syt7 is alternatively spliced (Sugita et al., 2001, Fukuda et al., 2002), and it is possible that the relative expression of different splice variants could determine the extent of facilitation or AR. The manner in which Syt7 and Syt1 interact to produce facilitation is not known. Finally, the extent of interactions between Syt7 and other proteins has not been characterized. Further studies will be required to distinguish between these possibilities, and to determine how Syt7 can play diverse roles across many different synapses.

Syt7 and Facilitation

This study adds to the list of synapses in which facilitation is mediated primarily by Syt7. At multiple hippocampal synapses and at corticothalamic synapses, paired-pulse plasticity is entirely mediated by Syt7 (Jackman et al., 2016). At PC and vestibular synapses, Syt7 mediates facilitation that is normally masked by depression, but that is revealed during frequency step trains or when P_R is reduced

(Turecek et al., 2017). However, in contrast to other synapses, some facilitation remains at grC to PC and SC synapses in Syt7 KOs

Previous studies suggest that the presence of Syt7 in presynaptic boutons does not always result in obvious facilitation. In many instances a high initial P_R results in partial vesicle depletion that obscures facilitation (Turecek et al., 2016b, Lu and Trussell, 2016, Muller et al., 2010). This occurs at vestibular and PC synapses that depress in normal external Ca^{2+}, but Syt7-dependent facilitation is revealed in low external Ca^{2+} when the initial probability is reduced (Turecek et al., 2017). This could explain the apparent lack of facilitation for cultured synapses and the zebrafish neuromuscular junction, but post-synaptic mechanisms such as receptor desensitization could also obscure facilitation. It is more difficult to understand why Syt7 does not mediate facilitation at the calyx of Held even when the initial P_R is lowered (Luo and Sudhof, 2017). It is possible that Syt7 expression levels are not sufficiently high at the calyx of Held to facilitate release. It will be informative to compare Syt7 expression levels at the calyx of Held with synapses where the role of Syt7 in facilitation is well established.

Syt7 and Asynchronous Release

It has been shown that Syt7 can mediate the prominent AR observed when fast Synaptotagmin isoforms are eliminated (Bacaj et al., 2013), and asynchronous events during prolonged trains at the zebra fish neuromuscular junction (Wen et al., 2010). It has also been observed that at the calyx of Held prolonged high frequency trains evoke a Syt7-dependent tonic current that has been attributed to AR (Luo and Sudhof, 2017). Here we show that a single stimulus can trigger Syt7-dependent AR even in wildtype animals where fast Synaptotagmin isoforms are present. We also used Sr^{2+} to examine AR because it had been proposed that the Ca^{2+} sensor that mediates AR had a higher sensitivity to Sr^{2+} than to Ca^{2+}. However, we found that AR triggered by Sr^{2+} was mediated by both Syt7 and Syt7-independent mechanisms. This suggests that although Sr^{2+} is a useful tool to produce large and prolonged AR, it is not particularly helpful in identifying the Ca^{2+} sensor for AR.

AR is not a prominent feature of most synapses, even those containing Syt7. Why does Syt7 evoke AR at grC synapses but not at others? One possibility is that AR occurs, but is obscured for technical

reasons. In SCs, synchronous release is rapid, allowing the detection of delayed events several milliseconds after stimulation. In PCs evoked EPSCs and quantal events are much smaller and slower, which can obscure short-lived AR (Diamond and Jahr, 1995, Atluri and Regehr, 1998, Rudolph et al., 2011). Another factor is the Ca^{2+} signal seen by Syt7. AR is highly Ca^{2+}-sensitive (Atluri and Regehr 2008). Parallel fiber boutons have large residual Ca^{2+} signals that could be effective at promoting Syt7-mediated AR (Brenowitz and Regehr, 2007), whereas residual Ca^{2+} signals elsewhere may not be sufficiently large to promote AR (Delvendahl et al., 2015, Scott and Rusakov, 2006). An additional factor is the presence of fast Synaptotagmin isoforms that can prevent AR (Kochubey and Schneggenburger, 2011, Xu et al., 2007, Chen et al., 2017a). It is unclear whether this is a clamping effect in which Syt1/2 directly suppresses AR, or whether it reflects competition between sensors. More generally other presynaptic proteins may suppress AR, just as complexin and Syt1/2 suppress spontaneous vesicle fusion (Xu et al., 2007, Yang et al., 2010).

Syt7-Independent AR and Facilitation

The mechanisms responsible for the short-lived components of AR and facilitation present in Syt7 KO animals are not known. Whether these components are also present in wildtype animals, or are compensatory mechanisms only present in Syt7 KO animals is also not known. There are several candidate mechanisms that could mediate the short-lived Ca^{2+}-dependent facilitation present in Syt7 KO animals (Jackman and Regehr, 2017). The remaining facilitation is much smaller in amplitude and decays ~3 times more rapidly than facilitation in wildtype animals, and is EGTA-sensitive suggesting it is Ca^{2+}-dependent. The remaining component could be mediated by a Ca^{2+} sensor with more rapid kinetics than Syt7. Another possibility is Ca^{2+}-dependent facilitation of Ca^{2+} influx through P/Q-type Ca^{2+} channels (Cuttle et al., 1998, Borst and Sakmann, 1998). P/Q-type channels account for a large fraction of the Ca^{2+} channels in grC synapses (Mintz et al., 1995). Modest enhancement of Ca^{2+} entry (~20%) would be sufficient to account for the remaining facilitation, but increases in Ca^{2+} entry could be difficult to detect if they are confined to those channels that trigger vesicle fusion. The small, transient component of AR remaining in Syt7 KO animals could also be mediated by an additional sensor (Kaeser and Regehr,

2014b, Saraswati et al., 2007, Yao et al., 2011), but see (Groffen et al., 2010, Pang et al., 2011). Another possibility is that Ca^{2+} increases in grC presynaptic boutons are sufficient to activate fast Synaptotagmins to a small extent and trigger a small amount of AR. Further experiments are needed to determine the mechanisms of Syt7-independent AR and facilitation and to determine if they are mediated by the same Ca^{2+} sensor, or whether they are mediated by distinct mechanisms.

Chapter 5

Neuronal regulation of fast Synaptotagmin isoforms controls the relative contributions of synchronous and asynchronous release

Josef Turecek & Wade Regehr

Neuron 101(3), 938-949

Author Contributions. J.T. and W.R. designed experiments. J.T. performed experiments and analyzed data. J.T. and W.R. wrote the paper.

Abstract

Neurotransmitter release can be synchronous and occur within milliseconds of action potential invasion, or asynchronous and persist for tens of milliseconds. The molecular determinants of release kinetics remain poorly understood. It has been hypothesized that asynchronous release dominates when fast Synaptotagmin isoforms are far from calcium channels or when specialized sensors, such as Synaptotagmin 7, are abundant. Here we test these hypotheses for GABAergic projections onto neurons of the inferior olive, where release in different subnuclei ranges from synchronous to asynchronous. Surprisingly, neither of the leading hypotheses accounts for release kinetics. Instead, we find that rapid Synaptotagmin isoforms are abundant in subnuclei with synchronous release, but absent where release is asynchronous. Viral expression of Synaptotagmin 1 transforms asynchronous synapses into synchronous ones. Thus, the nervous system controls levels of fast Synaptotagmin isoforms to regulate release kinetics, and thereby controls the ability of synapses to encode spike rates or precise timing.

INTRODUCTION

Neurotransmitter release can occur within a millisecond after action potential invasion (Katz and Miledi, 1965, Sabatini and Regehr, 1996, Borst and Sakmann, 1996), but many synapses also have a slow component of release that persists for tens to hundreds of milliseconds (Atluri and Regehr, 1998, Lu and Trussell, 2000, Hefft and Jonas, 2005, Iremonger and Bains, 2007, Daw et al., 2009, Best and Regehr, 2009, Peters et al., 2010). These components, known respectively as synchronous and asynchronous release, allow synapses to provide different types of signals and contribute to neural processing in diverse ways. Most consideration of synaptic transmission and neural computations has focused on the precisely timed signals provided by synchronous release (Abbott and Regehr, 2004), but asynchronous release also has important functional roles (Kaeser and Regehr, 2014b). Asynchronous release provided by fast-spiking interneurons in the cortex is well suited to suppressing epileptiform activity (Manseau et al., 2010). Asynchronous release can also build during sustained activation to provide a slow, long-lasting signal that is effective at activating high affinity receptors such as metabotropic receptors, or that can activate ionotropic receptors to provide graded inhibition independent of the precise timing of inputs (Hefft and Jonas, 2005, Daw et al., 2009, Best and Regehr, 2009). Synapses across the brain have a wide variety of release properties: some are exclusively synchronous, others exclusively asynchronous, and many combine both synchronous and asynchronous components.

The molecular determinants of the relative contributions of synchronous and asynchronous release to transmission are not known, even though each component has been studied extensively. Synchronous release is a consequence of fast Synaptotagmin (Syt) isoforms (Syt1, Syt2 & Syt9) sensing high local increases from nearby calcium channels that are opened by action potentials (Llinas et al., 1992, Borst and Sakmann, 1996, Schneggenburger and Neher, 2000, Xu et al., 2007, Eggermann et al., 2011). Numerous mechanisms have been proposed to mediate asynchronous release at different types of synapses. One possibility is that fast Syt isoforms are located far away from calcium channels and are only exposed to small, slow calcium signals. This hypothesis was motivated by the observation that introducing the slow buffer EGTA to presynaptic terminals eliminates asynchronous release while sparing

synchronous release (Atluri and Regehr, 1998, Hefft and Jonas, 2005, Iremonger and Bains, 2007). Alternatively, there is growing evidence supporting specialized slow, high-affinity calcium sensors mediating asynchronous release (Sun et al., 2007, Yao et al., 2011, Kochubey and Schneggenburger, 2011, Bacaj et al., 2013). Synaptotagmin 7 (Syt7) is such a sensor that mediates asynchronous release at several synapses (Wen et al., 2010, Bacaj et al., 2013, Luo et al., 2015, Luo and Sudhof, 2017, Chen et al., 2017c, Turecek and Regehr, 2018). This raises the possibility that the presence of sensors such as Syt7 might regulate release kinetics (although see (Jackman et al., 2016, Turecek et al., 2017)). It has been difficult to test these hypotheses because in most brain areas synapses from different presynaptic sources with diverse release kinetics are mixed together and it has been impractical to study them in isolation.

The IO has several technical advantages for understanding the factors that control the timing of neurotransmitter release. The IO provides climbing fibers that drive motor learning in the cerebellar cortex. Long-range projections from the DCN and vestibular nuclei (VN) are the primary sources of GABAergic inhibition and there are virtually no interneurons within the IO (Fredette and Mugnaini, 1991, Fredette et al., 1992) (Figure 1A). Inhibitory synapses are therefore relatively homogeneous relative to other brain regions. In addition, the IO has a stereotyped anatomy, and it is divided into subnuclei that communicate with specific regions of the cerebellar system, forming a feedback loop between the cerebellar cortex, DCN and IO (Voogd and Glickstein, 1998, Sugihara and Shinoda, 2004, Pijpers et al., 2005, Sugihara and Shinoda, 2007, Yu et al., 2014). The kinetics of GABA release can be different between subnuclei: release is synchronous in the dorsal cap of Kooy (DCK) (Urbano et al., 2006), and asynchronous in the principal IO (PIO) (Best and Regehr, 2009). Finally, inhibitory presynaptic boutons in the IO are larger and easier to optically resolve than synapses in other brain regions.

Here we study the mechanism that controls release kinetics for inhibitory inputs in the IO. Syt7 can be present at equal levels in neighboring regions with very different release kinetics, and the removal of Syt7 does not eliminate asynchronous release. This indicates that the Syt7 does not determine whether release is synchronous or asynchronous. We find that for inhibitory synapses in the IO, fast Syts are present at synapses with synchronous release but absent from synapses with exclusively asynchronous

release. Presynaptic expression of Syt1 at synapses that are normally asynchronous and lack Syt1 leads to highly synchronized release. These findings exclude the hypothesis that fast Syts mediate both synchronous and asynchronous release, with synchronous release occurring when fast Syts are close to calcium channels, and asynchronous release occurring when fast Syts are far from calcium channels. We find, instead, that it is the presence or absence of fast Syt isoforms that control release kinetics. Previously, the ability of Syt1 to both promote synchronous release and suppress asynchronous release had only been apparent in genetic experiments in which elimination of fast Syt isoforms both eliminates synchronous release and leads to more pronounced asynchronous release (Littleton et al., 1993, DiAntonio and Schwarz, 1994, Geppert et al., 1994, Yoshihara and Littleton, 2002, Sun et al., 2007, Kochubey and Schneggenburger, 2011, Bacaj et al., 2013, Luo and Sudhof, 2017, Chen et al., 2017b), and it had not been thought that synapses lacking fast Syts were present in wildtype animals. Here we see that inhibitory inputs to the IO tune their release kinetics by controlling the level of fast Syt isoforms.

RESULTS

The kinetics of GABA release is regionally segregated in the IO

In order to determine how the kinetics of GABA release are regionally segregated throughout the entire IO of mice, we measured the properties of IPSCs across many subnuclei. For each neuron, we evoked IPSCs with single stimuli for many trials, determined the rise time and decay time constant from the average response, and quantified the jitter in the time to peak from the individual trials (**Figure 5.1B, Figure 5.2 A-J**). These findings are summarized by plotting the color-coded properties as a function of spatial location within the IO (**Figure 5.1C, 5.2K, 5.2M**), and by plotting the properties for neurons within each subnucleus (**Figure 5.1D, 5.2L, 5.2N**).

We found that the properties of inhibitory post-synaptic currents (IPSCs) evoked by a single stimulus varied widely across different subnuclei of the IO. Release in the rostral dorsal cap of Kooy (rDCK) was exclusively synchronous (**Figure 5.1B, left**), as in rats (Urbano et al., 2006, Best and Regehr, 2009). Responses had a rapid rise, decayed smoothly with a single exponential decay, and exhibited no sign of asynchronous release. Quantification of the rise times and decay times from the average IPSCs,

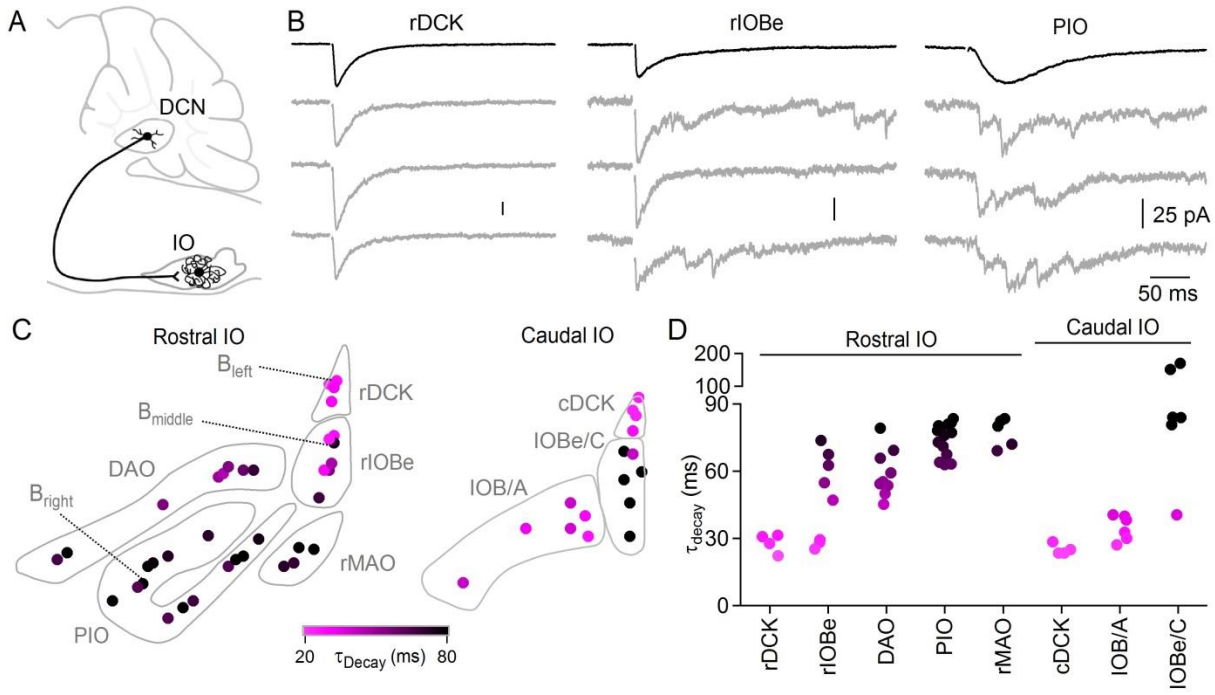

Figure 5.1: GABA release in the IO ranges from synchronous to asynchronous.

A, Sagittal view showing cells in the deep cerebellar nuclei (DCN) forming GABAergic synapses in the inferior olive (IO).

B, Evoked IPSCs in response to a single stimulus in the rostral dorsal cap of Kooy (rDCK, left), rostral beta subnucleus (rIOBe, middle) and principal IO (PIO, right), with averages (black) and single trials (gray).

C, Coronal outline of the rostral (left) and caudal (right) IO. Each marker is a single cell, the color map corresponds to the decay time of the averaged IPSC. (DAO, dorsal accessory olive; rMAO, medial accessory olive; cDCK, caudal dorsal cap of Kooy; IOB/A, subnuclei A-B; IOBe/C, beta/C subnuclei).

D, Plot of average decay time for individual cells in each IO subnucleus. Number of experiments in **Table 5.1.**

Table 5.1: Number of experiments

Figure	Subnucleus	Cells (WT/KO)	Mice (WT/KO)	Virus/stimulus	
5.1, 5.2	rDCK	4	3	None/electrical	
5.1, 5.2	rIOBe	8	6	None/electrical	
5.1, 5.2	DAO	9	8	None/electrical	
5.1, 5.3, 5.2	PIO	14/8	9/2	None/electrical	
5.1, 5.2	rMAO	4	3	None/electrical	
5.1, 5.2	cDCK	4	3	None/electrical	
5.1, 5.3, 5.2	IOB/A	6	5	None/electrical	
5.1, 5.3, 5.2	IOBe/C	7	5	None/electrical	
5.3	PIO	27/28	4/3	None/Max electrical	
5.4	rDCK	5/4	3/2	None/None (mIPSCs)	
5.4	rIOBe	5/5	2/1	None/None (mIPSCs)	
5.4	DAO	5/4	2/2	None/None (mIPSCs)	
5.4	PIO	7/8	2/4	None/None (mIPSCs)	
5.4	rMAO	4/4	3/2	None/None (mIPSCs)	
5.4	cDCK	4/6	2/3	None/None (mIPSCs)	
5.4	IOB/A	5/5	1/2	None/None (mIPSCs)	
5.4	IOBe/C	7/10	3/2	None/None (mIPSCs)	
5.10C	DAO	7	2	ChR2/optical	
5.10C	MAO	2	2	ChR2/optical	
5.10C,E-F	PIO	8	2	ChR2/optical	
5.10D	DAO	3	2	ChR2+Syt1/optical	
5.10D	MAO	2	2	ChR2+Syt1/optical	
5.10D,E-F	PIO	8	2	ChR2+Syt1/optical	
Figure	**Subnucleus**	**Label**	**Boutons (WT/KO)**	**Sections**	**Animals**
5.3, 5.4	rDCK	VGAT, Syt7	361/270	1/1	1/1
5.3, 5.4	rIOBe	VGAT, Syt7	1119/1088	1/1	1/1
5.3, 5.4	DAO	VGAT, Syt7	2778/5476	1/1	1/1
5.3, 5.4	PIO	VGAT, Syt7	2346/3889	1/1	1/1
5.3, 5.4	rMAO	VGAT, Syt7	3712/2908	1/1	1/1
5.3, 5.4	cDCK	VGAT, Syt7	375/453	1/1	1/1
5.3, 5.4	IOB/A	VGAT, Syt7	4169/6150	1/1	1/1
5.3, 5.4	IOBe/C	VGAT, Syt7	3437/1891	1/1	1/1
5.5E	RF	VGAT, Syt1/2	524-530	1	1
5.5F	DAO	VGAT, Syt1/2	534-570	1	1
5.6A,B, 5.6, 5.7	RF	VGAT, Syt1/2	11889	2	2
5.6, 5.7, 5.5	rDCK	VGAT, Syt1/2	1420	2	2
5.6, 5.7, 5.5	rIOBe	VGAT, Syt1/2	7022	2	2
5.6A,B, 5.6, 5.7	DAO	VGAT, Syt1/2	11132	2	2
5.6, 5.7, 5.5	rMAO	VGAT, Syt1/2	8467	2	2
5.6, 5.7, 5.5	PIO	VGAT, Syt1/2	16045	2	2
5.6, 5.7, 5.5	cDCK	VGAT, Syt1/2	2291	1	1
5.6, 5.7, 5.5	IOB/A	VGAT, Syt1/2	14871	1	1
5.6, 5.7, 5.5	IOBe/C	VGAT, Syt1/2	6258	1	1
5.6C,D, 5.6, 5.7	RF	VGLUT2, Syt1/2	985	1	1
5.8B	rDCK	VGLUT2, Syt1/2	851	1	1

Table 5.1 (Continued)

5.8B	rIOBe	VGLUT2, Syt1/2	909	1	1
5.6C,D, 5.8B	DAO	VGLUT2, Syt1/2	4644	1	1
5.8B	rMAO	VGLUT2, Syt1/2	1226	1	1
5.8B	PIO	VGLUT2, Syt1/2	7105	1	1
5.8C	RF	VGAT, GAD67	3872	1	1
5.8C	rDCK	VGAT, GAD67	863	1	1
5.8C	rIOBe	VGAT, GAD67	4008	1	1
5.8C	DAO	VGAT, GAD67	4580	1	1
5.8C	rMAO	VGAT, GAD67	5340	1	1
5.8C	PIO	VGAT, GAD67	6275	1	1

Table 5.2: Summary data for all IO subnuclei

Region	Release type	Decay (ms)	Half-rise (ms)	Jitter (ms)	Syt7 Int. (AU)	ΔmIPSC freq. Syt7 KO (Hz)	VGAT density, WT/KO (boutons/ μm^3)	% boutons lacking Syt1/2
RF	Sync.	N/A	N/A	N/A	0.14	N/A	0.058/0.058	1.6
rDCK	Sync.	28.0 ± 2.1	5.7 ± 0.3	1.6 ± 0.5	0.26	1.2 ± 0.6	0.048/0.054	16.2
rIOBe	Mixed	48.6 ± 6.7	5.4 ± 0.4	11.3 ± 4.8	0.35	5.3 ± 0.8	0.051/0.052	49.6
DAO	Async.	59.1 ± 3.5	14.6 ± 2.4	24.9 ± 2.9	0.46	8.1 ± 0.7	0.066/0.067	68.1
PIO	Async.	74.1 ± 1.9	20.3 ± 1.1	25.2 ± 1.8	0.45	10.1 ± 1.5	0.076/0.074	85.5
rMAO	Async.	77.4 ± 2.9	20.4 ± 1.1	26.4 ± 2.9	0.57	13.1 ± 3.9	0.082/0.086	89.5
cDCK	Sync.	25.1 ± 1.2	4.2 ± 0.3	0.8 ± 0.2	0.19	0.5 ± 0.5	0.059/0.053	5.0
IOB/A	Sync.	34.7 ± 2.3	5.1 ± 0.4	1.3 ± 0.3	0.33	0.6 ± 0.5	0.049/0.059	5.4
IOBe/C	Mixed	101.7 ± 19.9	11.0 ± 3.3	36.5 ± 7.8	0.31	3.7 ± 1.2	0.062/0.064	59.4

and the jitter in the time for individual trials revealed that IPSCs in the rDCK consistently exhibited synchronous release with no apparent contribution from asynchronous release (Urbano et al., 2006, Best and Regehr, 2009). These properties were consistent for all rDCK neurons (F**igure 5.1C,D, Figure 5.2K-N**). The properties of synapses in the principal IO (PIO) were very different (**Figure 5.1B, right**) (Best and Regehr, 2009). Individual trials consisted of many quantal events spread out over tens of milliseconds, and the average IPSC had a very slow rise time and a slow decay time. All cells within the PIO had a similar slow rise time, slow decay time and large jitter in time to peak. These properties are all consistent with synapses that release asynchronously and lack a synchronous component. IPSCs in the rostral beta subnucleus (rIOBe) had both synchronous and asynchronous components (**Figure 5.1B, middle**). This is apparent in individual trials in which there was a rapidly rising component that was accompanied by delayed events characteristic of asynchronous release. There was variability in synaptic properties within the rIOBe, suggesting that within this sub-nucleus asynchronous and synchronous release make variable contributions (**Figure 5.2B,C**). Most subnuclei in the rostral IO received asynchronous inhibitory inputs, whereas most subnuclei in the caudal IO had synchronous inhibitory inputs.

These findings establish that the kinetics of GABA release within the IO are diverse and range from purely synchronous, exclusively asynchronous, or a combination of both (**Figure 5.1D, Figure 5.2L,N**). Importantly, the release kinetics are regionally segregated, in contrast to most brain areas where synapses from many presynaptic sources are intermingled. We took advantage of regional segregation of synapses with vastly different kinetics to study the molecular properties that determine the ratio of synchronous to asynchronous release.

Assessing the role of Syt7 in Asynchronous Release in the IO

We began by testing the hypothesis that differential expression of Syt7 could account for differences in release kinetics. Syt7 is a high affinity calcium sensor that mediates asynchronous release at several synapses (Bacaj et al., 2013, Wen et al., 2010, Luo et al., 2015, Luo and Sudhof, 2017, Turecek and Regehr, 2018).We performed immunohistochemistry to determine the regional distribution of Syt7

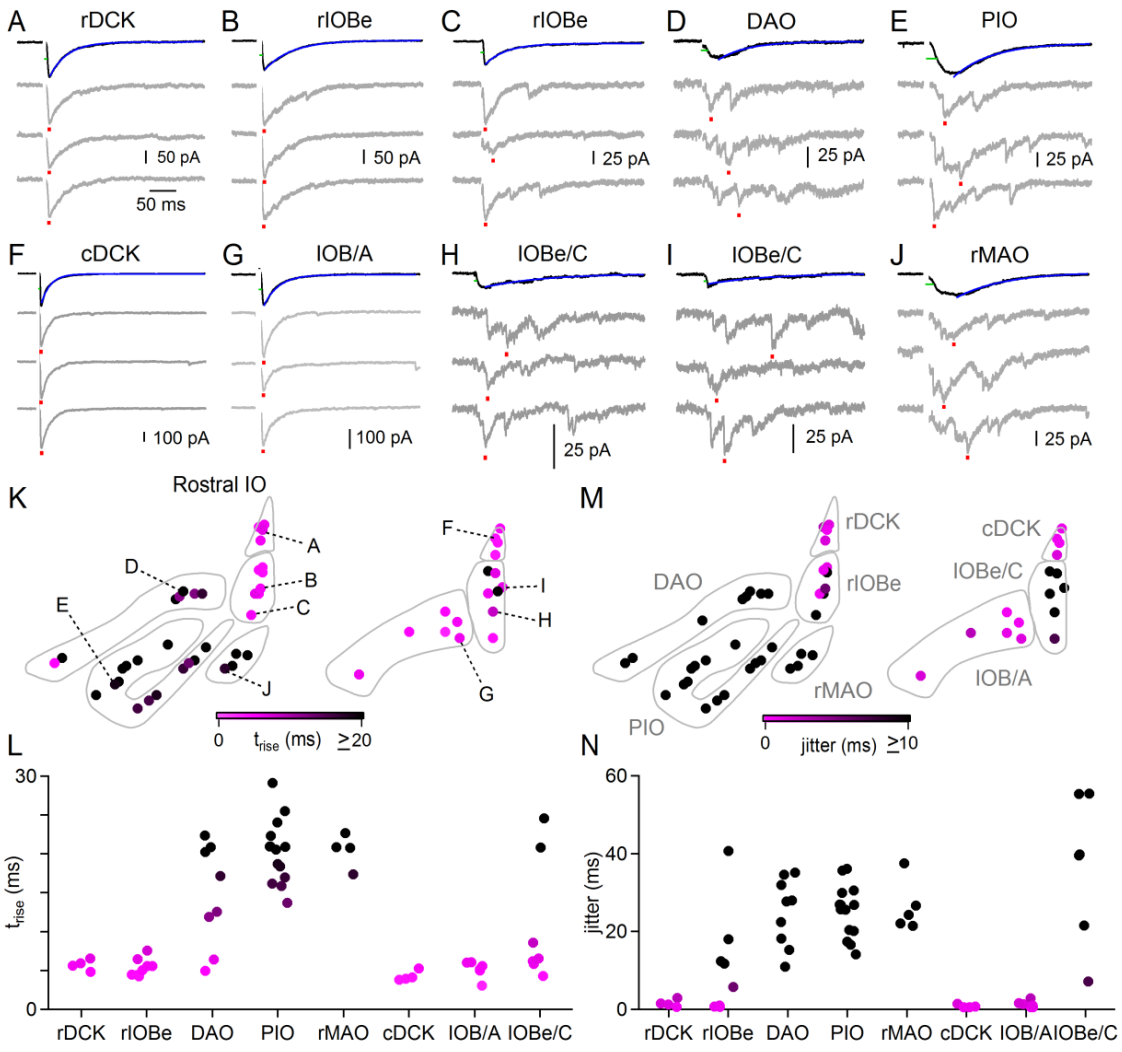

Figure 5.2: IPSCs from different subnuclei of the IO, related to Figure 1. Each subpanel shows the average IPSC (black traces) and three individual trials (gray) for a single cell. Measurements were performed on averaged currents. The decay time is fit to the average IPSC (blue) and the half-rise time of the average relative to stimulation onset is also shown (green). Red ticks indicate peak IPSC time used to calculate jitter. Recordings were performed in the rostral and caudal IO. Examples are shown for **A,** the rostral dorsal cap of Kooy (rDCK) which received exclusively synchronous input, **B, C,** rostral beta olive (rIOBe), which received either exclusively synchronous (**B**) or mixed input (**C**). **D,** Exclusively asynchronous release in the dorsal accessory olive (DAO), **E,** and principal olive (PIO). **F,** Exclusively synchronous release in the caudal dorsal cap of Kooy (cDCK), **G**, and the caudal subnuclei B & A

Figure 5.2 (Continued)

(IOB/A), **H, I**, Mostly asynchronous release in the caudal beta and C subnuclei (IOBe/C) **J**, and exclusively asynchronous release in the rostral medial accessory olive (rMAO). **K-N:** Asynchronous release has slow kinetics, characterized by longer decay times, slower rise times, and more jitter compared to synchronous release. Differences were observed for all three measures across subnuclei, but the kinetics of spontaneous IPSCs were similar for all regions (τ_{decay} = 35 ± 2 ms). **K**, Coronal map of all cells recorded in the rostral (left) and caudal (right) IO color-coded by the half-rise time (t_{rise}) of their input showing locations of cells in **A-J**. Areas in the rostral beta olive (rIOBe) had both synchronous components with rapid rise times, but in some cases had asynchronous release that was not captured by the rise time. **L**, Summary of rise times across all subnuclei of the IO with same color code as in **K**. **M**, Same as in **K**, but cells are color-coded by the jitter of inhibitory inputs (standard-deviation of peak time). **N**, Summary of jitter for cells across all subnuclei. Markers are individual cells.

within the IO (**Figure 5.3A,B**). Inhibitory synapses were identified with a VGAT antibody that was also used to identify the subnuclei in the rostral (**Figure 5.3A, top**) and caudal IO (**Figure 5.3B, top**). Syt7 was apparent in IO subnuclei in wildtype animals and absent in Syt7 KO animals (**Figure 5.3A, middle, Figure 5.3B, middle**). Syt7 is present at both excitatory and inhibitory synapses, and we therefore used VGAT signals to generate maps of Syt7 levels at inhibitory synapses (**Figure 5.3A, bottom, Figure 5.3B, bottom, Figure 5.4, see methods**). Subnuclei with asynchronous release tended to have higher Syt7 levels than subnuclei with synchronous release (**Figure 5.3C, D**), but there were notable exceptions. Syt7 was similarly high at inhibitory synapses in the IOB/A where release is exclusively synchronous, and in the IOBe/C where asynchronous release is prominent (**Figure 5.3E-G**). Thus, we conclude that Syt7 levels alone do not always explain differences in release kinetics in different regions of the IO, and that the abundance of Syt7 does not determine the synchrony of release.

We next examined asynchronous release in Syt7 KO mice. We used low intensity stimulation to measure kinetics in the PIO, where release is exclusively asynchronous. Low stimulus intensities evoked small responses, and the quantal events making up these responses were apparent. Surprisingly, the kinetics of asynchronous release were significantly slowed in Syt7 KOs (**Figure 5.3H-J**). This is evident when the time courses of normalized average synaptic currents are compared for wildtype and Syt7 KO animals (**Figure 5.3I**). In Syt7 KO animals there is a delay before a slowly rising synaptic current is apparent, and the synaptic current is much longer lasting than in wildtype animals (**Figure 5.3I**). To determine whether there were changes in the total amount of evoked release, we compared synaptic currents evoked by the same large stimulus intensity at which release was maximal (see methods, **Figure 5.3K-L**). There was considerable variability in the magnitude of synaptically evoked currents, presumably reflecting variability in the number of DCN axons stimulated. On average, there was a decrease in the amplitude of evoked release (wildtype: 914 ± 80 pA; Syt7 KO: 469 ± 35 pA; $p < 0.01$, Student's t-test), and as with low stimulus intensities the timecourse of release was consistently altered. However, the total amount of synaptic charge was not significantly different for wildtype and Syt7 KO mice because the decrement in the amplitude of asynchronous release was offset by a more prolonged

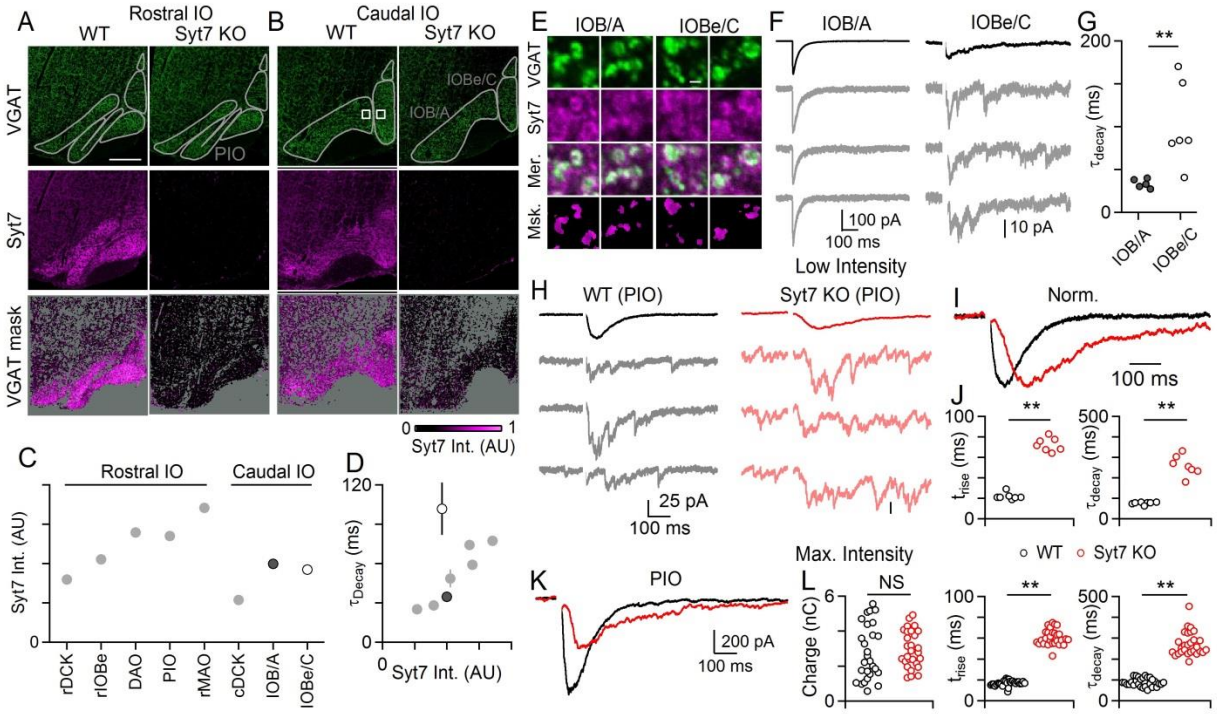

Figure 5.3: The presence of Syt7 does not confer asynchronous release onto DCN-IO synapses.

A, Coronal view of the rostral IO with subnuclei outlined immunostained for VGAT (top) and Syt7 (middle). VGAT was used as a mask to display the intensity of Syt7 at inhibitory synapses (bottom), with regions lacking VGAT staining shown in grey. Examples are from a wildtype (left) and Syt7 KO (right). Scalebar, 200 µm.

B, Same as in A, but for the caudal IO.

C, Median intensity of Syt7 in VGAT-positive boutons for each subnucleus (Syt7 KO signal subtracted).

D, Average IPSC decay time plotted against median Syt7 intensity at VGAT boutons for each subnucleus, with IOBe/C (white) and IOB/A (dark) highlighted. Markers are mean ± s.e.m. for decay time, and median Syt7 intensity for all measured boutons within each subnucleus.

E, Individual boutons in the caudal IO from the IOB/A (left), and IOBe/C (right) from areas indicated in B from a wildtype animal. Images are from single sections. Scalebar, 2 µm.

F, Example evoked synchronous IPSCs in the IOB/A (left), and asynchronous IPSCs from a cell in the IOBe/C (right), with averaged IPSCs (black) and individual trials shown (gray).

Figure 5.3 (Continued)

G, summary of decay kinetics of averaged IPSCs in the IOBe/C and IOB/A. Markers are individual cells.

H, Low intensity stimuli evoked asynchronous IPSCs from the PIO in a wildtype animal (left), and from a Syt7 KO (right) with averages (top) and individual trials (bottom).

I, Averaged IPSCs normalized to peak amplitudes for examples shown in H.

J, Half-rise (left) and time constants of decay (right) of averaged IPSCs for wildtype and Syt7 KOs.

K, Example IPSCs evoked by high intensity stimulation in the PIO of wildtype and Syt7 KOs.

L, Properties of currents evoked by maximal intensity showing amplitude (left), half-rise and decay (middle) times and total charge (right). Markers are individual cells. ** $p < 0.01$, unpaired two-tailed Student's t-test.

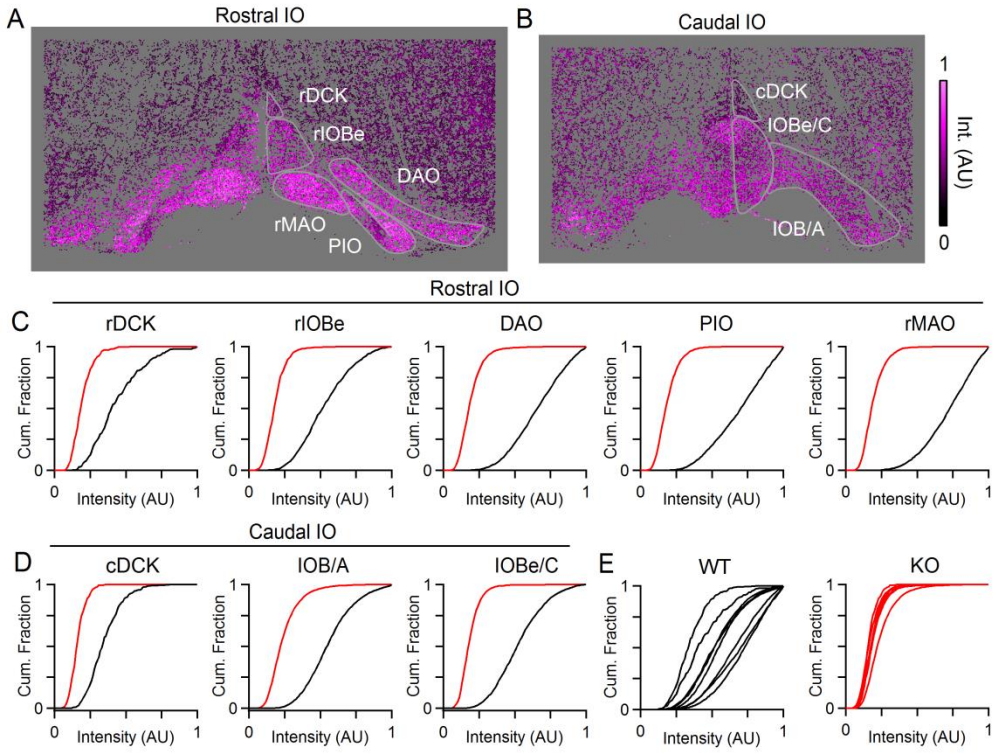

Figure 5.4: Syt7 levels at inhibitory synapses in the IO.

A, Map of Syt7 labeling in the rostral IO masked using VGAT fluorescence. Each dot is a VGAT bouton.

B, Same as in A, but for the caudal IO.

C, cumulative distribution of Syt7 levels for VGAT boutons for wildtype (black) and Syt7 KOs (red) for all subnuclei of the rostral IO.

D, same as in C, but for the caudal IO.

E, Overlaid cumulative distributions of Syt7 labeling for all wildtype (left) and Syt7 KO (right) subnuclei of the IO.

timecourse (wildtype: 2780 ± 300 pC; Syt7 KO: 2970 ± 200 pC; p = 0.60, Student's t-test, **Figure 5.3K-L**). Thus, elimination of Syt7 does not reduce the total amount of asynchronous release in the IO.

Release in Syt7 KO animals provided an important insight into IO synapses with different degrees of synchrony. When measuring evoked transmission in the PIO of Syt7 KO mice, there was a dramatic elevation of spontaneous release. This prompted us to measure mIPSC frequency in the presence of TTX in wildtype and Syt7 KOs. In wildtype animals, the rate of spontaneous release is low, and is similar for subnuclei receiving synchronous and asynchronous release (**Figure 5.5A**). In the rDCK, where release is synchronous, and the PIO where release is asynchronous, mIPSCs were infrequent in wildtype animals (Figure 5.5A, left). Across the IO mIPSCs are infrequent in all subnuclei in wildtypes (**Figure 5.5A, middle, right**). In Syt7 KOs, the rate of mIPSCs was elevated in the PIO, but not in the rDCK (**Figure 5.5B, left**). We found that across the IO, mIPSC frequency was specifically upregulated in regions where release is asynchronous, and was unchanged in areas receiving synchronous release (**Figure 5.5B, middle, right**). Across the IO the density of inhibitory synapses measured anatomically was unchanged in Syt7 KOs (**Table 5.2**). We grouped subnuclei into those receiving synchronous release (rDCK, cDCK, IOB/A), mixed synchronous and asynchronous release (rIOBe, IOBe/C), and exclusively asynchronous areas (DAO, PIO, MAO) and compared the mIPSC frequency for each subnucleus (**Figure 5.5C**). The greatest elevation of mIPSC frequency in Syt7 KO mice occurred for subnuclei where release is exclusively asynchronous (**Figure 5.5D**).

The differential enhancement of mIPSC frequency is consistent with the ability of Syt7 to clamp release. At the calyx of Held it is known that mEPSC frequency is unaltered in Syt7 KO animals, but mEPSC frequency is much higher in Syt7/Syt2 dKO mice than in Syt2 KO mice (Luo and Sudhof, 2017). This suggests that the ability of Syt7 to clamp release only becomes apparent in the absence of fast Syt isoforms, because elimination of Syt7 alone does not have an effect on spontaneous release at many synapses (Luo and Sudhof, 2017, Chen et al., 2017c, Turecek et al., 2017, Turecek and Regehr, 2018, Jackman et al., 2016, Bacaj et al., 2013, Luo et al., 2015). Here we see that mIPSC frequency is preferentially elevated in regions where asynchronous release is prominent. One possibility is that the

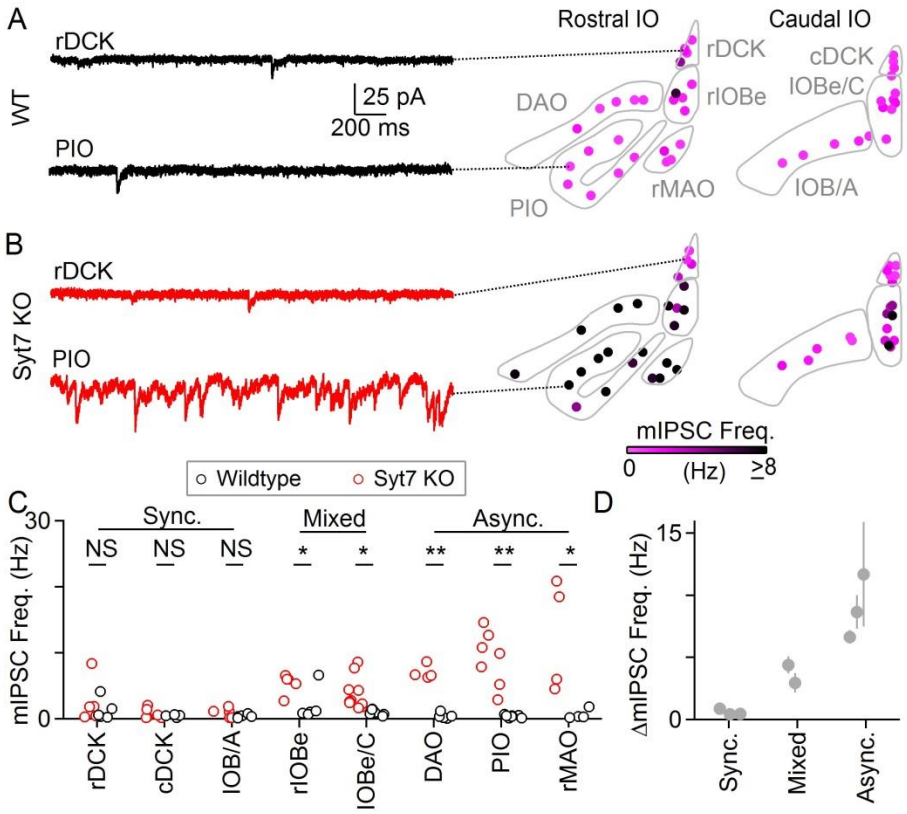

Figure 5.5: Syt7 clamps spontaneous release only in areas where there is prominent asynchronous release.

A, Examples of mIPSCs (left) from the rostral dorsal cap of Kooy (rDCK, top) and principal inferior olive (PIO, bottom) in a wildtype animal. Summary of all wildtype cells color-coded by mIPSC frequency in the rostral (middle) and caudal IO (right).

B, Examples of mIPSCs for the rDCK (top) and PIO (bottom) in a Syt7 KO. Summary for all Syt7 KO cells are shown for rostral (middle) and caudal IO (right).

C, Plot of mIPSC frequency for wildtype and Syt7 KO cells for each subnucleus. Subnuclei are arranged in order based on IPSC kinetics, ranging from predominantly synchronous (Sync.), to both synchronous and asynchronous (Mixed), to exclusively asynchronous (Async.). Data are individual cells.

D, Difference in average mIPSC frequency (Syt7 KO – wildtype; mean ± s.e.m.) for each subnucleus in C. *p<0.05, **p<0.01, two-tailed student's t-test.

differential effect of Syt7 KOs on mIPSC frequency is a consequence of the differential expression of fast Syt isoforms. Areas that have asynchronous release may lack fast Syt isoforms, and the elimination of Syt7 would then be expected to selectively elevate mIPSC frequency in these regions.

Asynchronous release is mediated by the absence of fast Syt isoforms

It is possible that asynchronous synapses in the IO lack fast Syt isoforms (Syt1, Syt2 and Syt9). It is well established that removing rapid Syt isoforms from synapses using molecular genetics eliminates synchronous release and promotes asynchronous release (DiAntonio and Schwarz, 1994, Geppert et al., 1994, Xu et al., 2007, Bacaj et al., 2013, Chen et al., 2017b), but this was thought to occur only under artificial conditions by genetically manipulating Syt expression. It is assumed that in wildtype animals, for transmission triggered by action potentials, synapses contain at least one of the rapid Syt isoforms. Neurons in the DCN do not express Syt9 (Mittelsteadt et al., 2009), so we determined whether Syt1 and Syt2 are present at inhibitory synapses in the IO.

We compared the expression of markers for GABAergic (VGAT) and glutamatergic (VGLUT2) synapses with the expression of Syt1/2 (staining simultaneously for both Syt1 and Syt2) using immunohistochemistry and confocal microscopy. VGAT, VGLUT2 (green) and Syt1/2 (purple) were present throughout the IO and surrounding reticular formation (RF) (**Figure 5.6A,C**). At high magnification GABAergic synapses were abundant in the RF and in the dorsal accessory olive (DAO), which is adjacent to the RF (**Figure 5.6B**). Merged images showed that Syt1/2 were present at GABAergic synapses in the RF (**Figure 5.6E, merged, white**), but were excluded from GABAergic boutons in the DAO (**Figure 5.6F, merged, green**). To determine whether Syt1/2 were specifically absent from GABAergic synapses, we analyzed Syt1/2-VGAT signal correlation for individual boutons (**Figure 5.7, see methods**). VGAT positive boutons were identified, and the degree of signal correlation of VGAT and Syt for each GABAergic bouton was measured as the Pearson's Correlation coefficient R^2. VGAT fluorescence was thresholded and each bouton was color-coded by the extent of Syt1/2-VGAT correlation (**Figure 5.6B, lower**). Syt1/2 and VGAT levels were highly correlated for individual boutons in the RF but not in the DAO. A similar analysis using VGLUT2 for glutamatergic synapses (**Figure**

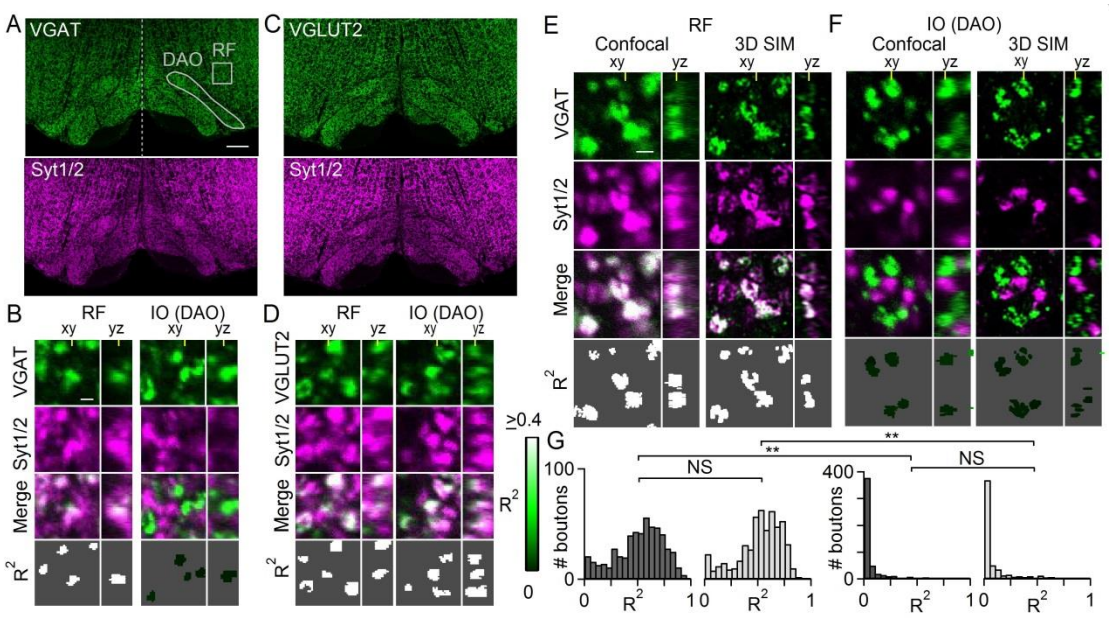

Figure 5.6: GABAergic synapses in some IO subnuclei lack sensors for fast vesicle fusion.

A, Coronal image of ventral brainstem immunostained for VGAT (top) and Syt1/Syt2 (bottom). Dashed line indicates midline, with reticular formation (RF) and dorsal accessory olive (DAO) outlined. Scalebar, 200 µm.

B, High-power single-plane view of VGAT-positive boutons in RF (left) and DAO (right). Raw images shown from top to bottom for VGAT, Syt1/2, merged channels, and correlation analysis. YZ and XY planes indicated by yellow ticks. Scalebar, 1 µm.

C, same as in **A** but for VGLUT2 and Syt1/2.

D, same as in **B**, but for VGLUT2.

E, Comparison of confocal (left) and 3D-SIM (right) in the RF. Scalebar, 1 µm.

F, Same as in **E**, but for the DAO. **G,** Distribution of correlation coefficient values for confocal (dark) and 3D-SIM (light) in the RF (left) and DAO (right). **p<0.01, K-S test.

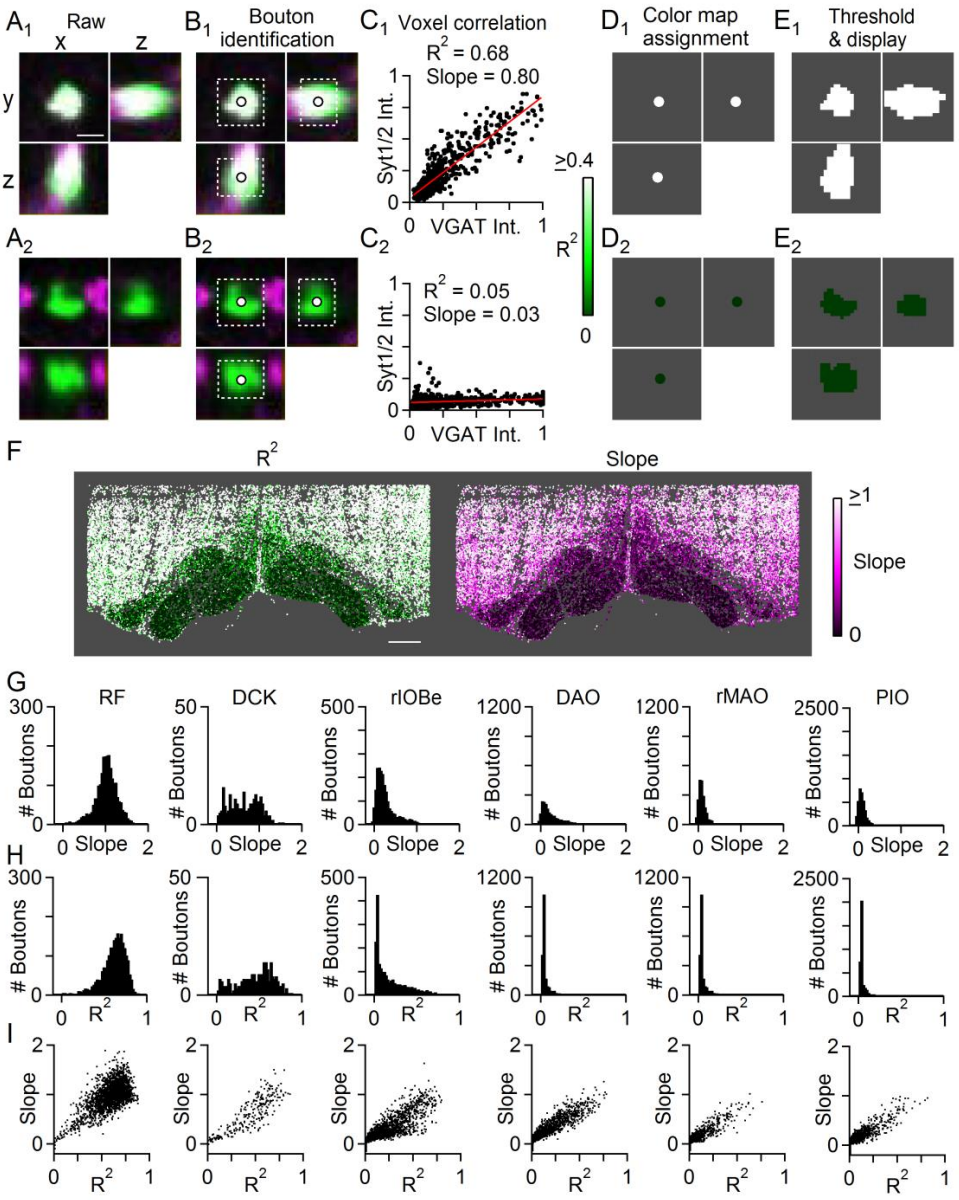

Figure 5.7: Co-localization analysis of VGAT and Syt1/2, In order to determine whether Syt1/2 were present at inhibitory synapses, we performed co-localization analysis by correlating the signal intensity of Syt1/2 and VGAT for each VGAT-positive bouton. We found that the advantages of this method are that it is relatively insensitive to differences in absolute signal strength and is insensitive to bouton morphology, which is highly variable. Examples of analysis are shown for a VGAT positive bouton containing fast Syts (**A_1-E_1**) and for a bouton that lacked fast Syts (**A_2-E_2**). **A,** Merged single plane

Figure 5.7 (Continued)

confocal images of VGAT (green) and Syt1/2 (magenta) in the xy, yz and xz planes (left) for an example bouton that was positive for Syt1/2 (**A_1**) or lacked Syt1/2 (**A_2**). Scalebar, 1 μm **B,** VGAT-positive boutons were identified as a local maxima and a 1.5 x 1.5 x 1.25 μm volume of interest (dashed) was drawn around the centroid of the bouton (marker). **C,** Within each region of interest, the intensity of Syt1/2 fluorescence was plotted vs. VGAT intensity for each voxel and linearly correlated (red). The degree of co-localization for each region of interest was measured as Pearson's correlation coefficient R^2. Intensity is normalized to the max intensity in the entire image stack, not within region of interest. **D,** To analyze the degree of correlation in different regions of the brainstem and IO, each bouton was represented at its location by a marker which was color-coded by its R^2 value. **E,** For display of high magnification images, a single plane of the VGAT channel was thresholded and color-coded by its R^2 value for each bouton. **F-I**, To determine whether there were differences in the magnitude of Syt1/2 expression across subnuclei, we also analyzed the slope of regression lines. We found that in the rIOBe, which receives mixed synchronous and asynchronous input, VGAT synapses where Syt1/2 were present had lower expression of Syt1/2 compared to regions with exclusively synchronous release, such as the RF. Thus, the asynchronous release in this region is driven by a lack of Syt1/2 at some synapses, but also could be compounded by lower Syt1/2 expression at synapses where Syt1/2 are present. **F**, Map of all VGAT-positive boutons in the ventral brainstem color-coded for R^2 (left) and the slope (right) of linear fits to Syt1/2 vs. VGAT signals. Scalebar, 200 μm. **G**, Distribution of slopes of linear fits for all VGAT-positive boutons in each subnucleus. **H**, Same as **G**, but for values of R^2. **I**, Plot of slope vs. R^2 for all boutons in each subnucleus. For all figures shown, R^2 was set to 0.01 for boutons with a negative slope.

5.6D, 5.8) showed that Syt1/2 were present at excitatory synapses in both the RF and DAO. We also repeated the same analysis using 3D structured illumination microscopy, which can reduce the point-spread function by half compared to confocal microscopy (**Figure 5.6E,F**). There was no difference in the correlation of Syt1/2 and VGAT between imaging methods, and differences in Syt1/2-VGAT correlations between the RF and DAO were apparent with both techniques (**Figure 5.6G**). Thus, Syt1/2 were present at excitatory and inhibitory synapses in the RF. In the DAO, Syt1/2 were present at excitatory synapses, consistent with synchronized glutamatergic release in the IO (**Figure 5.6B-G, 5.8**) (Best and Regehr, 2008). In contrast, Syt1/2 were excluded from GABAergic boutons within the DAO (**Figure 5.6B, 5.7**), where inhibitory transmission is asynchronous.

We next assessed the presence of Syt1/2 at inhibitory synapses across the ventral brainstem. High resolution images were acquired and the correlation of Syt1/2 and VGAT was analyzed for each inhibitory bouton (**Figure 5.9A**). As in Figure 4B, VGAT was used to identify GABAergic synapses. Syt1/2 were used to assess the presence of fast Syts but labeled both glutamatergic and GABAergic boutons. Thus, in merged images green labeling indicates GABAergic boutons where Syt1/2 are not present, purple indicates primarily glutamatergic boutons where Syt1/2 are present and VGAT is absent, and overlapping VGAT and Syt1/2 is white. Finally, R^2 images show the color-coded R^2 values for each GABAergic bouton (**Figure 5.9A**). Each subnucleus contained thousands of boutons allowing us to examine the distribution of Syt1/2-VGAT correlation within each subnucleus (**Figure 5.9B**). The regional dependence of Syt1/2 levels are apparent in the anatomical map displaying the R^2 of Syt1/2 and VGAT for inhibitory boutons in the entire ventral brainstem (**Figure 5.9C**). These results indicate that Syt1/2 are present at most GABAergic boutons in regions surrounding the IO (the RF), the rDCK, cDCK and the IOB/A. Syt1/2 are absent at most synapses in DAO, PIO and rMAO, and present at a fraction of synapses in rIOBe and IOBe/C.

In order to compare Syt1/2-VGAT correlation to the release kinetics in different regions, we made maps of the IO color-coded by the average time constant of IPSC decay in different subnuclei (Figure 5.9D) based on the data in Figure 1C. In order to summarize the anatomical data, we quantified

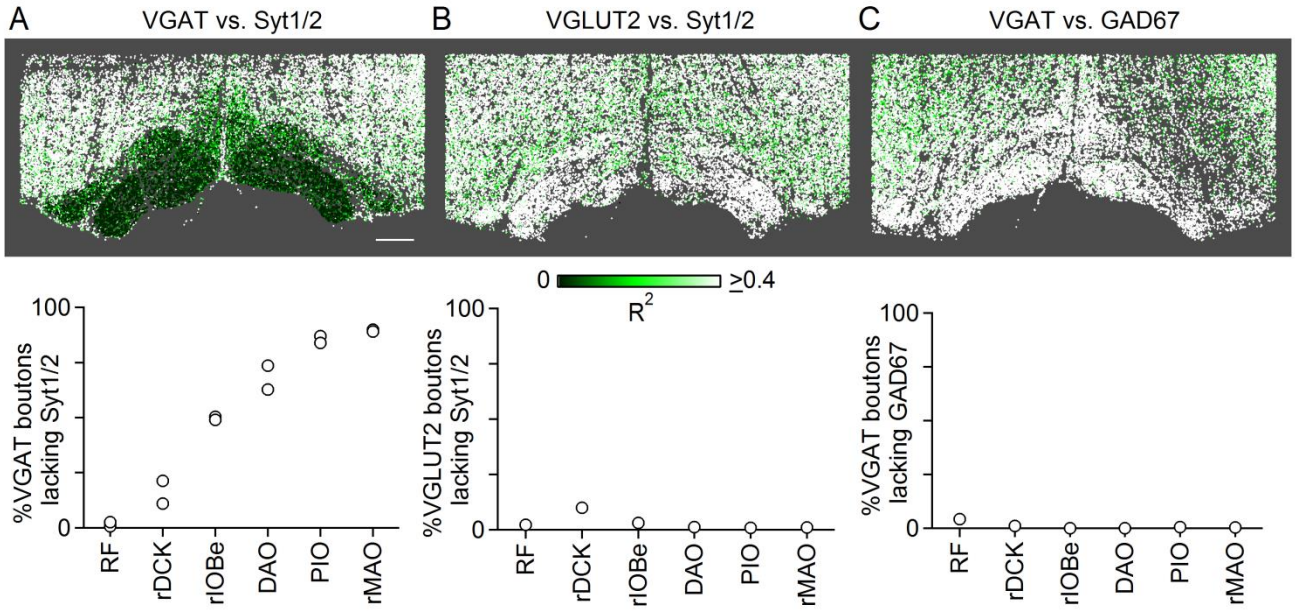

Figure 5.8: Co-localization of other markers. **A,** Mosaic of correlation analysis of VGAT and Syt1/2 for the ventral brainstem (top). The fraction of boutons lacking Syt1/2 ($R^2 < 0.1$) is plotted for the reticular formation (RF) and each subnucleus of the rostral IO (bottom). Scalebar, 200 µm. **B**, Same as in **A** but for immunostaining and analysis of VGLUT2 vs. Syt1/2. **C,** Same as in **A** but for staining and analysis of VGAT vs. GAD67. Markers on bottom are individual animals.

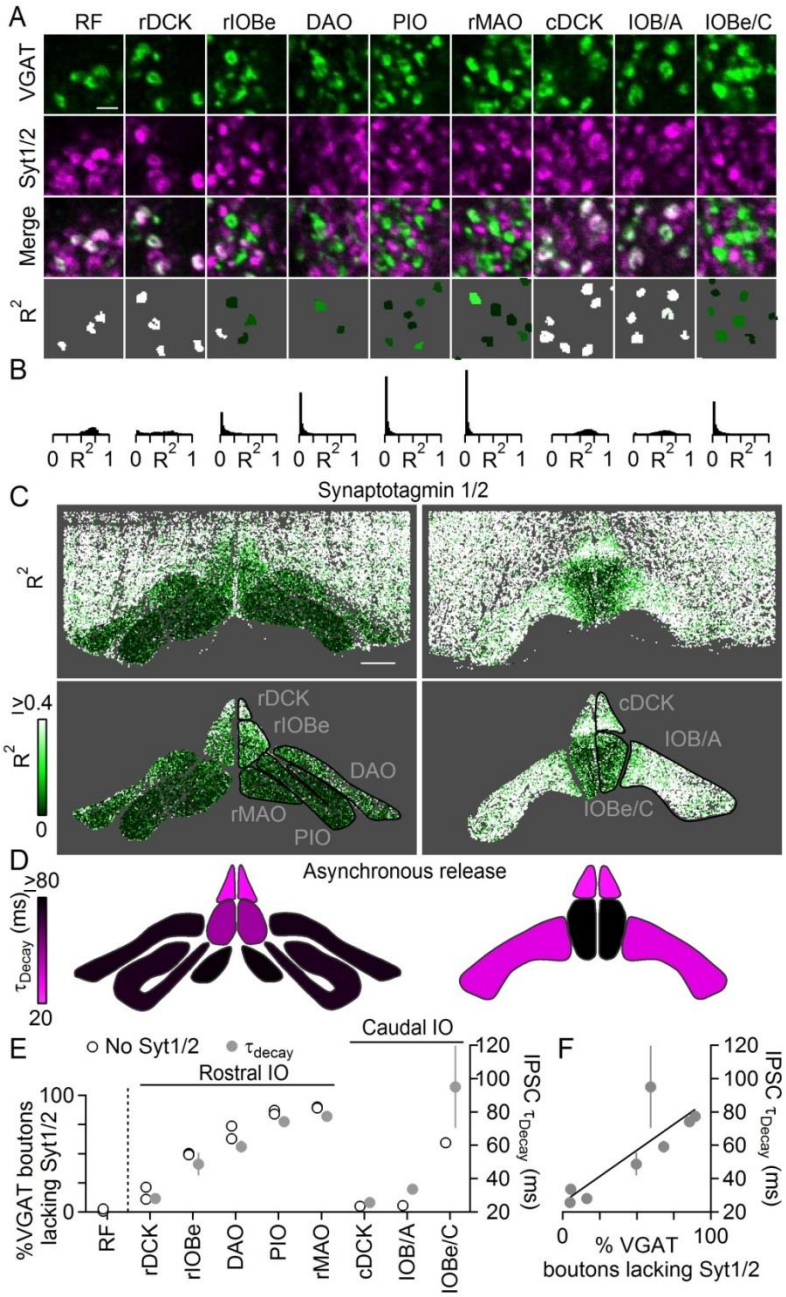

Figure 5.9: Lack of Syt1/2 in GABAergic synapses correlates to asynchronous release in the IO.

A, Example single-plane views of GABAergic boutons, Syt1/2, and correlation analysis for IO subnuclei. Scalebar, 2 µm. **B**, Distribution of correlation coefficient values for all regions normalized by number of boutons within each subnucleus. **C**, Map of correlation coefficient values for rostral (left) and caudal (right) ventral brainstem (top) with IO subnuclei segmented and labeled (bottom). Scalebar, 200 µm.

Figure 5.9 (Continued)

D, Map of the rostral (left) and caudal (right) IO color mapped for the average IPSC τ_{decay}. **E**, Plot of the fraction of GABAergic boutons lacking Syt1/2 ($R^2 < 0.1$, empty markers) and average IPSC decay time (filled gray) for subnuclei and reticular formation (RF). **F**, Plot of average IPSC decay time vs. fraction of VGAT boutons lacking Syt1/2 ($R^2 < 0.1$). Each marker is data from one subnucleus. Physiology data are mean ± s.e.m., anatomy are individual animals.

the fraction of inhibitory synapses lacking Syt1/2 (defined as $R^2 < 0.1$) for direct comparison to the average IPSC decay time (**Figure 5.9E, F**). Syt1/2 were present at most inhibitory synapses in the DCK and the IOB/A, which are regions where the average decay time is less than 30 ms and release is primarily synchronous. Syt1/2 were absent from most inhibitory synapses in DAO, PIO, MAO and IOBe/C, which are regions where the decay of the IPSC is slow and release is primarily asynchronous. Syt1/2 were absent in approximately half of synapses in the rIOBe, which is a region where inhibition has both synchronous and asynchronous components. Thus, there was a correlation between the absence of Syt1/2 at inhibitory synapses and the extent of asynchronous release (**Figure 5.9E, F**). Regions with prominent Syt1/2-VGAT correlation were mainly synchronous, and regions lacking Syt1/2-VGAT correlation had primarily asynchronous release.

Expression of Syt1 is sufficient to synchronize release at asynchronous synapses

These results suggest that a lack of Syt1/2 leads to asynchronous release for inhibitory synapses within the IO. If this is the case, then introducing Syt1 into these synapses should be sufficient to transform release from asynchronous to synchronous. We tested this prediction by presynaptically expressing channelrhodopsin-2 (ChR2-YFP) alone, or bicistronically expressing ChR2-YFP and Syt1 using AAVs (**Figure 5.10**). We then recorded light-evoked synaptic responses in regions of the IO that normally receive asynchronous inhibitory inputs. ChR2-YFP fluorescence was apparent in the IO and could be used to identify regions of the slice containing presynaptic fibers expressing ChR2 (**Figure 5.10A**). Inhibitory synapses that expressed ChR2 alone did not contain Syt1 (**Figure 5.10A**), but when ChR2 and Syt1 were both expressed, inhibitory YFP-expressing synapses also contained Syt1 (**Figure 5.10B**). When ChR2 alone was expressed, all optically-evoked responses in the PIO were asynchronous (**Figure 5.10C, E-F**). However, when ChR2 and Syt1 were expressed, IPSCs in every cell were synchronous with rapid rise times and decay times (**Figure 5.10D-F**). These findings show that the presence of a fast Syt isoform controls the kinetics of neurotransmitter release at these synapses.

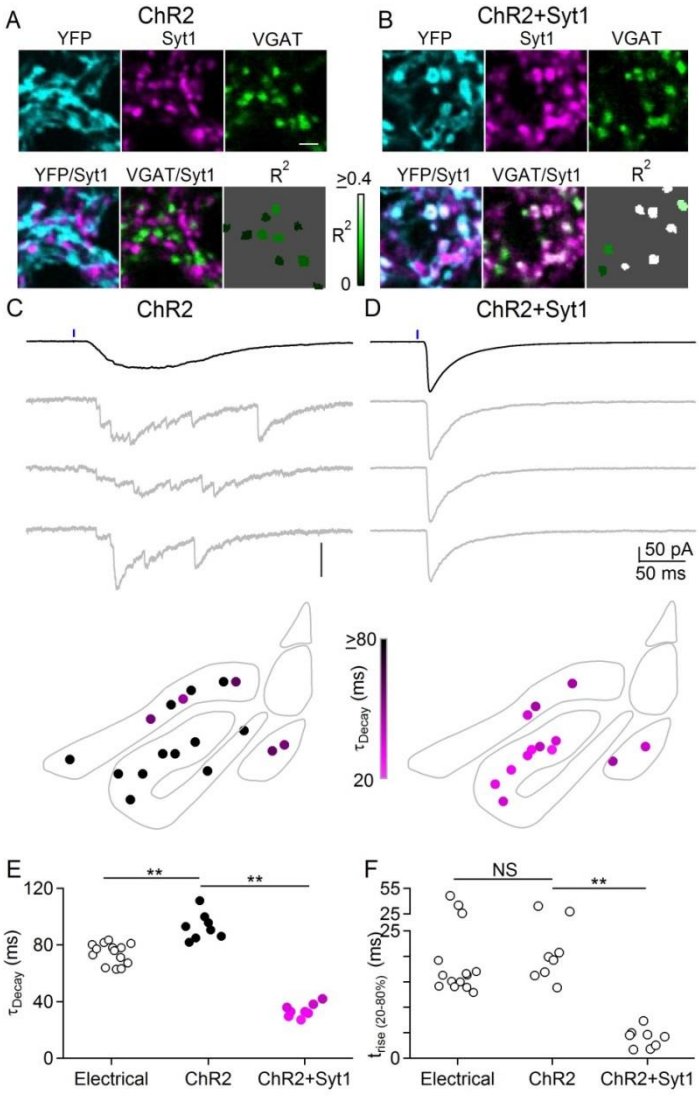

Figure 5.10: Expression of Syt1 is sufficient to drive synchronous release at typically asynchronous synapses. **A**, GABAergic boutons in the PIO expressing ChR2-YFP alone immunostained for VGAT and Syt1. Scalebar, 2 µm. **B**, Same as in **A** but expressing ChR2-YFP and Syt1. **C**, Release evoked by optical simulation in one cell when ChR2 was expressed alone (top) and map of decay time for all cells in the rostral IO (bottom) **D**, Same as in **C**, but for ChR2 and Syt1 expression. **E**, Summary of decay time for optical stimulation of ChR2 alone or ChR2+Syt1 in the PIO. **F**, Same as in **E** but for rise time. Markers are individual cells. **p<0.01, Two-tailed Student's t-test.

DISCUSSION

Our primary finding is that in wildtype animals the exclusion of fast Synaptotagmin isoforms at some specialized synapses leads to exclusively asynchronous release. The differential presence of Syt1/2 at inhibitory synapses across the IO is ideally suited to control the timing of GABA release and thereby tailor the properties of inhibition within each subnucleus.

Release kinetics in the IO are not determined by distance between fast Syts and Ca channels

Our findings exclude the hypothesis that synchronous release and asynchronous release are both mediated by fast Syt isoforms with release kinetics controlled by the distance between release sites and calcium channels within the IO. If this were the case, then fast Syts would be present at all inhibitory synapses across IO subnuclei regardless of whether they mediated synchronous or asynchronous release. However, we found that fast Syts are absent in inhibitory boutons within subnuclei that have exclusively asynchronous release. In addition, the ability of viral Syt1 expression to transform synapses from asynchronous to synchronous suggests that it is the presence or absence of Syt1 rather than some other mechanism such as calcium signaling that is the primary determinant of differential release kinetics. It is unclear whether asynchronous release at other synapses is mediated by similar mechanisms because synapses outside the IO have both synchronous and asynchronous components and appear to have an abundance of fast Syt isoforms.

The presence of Syt7 does not determine if a synapse is asynchronous

There is growing evidence supporting specialized slow, high-affinity calcium sensors mediating asynchronous release (Sun et al., 2007, Yao et al., 2011, Kochubey and Schneggenburger, 2011, Bacaj et al., 2013). Our findings indicate that the mere presence of such a calcium sensor cannot account for whether synapses in the IO are synchronous or asynchronous. Syt7, which mediates asynchronous release at several synapses (Wen et al., 2010, Bacaj et al., 2013, Luo et al., 2015, Luo and Sudhof, 2017, Chen et al., 2017c, Turecek and Regehr, 2018), is generally more prominent at asynchronous synapses in the IO, but it can also be present at comparable levels in regions with very different release kinetics. The remarkable feature of synapses in the IO is that despite the drastically altered kinetics in the absence of

Syt7, the total asynchronous release is not significantly different. The observation that the kinetics of asynchronous release are much slower in Syt7 KO animals suggests that Syt7 can control the kinetics of asynchronous release in wildtype animals. At other synapses, asynchronous release is affected to different degrees in Syt7 KO animals, but at every synapse some component of asynchronous release remains when Syt7 is absent. There can be a wide range of kinetics for the remaining component of asynchronous release (Bacaj et al., 2013, Luo and Sudhof, 2017, Turecek and Regehr, 2018, Weber et al., 2014). These results suggest that there are additional calcium sensors with different properties that can mediate asynchronous release at inhibitory synapses in the IO and elsewhere.

Even though Syt7 levels could not always account for the kinetics of release, the role of Syt7 in clamping release was negatively correlated with release synchrony and the presence of fast Syts. This is consistent with a previous study at the calyx of Held showing that the elimination of Syt7 does not increase spontaneous fusion in wildtype animals, but when Syt2 is eliminated the additional removal of Syt7 elevated mEPSC frequency (Luo and Sudhof, 2017). In IO subnuclei where Syt1 is present, there is synchronous release and the elimination of Syt7 had no effect on spontaneous release. In contrast, in IO subnuclei where Syt1 is absent, release is asynchronous and the elimination of Syt7 increased spontaneous release. Previous studies have also shown that the elimination of fast Syts leads to an elevation of spontaneous release (Littleton et al., 1993, Xu et al., 2009, Kochubey and Schneggenburger, 2011, Bacaj et al., 2013, Luo and Sudhof, 2017, Chen et al., 2017b). This raised the possibility that spontaneous fusion in subnuclei lacking fast Syts would be higher than in subnuclei where fast Syts are present. However, we found that this was not the case and that mIPSCs in wildtype animals were uniformly low in all IO subnuclei.

Fast Syts suppress asynchronous release

Our findings support the hypothesis that fast Syt isoforms suppress asynchronous release. In the simplest scheme for neurotransmitter release, fast Syts mediate synchronous release, another calcium sensor such as Syt7 mediates asynchronous release, and total release at a synapse reflects the summation of these two components. However, in the IO, Syt7 is present at inhibitory synapses in subnuclei such as

the IOB/A where release is synchronous. Syt7 is expressed at many synapses that have tightly synchronized release, and it has become apparent that the presence of a sensor capable of mediating asynchronous release does not necessarily lead to prominent asynchronous release. Our study establishes that within the IO asynchronous release is prominent when fast Syts are excluded from synapses. This is shown more explicitly in the PIO, DAO and rMAO where release is normally asynchronous, but where the viral expression of Syt1 promotes synchronous release and suppresses asynchronous release (**Figure 5.10**). Thus, the abilities of fast Syt isoforms to simultaneously promote synchronous release and suppress asynchronous release are used by DCN neurons to control the timing of GABA release in different IO subnuclei.

Synapses with both synchronous and asynchronous components

Synapses in numerous brain regions have mixed synchronous and asynchronous release that resembles GABA release in the rIOBe and IOBe/C of the IO. Our findings suggest there are two ways that regulating the levels of fast Syts could contribute to mixed synchronous and asynchronous release. One possibility is that boutons containing fast Syts mediate synchronous release, boutons lacking fast Syts mediate asynchronous release, and the ratio of synchronous to asynchronous release is determined by the fraction of synapses where fast Syts are present. Another possibility is that each synapse is capable of both synchronous and asynchronous release. We found that Syt1/2 levels were lower in regions with mixed synchronous/asynchronous release than for regions with purely synchronous release (**Figure 5.7G**). Thus, it is possible that individual synapses generally contribute both asynchronous and synchronous components, with the relative contribution at individual synapses dictated by the levels of fast Syts. If this is the case, when fast Syts are present but at very low levels and a sensor for asynchronous release is also present, both synchronous release and asynchronous release can occur at the same synapse. It will be necessary to study individual synapses to determine the extent to which single synapses can mediate both synchronous and asynchronous release.

Do low levels of fast Syts promote asynchronous release at other synapses?

The role of fast Syts in controlling the relative contributions of synchronous and asynchronous release raises the possibility that asynchronous release elsewhere is mediated by the absence or low abundance of fast Syt isoforms. It is difficult to test this hypothesis for several reasons, as most synapses lack the experimental advantages of the IO. Presynaptic boutons are typically smaller, more closely packed, and difficult to resolve optically in most brain regions. Moreover, synapses of diverse presynaptic origin are generally mixed together rather than being regionally segregated, making it impossible to correlate structural and functional experiments. It may therefore be necessary to devise new approaches to determine if Syt1/2 regulation is a general mechanism to control release timing at many types of synapses.

Functional roles of synchronous and asynchronous release in the IO

The differences in release kinetics in the IO suggest that release timing can be controlled in order to optimize synaptic function. Kinetic differences in DCN to IO synapses in different subnuclei are consistent with regional specializations that allow the cerebellum to perform different computations. Numerous specializations within the loop between the DCN, the IO, and the cerebellar cortex have been described previously. For example, neurons in the IO and cerebellar cortex have regional differences in their firing properties, and some cell types and synaptic connections are preferentially present only in specific lobules of the cerebellar cortex (Witter and De Zeeuw, 2015, Urbano et al., 2006, Guo et al., 2016). A defining feature of the IO is that in many regions IO neurons are electrically coupled via gap junctions, allowing them to provide synchronous climbing fiber activity to the cerebellar cortex. In some IO subnuclei, the absence of fast Syts leads to exclusively asynchronous release and it has been proposed that the slow release kinetics generate tonic inhibitory currents that are ideal for shunting gap-junctional coupling between IO neurons (Lang et al., 1996, Best and Regehr, 2009, Lefler et al., 2014). The asynchronous release in these subnuclei produces graded inhibition that is controlled by input frequency without regard to precise timing. Many presynaptic IO-projecting DCN neurons fire spontaneously, enabling persistent graded tonic inhibition (Najac and Raman, 2015). In other subnuclei, exclusively

synchronous inhibitory inputs are suited to precisely control spike timing rather than spike synchrony (Urbano et al., 2006). Mixed asynchronous and synchronous release could allow inhibition to both influence spike timing and provide graded inhibition of electrical coupling.

EXPERIMENTAL MODEL AND SUBJECT DETAILS

All animals were handled in accordance with NIH guidelines and protocols approved by Harvard Medical Area Standing Committee on Animals. All animals were housed according to Harvard Medical Area Standing Committee on Animals. Adult (≥P60) C57/BL6 of both sexes were obtained from Charles River. Syt7 KO and wildtype littermates (Chakrabarti et al., 2003) were bred from heterozygous crosses (Jackson labs). Experiments were initially performed blind but blinding was abandoned because Syt7 KOs could be easily identified by increased spontaneous release.

METHODS DETAILS

Viruses

AAV2/9-hSyn-hChR2(H134R)-EYFP was obtained from the University of Pennsylvania Vector Core. AAV2/9-hSyn-hChR2(H134R)-EYFP-2A-Syt1 was generated by the Boston Children's Virus Core. Experiments in **Figure 5.10** were performed blind to virus identity, and for all other experiments were not blinded.

Stereotaxic surgeries were performed on adult (≥P60) C57/BL6 male mice anesthetized with ketamine/xylazine (100/10 mg/kg) supplemented with isoflurane (1-4%). Viruses were injected through fine-tipped glass capillary needles via a Nanoject III (Drummond) mounted on a stereotaxic (Kopf). Unilateral (for anatomy) or bilateral (for electrophysiology) injections were made in the cerebellum targeting the DCN, 2.5 mm lateral, 2 mm posterior from lambda, 2.5 mm depth. 300-500 nL of virus suspension was delivered to each site at a rate of 100 nL/minute, and the needle was retracted 10 minutes following injection. Subcutaneous analgesic (buprenorphine 0.05 mg/kg) was administered for 48 hours post-surgery.

Slice preparation

Slices were obtained from adult (≥P60) C57/BL6 mice or from Syt7 KOs and wildtype littermates of both sexes (Chakrabarti et al., 2003). Animals were anesthetized using ketamine/xylazine (100/10 mg/kg) and transcardially perfused with solution composed of in mM: 110 Choline Cl, 2.5 KCl, 1.25 NaH_2PO_4, 25 $NaHCO_3$, 25 glucose, 0.5 $CaCl_2$, 7 $MgCl_2$, 3.1 Na Pyruvate, 11.6 Na Ascorbate, 0.002 (R,S)-CPP, 0.005 NBQX, oxygenated with 95% O2 / 5% CO_2, kept at 35°C. The back of the skull was removed and the hind brain was dissected by making a cut between the border of the cerebellum and midbrain. The dura was carefully removed from the hindbrain and the cut face was glued down. 250 μm thick coronal sections of the brainstem were made on a Leica 1200S vibratome and were then transferred to a holding chamber with ACSF containing in mM: 127 NaCl, 2.5 KCl, 1.25 NaH_2PO_4, 25 $NaHCO_3$, 25 glucose, 1.5 $CaCl_2$, 1 $MgCl_2$, and allowed to recover at 35°C for at least 20 minutes before cooling to room temperature. For experiments involving an AAV, electrophysiology was performed 10-20 days after injections.

Electrophysiology

All experiments were performed at room temperature with a flow rate of 3-5 ml/min. Recording ACSF had the same composition as incubation ACSF except external Ca^{2+} was raised to 2.5 mM and Mg^{2+} lowered to 0.5 mM to maximize the amount of release evoked by single stimuli. Borosilicate electrodes (1-2 MΩ) contained internal solution consisting in mM of: 110 CsCl, 10 HEPES, 10 TEA-Cl, 1 $MgCl_2$, 4 $CaCl_2$, 5 EGTA, 20 Cs-BAPTA, 2 QX314, 0.2 D600, pH to 7.3. Cells were held at -70 mV, and all experiments were performed in the presence of 5 μM NBQX to block AMPARs, 2.5 μM (R,S)-CPP to block NMDARs, and 0.5 μM strychnine to block glycine receptors. IO neurons have prominent subthreshold membrane potential oscillations (Llinas and Yarom, 1981a, Llinas and Yarom, 1981b, Llinas and Yarom, 1986, Turecek et al., 2016a) and conditions were adjusted to minimize oscillatory activity. 1 μM TTA-P2 was included in the ACSF to block t-type Ca^{2+} channels that can drive sub-threshold oscillations (Llinas and Yarom, 1981b). The blockade of t-type channels does not influence the

release of GABA in the IO (Best and Regehr, 2009). Trains of stimuli were avoided to prevent evoking electrically coupled bursts of IO neurons. Experiments were performed at room temperature to suppress oscillations. For most experiments, a glass monopolar stimulus electrode (2-3 MΩ) filled with ACSF was placed within the IO or in the surrounding reticular formation. Single stimuli were applied every 5 seconds at low stimulus intensities in which single asynchronous quantal events could be identified. For experiments measuring maximal charge in wildtype and Syt7 KOs, a glass monopolar stimulus electrode (2 MΩ) was placed in the dorsomedial edge of the dorsal PIO and cells were recorded 100 μm away in the dorsal PIO. Single stimuli were applied every 10 seconds, and the stimulation intensity was ramped from 10-100 μA. Total evoked charge typically reached maximal values between 30-80 μA, and the charge for one second after stimulation evoked by 100 μA stimulation was used as a measure of maximally evoked release. DCN axons expressing ChR2 were stimulated by 473 nm light (0.5-1 ms, 80 mW/mm^2) generated by an LED (Thorlabs). Illumination was guided through a 60x objective producing an 80 μm diameter spot that was positioned several hundred μm away from the recorded cell. All data are presented as individual cells unless otherwise noted. Whole-cell capacitance and series resistance was left uncompensated for all experiments. All currents were reversible at 0 mV, indicating that they were not mediated by gap junctions. For some cells, the $GABA_A$Rs antagonist SR95531 (5 μM) was washed in at the end of the experiments to ensure currents were mediated by $GABA_A$Rs. One hundred trials were typically collected per cell to ensure smooth averaged currents. Measurements of mIPSC frequency were performed in the presence of TTX (0.5 μM) and in slices unperturbed by stimulus electrodes. Raphe obscurus neurons along the midline could be identified physiologically by their passive membrane properties and were avoided.

Immunohistochemistry

Adult ($\geq$P60) male mice were anesthetized using ketamine/xylazine (100/10 mg/kg) and perfused transcardially with PBS followed by 4% paraformaldehyde (PFA) in PBS. Brains were removed and post-fixed overnight in PFA. The brainstem was mounted in 6% low-melting agarose and sliced coronally on a

Leica VT1000S vibratome (30-50 µm). For immunohistochemistry, sections of the IO were subdivided into rostral and caudal sections with the same criteria used for physiology experiments (see Quantification and Statistical Analysis). Free-floating slices were then permeabilized (0.2% triton X-100 in PBS) for 10 min and blocked for 1 hr (4% Normal Goat Serum in 0.1 % triton X-100) at room temperature, followed by incubation overnight at 4°C with primary antibodies (Mouse anti-Syt1, Synaptic Systems 105011, 1:500; Mouse anti-Syt2, Zirc znp-1, 1:200; Guinea-pig anti-VGAT, Synaptic Systems 131004, 1 µg/mL, 1:200; Guinea-pig anti-VGLUT2, Synaptic Systems 135404, 1 µg/mL, 1:1200, Mouse anti-Syt7, UC Davis/NIH NeuroMab Facility, clone N275/14, RRID: AB_11030371, 1 µg/mL, 1:100). Antibodies targeting Syt1 and Syt2 have been validated for immunohistochemistry in brainstem tissue using conditional knockout mice (Kochubey et al., 2016, Bouhours et al., 2017). Antibodies targeting Syt7 have been validated for staining in tissue using global knockout mice (Turecek et al., 2017). For all analyzed experiments presented here, antibodies for Syt1 and Syt2 were mixed together and labeled with the same secondary. To prevent background when co-staining with VGLUT2 and Syt1/2, Syt1/2 primary antibodies were applied alone overnight at 4°C, then VGLUT2 primary antibodies alone for 2 hrs at room temperature. Secondary antibodies were then applied for 2 hrs at room temperature (anti-Guinea-pig-AlexaFluor488, Abcam ab150185; anti-Guinea-pig-DyLight594, Abcam ab102376; anti-Mouse-AlexaFluor568, Abcam ab175473; anti-Mouse-AlexaFluor647, Abcam ab150115). Slices were mounted using #1.5 coverslips and Prolong Diamond Antifade mounting medium. Z-Stacks of each sample were collected on an Olympus Fluoview1000 confocal microscope with FluoView software using a 60X 1.42 NA oil immersion objective, and mosaics of the entire ventral brainstem were collected on a motorized stage. Acquisition settings were kept constant across the entire mosaic. Images were collected with xy resolution of 0.129 µm/pixel with 16 bit depth and z-spacing of 0.25 µm/section. Individual stacks were 132 x 132 x 3.25 µm in size.

For 3D-SIM, tissue was prepared as described above, but with minor modifications to optimize resolution. Slice thickness was reduced to 7-10 µm and slices were mounted on glass slides instead of free-floating. Immunostaining was then performed at 4°C. Blocking and permeabilization solution (4%

Normal Goat Serum in 0.01% triton X-100) was applied for 1 hr. Primary antibodies were applied for 45 minutes, followed by 1 hr incubation with secondary antibodies. Slides were mounted with precision cover glasses (thickness 170 ± 5 μm, Zeiss). Imaging was performed using a DeltaVision OMX V4 Blaze system (GE Healthcare). Images were collected using a 60X 1.42 NA oil immersion objective and each channel was collected on separate Edge 5.5 sCMOS cameras (PCO). Z-stacks were collected with xy resolution of 0.04 μm/pixel and z-spacing of 0.125 μm with 15 raw images collected per plane (five phases, three angles). Images were reconstructed with channel-specific measured optical transfer function and Weiner filter constant of 0.002 in softWoRx 6.1.3 (GE Healthcare). Stacks were collected in the dorsal accessory olive and adjacent reticular formation in 90 x 90 x 6.6 μm volumes.

QUANTIFICATION AND STATISTICAL ANALYSIS

Electrophysiology analysis

Recordings were collected with a Multiclamp 700B (Molecular Devices) in Igor Pro (Wavemetrics). Data was sampled at 20 kHz and filtered at 4 kHz. All analysis was performed using custom-written scripts in Matlab (Mathworks). Stimulus artifacts were blanked for clarity. For all cells, the average synaptic current was used to calculate the half-rise time, decay time and jitter. To calculate jitter, the time of peak current amplitude for each trial was measured, and the standard deviation of peak times was calculated. mIPSCs were detected using a first derivative and integration threshold using custom written scripts in Matlab. mIPSCs in Syt7 KOs were so frequent that individual events often summated, and therefore the amplitude of mIPSCs could not be reliably measured. For all cells, an image of the recording configuration showing the position of the recording and stimulation electrodes and full view of the IO were captured under a 5x objective using a CCD. Images were later used to assign cells to a common map of the IO (Paxinos and Franklin, 2001, Fu and Watson, 2012, Yu et al., 2014). Cells in the caudal IO were restricted to caudal sections in which the lateral arms of the IO were single bands of gray matter and no DAO or PIO was visible. Cells included in the rostral IO were restricted to rostral sections in which the IOBe and DCK were visible and the lateral aspect of the PIO and DAO was clearly defined.

Statistical significance for physiology experiments was assessed using unpaired two-tailed Student's t-test. All data are presented as individual cells unless otherwise noted.

Anatomical and co-localization analysis

Confocal images were not de-noised or processed in any way, and analysis were performed on raw data using custom-written scripts in Matlab. Images were prepared for display in ImageJ, making only minor increases in brightness in some cases.

For analysis of Syt7 levels, VGAT signals were used to identify VGAT-positive boutons. VGAT-positive boutons were identified as local maxima of signals in 2D images. A set VGAT intensity was used to threshold the VGAT channel, and the average Syt7 intensity within the thresholded region was used as the Syt7 level for that bouton. Subnuclei were identified using VGAT staining (see below), and the median Syt7 intensity was collected for wildtype and Syt7 KOs. The median Syt7 intensity for Syt7 KOs for each subnucleus was subtracted from median wildtype intensity for final analysis shown in **Figure 5.3**.

For co-localization analysis of VGAT and Syt1/2, we first attempted to assess co-localization using object-based methods in which VGAT and Syt1/2 boutons were detected and co-localization was measured as the nearest neighbor distance. However, this method was problematic because the morphology of boutons was heterogeneous and often poorly fit by a 3D Gaussian. We therefore used pixel-based co-localization that is much simpler and is also insensitive to the shape of boutons. Co-localization was determined by the degree of signal correlation using Pearson's correlation coefficient (**Figure 5.7A-E**). VGAT and Syt1/2 staining was robust with little background, which provided the high signal to noise required by this method. We limited our final analysis to determining whether Syt1/2 was present at synapses or not because quantitative conclusions can be difficult to draw from the degree of signal correlation. Similar analysis could not be performed for Syt7 and VGAT because Syt7 expression was diffuse.

VGAT-positive boutons were identified as local maxima of signals in each imaged 3D volume. For each identified VGAT synapse, a 1.5 x 1.5 x 1.25 μm volume of interest was drawn around the

bouton centroid. The intensity of VGAT signal and Syt1/2 signal was collected for each voxel within the region of interest and plotted against each other. Voxels in the periphery of the region of interest (outer 0.25 μm) that had strong VGAT signals from neighboring boutons were detected by a set intensity threshold and were ignored. The correlation between VGAT and Syt1/2 signal was measured using linear regression, obtaining a value of R^2 that was then used as a measure of co-localization. In many cases within the IO, VGAT and Syt1/2 were partially anti-correlated (slope of regression line < 0). In these cases R^2 was set to 0.01. Analysis was performed similarly for confocal and 3D SIM data.

For analysis of individual IO subnuclei, regions were outlined by visual inspection of a VGAT mosaic image. The reticular formation was drawn as a 170 x 170 x 3.25 μm volume just dorsal to the DAO, as shown in **Figure 5.6A**. In order to measure the density of VGAT-positive synapses for each nuclei in wildtype and Syt7 KOs, small 1000-3000 μm^3 volumes of neuropil were selected for analysis to avoid cell bodies and myelinated fiber tracts. Several nuclei were grouped because they were too small to be reliably distinguished and compared across experiments, such as the ventrolateral outgrowth which was incorporated into the rostral beta subnucleus. Others were grouped because the borders could not be clearly defined, such as the grouping of the caudal beta subnucleus and subnucleus C, and grouping of caudal subnuclei A and B. Statistical significance between distribution of R^2 values of different subnuclei were assessed using two-sample Kolmogorov-Smirnov tests. Summary points in **Figure 5.9E** are shown as average of left and right subnuclei from individual animals.

Chapter 6

Conclusion

Syt7 as a Ca sensor for short-term facilitation

In this thesis, we have shown that short-term facilitation is eliminated at five different synapses in Syt7 KOs. Under near physiological conditions facilitation was absent at CA3-CA1, perforant path, corticothalamic, PC-DCN, and VA-MVN synapses. No facilitation was observed in low Ca at CA3-CA1, PC-DCN and VA-MVN synapses, suggesting that facilitation was completely eliminated at these synapses, and that there are no additional mechanisms of facilitation remaining in the absence of Syt7. It has also been shown recently that Syt7 is involved in facilitation at cerebellar basket cell synapses. Thus, Syt7 mediates most facilitation at many different types of synapses in multiple brain regions.

Ca sensing by Syt7 is required for facilitation, suggesting that Syt7 may act as a Ca sensor for facilitation. However, loss of Syt7 can change other synaptic properties, such as recovery from depression and the kinetics or magnitude of asynchronous release. Thus, the function of Syt7 may be more complicated. Future experiments will be required to test the Ca affinity of Syt7 and its role in facilitation. If Syt7 is a Ca sensor for facilitation, altering the Ca sensitivity of Syt7 would be expected to change the strength of facilitation such that lowering the Ca affinity would result in more attenuated facilitation.

It is clear that there are other mechanisms of short-term facilitation, some of which are evident in the absence of Syt7. Facilitation was attenuated at PF-PC and PF-SC synapses in Syt7 KOs, but under near physiological conditions, the remaining component of facilitation was small and rapid. A substantial component of facilitation remains at hippocampal mossy fibers in the absence of Syt7. The remaining component is consistent with reported use-dependent changes in action potential waveform that can result in increased Ca entry during repetitive stimulation. It also been reported that the elimination of Syt7 does not affect facilitation at the Calyx of Held in low external Ca. Thus, there are additional mechanisms of short-term facilitation that are evident at multiple synapses.

We have shown that facilitation of Ca^{2+} entry through $Ca_V2.1$ channels likely plays little role in synaptic facilitation at CA3-CA1 synapses. It is unclear the extent to which $Ca_V2.1$ facilitation plays a role at PF-PC synapses because it is likely that Ca influx is altered in Ca-IMAA mice at PF synapses.

The role of Syt7 in asynchronous release and vesicle replenishment

In addition to mediating short-term facilitation, it has been shown that Syt7 can also play a role in asynchronous release at many synapses. We have shown in Chapter 4 that Syt7 contributes to asynchronous release at PF-PC synapses, and that the kinetics of asynchronous release are altered at DCN-IO synapses in Syt7 KOs. The role of Syt7 in PF synapses appears to be different than at DCN-IO synapses, because Syt7 plays a role in facilitation at PF synapses, but not at DCN-IO synapses. Mechanisms of asynchronous release in the absence of Syt7 also appear to be different between these synapses, because the remaining release at PF synapses has faster kinetics, whereas the release at DCN-IO synapses in Syt7 KOs is slower.

We have shown in Chapter 3 that Syt7 does not accelerate synaptic vesicle replenishment, at least at PC-DCN synapses. In contrast to other synapses (Chen & Jonas 2017b), it would appear that Syt7 impedes recovery from depression. It is unclear whether Syt7 is directly involved in vesicle replenishment at PC-DCN synapses, or whether the acceleration of recovery in Syt7 KOs is a compensatory mechanism.

Use-dependent recovery has been shown to occur at cerebellar climbing fiber synapses, and at the Calyx of Held. We have found that Syt7 is not expressed by climbing fibers, and it is unclear whether Syt7 plays a role in vesicle replenishment at the Calyx of Held. A role for Syt7 has been suggested for cerebellar basket cell synapses, but in contrast to previous work, Syt7 appears to play a weaker role that is limited to a slow phase of recovery from depression. Thus, the role of Syt7 in synaptic vesicle replenishment is unclear.

Potential mechanisms of Syt7 in facilitation and asynchronous release

Although we have shown that Syt7 plays a role in facilitation, how Syt7 enhances vesicle release is unclear. During facilitation Syt7 likely drives release mediated by fast Syts because release mediated by Syt7 in the absence of fast Syts is asynchronous. Syt7 differs from fast Syt isoforms in several ways. In contrast to Syts that drive synchronous release, Syt7 has been proposed to be present on the plasma membrane and excluded from synaptic vesicles. It is also known that Syt7 is capable of interacting with phospholipids and SNARE proteins in a Ca-dependent manner, but with a higher affinity than Syt1,2 or 9

(Sugita et al., 2002, Osborne et al., 2007). Phospholipid binding of Syt7 has also been shown to be slower than fast Syts (Hui et al., 2005), with unbinding rates 60-fold slower than Syt1 (Brandt et al., 2012). Thus, Syt7 is generally slower and has higher affinity for binding interactions that are likely to play a major role in its function.

The mechanism by which Syt1 triggers synchronous release is controversial, but it has been proposed that binding of phospholipids and SNAREs by Syt1 triggers release. Upon Ca binding, the top loops of the Syt1 C2B domain bind the plasma membrane whereas basic regions of Syt1 remain bound to SNAREs. The binding of Syt1 then induces a curvature in the plasma membrane that brings the vesicle and plasma membrane closer together, reducing the energy barrier for fusion. One possibility is that Syt7 could act in a similar way, but due to its slow kinetics and high Ca affinity, reduces the energy barrier for fusion to a much slower and weaker extent (Jackman and Regehr, 2017). However, much less is known about the biochemical properties of Syt7, and will be required to understand the mechanisms underlying its role in short term plasticity.

Another possibility is that Syt7 interacts with other proteins at synapses to promote release. It has been proposed that Syt7 could interact directly with Ca channels, but many synapses do not appear to have use-dependent changes in Ca entry, and no interaction has been shown between Ca channels and Syt7 or any other Syt isoform. Syt7 has been shown to interact with calmodulin, and the interaction with calmodulin has been proposed to be important for the role of Syt7 in vesicle replenishment in cultured neurons. Whether Syt7 and calmodulin could interact to change other synaptic properties is not known.

Controlling release synchrony at synapses

We have shown that Syt7 is expressed at many different synapses, but few synapses expressing Syt7 have prominent asynchronous release. At synapses where asynchronous release is prominent, mediates asynchronous release do various degrees, and in at least one the removal of Syt7 does not decrease the magnitude of asynchronous release.

Remaining mechanisms of facilitation and asynchronous release

Although Syt7 eliminated facilitation or asynchronous release at many synapses, there are some synapses where there are remaining components of release in the absence of Syt7. The remaining components suggest that there must be additional mechanisms capable of achieving short term facilitation and asynchronous release.

Appendix A

The calcium sensor Synaptotagmin 7 is required for synaptic facilitation

Skyler L. Jackman, Josef Turecek, Justine E. Belinsky, Wade G. Regehr

Nature, *529*(7584), 88.

Contributions

S.L.J., J.T., and W.G.R. designed experiments. J.E.B. performed stereotaxic surgeries, S.L.J. performed electrophysiology, and J.T measured Ca^{2+} and performed immunohistochemistry. S.L.J. and J.T. produced AAVs and analyzed experiments, and S.L.J. and W.G.R. wrote the manuscript.

Abstract

It has been known for over 70 years that synaptic strength is dynamically regulated in a use-dependent manner (Feng, 1940). At synapses with a low initial release probability, closely spaced presynaptic action potentials can result in facilitation, a short-term form of enhancement where each subsequent action potential evokes greater neurotransmitter release (Zucker and Regehr, 2002b). Facilitation can enhance neurotransmitter release manyfold and profoundly influence information transfer across synapses (Abbott and Regehr, 2004), but the underlying mechanism remains a mystery. Among the proposed mechanisms is that a specialized calcium sensor for facilitation transiently increases the probability of release (Zucker and Regehr, 2002b, Atluri and Regehr, 1996b) and is distinct from the fast sensors that mediate rapid neurotransmitter release. Yet such a sensor has never been identified, and its very existence has been disputed (Bertram et al., 1996, Felmy et al., 2003). Here we show that Synaptotagmin 7 (syt7) is a calcium sensor that is required for facilitation at multiple central synapses. In syt7 knockout mice, facilitation is eliminated even though the initial probability of release and presynaptic residual calcium signals are unaltered. Expression of wild-type syt7 in presynaptic neurons restored facilitation, whereas expression of a mutated syt7 with a calcium-insensitive C2A domain did not. By revealing the role of syt7 in synaptic facilitation, these results resolve a longstanding debate about a widespread form of short-term plasticity, and will enable future studies that may lead to a deeper understanding of the functional importance of facilitation.

Results

Several mechanisms for facilitation have been proposed (**Figure 7.1**). In the "buffer saturation" model, high concentrations of presynaptic Ca^{2+} buffer capture incoming Ca^{2+} before it binds to the rapid Synaptotagmin isoforms (1, 2 and 9) that trigger vesicle fusion at most synapses (Sudhof, 2013). If the Ca^{2+} buffer saturates during the first action potential, more Ca^{2+} reaches release sites during subsequent action potentials, producing facilitation (Felmy et al., 2003, Matveev et al., 2004). Yet many facilitating synapses lack sufficient presynaptic Ca^{2+} buffer to account for this form of facilitation (Blatow et al., 2003). Another theory suggests that a specialized Ca^{2+} sensor responds to the smaller, longer-lasting Ca^{2+} signals between action potentials (Atluri and Regehr, 1996b). Under one scenario, this sensor modulates Ca^{2+} channels to produce use-dependent increases in Ca^{2+} influx (Mochida et al., 2008). Several canditate proteins have been proposed to act in this manner (Sippy et al., 2003, Tsujimoto et al., 2002), but increased Ca^{2+} influx cannot account for facilitation at most synapses (Muller et al., 2008). Alternatively, an unidentified Ca^{2+} sensor could mediate facilitation by directly increasing the probability of release (*p*).

Syt7 is located presynaptically, and binds Ca^{2+} with high affinity and slow kinetics (Hui et al., 2005, Li et al., 1995, Sugita et al., 2001), making it a promising candidate sensor for the modest increases in residual Ca^{2+} that mediate facilitation. Previous studies suggest that syt7 contributes to a slow phase of transmission known as asynchronous release (Wen et al., 2010, Bacaj et al., 2013), and to Ca^{2+}-dependent recovery from depression (Liu et al., 2014), but the role of syt7 in facilitation was not examined because these studies employed synapses with prominent depression that obscures facilitation. We therefore examined synaptic transmission at four facilitating synapses: Schaffer collateral synapses between hippocampal CA3 and CA1 pyramidal cells(Blatow et al., 2003) (**Figure 7.2a**), thalamocortical synapses between layer 6 cortical pyramidal cells and thalamic relay cells (Descheenes and Hu, 1990) (**Figure 7.2b**), mossy fiber synapses between dentate granule and CA3 cells (Blatow et al., 2003) (**Figure 7.2c**), and perforant path synapses between layer II/III cells of the entorhinal cortex and dentate granule cells(Lomo, 1971) (**Figure 7.2d**). Immunohistochemistry shows that syt7 is present in regions where

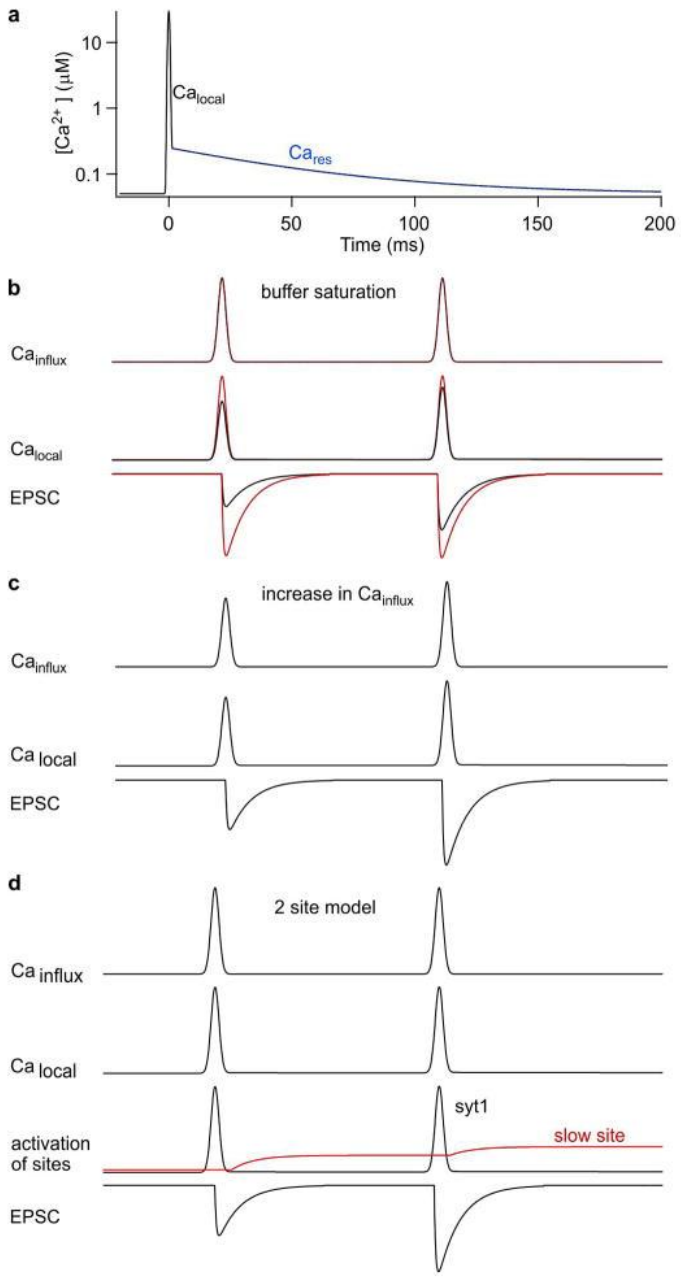

Figure 7.1. Possible mechanisms for synaptic facilitation.

It is established that calcium plays an important role in synaptic facilitation, and a number of mechanisms have been proposed that involve different aspects of calcium signaling(Zucker and Regehr, 2002b). Here we discuss the calcium signals that evoke rapid vesicle fusion, and also those thought to be involved in facilitation (**a**), and 3 mechanisms of facilitation are presented schematically(Regehr, 2012) (**b-d**). **a**, To understand the mechanisms that have been proposed to account for facilitation, it is important to

Figure 7.1 (Continued)

appreciate different aspects of presynaptic calcium signaling. Calcium signals are complex, but can be approximated by 2 components. An action potential opens calcium channels for less than a millisecond, and near open channels the calcium levels reach tens of micromolar. Release sites near calcium channels experience high local calcium levels (Ca_{local}) that are highly dependent on the distance from open calcium channels. Ca_{local} can be reduced by high concentrations of fast calcium buffers that rapidly bind calcium. In addition there is a residual calcium signal (Ca_{res}) that results from calcium equilibrating within presynaptic terminals, before calcium is gradually removed over tens to hundreds of milliseconds. The amplitude of Ca_{res} (and also total influx of Ca^{2+}, Ca_{influx}) is determined by *all* of the calcium channels that open, not only those that produce Ca_{local} that drives release, and after initial equilibration Ca_{res} is roughly uniform throughout the presynaptic bouton. It is generally accepted that fast synaptic transmission is produced by calcium binding to syt1, syt2 or syt9 which have low-affinity binding sites, fast kinetics, and require the binding of multiple calcium ions(Sudhof, 2013, Kaeser and Regehr, 2014a). The time course of release follows the time course of calcium channel opening, but with a brief delay (< 1 ms). Ca_{res} after a single stimulus is much smaller than Ca_{local}. Typical fluorescence-based approaches to measure calcium readily detect Ca_{res}, but are insensitive to Ca_{local} which is too localized and short-lived to measure. Note the y-axis is logarithmic to show both Ca_{local} and Ca_{res} in (**a**), but not in (**b-d**). **b**, For one mechanism of facilitation a fast calcium buffer is present in presynaptic terminals that binds calcium and reduces Ca_{local}. Stimulating twice in rapid succession results in the same calcium influx for both stimuli. If there is no fast presynaptic buffer, the amplitudes of Ca_{local} and the EPSCs are the same for both stimuli (red traces). If a fast high-affinity buffer is present (black traces), it reduces the initial Ca_{local} and reduces the amplitude of the initial EPSC, but if enough calcium enters and binds to the buffer, it reduces its ability to buffer calcium. As a result the second stimulus produces larger Ca_{local} than the first, and the EPSC is facilitated. **c**, A second possible mechanism is that more calcium enters for the second stimulus, and as a result there is more neurotransmitter release. This could arise from a spike broadening, or from the modulation of

Figure 7.1 (Continued)

calcium channels. It is possible that influx through all calcium channels in the presynaptic terminal would be increased, in which case both Ca_{res} and Ca_{local} would be increased. It is also possible that the only calcium channels that are modulated are the subset that produce Ca_{local} that triggers release, in which case Ca_{res} would not be significantly increased. **d**, Finally, it is possible that there is a specialized calcium sensor that produces facilitation that is distinct from syt1(Zucker and Regehr, 2002b, Kamiya and Zucker, 1994, Atluri and Regehr, 1996b). Previous studies have shown that such a sensor would need to be sensitive to Ca_{res} based on the observation that facilitation is altered at some synapses by manipulations that affect Ca_{res} without affecting Ca_{local}. According to this scheme, release is mediated by syt1 but calcium binding to a second sensor would increase *p*. The sensor is sufficiently slow that it does not influence release evoked by the first stimulus, but it able to influence release evoked by a second stimulus.

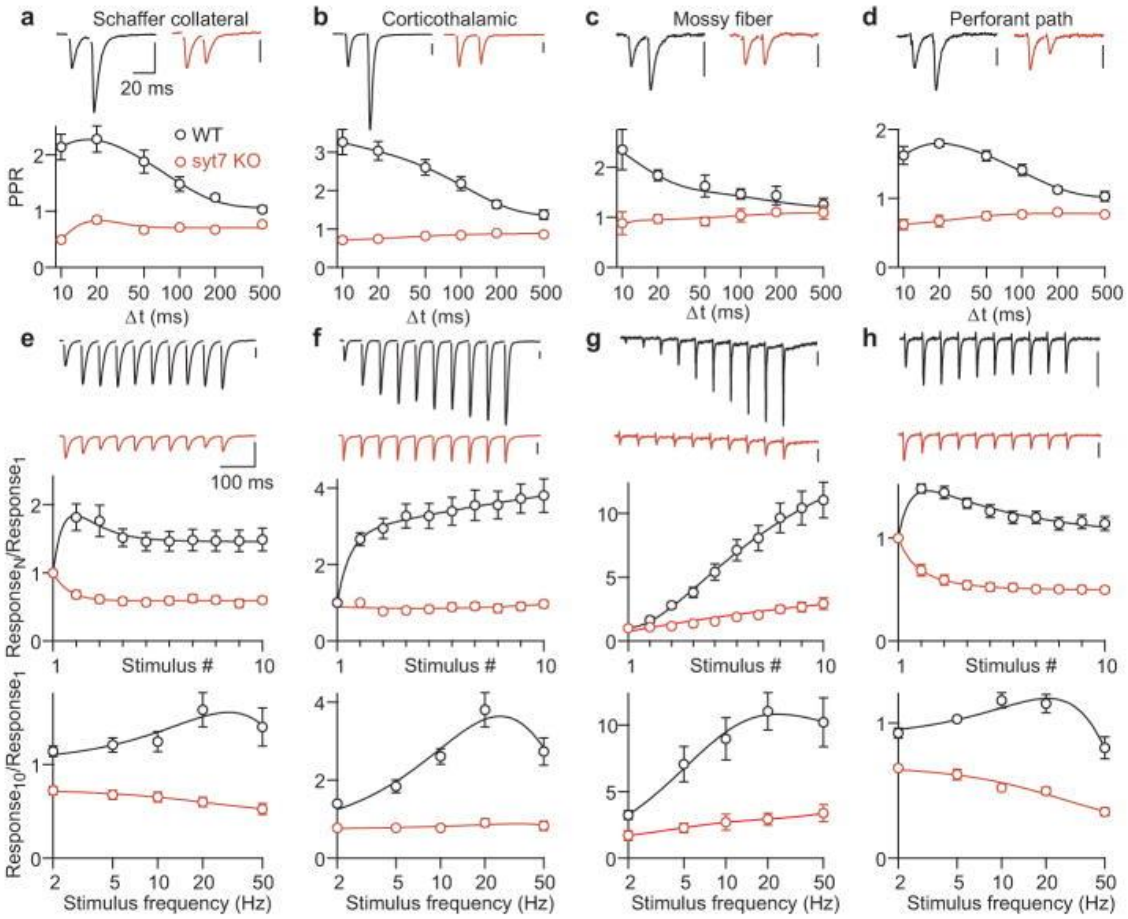

Figure 7.2: Facilitation is absent in syt7 KO mice.

a-d, Representative traces (top) and average paired-pulse ratios (PPR) at different interstimulus intervals (Δt) (bottom) recorded in slices prepared from WT (black) and syt7 KO animals (red). Postsynaptic responses were recorded using whole-cell voltage clamp from (**a**) hippocampal CA1 pyramidal cells, and (**b**) thalamic relay cells. fEPSPs were recorded from (**c**) hippocampal-mossy-fiber to CA3 synapses, and (**d**) lateral-performant-path synapses in the dentate gyrus. Vertical scale bars, 100 pA (**a,b**) and 100 μV (**c,d**). **e-h**, Synaptic responses to 20 Hz trains from the same preparations as **a-d** (top), normalized amplitudes during 20 Hz trains (middle), and normalized responses to the 10th stimulus as a function of stimulus frequency (bottom). Peak PPR was significantly different for WT and syt7 KO mice at all synapses, as was response$_{10}$/response$_1$ for 5 to 50 Hz trains ($P < 0.01$, Student's t-test). Data in this and subsequent figures represent mean ± SEM.

these synapses are located (**Figure 7.3, 7.4**). Facilitation is often assessed using pairs of closely-spaced stimuli. In slices from wild-type (WT) mice, paired-pulse facilitation resulted in ~2-fold enhancement of neurotransmitter release lasting several hundred milliseconds (**Figure 7.2a-d,** black traces). In syt7 knockout (KO) mice, paired-pulse facilitation was eliminated (**Figure 7.2a-d**, red traces). Sustained high frequency activation produces up to 10-fold enhancement in wild-type animals, but in knockouts facilitation is eliminated at all synapses except for mossy fiber synapses, where the remaining enhancement is consistent with use-dependent spike broadening that occurs at this synapse (Geiger and Jonas, 2000) (**Figure 7.2e-h, 7.5**).

The loss of facilitation in syt7 knockouts cannot be accounted for by slowed recovery from depression reported with syt7 deletion (Liu et al., 2014) because recovery from depression is too slow to strongly influence rapid facilitation, nor can it produce the large increase in release associated with facilitation. There are several possible explanations for the loss of facilitation in knockouts: (1) the presynaptic Ca^{2+} signal that induces facilitation could be altered, (2) the probability of release (p) for synaptic vesicles could be increased, which by promoting vesicle depletion would indirectly reduce facilitation, or (3) the mechanism for facilitation could be disrupted directly. We assessed these possibilities at the CA3→CA1 synapse.

Action-potential-evoked increases in presynaptic Ca^{2+} consist of a large, brief localized Ca^{2+} signal that activates the low-affinity Ca^{2+} sensor Synaptotagmin 1 to trigger neurotransmitter release (Geppert et al., 1994), and a small residual Ca^{2+} signal (Ca_{res}) that persists for tens of milliseconds and has been implicated in facilitation (Zucker and Regehr, 2002b). It is difficult to measure local Ca^{2+} signals that trigger release, but Ca_{res} is readily measured. We used a low-affinity Ca^{2+} indicator to measure the time course of Ca_{res} in CA3 presynaptic terminals, because facilitation can be attenuated by the accelerated decay of Ca_{res} (Atluri and Regehr, 1996b). Ca_{res} decayed similarly in wild-type and syt7 knockout animals (**Figure 7.6a**), indicating that the loss of facilitation in knockouts is not a consequence

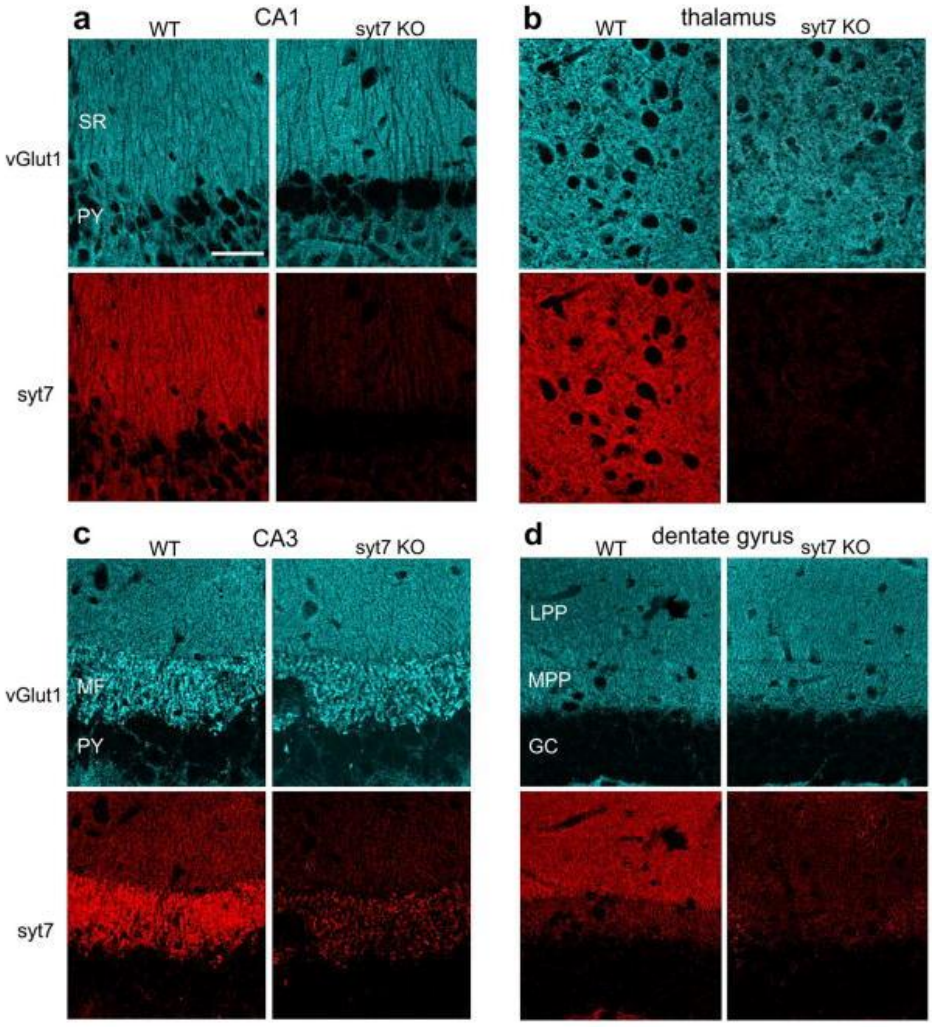

Figure 7.3: Immunohistochemistry of syt7 expression at 4 different synapses.

Fluorescent images of immunostaining for vGlut1 (top) and syt7 (bottom) in slices from WT and syt7 KO animals, showing (**a**) the stratum radiatum (SR) of hippocampal CA1 region, (**b**) the ventral thalamus, (**c**) mossy fibers (MF) in hippocampal CA3, and (**d**) the lateral and medial performant paths (LPP and MPP) in the outer molecular layer of the dentate gyrus. Notably, syt7 expression in WT animals was higher in the LPP, where synapses exhibit facilitation, compared to the MPP, where synapses exhibit depression. Scale bar, 50 μm. The presence of syt7 labeling in regions containing CA3→CA1 synapses, layer 6 to thalamus synapses, MF synapses and LPP→granule cell synapses that are also colabeled with antibodies to the presynaptic marker for glutamatergic synapses vGlut1, suggests that syt7 is located presynaptically

Figure 7.3 (Continued)

at these synapses. It is, however, difficult to obtain sufficient resolution with confocal microscopy in brain slices to unambiguously establish that syt7 is located presynaptically at these synapses. Importantly, the Allen Brain atlas suggests that the presynaptic cells for these synapses contain mRNA for syt7(Website:). Lastly, immunoelectron microscopy revealed selective staining of presynaptic boutons in the CA1 region of the hippocampus (Sugita et al., 2001).

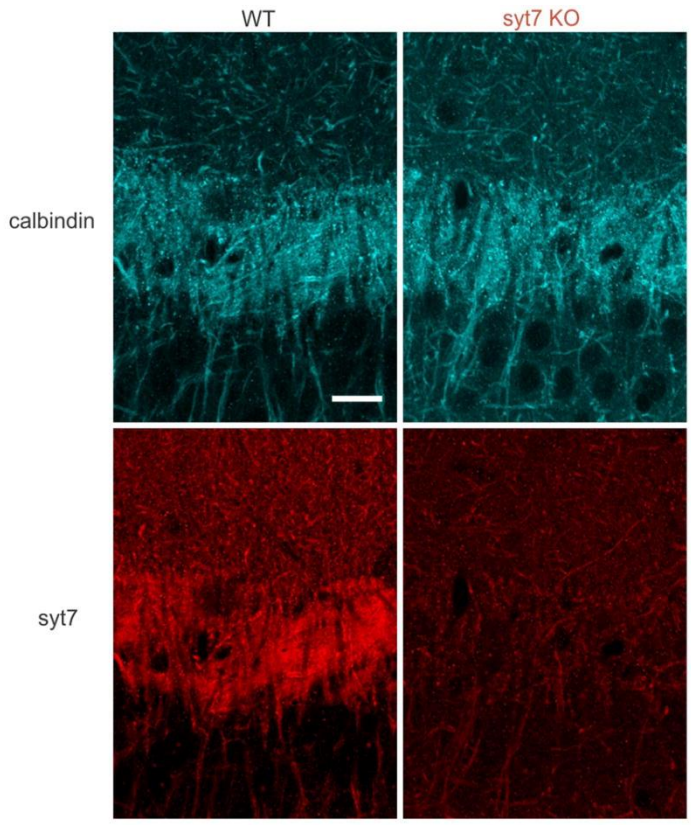

Figure 7.4: Immunohistochemistry of syt7 and calbindin expression at mossy fiber synapses.

Fluorescent images of immunostaining for calbindin-D28k, which predominantly labels mossy fibers in the CA3 region of the hippocampus(Celio, 1990, Blatow et al., 2003) (top) and syt7 (bottom) in slices from WT and syt7 KO animals. Colocalization of syt7 and calbindin staining in WT animals provides further support for the expression of syt7 in mossy fiber terminals. Scale bar, 20 μm.

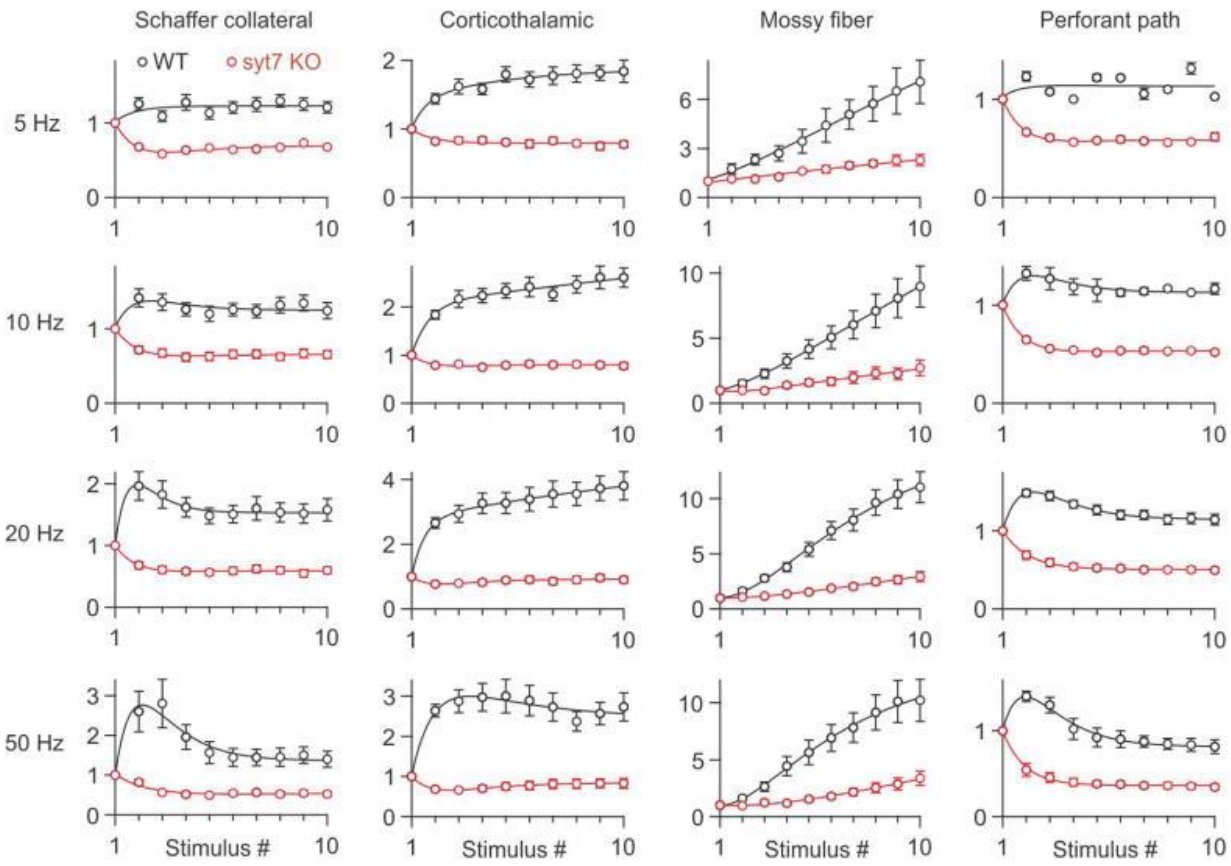

Figure 7.5: Loss of facilitation in syt7 KO animals at multiple frequencies.

Average normalized synaptic responses evoked by extracellular stimulation with trains at frequencies from 5-50 Hz at four synapses in slices from WT and syt7 KO animals. Enhancement during trains was eliminated for all synapses other than mossy fiber synapses, where significant enhancement was present by the 5th stimulus for 5 Hz and 10 Hz, the 3rd stimulus for 20 Hz and the 6th stimulus for 50 Hz (compared to 1 by a Wilcoxon signed rank test, $P < 0.05$). This indicates that another form of synaptic enhancement gradually builds during repetitive activation and is consistent with a specialized form of synaptic enhancement that has been described at mossy fiber synapses in which spike broadening gradually builds during repetitive activation and leads to increased calcium influx.

of accelerated Ca_{res} decay. We also used Ca_{res} as a measure of Ca_{influx} to determine whether there are use-dependent manner changes in Ca^{2+} entry. However, each of two closely spaced stimuli evoked the same incremental increase in Ca_{res} in both wild-types and knockouts (**Figure 7.6b**), indicating that use-dependent changes in total Ca_{influx} cannot account for facilitation. This suggests that if changes in Ca_{influx} contribute to facilitation at this synapse, they must be restricted to the small subset of presynaptic calcium channels that evoke neurotransmitter release. We repeated the experiment using a high-affinity Ca^{2+} indicator, where the degree of saturation during paired stimuli can be used to measure the magnitude of Ca_{res} evoked by the first stimulus (see Methods). We conclude that Ca_{influx} evoked by the first stimulus is the same in wild-type and knockout animals (**Figure 7.6c**).

We further explored the role of Ca^{2+} in facilitation by examining the Ca^{2+}-dependence of excitatory postsynaptic currents (EPSC) and facilitation. Raising extracellular Ca^{2+} leads to a steep increase in EPSC amplitude (**Figure 7.6d**), but a decrease in facilitation (**Figure 7.6e**, *black traces*) even though high extracellular Ca^{2+} should *increase* the Ca_{res} available to evoke facilitation. This paradox is resolved by realizing that increased Ca^{2+} influx elevates *p*, which depletes presynaptic vesicles, saturates release, and limits the extent of facilitation. The Ca^{2+}-dependence of EPSC amplitudes was unaffected in knockout animals (**Figure 7.6d**), but facilitation was absent for all values of external Ca^{2+} (**Figure 7.6e.f**). Meanwhile there was no difference in basal release properties measured by the rate of spontaneous EPSCs (**Figure 7.7**). These findings suggest that the loss of facilitation in knockouts is not a consequence of higher initial *p*, because facilitation was absent even when the initial *p* was strongly attenuated by reducing external Ca^{2+}.

To further test whether initial *p* is elevated in syt7 knockouts, we measured how field excitatory postsynaptic potentials (fEPSPs) scaled with stimulus intensity (Dingledine and Somjen, 1981) (**Figure 7.8a**). The slope of the fEPSP vs. presynaptic volley gives a relative measure of *p* (see Methods), which was unchanged in knockouts (**Figure 7.8b**). Moreover, the fEPSP to presynaptic volley ratio changed steeply with extracellular Ca^{2+}, showing that this method is sensitive to *p* (**Figure 7.8c, d**). We also assessed *p* using pharmacological blockade of synaptically-activated NMDARs by the use-dependent

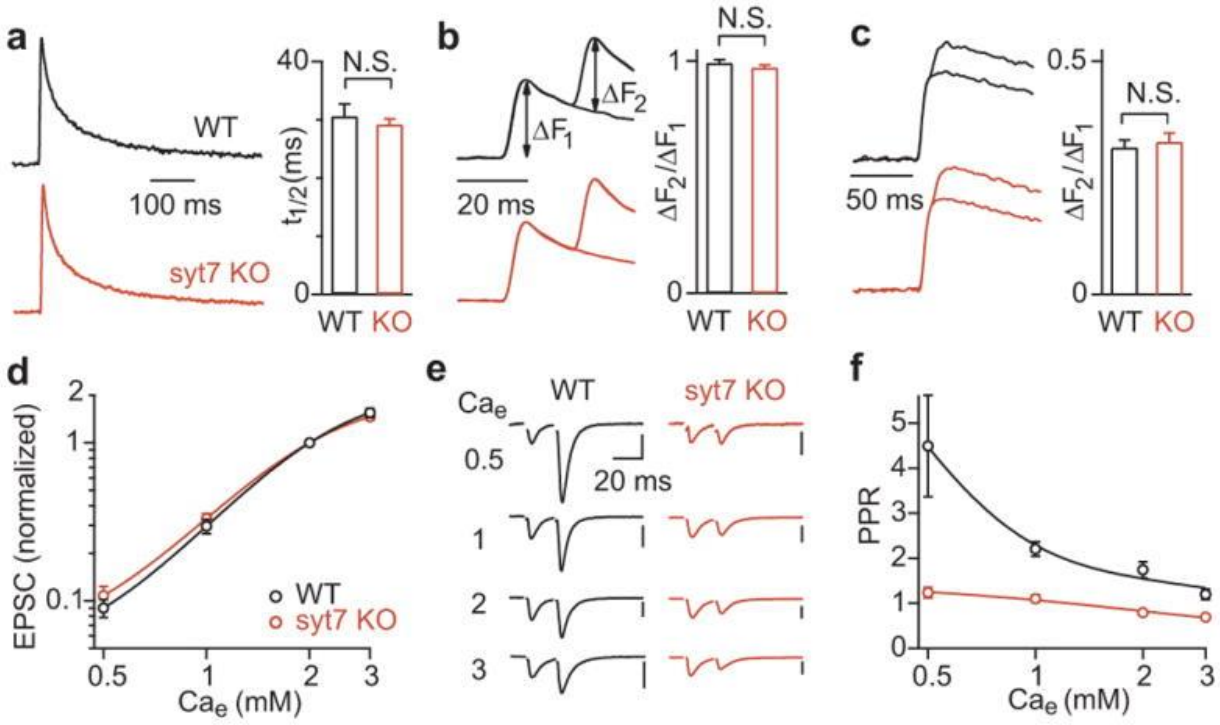

Figure 7.6: Facilitation is altered in syt7 KO animals despite similar presynaptic Ca^{2+} signals.

a, Presynaptic Ca_{res} evoked by a single stimulus recorded from Schaffer collateral fibers loaded with a low-affinity Ca^{2+} indicator (left), and Ca_{res} half-decay times (right). N.S. not significant. **b**, Ca_{res} signals recorded with low-affinity indicator evoked by 1 or 2 stimuli (left). The ratio of the increase in Ca_{res} evoked by the first (ΔF_1) and second (ΔF_2) stimuli (right). **c**, Ca_{res} signals recorded with high-affinity indicator evoked by 1 or 2 stimuli. **d**, Average EPSC amplitudes for CA3→CA1 synapses recorded in different external Ca^{2+} (Ca_e) concentrations, normalized to the amplitude in 2 mM Ca_e. **e**, EPSCs recorded in different Ca_e. Vertical scale bars, 50, 100, 200 and 300 pA in 0.5, 1, 2 and 3 mM Ca_e respectively. **f**, PPR for interstimulus interval of 20 ms recorded in different Ca_e. In 0.5 mM Ca^{2+} PPR in KOs (1.24 ± 0.12) was not significantly different from 1 ($P = 0.084$, Wilcoxon signed rank test).

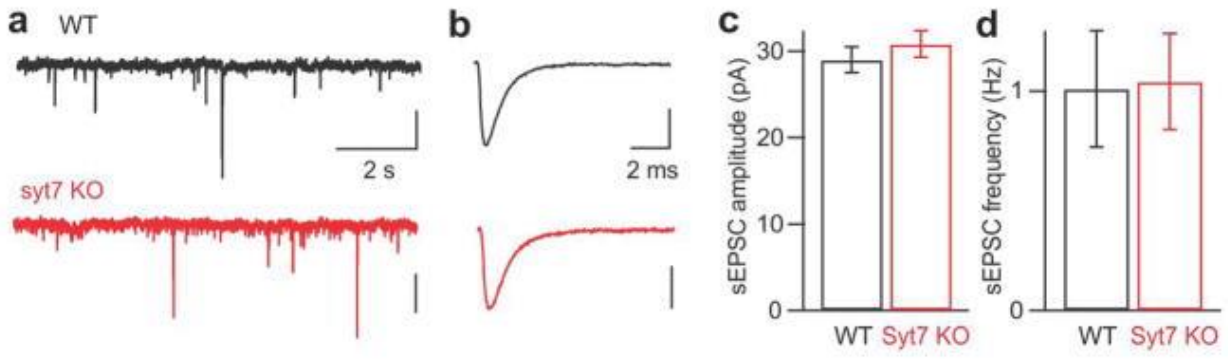

Figure 7.7: Spontaneous release is similar in WT and syt7 KO animals.

a, Representative sEPSCs recorded from voltage-clamped hippocampal CA1 cells in WT (black) and KO (red) animals. Vertical scale bars, 20 pA. **b**, Representative sEPSCs, averaged from >50 events recorded in WT and KO animals. Vertical scale bars, 10 pA. **c-d**, Average sEPSC (**c**) amplitude and (**d**) frequency in WT (N = 16) and syt7 KO animals (N = 18).

blocker MK801 (Manabe and Nicoll, 1994) (**Figure 7.8e-g**). This approach is widely-used to detect changes in *p*: An increase in *p* leads to more glutamate release, more activation of NMDARs, and a more rapid blockade of NMDA receptors, while a decrease in *p* leads to a slower blockade (**Figure 7.9**). The rate of blockade of NMDA-mediated field EPSPs (NMDA-fEPSP) was unaffected by syt7 deletion (**Figure 7.8**), indicating similar initial *p*. However, when we evoked NMDA-fEPSPs with trains of 3 stimuli (Manabe and Nicoll, 1994), amplitudes decayed more rapidly in wild-types (**Figure 7.8f, g**), suggesting that syt7 is required to increase *p* for the second and third stimuli. Thus, initial *p* and presynaptic Ca^{2+} signaling are unaffected by syt7 deletion, but knockouts lack the use-dependent increase in *p* that underlies facilitation. This suggests that the mechanism underlying facilitation is directly impaired by syt7 deletion.

Syt7 is implicated in neuroendocrine release (Sugita et al., 2001), insulin secretion (Gustavsson et al., 2008), and exocytosis of lysosomes (Martinez et al., 2000), which could all indirectly influence synaptic transmission in global syt7 knockouts. Therefore, to determine whether syt7 controls facilitation by acting in presynaptic neurons in a cell autonomous manner, we tested whether viral expression of syt7 in CA3 pyramidal cells of syt7 knockouts rescued facilitation. This approach is complicated by our inability to virally transduce all CA3 pyramidal cells, which prohibits the use of extracellular stimulation that would activate some presynaptic cells that express syt7 and others that do not. We overcame this problem with an adeno-associated virus (AAV) that drove bicistronic expression of both ChR2 and syt7, allowing optical stimulation of only those fibers expressing syt7.

Using conditions we have previously shown allow facilitation to be studied with optogenetic stimulation (see Methods), we confirmed that when ChR2 alone was expressed, optical and electrical stimulation produced similar facilitation in wild-types (**Figure 7.10a,e,f**), and similar depression in knockouts (**Figure 7.10b,e,f**). We next used a bicistronic vector to express both ChR2 and wild-type syt7 in knockout animals. Light-evoked responses exhibited facilitation, whereas electrically-evoked responses did not (**Figure 7.10c,e,f**). This suggests that bicistronic expression of ChR2 along with a presynaptic protein of interest offers a powerful new approach to characterize the effect of gene manipulation on

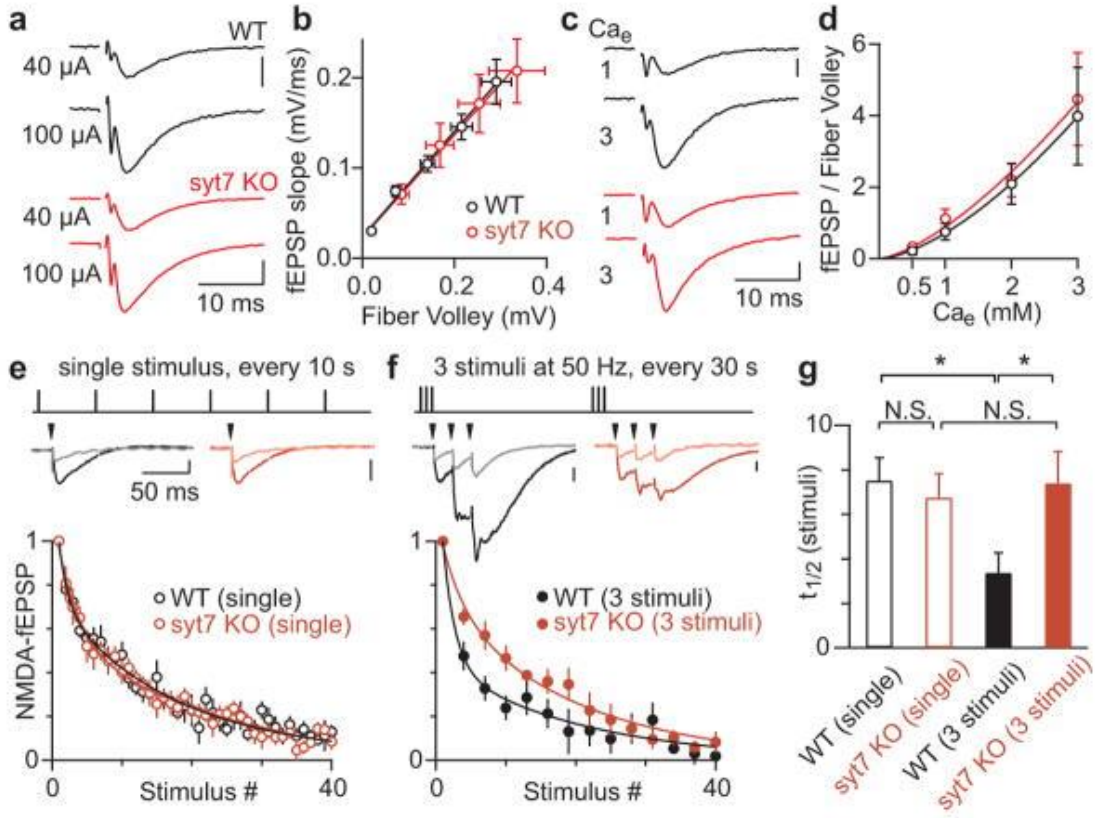

Figure 7.8: Change in the initial probability of release does not underlie the absence of facilitation in syt7 KO mice.

a, Extracellular recordings of presynaptic fiber volley and fEPSP evoked by the indicated stimulus intensities. Scale bar, 200 µV. **b**, fEPSP slope plotted against fiber volley amplitude, for 20-100 µA stimulation. **c**, fEPSPs recorded in 1 and 3 mM Ca_e. Scale bar, 100 µV. **d**, Average ratio of the fEPSP to the fiber volley in different Ca_e. **e**, (Top) Initial release probability was measured by stimulating Schaffer collaterals every 10 seconds while recording NMDA-fEPSPs before and after MK801 bath application. (Middle) Traces averaged from 10 trials before (dark traces), and trials 10-15 after MK801 application (light traces). (Bottom) Average NMDA-fEPSPs amplitudes evoked in the presence of MK801. **f**, Same as in (e) but with 3 stimuli at 50 Hz every 30 seconds. First response to trains is shown. **g**, Half-decay times of NMDA-fEPSP amplitudes in the presence of MK801. $*P < 0.05$, one-way ANOVA with Tukey's post hoc test.

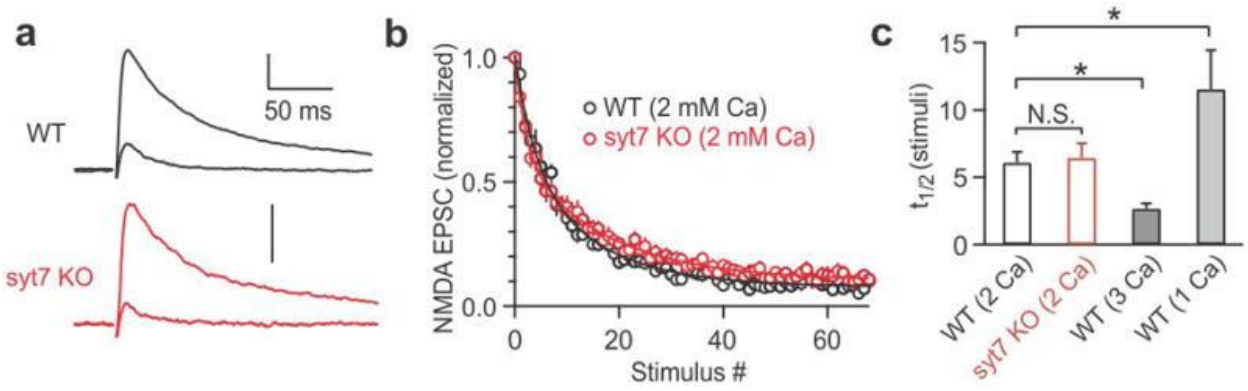

Figure 7.9: MK801 blockade of NMDA receptor-mediated EPSCs reveals similar initial release probability in WT and KO synapses.

a, Representative NMDA-EPSCs recorded in WT and KO animals before the application of MK801 (average of 10 traces) and after stimulation in the presence of MK801 (average response of 15-20th stimuli). Vertical scale bars, 100 pA. **b**, Average NMDA-EPSCs recorded in the presence of MK801, normalized to the first stimulus. **c**, Half-decay times of NMDA-EPSC amplitudes. *$P < 0.05$, one-way ANOVA with Tukey's post hoc test. N.S., not significant.

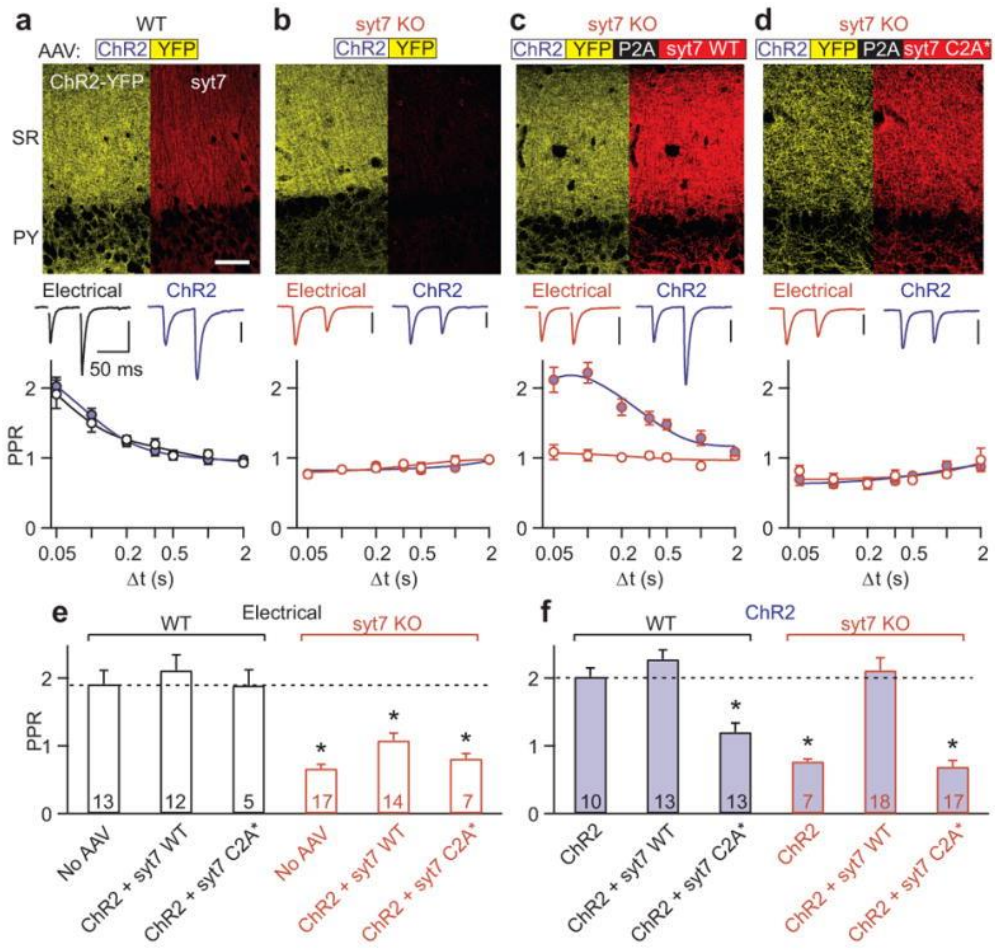

Figure 7.10: Viral expression of syt7 restores facilitation at Schaffer collateral synapses.

a-d, (Top) Fluorescence images of ChR2-YFP and syt7 immunostaining in the CA1 region after AAV injection into CA3 to express the indicated proteins in WT animals (**a**) or syt7 KO animals (**b-d**). Stratum pyramidale (PY) and stratum radiatum (SR). Scale bar, 100 μm. (Bottom) EPSCs and PPRs for responses evoked electrically (open symbols) and optically (blue symbols). In **a** and **b** only ChR2-YFP was expressed, in **c** both ChR2-YFP and syt7(WT) were expressed (separated by a P2A cleavage peptide) and in **d** ChR2-YFP and Ca^{2+}-insensitive syt7C2A* were expressed. **e-f**, Summary of PPRs for 50 ms interstimulus interval. Asterisks denote significant difference from responses evoked electrically in uninjected WT animals (**e**), or optically in WT animals expressing ChR2 alone (**f**). *$P < 0.05$, one-way ANOVA with Tukey's post hoc test.

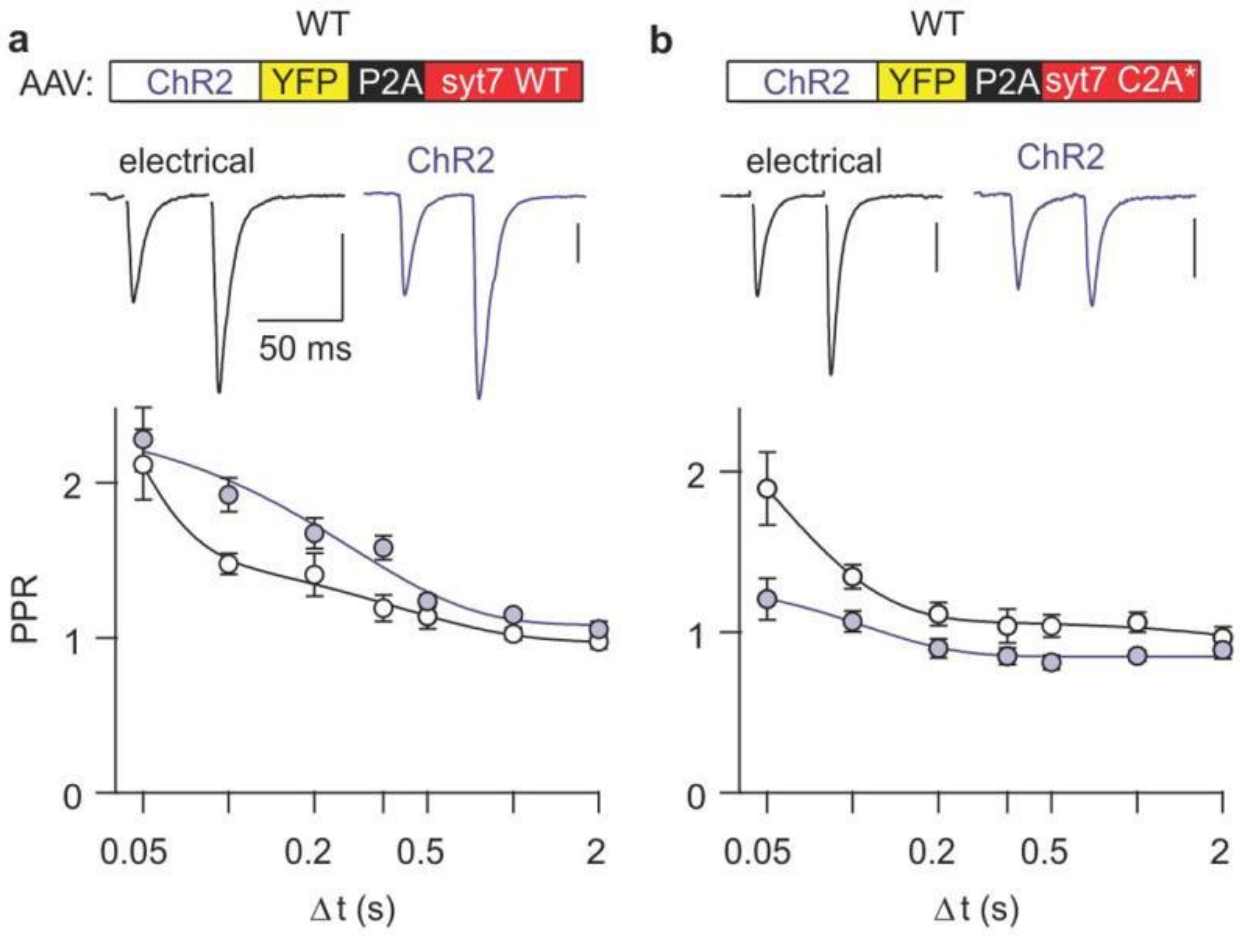

Figure 7.11: Effect of virally-expressed syt7 WT and syt7 C2A* in WT animals.

a-b, (Top) AAV was injected into the hippocampal CA3 region in WT animals to express ChR2 and (**a**) syt7 WT or (**b**) syt7 C2A*. (Bottom) Representative EPSCs and average paired-pulse ratios for responses evoked electrically and optically in WT slices with AAV-driven expression of (a) syt7 WT (electrical, N = 12; optical, N = 13) and (b) syt7 C2A* (electrical, N = 5; optical, N = 13). Vertical scale bars, 100 pA.

presynaptic function within intact neural circuits. When syt7 was expressed in wild-type animals the peak facilitation was unaffected (**Figure 7.10e,f**, **Figure 7.11a**). Thus, expressing syt7 in CA3 pyramidal cells rescued facilitation in a cell autonomous manner, with facilitation restored only at synapses expressing syt7 and ChR2.

To determine whether Ca^{2+}-binding by syt7 is important for facilitation, we assessed whether facilitation is rescued by syt7 with a mutated Ca^{2+}-insensitive C2A domain (syt7 C2A*). Previous studies established that Ca^{2+}-binding to the C2A domain of syt7 is required for syt7 to mediate asynchronous release(Bacaj et al., 2013). We found that syt7 C2A* did not rescue facilitation in knockouts (**Figure 7.10d-f**). Moreover, in wild-type animals, syt7 C2A* expression strongly attenuated facilitation (**Figure 7.10e,f**, **Figure 7.11b**), suggesting that syt7 C2A* competes with native syt7 to suppress facilitation.

Our results indicate that facilitation requires Ca^{2+}-binding to the C2A domain of syt7, and also provide insight into the role of syt7 in facilitation. We conclude that syt7 does not produce facilitation by altering the amplitude and time course of Ca_{res} (**Figure 7.6**), by increasing initial *p* (**Figure 7.8**), by acting as a Ca^{2+} buffer (**Figure 7.12**), or through use-dependent increases in the total Ca_{influx} (**Figure 7.1b, Figure 7.6**). The observation that initial *p* is unaltered in syt7 knockouts indicates that local Ca_{influx}, is unaffected for the first stimulus, but it is difficult to rule out the possibility that syt7 mediates a use-dependent increase in Ca_{influx} through the subset of channels that trigger vesicle fusion. There is, however, no evidence for syt7 associating with or regulating calcium channels. In contrast, syt7 is known to interact with syt1 and can mediate vesicle fusion(Sugita et al., 2001, Wen et al., 2010, Bacaj et al., 2013). The most parsimonious explanation is that syt7 acts as the hypothesized specialized Ca^{2+} sensor to elevate *p* during facilitation. Facilitated release exhibits rapid kinetics, suggesting that syt7 somehow increases the probability of syt1-dependent vesicle fusion. Whether this is through a direct interaction of syt7 with a fast Synaptotagmin isoform such as syt1 remains an open question. It is also unclear whether the recently described interaction between syt7 and calmodulin that promotes vesicle replenishment(Liu et al., 2014) is similarly required for facilitation. Finally, it is possible that at other synapses facilitation is mediated by

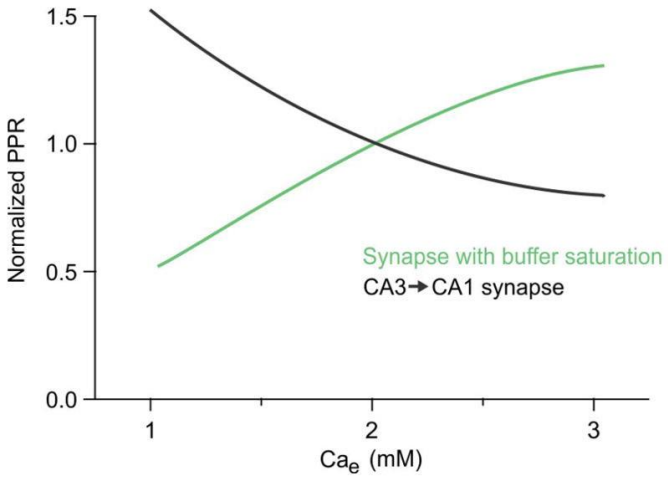

Figure 7.12: Evidence suggests that syt7 does not produce facilitation by acting as a local calcium buffer at the CA3→CA1 synapse.

This graph illustrates the general relationship between PPR and external calcium for synapses in which buffer saturation produces facilitation (green) and for facilitation observed at the CA3→CA1 synapse and many other synapses (black)(Blatow et al., 2003). It has been shown previously that the for buffer saturation mechanism (**Figure 7.1**) the amplitude of facilitation is reduced when Ca_{influx} is reduced by lowering external calcium(Blatow et al., 2003). This can be understood by considering that this form of facilitation is thought to require sufficient Ca_{influx} to saturate the endogenous buffer, and thereby reduce its ability to buffer calcium for subsequent stimuli. If Ca_{influx} is low then there is insufficient calcium entry to bind very much of the endogenous buffer, and little facilitation would result. In addition, as shown in **Figure 7.1** for a calcium buffer to produce facilitation it would need to buffer calcium sufficiently that it would reduce initial *p*. We have shown, however, that *p* is unaltered in syt7 knockouts. This is perhaps not surprising in light of the fact that syt7 is thought to be located on the plasma membrane, and in cases where this type of facilitation has been observed it is associated with high concentrations of a fast cytosolic buffer (Blatow et al., 2003).

additional specialized Ca^{2+} sensors or involves other mechanisms. Further studies are needed to clarify these issues.

Based primarily on theoretical considerations, facilitation is thought to profoundly influence both information transfer and network dynamics. In the hippocampus, the high-pass filtering imposed by facilitating synapses may account for the burst firing in place cells that encode spatial information(Klyachko and Stevens, 2006). In the auditory pathway, facilitation is proposed to counteract short-term depression in order to maintain linear transmission of rate-coded sound intensity(MacLeod et al., 2007). It has even been suggested that facilitation forms the basis of short-term memory, as facilitating recurrent connections within cortical networks could support the persistent activity states associated with working memory(Mongillo et al., 2008). In future studies the selective elimination of syt7 from specific cell types could allow the first direct tests of the impact of facilitation on neural circuits and behavior.

Methods

Animals and viruses

All mice were handled in accordance with NIH guidelines and protocols approved by Harvard Medical School. Syt7 KO mice(Chakrabarti et al., 2003) (Jackson Laboratory) and WT littermates of either sex were used. Statistical tests were not used to predetermine sample size. Blinding and randomization were not performed. AAV2/9-hSyn-hChR2(H134R)-EYFP and its pAAV backbone (Addgene 26973) were obtained from the University of Pennsylvania Vector Core. cDNA encoding the rat syt7 WT α isoform and C2A* mutant (D225A, D227A, D233A)(Bacaj et al., 2013) were generously provided by Taulant Bacaj and Thomas Sudhof. For rescue experiments involving syt7 with mutated Ca^{2+} binding domains, we used the mutated C2A* version instead of the C2A*C2B* double mutant, as mutation of both C2 domains leads to lower levels of expression. The porcine teschovirus-1 2A (P2A) cleavage sequence(Kim et al., 2011) and syt7 were inserted after the ChR2 C-terminus in the pAAV backbone (Genscript). Plasmid-driven expression of ChR2-YFP and syt7 was confirmed in HEK cells by syt7 immunostaining

and patch-clamp recording of ChR2 photocurrents. AAVs were produced and purified from HEK cells as previously described (Zolotukhin et al., 1999).

Stereotaxic surgeries were performed as described(Jackman et al., 2014). P18-P30 mice were anesthetized with ketamine/xylazine/acepromazine (100/10/3 mg/kg) supplemented with 1–4% isoflurane. Viruses were injected through glass capillary needles using a syringe (Hamilton) mounted on a stereotaxic instrument (Kopf). Injection coordinates from lambda were 2.69 mm (rostral), 3 mm (lateral), and 2.8 mm (ventral). 1 µl of virus suspension was delivered at a rate of 0.1 µl/min using a a microsyringe pump (WPI; UMP3) and microsyringe pump controller (WPI; Micro4). The needle was slowly retracted 5-10 minutes after injection, and the scalp incision was closed with gluture. Post-injection analgesic (buprenophrine, 0.05 mg/kg) was administered subcutaneously for 48 hrs.

Acute slice preparation

P30-P60 animals were euthanized under isoflurane anesthesia, 14-30 days after AAV injection. Brains were removed and placed in ice-cold solution containing (in mM): 234 sucrose, 25 $NaHCO_3$, 11 glucose, 7 $MgCl_2$, 2.5 KCl, 1.25 NaH_2PO_4, and 0.5 $CaCl_2$. 270 µm-thick transverse slices (hippocampal recordings) or 250 µm-thick sagittal slices (thalamic recordings) were prepared on a vibrotome (Leica, VT1000s), and a cut was made between CA3 and CA1 to prevent recurrent excitation. Slices were transferred for 30 min to 32°C artificial cerebrospinal solution (ACSF) containing (in mM): 125 NaCl, 26 $NaHCO_3$, 25 glucose, 2.5 KCl, 2 $CaCl_2$, 1.25 NaH2PO_4, and 1 $MgCl_2$, adjusted to 315 mOsm, and allowed to equilibrate to room temperature for >30 min. Experiments were performed at 33 ± 1°C with flow rates of 2 ml/min.

Electrophysiology

For ChR2 stimulation, 160 mW/mm^2 laser pulses (0.2-0.5 ms) from a 100 mW 473 nm laser (OptoEngine, MBL-III) were focused through the 60X objective of the microscope (Olympus, BX51WI) to produce a 80 µm diameter spot over the stratum radiatum, >500 µm from the recorded cell to avoid activating ChR2 in presynaptic boutons, which can artificially raise the probability of release and obscure facilitation(Jackman et al., 2014). Extracellular stimulation was performed with a stimulus isolation unit

(WPI, A360) using glass monopolar electrodes (0.5–1 MΩ) filled with ACSF. Stimulus electrodes were positioned ~500 μm from the recording electrode in the stratum radiatum (Schaffer collaterals), the internal capsule (corticothalamic), the hillus adjacent to the dentate granule cell layer (mossy fibers), and the outer molecular layer (lateral performant path). To ensure that mossy fiber responses were not contaminated by associational/commissural inputs the metabotropic glutamate receptor agonist DCG-IV (1 μM) was applied at the end of experiments to selectively block mossy fiber responses(Kamiya et al., 1996). Data were included only if responses were reduced by more than 80% (average reduction was 88 ± 1 % in WT and 90 ± 2% in syt7 KO mice), and the amplitude of mossy fiber responses was measured after subtracting the response remaining in the presence of DCG-VI. Stimulus trials were repeated at 0.1 Hz (0.033 Hz at mossy fibers to avoid potentiation), and artifacts were deleted for display. Recordings were acquired using an amplifier (Axon Instruments, Multiclamp 700B) controlled by custom software written in IgorPro (provided by Matthew Xu-Friedman, SUNY Buffalo) , and low-pass filtered at 2 kHz. Whole-cell recordings were obtained using borosilicate patch pipettes (2–5 MΩ) pulled with a horizontal puller (Sutter P-97). The internal recording solution contained (in mM): 150 Cs-gluconate, 3 KCl, 10 HEPES, 0.5 EGTA, 3 MgATP, 0.5 NaGTP, 5 phosphocreatine-tris, and 5 phosphocreatine-Na. pH = 7.2. Cells were held at -70 mV, and series resistance was monitored during recordings. fEPSPs were recorded in current-clamp mode with ACSF-filled patch pipettes (0.5-1 MΩ). Inhibition was blocked with picrotoxin (50 μM), and during fEPSP recordings, CPP (2 μM) and CGP (3 μM) was added to the bath. 4-10 trials were conducted for each stimulus frequency, and recordings were averaged over trials. Data in all figures represent the mean ± SEM. Average responses are displayed with double exponential or polynomial curves fit in IgorPro. Unless stated otherwise, statistical significance was assessed by unpaired two-tailed Student's t-test, or one-way ANOVA followed by Tukey's post hoc test.

Probability of release

To record NMDA-EPSCs cells were voltage clamped at +40 mV, and the internal solution contained (in mM): 85 Cs-methanesulfonate, 4 NaCl, 10 HEPES, 0.2 EGTA, 30 BAPTA, 2 MgATP, 0.4 NaGTP, 10 phosphocreatine-Na, 25 TEA, 5 QX-314, pH = 7.3. For recording NMDA-fEPSPs, Mg^{2+} was excluded

from ACSF to relieve Mg^{2+} block of NMDA receptors. Picrotoxin (100 μM) and NBQX (5 μM) were added to the bath, and stimulation was conducted at 0.1 Hz (unless otherwise indicated) for 5 minutes to obtain a baseline response. Stimulation was halted for 10 minutes while (+)-MK801 (40 μM) was added and allowed to equilibrate. For experiments involving fEPSPs vs. presynaptic volley, the postsynaptic response was measured by the slope of the fEPSP, while the amplitude of the presynaptic volley was used to determine the number of activated fibers. If *p* increases, the same number of activated presynaptic fibers will produce a larger fEPSP. The ratio between fEPSP and volley was determined by line fits to the linear regime of the input-output curve of individual experiments (20-80 μA stimuli).

The study of probability of release is complicated because many people use *p* to refer to the probability of release of a vesicle (p_v) and others refer to probability of release from an active zone ($p_{synapse}$) that contains N vesicles in its readily releasable pool (RRP). Thus, an increase in the size of the RRP for an active zone can increase $p_{synapse}$ even if p_v is unaltered. Although MK801 blockade (Manabe and Nicoll, 1994) and fEPSPs vs. presynaptic volley (Dingledine and Somjen, 1981) are both widely-used methods to detect changes in the probability of release, for both approaches it is conceivable (though unlikely) that increases in p_v could be obscured by a perfectly balanced decrease in the RRP size. However, the relationship between EPSC amplitude and extracellular Ca^{2+} is similar in WT and syt7 KO animals. This suggests there is no increase in p_v, which would cause this curve to saturate at lower values of Ca_e for syt7 KO animals. Moreover, the large differences in facilitation in WT and syt7 KO animals were even more pronounced when the probability of release was reduced 10-fold by lowering Ca_e from 2 mM to 0.5 mM, which is incompatible with an increase in p_v obscuring facilitation by depleting vesicles.

Ca^{2+} measurements

Ca^{2+} was measured as described previously(Atluri and Regehr, 1996b). Briefly, CA3 fibers were labelled for three minutes using an ACSF-filled pipette containing either magnesium green AM or fura-2 AM (240 μM) and 1% fast green, placed into the border of the CA3-CA1 field. A vacuum pipette placed above the loading site removed excess indicator. Slices were incubated for at least 1 hour and imaging was performed in stratum radiatum of CA1 at least 500 μm from the injection site using a 60X objective and

custom-built photodiode. Excitation was achieved using a tungsten (magnesium green) or xenon lamp (fura-2). Schaffer collaterals were stimulated using a glass electrode placed at least 300 μm from the imaging site. To prevent recurrent excitation, experiments were performed in the presence of NBQX (10 μM), CPP (2 μM) and picrotoxin (50 μM).

Magnesium green is a low-affinity calcium indicator(Zhao et al., 1996) (K_D=7 μM) that provides an approximately linear measure of Ca_{res}(Kreitzer and Regehr, 2000). As such it is well suited to measuring the time course of presynaptic Ca_{res} (**Figure 7.6A**) and detecting changes in Ca_{influx} during successive stimulations (**Figure 7.6B**). However, with the bulk loading approach the size of the fluorescence change is proportional to the number of stimulated fibers, so the absolute Ca_{res} signal is not readily quantified with magnesium green. In contrast, fura-2 has a high affinity for calcium (Brenowitz and Regehr, 2003, Grynkiewicz et al., 1985) (K_D = 131 nM) so it provides a saturating sublinear response to increases in Ca_{res} (Sabatini and Regehr, 1995, Maravall et al., 2000, Sabatini and Svoboda, 2000). This can be used to test for changes in the absolute size of Ca_{influx} because a change in the Ca_{influx} per stimulus would change the ratio between the fluorescence change produced by the first and second stimuli.

Immunohistochemistry

Two to four weeks after AAV injection, mice were anesthetized with ketamine and transcardially perfused with 4% PFA in PBS. The brain was removed and post-fixed for 24 hours. Slices (50 μm thick) were permeabilized (PBS + 0.4% Triton X-100) for 30 minutes and then prepared in blocking solution (PBS + 0.2% Triton X-100 + 2% normal goat serum [PBST]) for 30 min at room temperature. Slices were incubated overnight at 4°C in PBST with primary antibodies (anti-syt7 [Synaptic Systems, 105173], 1 μg/ml; 1:200, targeting AA 46-133 of syt7α, anti-vGlut1 [Synaptic Systems, 135304], 1 μg/ml; 1:500, and anti-calbindin-D28k [Sigma Aldrich, C9848], 1 μg/ml; 1:500), followed by incubation with secondary antibodies in PBST for 2 hr at room temperature. For both WT and syt7 KO mice, images from each brain region were acquired on a laser scanning confocal (Olympus, FluoView1200) using the same laser/microscope settings and processed in ImageJ identically.

Appendix B

The role of CaV2.1 channel facilitation in synaptic facilitation

Christopher Weyrer, Josef Turecek, Zachary Niday, Pin W Liu, Evanthia Nanou, William A Catterall, Bruce P Bean, Wade G Regehr

Cell reports, 26(9), 2289-2297.

Contributions: C.W., J.T., B.P.B. and W.G.R. conceived the experiments. C.W. conducted experiments in Figsures 8.1B-D, Figures 8.2 and 8.3. J.T. conducted experiments in Figures 8.1C and D, Figure 8.2B and Figure 8.3. Z.N. conducted experiments in Figure 8.4 and Figure 8.5. P.W.L. conducted experiments in Figure 8.1A. C.W., J.T., P.W.L. and B.P.B. conducted analyses. C.W. made illustrations. E.N. and W.A.C. helped with animals and the manuscript. C.W., B.P.B. and W.G.R. wrote the manuscript, with input from all authors.

Abstract

Activation of $Ca_V2.1$ voltage-gated calcium channels is facilitated by preceding calcium entry. Such self-modulatory facilitation is thought to contribute to synaptic facilitation. Using knock-in mice with mutated $Ca_V2.1$ channels that do not facilitate (Ca IM-AA mice), we surprisingly found that under conditions of physiological calcium and near-physiological temperatures, synaptic facilitation at hippocampal CA3 to CA1 synapses was not attenuated in Ca IM-AA mice and facilitation was paradoxically more prominent at two cerebellar synapses. Enhanced facilitation at these synapses is consistent with a decrease in initial calcium entry, suggested by an action potential-evoked $Ca_V2.1$ current reduction in Purkinje cells from Ca IM-AA mice. In wild-type mice, $Ca_V2.1$ facilitation during high-frequency action potential trains was very small. Thus, for the synapses studied, facilitation of calcium entry through $Ca_V2.1$ channels makes surprisingly little contribution to synaptic facilitation. Instead, $Ca_V2.1$ facilitation offsets $Ca_V2.1$ inactivation to produce remarkably stable calcium influx during high frequency activation.

Introduction

Synaptic facilitation is a widespread form of use-dependent enhancement of neurotransmitter release that lasts for hundreds of milliseconds (Zucker and Regehr, 2002). Facilitation can counteract depression (Turecek et al., 2016, 2017), act as a temporal filter (Abbott and Regehr, 2004), is implicated

in working memory (Itskov et al., 2011; Mongillo et al., 2008) and has been proposed to serve many other functional roles (Jackman and Regehr, 2017). Multiple mechanisms have been suggested to account for synaptic facilitation (Jackman and Regehr, 2017), including local saturation of calcium buffer (Blatow et al., 2003; Rozov et al., 2001), a specialized high affinity calcium sensor such as Synaptotagmin 7 (Jackman et al., 2016), and facilitation of calcium entry through voltage gated calcium channels (Mochida et al., 2008; Nanou and Catterall, 2018; Nanou et al., 2016a).

Alterations in calcium entry have long been of special interest as a means of regulating neurotransmitter release, because at most synapses release is highly sensitive to small changes in calcium entry (Dodge and Rahamimoff, 1967; Katz and Miledi, 1968). Typically, release varies as $(Ca_{influx})^4$ such that a 20% increase in Ca_{influx} doubles synaptic strength (Cuttle et al., 1998; Díaz-Rojas et al., 2015; Dodge and Rahamimoff, 1967; Neher and Sakaba, 2008). Most types of calcium channels exhibit calcium-dependent inactivation (Ben-Johny and Yue, 2014; Catterall and Few, 2008; Christel and Lee, 2012). However, $Ca_V2.1$ channels, which play a crucial role in transmission at many synapses, can exhibit use-dependent facilitation of calcium current (Ben-Johny and Yue, 2014; Christel and Lee, 2012; Cuttle et al., 1998; Inchauspe et al., 2004; Lee et al., 2000; Liang et al., 2003). Calmodulin (CaM) is crucially involved in $Ca_V2.1$ channel facilitation (Lee et al., 1999, 2000). CaM pre-associates with $Ca_V2.1$ channels (Erickson et al., 2001), and upon Ca^{2+} binding to its C-terminus (DeMaria et al., 2001), it interacts with the IQ-like motif (IM) containing the amino acids isoleucine (I) and methionine (M) (DeMaria et al., 2001; Lee et al., 2003). Changing these amino acids to alanines (IM-AA) abolishes $Ca_V2.1$ channel facilitation (DeMaria et al., 2001; Lee et al., 2003; Zühlke et al., 2000) (**Figure 8.1A left**).

Because of the sensitivity of transmitter release to small changes in calcium entry, it is expected that calcium-dependent facilitation of calcium entry through $Ca_V2.1$ channels should produce synaptic facilitation. Indeed, at the calyx of Held synapse (Borst and Sakmann, 1998; Cuttle et al., 1998), as well as at synapses between cultured Purkinje cells (Díaz-Rojas et al., 2015), synaptic facilitation was accompanied by use-dependent increases in presynaptic calcium currents. The finding that in $Ca_V2.1$

knockout mice at the calyx of Held, calcium current facilitation was eliminated and synaptic facilitation was strongly attenuated (Inchauspe et al., 2004; Ishikawa et al., 2005) supported a central role for $Ca_V2.1$ in synaptic facilitation. Similarly, synaptic transmission between cultured superior cervical ganglion (SCG) neurons is normally mediated by non-facilitating $Ca_V2.2$ channels, and these synapses do not facilitate (Ben-Johny and Yue, 2014; Liang et al., 2003; Nanou and Catterall, 2018). However, upon expression of $Ca_V2.1$ channels and subsequent blockade of $Ca_V2.2$ channels in SCG neurons, $Ca_V2.1$ channels facilitated along with synaptic transmission. In contrast, the expression of non-facilitating mutated IM-AA $Ca_V2.1$ channels led to strongly reduced facilitation of SCG synapses (Mochida et al., 2003, 2008). Ca IM-AA knock-in mice, in which $Ca_V2.1$ channels were replaced with mutated IM-AA $Ca_V2.1$ channels, are a powerful tool for testing the contribution of $Ca_V2.1$ facilitation to synaptic facilitation (Nanou et al., 2016b, 2016a, 2018). Synaptic facilitation was eliminated or attenuated at some synapses in Ca IM-AA mice, suggesting that facilitation of $Ca_V2.1$ channels can account for a significant fraction of synaptic facilitation at the neuromuscular junction, CA3 to CA1 (CA3-CA1) and CA3 to parvalbumin-expressing (PV) basket cell synapses (Nanou et al., 2016b, 2016a, 2018).

However, many factors can influence short-term synaptic plasticity, and the contribution of $Ca_V2.1$ channel facilitation to synaptic facilitation under physiological conditions of temperature and external calcium (Ca_{ext}) with calcium entry during action potential waveforms is still unclear. Quantification of facilitation of voltage-clamped $Ca_V2.1$ channels has mostly been performed at room temperature, often using voltage steps lasting longer than action potentials and with relatively high Ca_{ext}. Temperature is a crucial factor, because action potential width, calcium channel activation kinetics, and kinetics of protein-protein interactions are all strongly temperature-dependent. Prolonged voltage steps and high external calcium (Ca_{ext}) may tend to increase the extent of $Ca_V2.1$ channel facilitation. Many previous studies characterizing $Ca_V2.1$ channel facilitation in synaptic facilitation were performed in the presence of $Ca_V2.2$ antagonists to isolate effects on $Ca_V2.1$ channels. However, inhibiting calcium entry through $Ca_V2.2$ channels could potentially modify many calcium-dependent processes in presynaptic terminals and decrease the initial probability of release. In addition, at many synapses the deletion of

Synaptotagmin 7 eliminates synaptic facilitation even though this should not affect calcium channel facilitation and does not produce alterations in presynaptic calcium signals (Jackman et al., 2016). We therefore assessed the contribution of $Ca_V2.1$ facilitation to synaptic facilitation under conditions of physiological Ca_{ext} (1.5 mM), at near-physiological temperatures and in the absence of $Ca_V2.2$ blockers. Under these conditions, we unexpectedly found that synaptic facilitation at three different synapses was not attenuated in Ca IM-AA mice. Also, under similar conditions of temperature and Ca_{ext}, wild type $Ca_V2.1$ channel facilitation surprisingly was very small. We therefore conclude that at the synapses we tested, $Ca_V2.1$ channel facilitation makes surprisingly little contribution to synaptic facilitation under conditions of physiological calcium and temperature and may instead serve primarily to counteract calcium channel inactivation.

Results

In order to determine the role of facilitation of calcium entry in synaptic transmission, we studied knock-in mice (Ca IM-AA mice) in which wild type (WT) $Ca_V2.1$ calcium channels are replaced by $Ca_V2.1$ calcium channels containing an IQ-like motif (IM) that has been mutated to prevent calcium-dependent facilitation of calcium entry (DeMaria et al., 2001; Lee et al., 2003; Mochida et al., 2008; Nanou et al., 2016a) (**Figure 8.1A, left**). We initially characterized the properties of calcium entry in acutely dissociated PCs using conditions similar to those used previously (30 stimuli at 100 Hz, 5 ms voltage steps at room temperature in 10 mM external Ca^{2+}). Maximal use-dependent facilitation of calcium currents of ~19% was apparent in wild type mice, which was replaced by maximal use-dependent depression of ~26% in Ca IM-AA mice (**Figure 8.1A, right, Table 8.1**). These findings confirm that calcium-dependent facilitation of $Ca_V2.1$ calcium channels in cerebellar Purkinje neurons is eliminated in the Ca IM-AA mice, as described previously for $Ca_V2.1$ channels in hippocampal neurons (DeMaria et al., 2001; Lee et al., 2003; Mochida et al., 2008; Nanou et al., 2016a). They also illustrate how calcium-dependent facilitation can serve to offset calcium-dependent inactivation in Cav2.1 channels in native neurons.

We then sought to determine the extent to which facilitation of calcium entry contributes to facilitation of synaptic transmission in physiological Ca_{ext} (1.5 mM) at 33-36 °C in the absence of $Ca_V2.2$ channel antagonists. We performed experiments in the presence of $GABA_A$ receptor blockers to better isolate EPSCs for quantification, and also in the presence of $GABA_B$ receptor blockers to avoid confounding changes in synaptic strength resulting from $GABA_B$–mediated presynaptic inhibition, especially during trains. To obtain a more complete picture of the role of $Ca_V2.1$ facilitation in synaptic facilitation, we studied three types of synapses with diverse properties. We used acute brain slices and stimulated synaptic inputs with pairs of pulses separated by different inter-stimulus intervals (ISIs) to determine paired-pulse plasticity of the postsynaptic currents (PSCs).

Contrary to the expectation that synaptic facilitation would be attenuated in Ca IM-AA mice, at hippocampal CA3-CA1 synapses the amplitudes and decays of exponential fits were not statistically significantly different in wild type and Ca IM-AA mice (**Figure 8.1B, Table 8.1**). Even more surprisingly, synaptic facilitation was actually enhanced in the Ca IM-AA mice at the cerebellar parallel fiber to PC (PF-PC) synapse. In WT animals, PPR peaked at 10 ms with a 2.7-fold increase and decayed with a time constant of 47 ms. In Ca IM-AA mice, the maximal mean PPR was virtually identical for short ISIs (2.8-fold at 10 ms), but facilitation was longer lived and decayed with a time constant of 85 ms. While the amplitudes of the exponential facilitation fit are not significantly different, the decay time constants are significantly different (**Figure 8.1C, Table 8.1**). Thus, unexpectedly, facilitation is actually

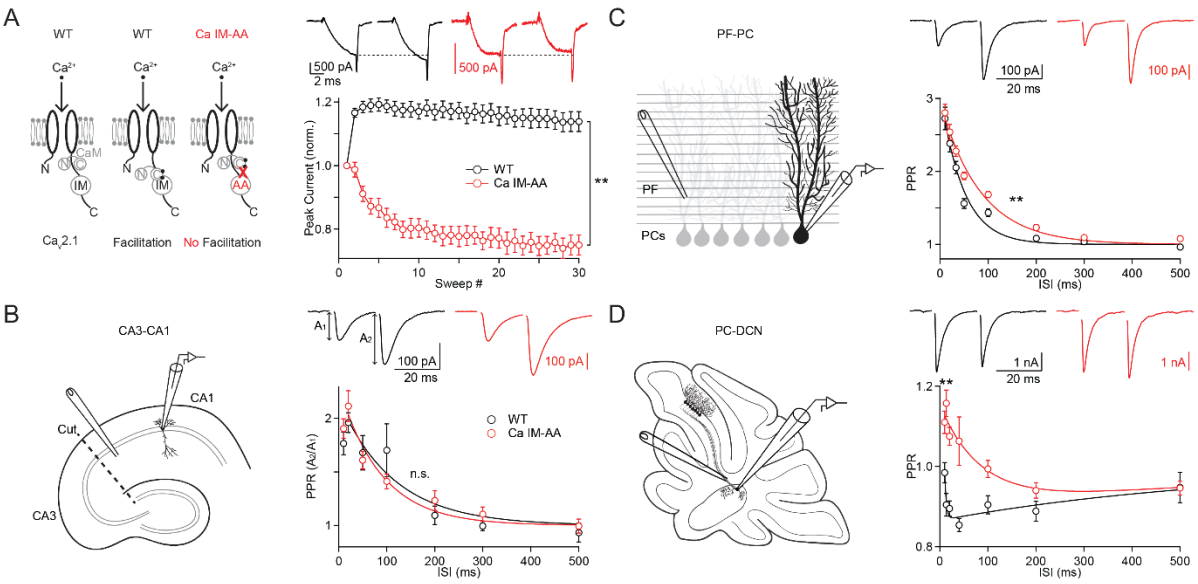

Figure 8.1. Paired-pulse synaptic facilitation does not decrease in the absence of $Ca_V2.1$ channel facilitation.

(A, left) Schematic of $Ca_V2.1$ channel facilitation (IM: IQ-like motif, CaM: Calmodulin)

(A, right) Use-dependent facilitation of $Ca_V2.1$ current is eliminated in Ca IM-AA mice. Top: Voltage steps and resulting calcium currents in dissociated PCs from WT (black) and Ca IM-AA (red) mice. Bottom: Average responses (normalized to current evoked by first stimulus) plotted versus the number of sweeps for 5 ms voltage steps at 100 Hz. Calcium current experiments were performed in 10 mM Ca_{ext} at room temperature.

(B-D) Synaptic experiments were performed on wild type (WT, black) and Ca IM-AA (red) mice at (B) the hippocampal CA3 to CA1 (CA3-CA1) synapse, (C) the cerebellar parallel fiber to PC (PF-PC) synapse and (D) the cerebellar PC to deep cerebellar nuclei synapse (PC-DCN). Synaptic experiments were performed in 1.5 mM Ca_{ext} at near-physiological temperatures.

(B-D) (left) Schematics show the experimental configurations in which synaptic inputs were stimulated twice with an extracellular electrode and synaptic currents were recorded in whole-cell voltage clamp.

Figure 8.1 (Continued)

(B-D) (top right) Representative EPSCs with an inter-stimulus interval (ISI) of 20 ms are shown for WT (black) and Ca IM-AA (red) mice.

(B-D) (bottom right) Average paired-pulse ratio ($PPR=A_1/A_2$) is plotted as a function of ISI.

Statistical significance (unpaired student's t-test or permutation test; see **Table 8.1**): **: $p<0.01$; not significant (n.s.)

Data shown as mean ± SEM. Fits as mean ± SD.

Table 8.1: Statistical Tests.

Figure	Measurement	Genotype	n/N	Mean ± SEM or Fit ± SD	Statistical test	p
8.1A	I_{peak}: $Sweep_{30}/Sweep_1$	WT	17/4	1.14 ± 0.03	Student's t-test	<0.01 **
		IMAA	11/4	0.75 ± 0.03		
8.1B	A_{PPR}	WT	10/5	0.98 ± 0.12	Permutation	0.21
		IMAA	11/5	1.04 ± 0.09		
8.1B	τ_{PPR}	WT	10/5	114 ± 35 ms	Permutation	0.27
		IMAA	11/5	88 ± 18 ms		
8.1C	A_{PPR}	WT	18/3	1.70 ± 0.09	Permutation	0.54
		IMAA	29/4	1.73 ± 0.06		
8.1C	τ_{PPR}	WT	18/3	47 ± 6 ms	Permutation	<0.01 **
		IMAA	29/4	85 ± 9 ms		
8.1D	Max PPR	WT	11/5	1.03 ± 0.04	Student's t-test	<0.01 **
		IMAA	9/4	1.21 ± 0.02		
8.2A	A_{Train}, 100 Hz	WT	14/6	1.40 ± 0.04	Permutation	0.65
		IMAA	12/5	1.30 ± 0.02		
8.2A	A_{Train}, 50 Hz	WT	14/6	1.85 ± 0.03	Permutation	0.68
		IMAA	14/6	1.68 ± 0.03		
8.2A	A_{Train}, 20 Hz	WT	13/5	0.92 ± 0.01	Permutation	0.45
		IMAA	13/6	0.89 ± 0.02		
8.2B	A_{Train}, 50 Hz	WT	11/3	2.09 ± 0.02	Permutation	0.02 *
		IMAA	13/4	3.26 ± 0.03		
8.2B	A_{Train}, 20 Hz	WT	11/3	0.75 ± 0.01	Permutation	0.01 *
		IMAA	13/4	1.39 ± 0.04		
8.2B	A_{Train}, 5 Hz	WT	11/3	0.02 ± 0.33	Permutation	0.13
		IMAA	12/4	0.07 ± 0.03		
8.3D	%ΔIPSC, 10-100 Hz	WT	5/3	174 ± 10%	Student's t-test	0.03 *
		IMAA	6/3	139 ± 10%		
8.3E	$IPSC_{SS}$ 100 Hz	WT	5/3	0.26 ± 0.02	Student's t-test	<0.01 **
		IMAA	6/3	0.47 ± 0.03		
8.4A	I_{peak}: $Sweep_2/Sweep_1$ 10 ms	WT	7/2	1.00 ± 0.01	Student's t-test	0.37
		IMAA	9/3	0.99 ± 0.01		
8.4C	I_{peak}: $Sweep_{30}/Sweep_1$, 100 Hz	WT	7/2	1.01 ± 0.01	Student's t-test	0.02 *
		IMAA	9/3	0.95 ± 0.02		
8.4C	I_{peak}: $Sweep_{30}/Sweep_1$, 50 Hz	WT	4/2	1.01 ± 0.02	Student's t-test	0.33
		IMAA	5/2	0.97 ± 0.03		
8.4D	I_{peak}: $Sweep_2/Sweep_1$ 10 ms	WT	7/2	1.02 ± 0.01	Student's t-test	0.1
		IMAA	9/3	1.00 ± 0.01		
8.4F	I_{peak}: $Sweep_{30}/Sweep_1$, 100 Hz	WT	7/2	1.01 ± 0.02	Student's t-test	<0.01 **
		IMAA	9/3	0.94 ± 0.01		
8.4F	I_{peak}: $Sweep_{30}/Sweep_1$, 50 Hz	WT	4/2	0.98 ± 0.01	Student's t-test	0.31
		IMAA	5/2	0.96 ± 0.02		

larger in Ca IM-AA mice than in wild type mice at PF-PC synapses for some ISIs. The results were even more surprising at the PC to deep cerebellar nuclei (PC-DCN) synapse. Short-term plasticity at this synapse is complicated and consists of a combination of facilitation and depression (Turecek et al., 2016, 2017). In 1.5 mM external calcium the initial probability of release is sufficiently high that depression dominates the PPR in wild type animals. Surprisingly, in PC-DCN synapses of Ca IM-AA mice, synaptic facilitation was prominent, whereas in WT mice synaptic depression dominated (**Figure 8.1D, Table 8.1**). Thus, at all three synapses tested, two glutamatergic and one GABAergic, the maximal paired-pulse facilitation was either the same or larger in Ca IM-AA mice in 1.5 mM Ca_{ext} at near-physiological temperatures.

Neurons often fire in bursts under physiological conditions. We therefore examined short-term plasticity during synaptic activation consisting of ten electrical pulses at different frequencies using a similar approach and experimental conditions used to study paired-pulse plasticity (**Figure 8.2**). For wild type mice at hippocampal CA3-CA1 synapse, synaptic enhancement plateaued at 2-3-fold and the extent of synaptic enhancement was frequency dependent (**Figure 8.2A, black, Table 8.1**). The maximal train facilitation and frequency-dependence of synaptic enhancement was unaltered in Ca IM-AA mice (**Figure 8.2A, red, Table 8.1**). For the PF-PC synapse in wild type mice, the synaptic enhancement reached 3-fold and the extent of synaptic enhancement was also frequency dependent (**Figure 8.2B, black, Table 8.1**). We found, however, that the maximal enhancement of PF-PC synapses was significantly larger in Ca IM-AA mice during trains (up to 4-fold), which is consistent with the prolonged decay of paired-pulse facilitation in Ca IMAA mice (**Figure 8.1C, Table 8.1**).

A different approach was required for the PC-DCN synapse. PCs fire spontaneously at frequencies of 10 Hz to over 100 Hz, and therefore sustained synaptic activation is more physiologically relevant. Wild type PC-DCN synapses depress until they reach a steady-state amplitude (Turecek et al., 2016, 2017) (**Figure 8.3A, B, E, black, Table 8.1**). At most depressing synapses steady-state amplitudes are smaller as the frequency of activation is increased, but at PC-DCN synapses this is not the case and

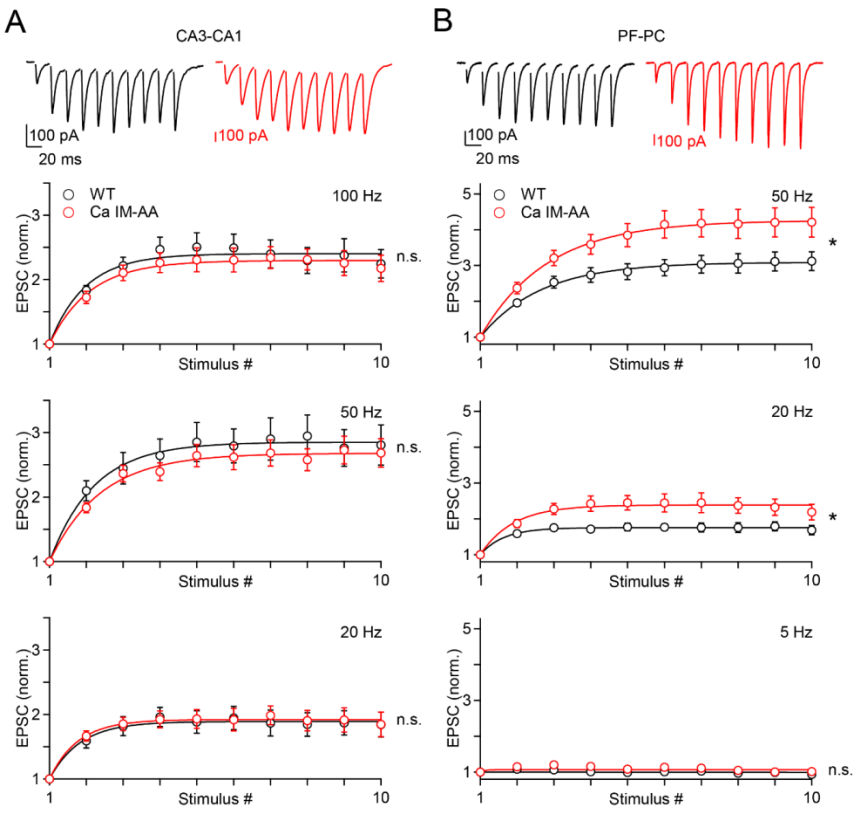

Figure 8.2. Synaptic train facilitation does not decrease in Ca IM-AA mice.

Experiments were performed in wild type (WT, black) and Ca IM-AA (red) mice at hippocampal CA3-CA1 synapses (A) and cerebellar PF-PC synapses (B).

(A, B) (top) Representative EPSCs evoked by a 50 Hz train.

(A, B) (middle, bottom) Summary of normalized average EPSC amplitudes for the indicated stimulus frequencies.

Statistical significance (permutation test; see **Table 8.1**): *: $p<0.05$; not significant (n.s.)

Data shown as mean ± SEM. Fits as mean ± SD.

steady-state amplitudes of the PC-DCN synapse are frequency invariant over a broad range of stimulus frequencies in WT animals (**Figure 8.3B, black**). Even though depression dominates short-term plasticity during trains, the net plasticity reflects a combination of facilitation and depression, and facilitation is essential for the frequency invariance of this synapse. The elimination of facilitation is predicted to lead to a frequency dependent synapse (Turecek et al., 2017). However, this was not the case. In Ca IM-AA mice, synaptic responses facilitated slightly at the start of stimulation and responses reached steady-state levels that were elevated relative to WT animals, but steady-state responses remained frequency invariant (**Figure 8.3A, B**). Facilitation can be studied more directly by stimulating with a 10 Hz trains and abruptly increasing the stimulus frequency to 100 Hz (**Figure 8.3C, D, black, Table 8.1**). Facilitation was actually much more prominent in Ca IM-AA mice than in wild type mice. Thus, synaptic responses evoked by stimulus trains are inconsistent with responses predicted to occur if facilitation of influx through $Ca_V2.1$ is the primary mechanism of facilitation.

The larger synaptic facilitation in Ca IM-AA mice observed at the PF-PC and PC-DCN synapses, suggests that some additional aspect of transmission is altered in Ca IM-AA mice. One possible explanation is that initial calcium influx is decreased in Ca IM-AA mice. At many synapses reducing calcium influx lowers the initial probability of release, thereby decreasing vesicle depletion and increasing synaptic facilitation (Jackman and Regehr, 2017; Zucker and Regehr, 2002). We have previously examined the properties of the PC to DCN synapse in wild type animals in normal (1.5 mM) and 1.0 mM Ca_{ext} (Turecek et al., 2017). The responses measured in 1.5 mM Ca_{ext} previously and in the current study were very similar (**Figure 8.3E**). In contrast, the responses of PC-DCN synapses in Ca IM-AA mice in 1.5 mM Ca_{ext} were similar to synaptic responses measured previously in wild type animals in 1.0 mM Ca_{ext} (Turecek et al., 2017) (**Figure 8.3E**). These findings suggest that a large reduction in presynaptic calcium entry could account for the synaptic responses of PC-DCN synapses in Ca IM-AA mice.

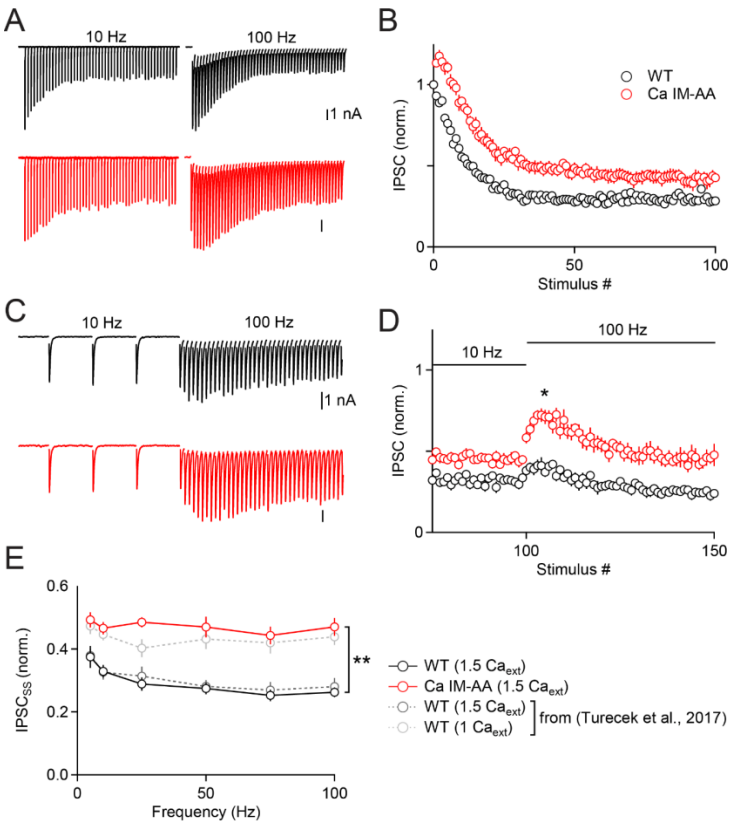

Figure 8.3. Elimination of $Ca_V2.1$ channel facilitation paradoxically increases train facilitation at the PC-DCN synapse. PC axons were stimulated with stimulus trains and the resulting IPSCs were recorded from DCN neurons for WT (black) and Ca IM-AA (red) mice.

(A) Representative IPSCs evoked by10 Hz and a 100 Hz trains are shown.

(B) Summary of normalized IPSC amplitudes evoked by 10 Hz stimulation.

(C) Synaptic currents are shown for 10 Hz stimulation followed by 100 Hz stimulation.

(D) Summary of IPSC amplitudes evoked by an abrupt increase from 10 Hz to 100 Hz stimulation. Statistical significance (unpaired student's t-test; see **Table 8.1**): *: $p<0.05$.

(E) Normalized average steady-state IPSC amplitudes ($IPSC_{SS}$) are plotted for 5 – 150 Hz stimulation. Dashed lines indicate summaries from previous studies (Turecek et al., 2017) for WT animals at different levels of external calcium (Ca_{ext}). 100 Hz $IPSC_{SS}$ significantly different between WT and Ca IMAA animals (**: $p<0.01$; unpaired student's t-test; see **Table 8.1**).

Data shown as mean ± SEM. Fits as mean ± SD.

Given the large effect of the IM-AA mutation on $Ca_V2.1$ channel facilitation described previously (Nanou et al., 2016b, 2016a) and in **Figure 8.1A**, the observation that, in 1.5 Ca_{ext}, at 33-36 °C and without blocking other voltage-gated calcium channels, synaptic facilitation was not attenuated in Ca IM-AA mice (**Figure 8.1B-D, 8.2 and 8.3**) was surprising. One possible explanation is that calcium current experiments were performed under conditions that tended to maximize facilitation of $Ca_V2.1$ channels for biophysical studies (10 mM Ca_{ext}, room temperature, and 5 ms voltage steps). In previous studies measuring presynaptic calcium levels with fluorescent indicators at 34°C in 2 mM Ca_{ext} for pairs of stimuli we did not detect significant use-dependent changes in presynaptic calcium influx for hippocampal CA3 pyramidal cells and cerebellar granule cells (Brenowitz and Regehr, 2007; Jackman et al., 2016). Measurements of changes in presynaptic calcium levels in cerebellar granule cells induced by brief trains at 34°C are consistent with small increases in calcium entry by the end of the train (Kreitzer and Regehr, 2000), but such increases could also arise from buffer saturation (Klingauf and Neher, 1997; Neher, 1998). Voltage clamp methods can provide precise quantification of calcium entry free from such ambiguity. Previous voltage clamp experiments indicated that the extent of facilitation of calcium entry is reduced in low Ca_{ext}, elevated temperatures, and brief depolarizations (1 mM Ca_{ext}, 32 °C, 1 ms step depolarizations) (Benton and Raman, 2009; Kreiner et al., 2010). The dependence of facilitation on Ca_{ext}, temperature and voltage steps prompted us to examine facilitation of calcium currents in physiological Ca_{ext} (1.5 mM) at 37 °C with trains of action potential waveforms. Experiments were performed on the somata of acutely dissociated PCs, which have a high density of $Ca_V2.1$ channels. Although the bulk residual calcium signals in presynaptic boutons and somata differ because of their very different surface-to-volume characteristics, facilitation of calcium entry is thought to be dependent on local calcium signaling near the point of entry through calcium channels, which does not depend on residual calcium signals (Borst and Sakmann, 1998; DeMaria et al., 2001; Lee et al., 2000). Voltage commands used both narrow waveforms measured from the somata of PCs and broad waveforms measured from hippocampal pyramidal cells. These waveforms span the range of action potential shapes typical of central neurons including those recorded in presynaptic boutons (Bischofberger et al., 2002; Boudkkazi et al., 2011; Foust

et al., 2011; Geiger and Jonas, 2000; Hee Kim et al., 2010; Hoppa et al., 2014; Rowan et al., 2014), thereby accounting for possible differences in action potential width between soma and presynaptic terminals.

We began by focusing on the initial pair of pulses during pulse trains to compare $Ca_V2.1$ facilitation with synaptic PPR (**Figure 8.2**). $Ca_V2.1$ calcium currents were isolated pharmacologically. Surprisingly, for identical action potentials (recorded from spontaneously active PCs with physiological Ca_{ext} and temperature) separated by 10 ms, there was no significant facilitation of calcium currents (I_{Ca2}/I_{Ca1}) in WT mice and little difference between WT and Ca IM-AA mice (**Figure 8.4A, Table 8.1**). In wild type animals,100 Hz stimulation evoked remarkably stable calcium currents, as is shown for the initial 10 stimuli of the train (**Figure 8.4B**), and as is summarized for the 30 stimuli (**Figure 8.4C**). The ratio of the amplitudes of the currents evoked by the 30^{th} stimulus and first stimulus is $I_{Ca30}/I_{Ca1} = 1.01 \pm 0.01$ in wild type animals, whereas in Ca IM-AA mice there was a decrement in calcium entry ($I_{Ca30}/I_{Ca1} = 0.95 \pm 0.02$). For 50 Hz stimulation there was no significant alteration of calcium current even with sustained activation in either wild type ($I_{Ca30}/I_{Ca1} = 0.99 \pm 0.01$) or Ca IM-AA mice ($I_{Ca30}/I_{Ca1} = 0.96 \pm 0.02$).

It is possible that the properties of the action potential waveform could influence facilitation of calcium entry. The action potentials of Purkinje cells are particularly brief. The action potential waveform used in **Figure 8.4A-C** had a width at half-amplitude of ~0.20 ms, typical of Purkinje neuron action potentials at 37 °C (Carter and Bean, 2009). Many other types of neurons using $Ca_V2.1$ channels to trigger synaptic release have significantly longer-lasting action potentials. We therefore also studied calcium channel facilitation using the broader waveforms recorded from hippocampal pyramidal cells, which had a width at half-amplitude of 0.92 ms (**Figure 8.4D-F**). Experiments were again performed in PCs where $Ca_V2.1$ currents are dominant and readily isolated. As expected, the resulting calcium currents were longer lasting than those evoked by PC waveforms, but there was little difference in the properties of facilitation from those obtained when PC waveforms were used (**Figure 8.4D-F, Table 8.1**). There was no facilitation of calcium entry for pairs (**Figure 8.4D**) and there were no obvious changes in calcium

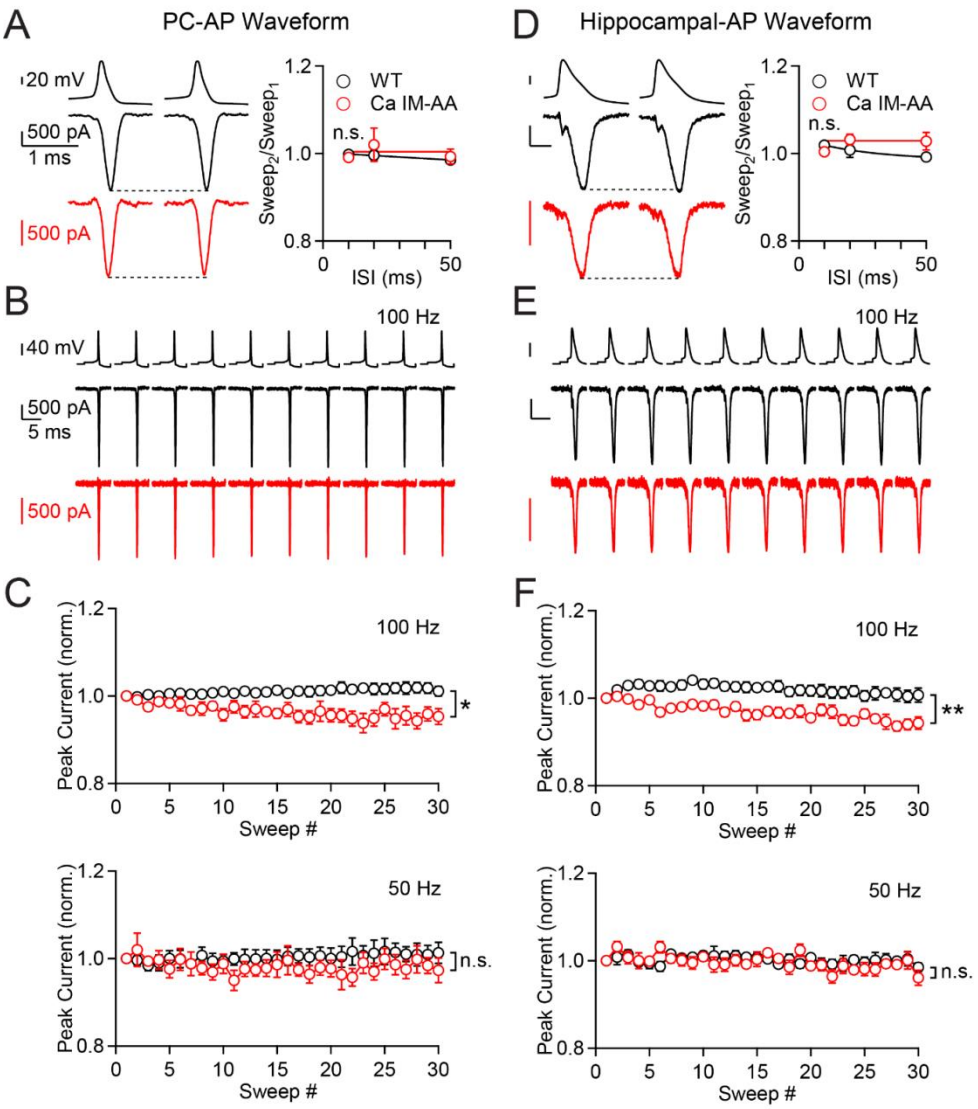

Figure 8.4. $Ca_V2.1$channel facilitation is small in physiological Ca_{ext} at physiological temperatures.

Experiments were performed in acutely dissociated Purkinje cells (PCs) at 37 °C with 1.5 mM Ca_{ext}. Calcium currents were evoked by trains of action potential (AP) waveforms from cerebellar PCs (PC, left) and hippocampal pyramidal cells (right).

(A left, D left) Currents evoked by representative PC (A, left) and hippocampal (D, left) AP waveforms are shown for wild type (black) and Ca IM-AA (red) mice. Same scale values for A and D.

Figure 8.4 (Continued)

(A right, D right) Summary of the ratio of calcium current evoked by second and first stimuli plotted for different inter-sweep intervals (ISIs) and AP waveforms (data from trains in C and F), each sweep corresponding to an AP waveform stimulus.

(B,E) Representative PC (B) and CA1 (E) AP waveforms and PC responses for the first ten sweeps of a 100 Hz train. Same scale values for B and E .

(C, F) Normalized peak calcium current evoked by different frequency trains plotted versus the sweep number, each sweep corresponding to an AP waveform stimulus.

Statistical significance (unpaired student's t-test; see **Table 8.1**): *: $p<0.05$; **: $p<0.01$, not significant (n.s.)

Data shown as mean ± SEM. Fits as mean ± SD.

entry for the first 10 stimuli at 100 Hz (**Figure 8.4E**). Similar to the results with Purkinje neuron action potential waveforms (maximal facilitation of ~ 2%), with long trains of hippocampal neuron action potential waveforms at 100 Hz, the currents were remarkably stable in WT neurons (maximal facilitation of ~ 4%), but showed a maximal decrease of ~ 6% over the course of 30 stimuli in Ca IM-AA neurons (**Figure 8.4F, Table 8.1**) as if the main difference during 100 Hz trains is an unmasking of cumulative calcium current inactivation. These findings suggest for a broad range of presynaptic waveforms, calcium entry in physiological Ca_{ext} at a physiological temperature produces little or no net facilitation of $Ca_V2.1$ currents but rather acts to compensate for cumulative inactivation, with the result being remarkable stability of calcium entry during high-frequency trains.

The synaptic properties at PF-PC synapses and PC-DCN synapses in the mutant animals are consistent with a reduction in presynaptic calcium influx. Expression levels are often altered in knock-in animals, either as a result of perturbing introns or as a result of the mutations in the protein of interest. For example, disruption of Ca^{2+}/calmodulin binding reduces surface membrane expression of $Ca_V1.2$ channels (Wang et al., 2007). We therefore compared calcium current densities in wild type and Ca IM-AA mice. Previous studies found that the IM-AA mutation does not alter maximal current densities in cultured hippocampal neurons (Nanou et al., 2016a), which is consistent with the synaptic properties we observed at the hippocampal CA3 to CA1 synapses. However, the more pronounced increase of facilitation we observe at PF-PC and PC-DCN synapses would be consistent with small decreases in calcium entry in cerebellar granule cells and substantial decreases in PCs. We therefore quantified the magnitudes of the calcium currents evoked by 5 ms voltage steps in 1.5 mM Ca_{ext} at 37°C in PCs (**Figure 8.5**). There was a sizeable difference ($p<0.01$) in the magnitudes of calcium currents in wild type mice (1.29 ± 0.13 nA) and in Ca IM-AA mice (0.57 ± 0.05 nA), different from the situation in hippocampal neurons (Nanou et al., 2016a). Thus, in some cell types, there is a large reduction in calcium currents in Ca IM-AA mice, which would explain the observed increases in synaptic facilitation at some synapses in Ca IM-AA mice.

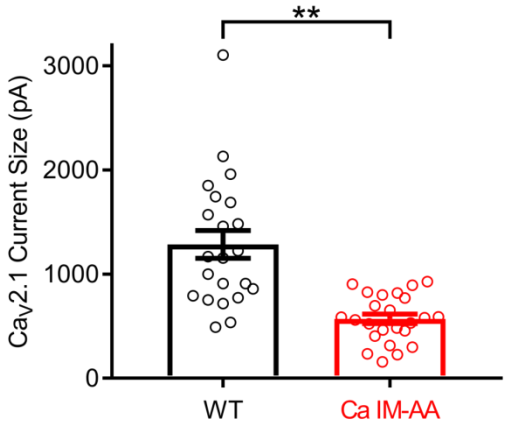

Figure 8.5: Comparison of WT vs. Ca IM-AA Ca current sizes recorded in 1.5 mM Ca_{ext} at 37 °C with 5 ms voltage steps. Average $Ca_V2.1$current sizes were 1286 ± 133 pA (n=22, N=6) for WT animals and 572 ± 46 pA (n=24, N=6) for Ca IM-AA animals. They are significantly different (unpaired student's t-test, **: $p<0.01$).

Discussion

Our main finding is that under physiological conditions of temperature and Ca_{ext}, facilitation of native neuronal $Ca_V2.1$ channels is surprisingly small and under similar conditions of temperature and Ca_{ext} and the absence of $Ca_V2.2$ blockers, $Ca_V2.1$ channel facilitation is clearly not the major factor underlying synaptic facilitation at CA3-CA1, PF-PC or PC-DCN synapses.

Small facilitation of $Ca_V2.1$ in physiological Ca_{ext} and temperature

We were surprised by the small facilitation of $Ca_V2.1$ currents under our conditions, because many previous studies observed much larger $Ca_V2.1$ facilitation. Paired-pulse facilitation of calcium currents mediated by $Ca_V2.1$ has been observed at the calyx of Held of (5-20% enhancement, (Borst and Sakmann, 1998; Cuttle et al., 1998; Inchauspe et al., 2004; Ishikawa et al., 2005; Müller et al., 2008)), in Purkinje cells (10%, (Díaz-Rojas et al., 2015)), and in transfected cells (10-35%, (DeMaria et al., 2001; Lee et al., 2000, 2003; Mochida et al., 2008). Facilitation of calcium entry has also been documented during high frequency trains, at the calyx of Held (10-100% enhancement (Borst and Sakmann, 1998; Cuttle et al., 1998; Müller et al., 2008)), in PCs (5 – 25%, (Adams et al., 2010; Benton and Raman, 2009; Chaudhuri et al., 2005), and in transfected cells (20-35%, (DeMaria et al., 2001; Lee et al., 2000, 2003; Mochida et al., 2008). However, most previous studies used non-physiological conditions that may have contributed to the large facilitation of calcium entry. In most studies, calcium currents were evoked by 1 to 10 ms repetitive voltage steps. As shown previously at the calyx of Held, larger facilitation occurs when voltage steps are used rather than action potential waveforms, most likely because such voltage steps evoke larger calcium influx (Cuttle et al., 1998; Di Guilmi et al., 2014). Similarly, many previous studies were performed in 5-10 mM external calcium, which elevates initial calcium entry and produces more facilitation of calcium entry (Chaudhuri et al., 2005). Previous studies suggest that use-dependent changes in calcium entry are much smaller when experiments are performed with brief voltage steps, in low external calcium and at elevated temperatures (1 ms step, 1 mM Ca_{ext}, 32 °C; (Chaudhuri et al., 2005)). Our own results highlight the strong influence of experimental conditions in regulating use-dependent changes in calcium entry. We did not observe paired-pulse changes in calcium entry using

action potential waveform stimuli with physiological conditions of temperature and Ca_{ext}, but we observed large paired-pulse increases in calcium entry in wild type animals and decreases in Ca IM-AA mice (**Figure 8.1A, right**) when experiments were performed with 5 ms voltage steps at room temperature in elevated calcium.

Our results show that in physiological Ca_{ext} at physiological temperature, $Ca_V2.1$ channel facilitation is small regardless of whether a rapid PC waveform or a slow hippocampal waveform was used to evoke calcium entry. These waveforms span the range of action potential shapes typical of central neurons, including those in presynaptic boutons (Bischofberger et al., 2002; Boudkkazi et al., 2011; Foust et al., 2011; Geiger and Jonas, 2000; Hee Kim et al., 2010; Hoppa et al., 2014; Rowan et al., 2014). Thus, our results suggest that facilitation of calcium entry is likely to be small for a broad range of presynaptic waveforms. In addition, it is actually local calcium increases near open calcium channels that facilitate entry through $Ca_V2.1$ channels (Borst and Sakmann, 1998; DeMaria et al., 2001; Lee et al., 2000). Being responsible for controlling the extent of facilitation of calcium entry, such localized calcium increases are expected to be similar for channels in the soma and in presynaptic terminals. Also, the similarity of facilitation in WT and Ca IM-AA mice at CA3 to CA1 synapses suggests that there is no facilitation of total calcium entry in the presynaptic boutons of these synapses.

Synaptic facilitation in physiological Ca_{ext} at near-physiological temperatures

Our finding that facilitation of calcium entry does not contribute to synaptic facilitation at CA3-CA1, PF-PC and PC-DCN synapses in physiological Ca_{ext} at near-physiological temperatures, contrasts with previous demonstrations that $Ca_V2.1$ channel facilitation can contribute to the facilitation of numerous synapses under other conditions. $Ca_V2.1$ facilitation has been proposed to account for ~40% (Müller et al., 2008) or up to 100% (Inchauspe et al., 2004) of synaptic paired pulse facilitation (PPF) at the calyx of Held synapse, up to ~100% of PPF at synapses made by cultured PCs (Díaz-Rojas et al., 2015), and up to 100% of PPF of cultured SCG synapses (Mochida et al., 2008). Previous studies in wild type and Ca IM-AA mice found that calcium channel facilitation can account for up to ~60% of the maximal synaptic paired-pulse facilitation at NMJ synapses (Nanou et al., 2016b), for close to ~100% of

maximal PPF at cultured hippocampal synapses (Nanou et al., 2016a), and up to ~50% of peak PPF at hippocampal synapses in slices (Nanou et al., 2016a). However, there is no conflict between our results and previous experiments, which were performed in very different experimental conditions. These previous studies were conducted primarily at room temperature, which could have led to more prominent $Ca_V2.1$ channel facilitation than we observed at near-physiological temperatures. In addition, previous studies on facilitation at hippocampal synapses in slices (Nanou et al., 2016a, 2018) and at NMJ synapses (Nanou et al., 2016b), were performed in the presence of ω-conotoxin GVIA to inhibit $Ca_V2.2$ channels. This accentuates the contribution of $Ca_V2.1$ channels to synaptic transmission at synapses such as the CA3 to CA1 synapse where release is mediated by both $Ca_V2.1$ and $Ca_V2.2$ channels. Inhibiting $Ca_V2.2$ channels is useful for detecting effects from modification of $Ca_V2.1$ channels, but leaving the currents from $Ca_V2.2$ channels intact is preferable for using the IM-AA knock-in animals to quantify the effects of $Ca_V2.1$ facilitation under more physiological conditions. Our results not only show that $Ca_V2.1$ current facilitation is small for WT Purkinje cells under physiological conditions, but also that our tested synapses do not lose their prominent synaptic facilitation due to a loss of $Ca_V2.1$ current facilitation (IM-AA mutation).

Calcium Current Reduction in Ca IM-AA mice

We found that calcium currents in PC somata were about half as large in Ca IM-AA mice as in wild type mice, suggesting a significant decrease in channel expression. In addition, the increased synaptic facilitation and short-term plasticity at PC to DCN synapses and granule cell to PC synapses in Ca IM-AA mice is consistent with a reduction in presynaptic calcium entry in the presynaptic boutons of both granule cells (glutamatergic) and PCs (GABAergic). It has been established that a decrease in calcium entry increases the extent of facilitation indirectly, presumably by lowering the initial probability of release, which decreases depression associated with vesicle depletion and prevents the saturation of release (Dittman et al., 2000). However, it does not appear that $Ca_V2.1$ channel density is reduced in all types of cells, because there is no indication that calcium channel density is reduced at the CA3 to CA1 synapse, consistent with the earlier observation of no change in the amplitudes of $Ca_V2.1$ currents in

cultured hippocampal neurons of Ca IM-AA animals (Nanou et al., 2016a) and our results for CA3-CA1 synapses (**Figure 8.1B**). Although the reason for the reduced $Ca_V2.1$ channel density in some cell types in Ca IM-AA mice is not known, even a small decrement in calcium channel density can strongly reduce the initial synaptic strength, which in turn increases synaptic facilitation. These results raise the possibility that changes in $Ca_V2.1$ channel density in some types of neurons could contribute to behavioral phenotypes that have been observed in Ca IM-AA mice (Nanou et al., 2016b, 2016c). We note however that a reduction in $Ca_V2.1$ current density is only one factor that may influence the balance of synaptic depression and facilitation in Ca IM-AA animals. A reduction in synaptic depression similar to that we saw in (PC-DCN) synapses is also seen in Ca IM-AA mice for the synapse of PV basket cells onto CA1 neurons (Nanou et al., 2018), in which case comparison with similar effects in CaBP1/caldendrin KO mice suggested mediation by altered binding of CaBP1 at the calcium sensor site. We currently have little knowledge of what calcium-binding proteins are present in presynaptic terminals of various neurons. CaBP1/caldendrin does not appear to be prominent in Purkinje neurons (Kim et al., 2014) but may be involved in altered plasticity of other synapses in Ca IM-AA mice.

A physiological role for $Ca_V2.1$ facilitation

In addition to self-facilitation, $Ca_V2.1$ channels also undergo both voltage-dependent and calcium-mediated inactivation. Interestingly, previous studies have shown that for native $Ca_V2.1$ channels in Purkinje neurons, cumulative inactivation is much more prominent than for $Ca_V2.1$ channels studied in heterologous transfection systems (Benton and Raman, 2009; Kreiner et al., 2010). Our own results show that in physiological Ca_{ext} at physiological temperatures, $Ca_V2.1$ facilitation in WT neurons does a remarkably good job of offsetting cumulative inactivation for the stimulation protocols commonly used to study synaptic facilitation. The resulting lack of net use-dependent changes in calcium entry in wild type animals supports the hypothesis that one role of $Ca_V2.1$ facilitation is to offset inactivation to reduce use-dependence of calcium entry (Benton and Raman, 2009). In Ca IM-AA mice, 100 Hz stimulation leads to a maximal reduction in calcium entry of ~6%, which would result in a small but significant use-dependent synaptic depression of about 26%. We conclude that under physiological conditions, $Ca_V2.1$ facilitation

acts to minimize use-dependent reduction in calcium entry that would otherwise occur and thereby minimizes a potential contribution of reduction in calcium entry to short-term plasticity. This function may be particularly valuable at synapses like the CA3-CA1 synapse where transmission is mediated by a combination of $Ca_V2.2$ channels (showing only calcium-mediated inactivation) and $Ca_V2.1$ channels (with both inactivation and facilitation).

Methods

Mice

Animal procedures have been carried out in accordance with the NIH guidelines and protocols were approved by the Harvard Medical Area Standing Committee on Animals. Ca IM-AA mice in which isoleucine and methionine of the $Ca_V2.1$ channel IM motif have been mutated to alanines were originally generated by "Ingenious Targeting Laboratory" (Nanou et al., 2016b, 2016a) and was transferred from the William Catterall laboratory at the University of Washington to Harvard Medical School. WT controls were derived from the same Ca IM-AA mouse line. Mice of either sex were used. Experimenters were blinded to the genotype of the mouse for all experiments.

Method Details

Preparation of dissociated Purkinje neurons

Mice were deeply anesthetized with isoflurane and killed by decapitation. The cerebellum was quickly removed and placed into ice-cold solution consisting of 110 mM NaCl, 2.5 mM KCl, 10 mM HEPES, 25 mM glucose, 75 mM sucrose, 7.5 mM $MgCl_2$, pH adjusted to 7.4 with NaOH. The cerebellum was cut into (~1 mm^3) chunks and was treated for 10–20 min at room temperature with 3 mg/mL protease XXIII (Sigma Life Science) dissolved in a dissociation solution consisting of 82 mM Na_2SO_4 , 30 mM K_2SO_4 , 5 mM $MgCl_2$, 10 mM glucose, and 10 mM HEPES, pH adjusted to 7.4 with NaOH. The protease solution was then replaced by ice-cold dissociation solution containing 1 mg/mL trypsin inhibitor and 1 mg/mL bovine serum albumin and the chunks were kept on ice in this solution until immediately before use. To release individual cells, the tissue was passed through Pasteur pipettes with fire-polished tips. A drop of the suspension was placed in the recording chamber and diluted with a large volume of Tyrode's

solution, consisting of 155 mM NaCl, 3.5 mM KCl, 1.5 mM $CaCl_2$, 1 mM $MgCl_2$, 10 mM glucose, 10 mM HEPES, pH adjusted to 7.4 with approximately 5 mM NaOH. Purkinje neurons could be recognized by their large size and a single large dendritic stump. The used age range was P16-P19 for Figure 8.1A, P15-P17 for Figure 8.4 and P11-P17 for the current size comparisons.

Electrophysiology of dissociated Purkinje neurons

P-type calcium current in dissociated Purkinje neurons: Whole-cell patch-clamp recordings were obtained with a Multiclamp 700B amplifier (Molecular Devices), and Digidata 1322A A/D converter (Molecular Devices), and Clampex 10.3.1.5 software (Molecular Devices). Data were analyzed using Igor-Pro 6.12A (Wavemetrics) using DataAccess (Bruxton) to read Clampex files and using Microsoft Excel. Recording were made with borosilicate glass electrodes (VWR International) wrapped with Parafilm to reduce pipette capacitance. Pipette resistances were 1.2-3.0 MΩ when filled with the internal solution containing (in mM) 139.5 K-methanesulfonate, 5 tetraethylammonium (TEA) Cl, 10 NaCl, 2 $MgCl_2$, 1 EGTA, 0.2 $CaCl_2$, 4 MgATP, 0.3 GTP (Tris salt), 14 creatine phosphate (Tris salt), and 10 HEPES with pH adjusted to 7.35 with KOH. Series resistance (typically 3-6 MΩ) was compensated during voltage-clamp recording by 70% and monitored throughout the experiment. Voltages are corrected for a liquid junction potential of -8 mV between the internal solution and the external Tyrode's solution in which membrane current was zeroed before the start of the experiment. After a gigaohm seal, whole-cell configuration were established, the cell was lifted off the bottom of the recording chamber and placed in front of an array of quartz fiber flow pipes (250 μm internal diameter, 350 μm external diameter) glued onto an aluminum rod whose temperature was controlled by resistive heating elements and a feedback-controlled temperature controller (TC-344B, Warner Instruments). Solutions were changed (in ~1 s) by moving the cell from one pipe to another. Initial voltage clamp recordings to assay calcium current facilitation were performed at room temperature using an external solution of 10 mM $CaCl_2$, 155 mM TEACl, 10 mM HEPES, pH adjusted to 7.4 with TEA-OH. In order to isolate P-type ($Ca_V2.1$) current, the solution contained inhibitors for L-type, N-type, and T-type current (2 μM nimodipine, 1 μM conotoxin GVIA, and 1 μM TTA-A2) along with 1 μM tetrodotoxin (TTX) to inhibit outward currents through

sodium channels. For recording P-type current flowing during action potential waveforms at physiological temperatures and with physiological calcium concentrations, the external solution contained 1.5 mM $CaCl_2$, 1 mM $MgCl_2$, 155 mM TEACl, 20 mM glucose, 10 HEPES, pH adjusted to 7.4 with TEA-OH, with 1 μM TTX, 2 μM nimodipine, 1 μM conotoxin GVIA, and 1 μM TTA-A2. The process of dialyzing cells to make whole-cell recordings did not disrupt calcium current facilitation, because it was robust and showed no tendency to run down in the experiments using 10 mM Ca^{2+} at room temperature with voltage steps. Recordings of action potential-evoked calcium currents were made at 37 °C.

Action potential waveforms were previously recorded at 37 °C in acutely dissociated CA1 pyramidal neurons and Purkinje cells using an intracellular solution containing 139.5 mM K-methanesulfonate, 10 mM NaCl, 2 mM $MgCl_2$, 1 mM EGTA, 0.2 mM $CaCl_2$, 4 mM MgATP, 0.3 mM GTP (Tris salt), 14 mM creatine phosphate (Tris salt), 10 mM HEPES, pH adjusted to 7.35 with KOH, and an external Tyrode's solution containing 155 mM NaCl, 3.5 mM KCl, 1.5 mM $CaCl_2$, 1 mM $MgCl_2$, 10 mM glucose and 10 mM HEPES with pH adjusted to 7.4 with NaOH.

In the voltage clamp recordings of P-type current, capacity currents were reduced during recording using the amplifier circuitry. In the voltage clamp experiments using step depolarizations, remaining capacity currents along with leak currents were corrected during analysis using the current evoked by a 5 mV hyperpolarization to define remaining capacity currents and leak current, which was assumed to be ohmic. For action potential waveforms, capacity and leak currents were corrected by recording the response to the action potential waveform inverted and scaled down by a factor of 4, and signal-averaging over 4 applications of this waveform. However, this correction was imperfect, particularly for the fast-rising and fast-falling Purkinje cell action potential waveforms. Therefore, to better isolate calcium current free from contaminating capacity current artifacts, after recording the P-type currents, we repeated the stimulation in a calcium-free solution, containing 5 mM $MgCl_2$, 155 mM TEACl, 20 mM glucose and 10 mM HEPES with pH adjusted to 7.4 with TEA-OH. Calcium currents

were determined by subtracting the currents in Ca-free solutions from those in the Ca-containing solutions. $Sweep_2/Sweep_1$ in Figure 8.4A and D was created using the first 2 points from stimulus trains.

Preparation of acute brain slices

Mice were anesthetized with isoflurane and decapitated. A Leica VT1200S vibratome was used to cut acute slices with a thickness ranging from 250 to 270 μm. For CA3-CA1 and PF-PC recordings, slices were prepared using ice-cold choline-based oxygenated (95% O2, 5% CO2) cutting solution containing (in mM): 110 Choline-Cl, 7 $MgSO_4$ or $MgCl_2$, 2.5 KCl, 1.2 NaH_2PO_4, 0.5 $CaCl_2$, 25 glucose, 11.6 Na-Ascorbate, 2.4 Na-Pyruvate and 25 $NaHCO_3$. Transverse hippocampal and cerebellar slices were cut for CA3-CA1 and PF-PC recordings. A subset of hippocampal slices were prepared using a Leica VT1000S vibratome and ice-cold oxygenated (95% O_2, 5% CO_2) sucrose-based cutting solution containing (in mM): 234 sucrose, 25 $NaHCO_3$, 11 glucose, 7 $MgCl_2$, 2.5 KCl, 1.25 NaH_2PO_4 and 0.5 $CaCl_2$. A cut was made between the CA3 and CA1 regions of the hippocampal slices when they were still cold. Antagonists were not included in the external solution of the holding chamber. Slices for PC-DCN recordings were prepared as previously described (Turecek et al., 2016, 2017). Choline-Cl slicing solution as described above was supplemented with (in μM) 5 CPP, 5 NBQX and warmed to 35°C to make parasagittal slices. Acute brain slices were transferred to a holding chamber and incubated at ~32-34 °C for 20-30 min in oxygenated (95% O_2, 5% CO_2) artificial cerebrospinal fluid (ACSF) containing (in mM): 125 NaCl, 26 $NaHCO_3$, 1.25 NaH_2PO_4, 2.5 KCl, 25 glucose, 1.5 $CaCl_2$ and 1 $MgCl_2$. After incubation, brain slices were kept at room temperature (RT) until they were transferred individually to a recording chamber.

Electrophysiology of acute brain slices

Brain slices were transferred/mounted onto poly-L-lysine coated coverslips and/or via harp and submerged in oxygenated ACSF. The composition of the ACSF was as described above unless otherwise noted. Whole-cell voltage-clamp recordings were performed at 33-36°C. For all experiments, series resistance was compensated up to 80% and ISIs were randomized.

CA3-CA1 recordings were performed similar to (Jackman et al., 2016). P25-31 (PPR) and P25-32 (trains) animals were used. ACSF was supplemented with (in μM): 100 picrotoxin, 2 CPP and 2 CGP-55845.

CA1 neurons were held at -60 mV. Borosilicate recording electrodes were filled with (in mM): 100 CsCl, 75 CsFl, 10 EGTA, 10 HEPES and 5 QX-314-Cl. For electrical stimulation a glass monopolar pipette was filled with ACSF and placed in the stratum radiatum. Initial EPSC sizes were kept at 50 to 250 pA.

For PF-PC recordings, ACSF was supplemented with (in μM): 100 picrotoxin or 1.25 gabazine, 2 CGP 55845 and 1 AM-251 (for trains only). P18-22 (PPR) and P19-22 (trains) animals were used. Purkinje cells were held at -60 mV. Recording electrodes contained the same internal solution as for CA3-CA1 recordings. Stimulation was performed within the inner third of the molecular layer and avoided the ascending branch of parallel fibers. EPSC1 sizes were between 50 and 250 pA in order to maintain voltage clamp.

PC-DCN recordings were performed as previously described (Turecek et al., 2016, 2017). P22-32 animals were used. ACSF was supplemented with (in μM): 5 NBQX, 2 CPP, 0.5 strychnine. DCN neurons were held at -30 to -40 mV. Recording electrodes were filled with (in mM): 110 CsCl, 10 HEPES, 10 TEA-Cl, 1 $MgCl_2$, 4 $CaCl_2$, 5 EGTA, 20 Cs-BAPTA, 2 QX314, 0.2 D600. A glass monopolar stimulus electrode was placed in the white matter surrounding the DCN, as previously described. Trains of various frequencies were applied with 100 stimuli, followed by 100 stimuli at 100Hz. Synaptic recordings were collected at 10 - 20 kHz and filtered at 2 - 10 kHz using an Axon Multiclamp 700B and digitized with an ITC-18 using mafPC (courtesy of Matthew A. Xu-Friedman) and custom procedures (courtesy of Skyler L. Jackman) in IgorPro (Wavemetrics). Data analysis was performed using custom scripts written in IgorPro (mainly courtesy of Skyler L. Jackman), Microsoft Excel and Matlab (Mathworks), available upon request. For presented data, stimulus artifacts were blanked for clarity. The number of experiments are shown in **Table 8.1** as number of cells (n) and number of animals (N). In text, fit coefficients are shown ± SD, and all other measurements are presented as mean ± SEM.

EPSC/IPSC amplitude was measured from averaged trials as the peak current with baseline collected just prior to the stimulus onset. During high frequency stimulation or when ISIs were small, EPSC/IPSCs did not fully decay between stimuli. For trains the baseline was measured by extrapolating a single exponential fit to the previous EPSC/IPSC. For PPR, for short ISIs the amplitude of EPSC2 was

determined by subtracting EPSC1 collected for long ISI trials. For PC-DCN recordings, a subset of paired-pulse ratios was collected from train data (40 and 50 ms ISIs were pooled). PC-DCN steady-state values were measured as the average of the 50-70th IPSC size.

PPR curves for CA3-CA1 and PF-PC synapses were fit with a single exponential of the form: $(1 + Ae^{-(t-t0)/\tau})$, with t_0 as the inter-stimulus interval leading to maximal PPR. PPR curves for PC-DCN synapses were more complicated and were poorly fit by a single exponential, and therefore only the peak PPR was compared. Train data for CA3-CA1 and PF-PC synapses was fit with a single exponential fit of the form $((1 + A) - Ae^{-(t/\tau)})$.

Quantification and statistical analysis

Statistics were performed using Graphpad Prism, Microsoft Excel, Igor Pro and custom written scripts in Matlab. Statistical tests are indicated in **Table 8.1**. Comparisons were performed using unpaired two-tailed Student's t-test unless otherwise noted (see **Table 8.1**) and set with significance level of $P < 0.05$ (*). Same standard deviation was assumed for both tested populations. Single exponential fits to PPR and synaptic train data were compared using permutation tests, as described previously (Turecek and Regehr, 2018). Briefly, wild type and Ca IM-AA data were randomly assigned to two groups. Each group was averaged and fit with PPR = $(1 + Ae^{-(t-t0)/\tau})$ or $EPSC_{train} = ((1 + A) - Ae^{-(t/\tau)})$. The differences between fit coefficients of the two groups (residuals, $A_1 - A_2$; $\tau_1 - \tau_2$) were taken. 10000 repetitions were performed to generate a distribution of residuals. The observed difference between wild type and Ca-IMAA fit coefficients was then compared to the generated distribution of residuals. P-values were obtained as the number of generated residuals greater than the observed difference, with significance set to $p < 0.05$.

References

ABBOTT, L. F. & REGEHR, W. G. 2004. Synaptic computation. *Nature,* 431**,** 796-803.

ABBOTT, L. F., VARELA, J. A., SEN, K. & NELSON, S. B. 1997. Synaptic depression and cortical gain control. *Science,* 275**,** 220-4.

ARENZ, A., SILVER, R. A., SCHAEFER, A. T. & MARGRIE, T. W. 2008. The contribution of single synapses to sensory representation in vivo. *Science,* 321**,** 977-80.

ARMSTRONG, D. M. & EDGLEY, S. A. 1984a. Discharges of nucleus interpositus neurones during locomotion in the cat. *J Physiol,* 351**,** 411-32.

ARMSTRONG, D. M. & EDGLEY, S. A. 1984b. Discharges of Purkinje cells in the paravermal part of the cerebellar anterior lobe during locomotion in the cat. *J Physiol,* 352**,** 403-24.

ATLURI, P. P. & REGEHR, W. G. 1996a. Determinants of the time course of facilitation at the granule cell to Purkinje cell synapse. *J Neurosci,* 16**,** 5661-71.

ATLURI, P. P. & REGEHR, W. G. 1996b. Determinants of the time course of facilitation at the granule cell to Purkinje cell synapse. *Journal of Neuroscience,* 16**,** 5661-5671.

ATLURI, P. P. & REGEHR, W. G. 1998. Delayed release of neurotransmitter from cerebellar granule cells. *J Neurosci,* 18**,** 8214-27.

BABAI, N., KOCHUBEY, O., KELLER, D. & SCHNEGGENBURGER, R. 2014. An alien divalent ion reveals a major role for Ca2+ buffering in controlling slow transmitter release. *J Neurosci,* 34**,** 12622-35.

BACAJ, T., WU, D., YANG, X., MORISHITA, W., ZHOU, P., XU, W., MALENKA, R. C. & SUDHOF, T. C. 2013. Synaptotagmin-1 and Synaptotagmin-7 trigger synchronous and asynchronous phases of neurotransmitter release. *Neuron,* 80**,** 947-59.

BAGNALL, M. W., MCELVAIN, L. E., FAULSTICH, M. & DU LAC, S. 2008. Frequency-independent synaptic transmission supports a linear vestibular behavior. *Neuron,* 60**,** 343-52.

BAGNALL, M. W., ZINGG, B., SAKATOS, A., MOGHADAM, S. H., ZEILHOFER, H. U. & DU LAC, S. 2009. Glycinergic projection neurons of the cerebellum. *J Neurosci,* 29**,** 10104-10.

BAKKEN, T. E., MILLER, J. A., DING, S. L., SUNKIN, S. M., SMITH, K. A., NG, L., SZAFER, A., DALLEY, R. A., ROYALL, J. J., LEMON, T., SHAPOURI, S., AIONA, K., ARNOLD, J., BENNETT, J. L., BERTAGNOLLI, D., BICKLEY, K., BOE, A., BROUNER, K., BUTLER, S., BYRNES, E., CALDEJON, S., CAREY, A., CATE, S., CHAPIN, M., CHEN, J., DEE, N., DESTA, T., DOLBEARE, T. A., DOTSON, N.,

EBBERT, A., FULFS, E., GEE, G., GILBERT, T. L., GOLDY, J., GOURLEY, L., GREGOR, B., GU, G., HALL, J., HARADON, Z., HAYNOR, D. R., HEJAZINIA, N., HOERDER-SUABEDISSEN, A., HOWARD, R., JOCHIM, J., KINNUNEN, M., KRIEDBERG, A., KUAN, C. L., LAU, C., LEE, C. K., LEE, F., LUONG, L., MASTAN, N., MAY, R., MELCHOR, J., MOSQUEDA, N., MOTT, E., NGO, K., NYHUS, J., OLDRE, A., OLSON, E., PARENTE, J., PARKER, P. D., PARRY, S., PENDERGRAFT, J., POTEKHINA, L., REDING, M., RILEY, Z. L., ROBERTS, T., ROGERS, B., ROLL, K., ROSEN, D., SANDMAN, D., SARREAL, M., SHAPOVALOVA, N., SHI, S., SJOQUIST, N., SODT, A. J., TOWNSEND, R., VELASQUEZ, L., WAGLEY, U., WAKEMAN, W. B., WHITE, C., BENNETT, C., WU, J., YOUNG, R., YOUNGSTROM, B. L., WOHNOUTKA, P., GIBBS, R. A., ROGERS, J., HOHMANN, J. G., HAWRYLYCZ, M. J., HEVNER, R. F., MOLNAR, Z., PHILLIPS, J. W., DANG, C., JONES, A. R., AMARAL, D. G., BERNARD, A. & LEIN, E. S. 2016. A comprehensive transcriptional map of primate brain development. *Nature,* 535**,** 367-75.

BEKKERS, J. M. 2003. Convolution of mini distributions for fitting evoked synaptic amplitude histograms. *J Neurosci Methods,* 130**,** 105-14.

BERTRAM, R., SHERMAN, A. & STANLEY, E. F. 1996. Single-domain/bound calcium hypothesis of transmitter release and facilitation. *Journal of Neurophysiology,* 75**,** 1919-1931.

BEST, A. R. & REGEHR, W. G. 2008. Serotonin evokes endocannabinoid release and retrogradely suppresses excitatory synapses. *J Neurosci,* 28**,** 6508-15.

BEST, A. R. & REGEHR, W. G. 2009. Inhibitory regulation of electrically coupled neurons in the inferior olive is mediated by asynchronous release of GABA. *Neuron,* 62**,** 555-65.

BLATOW, M., CAPUTI, A., BURNASHEV, N., MONYER, H. & ROZOV, A. 2003. Ca2+ buffer saturation underlies paired pulse facilitation in calbindin-D28k-containing terminals. *Neuron,* 38**,** 79-88.

BORST, J. G. 2010. The low synaptic release probability in vivo. *Trends Neurosci,* 33**,** 259-66.

BORST, J. G., HELMCHEN, F. & SAKMANN, B. 1995. Pre- and postsynaptic whole-cell recordings in the medial nucleus of the trapezoid body of the rat. *J Physiol,* 489 (Pt 3)**,** 825-40.

BORST, J. G. & SAKMANN, B. 1996. Calcium influx and transmitter release in a fast CNS synapse. *Nature,* 383**,** 431-4.

BORST, J. G. & SAKMANN, B. 1998. Facilitation of presynaptic calcium currents in the rat brainstem. *J Physiol,* 513 (Pt 1)**,** 149-55.

BOUHOURS, B., GJONI, E., KOCHUBEY, O. & SCHNEGGENBURGER, R. 2017. Synaptotagmin2 (Syt2) Drives Fast Release Redundantly with Syt1 at the Output Synapses of Parvalbumin-Expressing Inhibitory Neurons. *J Neurosci,* 37**,** 4604-4617.

BRANDT, D. S., COFFMAN, M. D., FALKE, J. J. & KNIGHT, J. D. 2012. Hydrophobic contributions to the membrane docking of Synaptotagmin 7 C2A domain: mechanistic contrast between isoforms 1 and 7. *Biochemistry,* 51**,** 7654-64.

BRENOWITZ, S., DAVID, J. & TRUSSELL, L. 1998. Enhancement of synaptic efficacy by presynaptic GABA(B) receptors. *Neuron,* 20**,** 135-41.

BRENOWITZ, S. D. & REGEHR, W. G. 2003. Calcium dependence of retrograde inhibition by endocannabinoids at synapses onto Purkinje cells. *J Neurosci,* 23**,** 6373-84.

BRENOWITZ, S. D. & REGEHR, W. G. 2007. Reliability and heterogeneity of calcium signaling at single presynaptic boutons of cerebellar granule cells. *J Neurosci,* 27**,** 7888-98.

BRENOWITZ, S. D. & REGEHR, W. G. 2014. Presynaptic calcium measurements using bulk loading of acetoxymethyl indicators. *Cold Spring Harb Protoc,* 2014**,** pdb prot081828.

CALAKOS, N., SCHOCH, S., SUDHOF, T. C. & MALENKA, R. C. 2004. Multiple roles for the active zone protein RIM1alpha in late stages of neurotransmitter release. *Neuron,* 42**,** 889-96.

CARTER, A. G. & REGEHR, W. G. 2000. Prolonged synaptic currents and glutamate spillover at the parallel fiber to stellate cell synapse. *J Neurosci,* 20**,** 4423-34.

CELIO, M. R. 1990. Calbindin D-28k and parvalbumin in the rat nervous system. *Neuroscience,* 35**,** 375-475.

CHAKRABARTI, S., KOBAYASHI, K. S., FLAVELL, R. A., MARKS, C. B., MIYAKE, K., LISTON, D. R., FOWLER, K. T., GORELICK, F. S. & ANDREWS, N. W. 2003. Impaired membrane resealing and autoimmune myositis in Synaptotagmin VII-deficient mice. *J Cell Biol,* 162**,** 543-9.

CHANDA, S. & XU-FRIEDMAN, M. A. 2010. A low-affinity antagonist reveals saturation and desensitization in mature synapses in the auditory brain stem. *J Neurophysiol,* 103**,** 1915-26.

CHEN, C., ARAI, I., SATTERFIELD, R., YOUNG, S. M., JR. & JONAS, P. 2017a. Synaptotagmin 2 Is the Fast Ca2+ Sensor at a Central Inhibitory Synapse. *Cell Rep,* 18**,** 723-736.

CHEN, C., ARAI, I., SATTERFIELD, R., YOUNG, S. M., JR. & JONAS, P. 2017b. Synaptotagmin 2 Is the Fast Ca(2+) Sensor at a Central Inhibitory Synapse. *Cell Rep,* 18**,** 723-736.

CHEN, C., BLITZ, D. M. & REGEHR, W. G. 2002. Contributions of receptor desensitization and saturation to plasticity at the retinogeniculate synapse. *Neuron,* 33**,** 779-88.

CHEN, C. & REGEHR, W. G. 1997. The mechanism of cAMP-mediated enhancement at a cerebellar synapse. *J Neurosci,* 17**,** 8687-94.

CHEN, C., SATTERFIELD, R., YOUNG, S. M., JR. & JONAS, P. 2017c. Triple Function of Synaptotagmin 7 Ensures Efficiency of High-Frequency Transmission at Central GABAergic Synapses. *Cell Rep,* 21**,** 2082-2089.

CHEN, C. H., FREMONT, R., ARTEAGA-BRACHO, E. E. & KHODAKHAH, K. 2014. Short latency cerebellar modulation of the basal ganglia. *Nat Neurosci,* 17**,** 1767-75.

CHEN, S., AUGUSTINE, G. J. & CHADDERTON, P. 2016. The cerebellum linearly encodes whisker position during voluntary movement. *Elife,* 5.

CHICKA, M. C., HUI, E., LIU, H. & CHAPMAN, E. R. 2008. Synaptotagmin arrests the SNARE complex before triggering fast, efficient membrane fusion in response to Ca2+. *Nat Struct Mol Biol,* 15**,** 827-35.

COOK, D. L., SCHWINDT, P. C., GRANDE, L. A. & SPAIN, W. J. 2003. Synaptic depression in the localization of sound. *Nature,* 421**,** 66-70.

CUTTLE, M. F., TSUJIMOTO, T., FORSYTHE, I. D. & TAKAHASHI, T. 1998. Facilitation of the presynaptic calcium current at an auditory synapse in rat brainstem. *J Physiol,* 512 (Pt 3)**,** 723-9.

DAW, M. I., TRICOIRE, L., ERDELYI, F., SZABO, G. & MCBAIN, C. J. 2009. Asynchronous transmitter release from cholecystokinin-containing inhibitory interneurons is widespread and target-cell independent. *J Neurosci,* 29**,** 11112-22.

DE SOLAGES, C., SZAPIRO, G., BRUNEL, N., HAKIM, V., ISOPE, P., BUISSERET, P., ROUSSEAU, C., BARBOUR, B. & LENA, C. 2008. High-frequency organization and synchrony of activity in the purkinje cell layer of the cerebellum. *Neuron,* 58**,** 775-88.

DE ZEEUW, C. I., WYLIE, D. R., STAHL, J. S. & SIMPSON, J. I. 1995. Phase relations of Purkinje cells in the rabbit flocculus during compensatory eye movements. *J Neurophysiol,* 74**,** 2051-64.

DEL CASTILLO, J. & KATZ, B. 1954. Statistical factors involved in neuromuscular facilitation and depression. *J Physiol,* 124**,** 574-85.

DELVENDAHL, I., JABLONSKI, L., BAADE, C., MATVEEV, V., NEHER, E. & HALLERMANN, S. 2015. Reduced endogenous Ca2+ buffering speeds active zone Ca2+ signaling. *Proc Natl Acad Sci U S A,* 112**,** E3075-84.

DESCHEENES, M. & HU, B. 1990. Electrophysiology and Pharmacology of the Corticothalamic Input to Lateral Thalamic Nuclei: an Intracellular Study in the Cat. *Eur J Neurosci,* 2**,** 140-152.

DIAMOND, J. S. & JAHR, C. E. 1995. Asynchronous release of synaptic vesicles determines the time course of the AMPA receptor-mediated EPSC. *Neuron,* 15**,** 1097-107.

DIANTONIO, A. & SCHWARZ, T. L. 1994. The effect on synaptic physiology of Synaptotagmin mutations in Drosophila. *Neuron,* 12**,** 909-20.

DINGLEDINE, R. & SOMJEN, G. 1981. Calcium dependence of synaptic transmission in the hippocampal slice. *Brain Research,* 207**,** 218-222.

DITTMAN, J. S., KREITZER, A. C. & REGEHR, W. G. 2000. Interplay between facilitation, depression, and residual calcium at three presynaptic terminals. *J Neurosci,* 20**,** 1374-85.

DITTMAN, J. S. & REGEHR, W. G. 1997. Mechanism and kinetics of heterosynaptic depression at a cerebellar synapse. *J Neurosci,* 17**,** 9048-59.

DITTMAN, J. S. & REGEHR, W. G. 1998. Calcium dependence and recovery kinetics of presynaptic depression at the climbing fiber to Purkinje cell synapse. *J Neurosci,* 18**,** 6147-62.

DOBRUNZ, L. E. & STEVENS, C. F. 1997. Heterogeneity of release probability, facilitation, and depletion at central synapses. *Neuron,* 18**,** 995-1008.

DODGE, F. A., JR., MILEDI, R. & RAHAMIMOFF, R. 1969. Strontium and quantal release of transmitter at the neuromuscular junction. *J Physiol,* 200**,** 267-83.

DULUBOVA, I., KHVOTCHEV, M., LIU, S., HURYEVA, I., SUDHOF, T. C. & RIZO, J. 2007. Munc18-1 binds directly to the neuronal SNARE complex. *Proc Natl Acad Sci U S A,* 104**,** 2697-702.

DULUBOVA, I., SUGITA, S., HILL, S., HOSAKA, M., FERNANDEZ, I., SUDHOF, T. C. & RIZO, J. 1999. A conformational switch in syntaxin during exocytosis: role of munc18. *EMBO J,* 18**,** 4372-82.

DUM, R. P. & STRICK, P. L. 2003. An unfolded map of the cerebellar dentate nucleus and its projections to the cerebral cortex. *J Neurophysiol,* 89**,** 634-9.

EGGERMANN, E., BUCURENCIU, I., GOSWAMI, S. P. & JONAS, P. 2011. Nanodomain coupling between Ca(2)(+) channels and sensors of exocytosis at fast mammalian synapses. *Nat Rev Neurosci,* 13**,** 7-21.

FELMY, F., NEHER, E. & SCHNEGGENBURGER, R. 2003. Probing the intracellular calcium sensitivity of transmitter release during synaptic facilitation. *Neuron,* 37**,** 801-11.

FENG, T. P. 1940. Studies on the neuromuscular junction. XVIII. The local potentials around n-m junctions induced by single and multiple volleys. *Chinese Journal of Physiology,* 15**,** 367-404.

FLANNERY, A. R., CZIBENER, C. & ANDREWS, N. W. 2010. Palmitoylation-dependent association with CD63 targets the Ca2+ sensor Synaptotagmin VII to lysosomes. *J Cell Biol,* 191**,** 599-613.

FORSYTHE, I. D., TSUJIMOTO, T., BARNES-DAVIES, M., CUTTLE, M. F. & TAKAHASHI, T. 1998. Inactivation of presynaptic calcium current contributes to synaptic depression at a fast central synapse. *Neuron,* 20**,** 797-807.

FOSTER, K. A., KREITZER, A. C. & REGEHR, W. G. 2002. Interaction of postsynaptic receptor saturation with presynaptic mechanisms produces a reliable synapse. *Neuron,* 36**,** 1115-26.

FOSTER, K. A. & REGEHR, W. G. 2004. Variance-mean analysis in the presence of a rapid antagonist indicates vesicle depletion underlies depression at the climbing fiber synapse. *Neuron,* 43**,** 119-31.

FREDETTE, B. J., ADAMS, J. C. & MUGNAINI, E. 1992. GABAergic neurons in the mammalian inferior olive and ventral medulla detected by glutamate decarboxylase immunocytochemistry. *J Comp Neurol,* 321**,** 501-14.

FREDETTE, B. J. & MUGNAINI, E. 1991. The GABAergic cerebello-olivary projection in the rat. *Anat Embryol (Berl),* 184**,** 225-43.

FU, Y. H. & WATSON, C. 2012. The arcuate nucleus of the C57BL/6J mouse hindbrain is a displaced part of the inferior olive. *Brain Behav Evol,* 79**,** 191-204.

FUKUDA, M., KANNO, E., SATOH, M., SAEGUSA, C. & YAMAMOTO, A. 2004. Synaptotagmin VII is targeted to dense-core vesicles and regulates their Ca2+ -dependent exocytosis in PC12 cells. *J Biol Chem,* 279**,** 52677-84.

FUKUDA, M., OGATA, Y., SAEGUSA, C., KANNO, E. & MIKOSHIBA, K. 2002. Alternative splicing isoforms of Synaptotagmin VII in the mouse, rat and human. *Biochem J,* 365**,** 173-80.

GALARRETA, M. & HESTRIN, S. 1998. Frequency-dependent synaptic depression and the balance of excitation and inhibition in the neocortex. *Nat Neurosci,* 1**,** 587-94.

GAUCK, V. & JAEGER, D. 2000. The control of rate and timing of spikes in the deep cerebellar nuclei by inhibition. *J Neurosci,* 20**,** 3006-16.

GEIGER, J. R. & JONAS, P. 2000. Dynamic control of presynaptic Ca(2+) inflow by fast-inactivating K(+) channels in hippocampal mossy fiber boutons. *Neuron,* 28**,** 927-39.

GEPPERT, M., GODA, Y., HAMMER, R. E., LI, C., ROSAHL, T. W., STEVENS, C. F. & SUDHOF, T. C. 1994. Synaptotagmin I: a major Ca2+ sensor for transmitter release at a central synapse. *Cell,* 79**,** 717-27.

GODA, Y. & STEVENS, C. F. 1994. Two components of transmitter release at a central synapse. *Proc Natl Acad Sci U S A,* 91**,** 12942-6.

GROFFEN, A. J., MARTENS, S., DIEZ ARAZOLA, R., CORNELISSE, L. N., LOZOVAYA, N., DE JONG, A. P., GORIOUNOVA, N. A., HABETS, R. L., TAKAI, Y., BORST, J. G., BROSE, N., MCMAHON, H. T. & VERHAGE, M. 2010. Doc2b is a high-affinity Ca2+ sensor for spontaneous neurotransmitter release. *Science,* 327**,** 1614-8.

GRYNKIEWICZ, G., POENIE, M. & TSIEN, R. Y. 1985. A new generation of Ca2+ indicators with greatly improved fluorescence properties. *J Biol Chem,* 260**,** 3440-50.

GUO, C., WITTER, L., RUDOLPH, S., ELLIOTT, H. L., ENNIS, K. A. & REGEHR, W. G. 2016. Purkinje Cells Directly Inhibit Granule Cells in Specialized Regions of the Cerebellar Cortex. *Neuron,* 91**,** 1330-1341.

GUSTAVSSON, N., LAO, Y., MAXIMOV, A., CHUANG, J. C., KOSTROMINA, E., REPA, J. J., LI, C., RADDA, G. K., SUDHOF, T. C. & HAN, W. 2008. Impaired insulin secretion and glucose intolerance in Synaptotagmin-7 null mutant mice. *Proc Natl Acad Sci U S A,* 105**,** 3992-7.

GUSTAVSSON, N., WEI, S. H., HOANG, D. N., LAO, Y., ZHANG, Q., RADDA, G. K., RORSMAN, P., SUDHOF, T. C. & HAN, W. 2009. Synaptotagmin-7 is a principal Ca2+ sensor for Ca2+ -induced glucagon exocytosis in pancreas. *J Physiol,* 587**,** 1169-78.

HALLERMANN, S., PAWLU, C., JONAS, P. & HECKMANN, M. 2003. A large pool of releasable vesicles in a cortical glutamatergic synapse. *Proc Natl Acad Sci U S A,* 100**,** 8975-80.

HAN, V. Z., MAGNUS, G., ZHANG, Y., WEI, A. D. & TURNER, E. E. 2014. Bidirectional modulation of deep cerebellar nuclear cells revealed by optogenetic manipulation of inhibitory inputs from Purkinje cells. *Neuroscience,* 277**,** 250-66.

HECK, D. H., DE ZEEUW, C. I., JAEGER, D., KHODAKHAH, K. & PERSON, A. L. 2013. The neuronal code(s) of the cerebellum. *J Neurosci,* 33**,** 17603-9.

HEFFT, S. & JONAS, P. 2005. Asynchronous GABA release generates long-lasting inhibition at a hippocampal interneuron-principal neuron synapse. *Nat Neurosci,* 8**,** 1319-28.

HEINEY, S. A., WOHL, M. P., CHETTIH, S. N., RUFFOLO, L. I. & MEDINA, J. F. 2014. Cerebellar-dependent expression of motor learning during eyeblink conditioning in head-fixed mice. *J Neurosci,* 34**,** 14845-53.

HESSLOW, G. & IVARSSON, M. 1994. Suppression of cerebellar Purkinje cells during conditioned responses in ferrets. *Neuroreport,* 5**,** 649-52.

HUA, Y. & SCHELLER, R. H. 2001. Three SNARE complexes cooperate to mediate membrane fusion. *Proc Natl Acad Sci U S A,* 98**,** 8065-70.

HUI, E., BAI, J., WANG, P., SUGIMORI, M., LLINAS, R. R. & CHAPMAN, E. R. 2005. Three distinct kinetic groupings of the Synaptotagmin family: candidate sensors for rapid and delayed exocytosis. *Proc Natl Acad Sci U S A,* 102**,** 5210-4.

HUI, E., JOHNSON, C. P., YAO, J., DUNNING, F. M. & CHAPMAN, E. R. 2009. Synaptotagmin-mediated bending of the target membrane is a critical step in Ca(2+)-regulated fusion. *Cell,* 138**,** 709-21.

IREMONGER, K. J. & BAINS, J. S. 2007. Integration of asynchronously released quanta prolongs the postsynaptic spike window. *J Neurosci,* 27**,** 6684-91.

JACKMAN, S. L., BENEDUCE, B. M., DREW, I. R. & REGEHR, W. G. 2014. Achieving high-frequency optical control of synaptic transmission. *J Neurosci,* 34**,** 7704-14.

JACKMAN, S. L. & REGEHR, W. G. 2017. The Mechanisms and Functions of Synaptic Facilitation. *Neuron,* 94**,** 447-464.

JACKMAN, S. L., TURECEK, J., BELINSKY, J. E. & REGEHR, W. G. 2016. The calcium sensor Synaptotagmin 7 is required for synaptic facilitation. *Nature,* 529**,** 88-91.

JAHN, R. & FASSHAUER, D. 2012. Molecular machines governing exocytosis of synaptic vesicles. *Nature,* 490**,** 201-7.

JAISWAL, J. K., CHAKRABARTI, S., ANDREWS, N. W. & SIMON, S. M. 2004. Synaptotagmin VII restricts fusion pore expansion during lysosomal exocytosis. *PLoS Biol,* 2**,** E233.

JIRENHED, D. A., BENGTSSON, F. & HESSLOW, G. 2007. Acquisition, extinction, and reacquisition of a cerebellar cortical memory trace. *J Neurosci,* 27**,** 2493-502.

JONES, M. V., JONAS, P., SAHARA, Y. & WESTBROOK, G. L. 2001. Microscopic kinetics and energetics distinguish GABA(A) receptor agonists from antagonists. *Biophys J,* 81**,** 2660-70.

KAESER-WOO, Y. J., YANG, X. & SUDHOF, T. C. 2012. C-terminal complexin sequence is selectively required for clamping and priming but not for Ca2+ triggering of synaptic exocytosis. *J Neurosci,* 32**,** 2877-85.

KAESER, P. S. & REGEHR, W. G. 2014a. Molecular mechanisms for synchronous, asynchronous, and spontaneous neurotransmitter release. *Annual Review of Physiology,* 76**,** 333-63.

KAESER, P. S. & REGEHR, W. G. 2014b. Molecular mechanisms for synchronous, asynchronous, and spontaneous neurotransmitter release. *Annu Rev Physiol,* 76**,** 333-63.

KAMIYA, H., SHINOZAKI, H. & YAMAMOTO, C. 1996. Activation of metabotropic glutamate receptor type 2/3 suppresses transmission at rat hippocampal mossy fibre synapses. *J Physiol,* 493 (Pt 2)**,** 447-55.

KAMIYA, H. & ZUCKER, R. S. 1994. Residual Ca2+ and short-term synaptic plasticity. *Nature,* 371**,** 603-6.

KATZ, B. & MILEDI, R. 1965. The Measurement of Synaptic Delay, and the Time Course of Acetylcholine Release at the Neuromuscular Junction. *Proc R Soc Lond B Biol Sci,* 161**,** 483-95.

KAWAGUCHI, S. Y. & SAKABA, T. 2015. Control of inhibitory synaptic outputs by low excitability of axon terminals revealed by direct recording. *Neuron,* 85**,** 1273-88.

KIM, J. H., LEE, S. R., LI, L. H., PARK, H. J., PARK, J. H., LEE, K. Y., KIM, M. K., SHIN, B. A. & CHOI, S. Y. 2011. High cleavage efficiency of a 2A peptide derived from porcine teschovirus-1 in human cell lines, zebrafish and mice. *PLoS One,* 6**,** e18556.

KLYACHKO, V. A. & STEVENS, C. F. 2006. Excitatory and feed-forward inhibitory hippocampal synapses work synergistically as an adaptive filter of natural spike trains. *PLoS Biol,* 4**,** e207.

KOCHUBEY, O., BABAI, N. & SCHNEGGENBURGER, R. 2016. A Synaptotagmin Isoform Switch during the Development of an Identified CNS Synapse. *Neuron,* 90**,** 984-99.

KOCHUBEY, O. & SCHNEGGENBURGER, R. 2011. Synaptotagmin increases the dynamic range of synapses by driving Ca(2)+-evoked release and by clamping a near-linear remaining Ca(2)+ sensor. *Neuron,* 69**,** 736-48.

KREITZER, A. C., GEE, K. R., ARCHER, E. A. & REGEHR, W. G. 2000. Monitoring presynaptic calcium dynamics in projection fibers by in vivo loading of a novel calcium indicator. *Neuron,* 27**,** 25-32.

KREITZER, A. C. & REGEHR, W. G. 2000. Modulation of transmission during trains at a cerebellar synapse. *J Neurosci,* 20**,** 1348-57.

KUENZEL, T., BORST, J. G. & VAN DER HEIJDEN, M. 2011a. Factors controlling the input-output relationship of spherical bushy cells in the gerbil cochlear nucleus. *J Neurosci,* 31**,** 4260-73.

KUENZEL, W. J., MEDINA, L., CSILLAG, A., PERKEL, D. J. & REINER, A. 2011b. The avian subpallium: new insights into structural and functional subdivisions occupying the lateral subpallial wall and their embryological origins. *Brain Res,* 1424**,** 67-101.

LABRAKAKIS, C., LORENZO, L. E., BORIES, C., RIBEIRO-DA-SILVA, A. & DE KONINCK, Y. 2009. Inhibitory coupling between inhibitory interneurons in the spinal cord dorsal horn. *Mol Pain,* 5**,** 24.

LANG, E. J., SUGIHARA, I. & LLINAS, R. 1996. GABAergic modulation of complex spike activity by the cerebellar nucleoolivary pathway in rat. *J Neurophysiol,* 76**,** 255-75.

LEE, H. K., YANG, Y., SU, Z., HYEON, C., LEE, T. S., LEE, H. W., KWEON, D. H., SHIN, Y. K. & YOON, T. Y. 2010. Dynamic Ca2+-dependent stimulation of vesicle fusion by membrane-anchored Synaptotagmin 1. *Science,* 328**,** 760-3.

LEFLER, Y., YAROM, Y. & UUSISAARI, M. Y. 2014. Cerebellar inhibitory input to the inferior olive decreases electrical coupling and blocks subthreshold oscillations. *Neuron,* 81**,** 1389-1400.

LEIN, E. S., HAWRYLYCZ, M. J., AO, N., AYRES, M., BENSINGER, A., BERNARD, A., BOE, A. F., BOGUSKI, M. S., BROCKWAY, K. S., BYRNES, E. J., CHEN, L., CHEN, T. M., CHIN, M. C., CHONG, J., CROOK, B. E., CZAPLINSKA, A., DANG, C. N., DATTA, S., DEE, N. R., DESAKI, A. L., DESTA, T., DIEP, E., DOLBEARE, T. A., DONELAN, M. J., DONG, H. W., DOUGHERTY, J. G., DUNCAN, B. J., EBBERT, A. J., EICHELE, G., ESTIN, L. K., FABER, C., FACER, B. A., FIELDS, R., FISCHER, S. R., FLISS, T. P., FRENSLEY, C., GATES, S. N., GLATTFELDER, K. J., HALVERSON, K. R., HART, M. R., HOHMANN, J. G., HOWELL, M. P., JEUNG, D. P., JOHNSON, R. A., KARR, P. T., KAWAL, R., KIDNEY, J. M., KNAPIK, R. H., KUAN, C. L., LAKE, J. H., LARAMEE, A. R., LARSEN, K. D., LAU, C., LEMON, T. A., LIANG, A. J., LIU, Y., LUONG, L. T., MICHAELS, J., MORGAN, J. J., MORGAN, R. J., MORTRUD, M. T., MOSQUEDA, N. F., NG, L. L., NG, R., ORTA, G. J., OVERLY, C. C., PAK, T. H., PARRY, S. E., PATHAK, S. D., PEARSON, O. C., PUCHALSKI, R. B., RILEY, Z. L., ROCKETT, H. R., ROWLAND, S. A., ROYALL, J. J., RUIZ, M. J., SARNO, N. R., SCHAFFNIT, K., SHAPOVALOVA, N. V., SIVISAY, T., SLAUGHTERBECK, C. R., SMITH, S. C., SMITH, K. A., SMITH, B. I., SODT, A.

J., STEWART, N. N., STUMPF, K. R., SUNKIN, S. M., SUTRAM, M., TAM, A., TEEMER, C. D., THALLER, C., THOMPSON, C. L., VARNAM, L. R., VISEL, A., WHITLOCK, R. M., WOHNOUTKA, P. E., WOLKEY, C. K., WONG, V. Y., WOOD, M., et al. 2007. Genome-wide atlas of gene expression in the adult mouse brain. *Nature,* 445**,** 168-76.

LI, C., ULLRICH, B., ZHANG, J. Z., ANDERSON, R. G., BROSE, N. & SUDHOF, T. C. 1995. Ca(2+)-dependent and -independent activities of neural and non-neural Synaptotagmins. *Nature,* 375**,** 594-9.

LI, F., PINCET, F., PEREZ, E., ENG, W. S., MELIA, T. J., ROTHMAN, J. E. & TARESTE, D. 2007. Energetics and dynamics of SNAREpin folding across lipid bilayers. *Nat Struct Mol Biol,* 14**,** 890-6.

LIPSTEIN, N., SAKABA, T., COOPER, B. H., LIN, K. H., STRENZKE, N., ASHERY, U., RHEE, J. S., TASCHENBERGER, H., NEHER, E. & BROSE, N. 2013. Dynamic control of synaptic vesicle replenishment and short-term plasticity by Ca(2+)-calmodulin-Munc13-1 signaling. *Neuron,* 79**,** 82-96.

LITTLETON, J. T., STERN, M., SCHULZE, K., PERIN, M. & BELLEN, H. J. 1993. Mutational analysis of Drosophila Synaptotagmin demonstrates its essential role in Ca(2+)-activated neurotransmitter release. *Cell,* 74**,** 1125-34.

LIU, H., BAI, H., HUI, E., YANG, L., EVANS, C. S., WANG, Z., KWON, S. E. & CHAPMAN, E. R. 2014. Synaptotagmin 7 functions as a Ca2+-sensor for synaptic vesicle replenishment. *Elife,* 3**,** e01524.

LLINAS, R., SUGIMORI, M. & SILVER, R. B. 1992. Microdomains of high calcium concentration in a presynaptic terminal. *Science,* 256**,** 677-9.

LLINAS, R. & YAROM, Y. 1981a. Electrophysiology of mammalian inferior olivary neurones in vitro. Different types of voltage-dependent ionic conductances. *J Physiol,* 315**,** 549-67.

LLINAS, R. & YAROM, Y. 1981b. Properties and distribution of ionic conductances generating electroresponsiveness of mammalian inferior olivary neurones in vitro. *J Physiol,* 315**,** 569-84.

LLINAS, R. & YAROM, Y. 1986. Oscillatory properties of guinea-pig inferior olivary neurones and their pharmacological modulation: an in vitro study. *J Physiol,* 376**,** 163-82.

LOMO, T. 1971. Potentiation of monosynaptic EPSPs in the perforant path-dentate granule cell synapse. *Exp Brain Res,* 12**,** 46-63.

LORTEIJE, J. A., RUSU, S. I., KUSHMERICK, C. & BORST, J. G. 2009. Reliability and precision of the mouse calyx of Held synapse. *J Neurosci,* 29**,** 13770-84.

LU, H. W. & TRUSSELL, L. O. 2016. Spontaneous Activity Defines Effective Convergence Ratios in an Inhibitory Circuit. *J Neurosci,* 36**,** 3268-80.

LU, T. & TRUSSELL, L. O. 2000. Inhibitory transmission mediated by asynchronous transmitter release. *Neuron,* 26**,** 683-94.

LUO, F., BACAJ, T. & SUDHOF, T. C. 2015. Synaptotagmin-7 Is Essential for Ca2+-Triggered Delayed Asynchronous Release But Not for Ca2+-Dependent Vesicle Priming in Retinal Ribbon Synapses. *J Neurosci,* 35**,** 11024-33.

LUO, F. & SUDHOF, T. C. 2017. Synaptotagmin-7-Mediated Asynchronous Release Boosts High-Fidelity Synchronous Transmission at a Central Synapse. *Neuron,* 94**,** 826-839 e3.

MACLEOD, K. M., HORIUCHI, T. K. & CARR, C. E. 2007. A role for short-term synaptic facilitation and depression in the processing of intensity information in the auditory brain stem. *J Neurophysiol,* 97**,** 2863-74.

MANABE, T. & NICOLL, R. A. 1994. Long-term potentiation: evidence against an increase in transmitter release probability in the CA1 region of the hippocampus. *Science,* 265**,** 1888-92.

MANSEAU, F., MARINELLI, S., MENDEZ, P., SCHWALLER, B., PRINCE, D. A., HUGUENARD, J. R. & BACCI, A. 2010. Desynchronization of neocortical networks by asynchronous release of GABA at autaptic and synaptic contacts from fast-spiking interneurons. *PLoS Biol,* 8.

MARAVALL, M., MAINEN, Z. F., SABATINI, B. L. & SVOBODA, K. 2000. Estimating intracellular calcium concentrations and buffering without wavelength ratioing. *Biophys J,* 78**,** 2655-67.

MARTENS, S., KOZLOV, M. M. & MCMAHON, H. T. 2007. How Synaptotagmin promotes membrane fusion. *Science,* 316**,** 1205-8.

MARTINEZ, I., CHAKRABARTI, S., HELLEVIK, T., MOREHEAD, J., FOWLER, K. & ANDREWS, N. W. 2000. Synaptotagmin VII regulates Ca(2+)-dependent exocytosis of lysosomes in fibroblasts. *J Cell Biol,* 148**,** 1141-49.

MATVEEV, V., ZUCKER, R. S. & SHERMAN, A. 2004. Facilitation through buffer saturation: Constraints on endogenous buffering properties. *Biophysical Journal,* 86**,** 2691-2709.

MAXIMOV, A., LAO, Y., LI, H., CHEN, X., RIZO, J., SORENSEN, J. B. & SUDHOF, T. C. 2008. Genetic analysis of Synaptotagmin-7 function in synaptic vesicle exocytosis. *Proc Natl Acad Sci U S A,* 105**,** 3986-91.

MCDEVITT, C. J., EBNER, T. J. & BLOEDEL, J. R. 1987. Relationships between simultaneously recorded Purkinje cells and nuclear neurons. *Brain Res,* 425**,** 1-13.

MCELVAIN, L. E., BAGNALL, M. W., SAKATOS, A. & DU LAC, S. 2010. Bidirectional plasticity gated by hyperpolarization controls the gain of postsynaptic firing responses at central vestibular nerve synapses. *Neuron,* 68**,** 763-75.

MCELVAIN, L. E., FAULSTICH, M., JEANNE, J. M., MOORE, J. D. & DU LAC, S. 2015. Implementation of linear sensory signaling via multiple coordinated mechanisms at central vestibular nerve synapses. *Neuron,* 85**,** 1132-44.

MEDINA, J. F. & LISBERGER, S. G. 2009. Encoding and decoding of learned smooth-pursuit eye movements in the floccular complex of the monkey cerebellum. *J Neurophysiol,* 102**,** 2039-54.

MEINRENKEN, C. J., BORST, J. G. & SAKMANN, B. 2002. Calcium secretion coupling at calyx of Held governed by nonuniform channel-vesicle topography. *J Neurosci,* 22**,** 1648-67.

MENNERICK, S. & MATTHEWS, G. 1996. Ultrafast exocytosis elicited by calcium current in synaptic terminals of retinal bipolar neurons. *Neuron,* 17**,** 1241-9.

MERCER, A. A., PALARZ, K. J., TABATADZE, N., WOOLLEY, C. S. & RAMAN, I. M. 2016. Sex differences in cerebellar synaptic transmission and sex-specific responses to autism-linked Gabrb3 mutations in mice. *Elife,* 5.

MINTZ, I. M., SABATINI, B. L. & REGEHR, W. G. 1995. Calcium control of transmitter release at a cerebellar synapse. *Neuron,* 15**,** 675-88.

MITTELSTEADT, T., SEIFERT, G., ALVAREZ-BARON, E., STEINHAUSER, C., BECKER, A. J. & SCHOCH, S. 2009. Differential mRNA expression patterns of the Synaptotagmin gene family in the rodent brain. *J Comp Neurol,* 512**,** 514-28.

MOCHIDA, S., FEW, A. P., SCHEUER, T. & CATTERALL, W. A. 2008. Regulation of presynaptic Ca(V)2.1 channels by Ca2+ sensor proteins mediates short-term synaptic plasticity. *Neuron,* 57**,** 210-6.

MOLGO, J. & VAN DER KLOOT, W. 1991. Quantal release and facilitation at frog neuromuscular junctions at about 0 degrees C. *J Neurophysiol,* 65**,** 834-40.

MONGILLO, G., BARAK, O. & TSODYKS, M. 2008. Synaptic theory of working memory. *Science,* 319**,** 1543-6.

MULLER, M., FELMY, F. & SCHNEGGENBURGER, R. 2008. A limited contribution of Ca2+ current facilitation to paired-pulse facilitation of transmitter release at the rat calyx of Held. *J Physiol,* 586**,** 5503-20.

MULLER, M., GOUTMAN, J. D., KOCHUBEY, O. & SCHNEGGENBURGER, R. 2010. Interaction between facilitation and depression at a large CNS synapse reveals mechanisms of short-term plasticity. *J Neurosci,* 30**,** 2007-16.

NAJAC, M. & RAMAN, I. M. 2015. Integration of Purkinje cell inhibition by cerebellar nucleo-olivary neurons. *J Neurosci,* 35**,** 544-9.

NEHER, E. 2015. Merits and Limitations of Vesicle Pool Models in View of Heterogeneous Populations of Synaptic Vesicles. *Neuron,* 87**,** 1131-42.

NEHER, E. & SAKABA, T. 2001. Combining deconvolution and noise analysis for the estimation of transmitter release rates at the calyx of held. *J Neurosci,* 21**,** 444-61.

NEHER, E. & SAKABA, T. 2008. Multiple roles of calcium ions in the regulation of neurotransmitter release. *Neuron,* 59**,** 861-72.

OHMAE, S. & MEDINA, J. F. 2015. Climbing fibers encode a temporal-difference prediction error during cerebellar learning in mice. *Nat Neurosci,* 18**,** 1798-803.

OSBORNE, S. L., WALLIS, T. P., JIMENEZ, J. L., GORMAN, J. J. & MEUNIER, F. A. 2007. Identification of secretory granule phosphatidylinositol 4,5-bisphosphate-interacting proteins using an affinity pulldown strategy. *Mol Cell Proteomics,* 6**,** 1158-69.

OUARDOUZ, M. & SASTRY, B. R. 2000. Mechanisms underlying LTP of inhibitory synaptic transmission in the deep cerebellar nuclei. *J Neurophysiol,* 84**,** 1414-21.

PANG, Z. P., BACAJ, T., YANG, X., ZHOU, P., XU, W. & SUDHOF, T. C. 2011. Doc2 supports spontaneous synaptic transmission by a Ca(2+)-independent mechanism. *Neuron,* 70**,** 244-51.

PAXINOS, G. & FRANKLIN, K. B. J. 2001. *The mouse brain in stereotaxic coordinates,* San Diego, Calif. London, Academic.

PEDROARENA, C. M. & SCHWARZ, C. 2003. Efficacy and short-term plasticity at GABAergic synapses between Purkinje and cerebellar nuclei neurons. *J Neurophysiol,* 89**,** 704-15.

PERSON, A. L. & RAMAN, I. M. 2012a. Purkinje neuron synchrony elicits time-locked spiking in the cerebellar nuclei. *Nature,* 481**,** 502-5.

PERSON, A. L. & RAMAN, I. M. 2012b. Synchrony and neural coding in cerebellar circuits. *Front Neural Circuits,* 6**,** 97.

PETERS, J. H., MCDOUGALL, S. J., FAWLEY, J. A., SMITH, S. M. & ANDRESEN, M. C. 2010. Primary afferent activation of thermosensitive TRPV1 triggers asynchronous glutamate release at central neurons. *Neuron,* 65**,** 657-69.

PIJPERS, A., VOOGD, J. & RUIGROK, T. J. 2005. Topography of olivo-cortico-nuclear modules in the intermediate cerebellum of the rat. *J Comp Neurol,* 492**,** 193-213.

PUGH, J. R. & RAMAN, I. M. 2005. GABAA receptor kinetics in the cerebellar nuclei: evidence for detection of transmitter from distant release sites. *Biophys J,* 88**,** 1740-54.

PUGH, J. R. & RAMAN, I. M. 2006. Potentiation of mossy fiber EPSCs in the cerebellar nuclei by NMDA receptor activation followed by postinhibitory rebound current. *Neuron,* 51**,** 113-23.

QUINN, G. P. & KEOUGH, M. J. 2002. *Experimental design and data analysis for biologists,* Cambridge, UK ; New York, Cambridge University Press.

RAGOZZINO, D., WOODWARD, R. M., MURATA, Y., EUSEBI, F., OVERMAN, L. E. & MILEDI, R. 1996. Design and in vitro pharmacology of a selective gamma-aminobutyric acidC receptor antagonist. *Mol Pharmacol,* 50**,** 1024-30.

RAHAMIMOFF, R. & YAARI, Y. 1973. Delayed release of transmitter at the frog neuromuscular junction. *J Physiol,* 228**,** 241-57.

RANCZ, E. A., ISHIKAWA, T., DUGUID, I., CHADDERTON, P., MAHON, S. & HAUSSER, M. 2007. High-fidelity transmission of sensory information by single cerebellar mossy fibre boutons. *Nature,* 450**,** 1245-8.

RAO, S. K., HUYNH, C., PROUX-GILLARDEAUX, V., GALLI, T. & ANDREWS, N. W. 2004. Identification of SNAREs involved in Synaptotagmin VII-regulated lysosomal exocytosis. *J Biol Chem,* 279**,** 20471-9.

REEBER, S. L., OTIS, T. S. & SILLITOE, R. V. 2013. New roles for the cerebellum in health and disease. *Front Syst Neurosci,* 7**,** 83.

REGEHR, W. G. 2012. Short-term presynaptic plasticity. *Cold Spring Harb Perspect Biol,* 4**,** a005702.

REGEHR, W. G. & ATLURI, P. P. 1995. Calcium transients in cerebellar granule cell presynaptic terminals. *Biophys J,* 68**,** 2156-70.

REGEHR, W. G. & TANK, D. W. 1991. Selective fura-2 loading of presynaptic terminals and nerve cell processes by local perfusion in mammalian brain slice. *J Neurosci Methods,* 37**,** 111-9.

RIBAK, C. E., TONG, W. M. & BRECHA, N. C. 1996. Astrocytic processes compensate for the apparent lack of GABA transporters in the axon terminals of cerebellar Purkinje cells. *Anat Embryol (Berl),* 194**,** 379-90.

RITZAU-JOST, A., DELVENDAHL, I., RINGS, A., BYCZKOWICZ, N., HARADA, H., SHIGEMOTO, R., HIRRLINGER, J., EILERS, J. & HALLERMANN, S. 2014. Ultrafast action potentials mediate kilohertz signaling at a central synapse. *Neuron,* 84**,** 152-163.

ROBINSON, D. A. 1981. The use of control systems analysis in the neurophysiology of eye movements. *Annu Rev Neurosci,* 4**,** 463-503.

RUDOLPH, S., OVERSTREET-WADICHE, L. & WADICHE, J. I. 2011. Desynchronization of multivesicular release enhances Purkinje cell output. *Neuron,* 70**,** 991-1004.

RUIZ, R., CANO, R., CASANAS, J. J., GAFFIELD, M. A., BETZ, W. J. & TABARES, L. 2011. Active zones and the readily releasable pool of synaptic vesicles at the neuromuscular junction of the mouse. *J Neurosci,* 31**,** 2000-8.

SABATINI, B. L. & REGEHR, W. G. 1995. Detecting changes in calcium influx which contribute to synaptic modulation in mammalian brain slice. *Neuropharmacology,* 34**,** 1453-67.

SABATINI, B. L. & REGEHR, W. G. 1996. Timing of neurotransmission at fast synapses in the mammalian brain. *Nature,* 384**,** 170-2.

SABATINI, B. L. & SVOBODA, K. 2000. Analysis of calcium channels in single spines using optical fluctuation analysis. *Nature,* 408**,** 589-93.

SAFO, P. K. & REGEHR, W. G. 2005. Endocannabinoids control the induction of cerebellar LTD. *Neuron,* 48**,** 647-59.

SAKABA, T. 2008. Two Ca(2+)-dependent steps controlling synaptic vesicle fusion and replenishment at the cerebellar basket cell terminal. *Neuron,* 57**,** 406-19.

SAKABA, T. & NEHER, E. 2001. Calmodulin mediates rapid recruitment of fast-releasing synaptic vesicles at a calyx-type synapse. *Neuron,* 32**,** 1119-31.

SARASWATI, S., ADOLFSEN, B. & LITTLETON, J. T. 2007. Characterization of the role of the Synaptotagmin family as calcium sensors in facilitation and asynchronous neurotransmitter release. *Proc Natl Acad Sci U S A,* 104**,** 14122-7.

SCHMIDT, H., BRACHTENDORF, S., ARENDT, O., HALLERMANN, S., ISHIYAMA, S., BORNSCHEIN, G., GALL, D., SCHIFFMANN, S. N., HECKMANN, M. & EILERS, J. 2013. Nanodomain coupling at an excitatory cortical synapse. *Curr Biol,* 23**,** 244-9.

SCHNEGGENBURGER, R. & NEHER, E. 2000. Intracellular calcium dependence of transmitter release rates at a fast central synapse. *Nature,* 406**,** 889-93.

SCHONN, J. S., MAXIMOV, A., LAO, Y., SUDHOF, T. C. & SORENSEN, J. B. 2008. Synaptotagmin-1 and -7 are functionally overlapping Ca2+ sensors for exocytosis in adrenal chromaffin cells. *Proc Natl Acad Sci U S A,* 105**,** 3998-4003.

SCOTT, R. & RUSAKOV, D. A. 2006. Main determinants of presynaptic Ca2+ dynamics at individual mossy fiber-CA3 pyramidal cell synapses. *J Neurosci,* 26**,** 7071-81.

SEARL, T. J. & SILINSKY, E. M. 2002. Evidence for two distinct processes in the final stages of neurotransmitter release as detected by binomial analysis in calcium and strontium solutions. *J Physiol,* 539**,** 693-705.

SHIN, O. H., RHEE, J. S., TANG, J., SUGITA, S., ROSENMUND, C. & SUDHOF, T. C. 2003. Sr2+ binding to the Ca2+ binding site of the Synaptotagmin 1 C2B domain triggers fast exocytosis without stimulating SNARE interactions. *Neuron,* 37**,** 99-108.

SIMS, R. E. & HARTELL, N. A. 2005. Differences in transmission properties and susceptibility to long-term depression reveal functional specialization of ascending axon and parallel fiber synapses to Purkinje cells. *J Neurosci,* 25**,** 3246-57.

SIPPY, T., CRUZ-MARTIN, A., JEROMIN, A. & SCHWEIZER, F. E. 2003. Acute changes in short-term plasticity at synapses with elevated levels of neuronal calcium sensor-1. *Nat Neurosci,* 6**,** 1031-8.

STEIN, A., RADHAKRISHNAN, A., RIEDEL, D., FASSHAUER, D. & JAHN, R. 2007. Synaptotagmin activates membrane fusion through a Ca2+-dependent trans interaction with phospholipids. *Nat Struct Mol Biol,* 14**,** 904-11.

STEVENS, C. F. & WESSELING, J. F. 1998. Activity-dependent modulation of the rate at which synaptic vesicles become available to undergo exocytosis. *Neuron,* 21**,** 415-24.

SUDHOF, T. C. 2013. A molecular machine for neurotransmitter release: Synaptotagmin and beyond. *Nature Medicine,* 19**,** 1227-1231.

SUDHOF, T. C. & ROTHMAN, J. E. 2009. Membrane fusion: grappling with SNARE and SM proteins. *Science,* 323**,** 474-7.

SUGIHARA, I. & SHINODA, Y. 2004. Molecular, topographic, and functional organization of the cerebellar cortex: a study with combined aldolase C and olivocerebellar labeling. *J Neurosci,* 24**,** 8771-85.

SUGIHARA, I. & SHINODA, Y. 2007. Molecular, topographic, and functional organization of the cerebellar nuclei: analysis by three-dimensional mapping of the olivonuclear projection and aldolase C labeling. *J Neurosci,* 27**,** 9696-710.

SUGITA, S., HAN, W., BUTZ, S., LIU, X., FERNANDEZ-CHACON, R., LAO, Y. & SUDHOF, T. C. 2001. Synaptotagmin VII as a plasma membrane Ca(2+) sensor in exocytosis. *Neuron,* 30**,** 459-73.

SUGITA, S., SHIN, O. H., HAN, W., LAO, Y. & SUDHOF, T. C. 2002. Synaptotagmins form a hierarchy of exocytotic Ca(2+) sensors with distinct Ca(2+) affinities. *EMBO J,* 21**,** 270-80.

SULLIVAN, W. E. & KONISHI, M. 1984. Segregation of stimulus phase and intensity coding in the cochlear nucleus of the barn owl. *J Neurosci,* 4**,** 1787-99.

SUN, J., PANG, Z. P., QIN, D., FAHIM, A. T., ADACHI, R. & SUDHOF, T. C. 2007. A dual-Ca2+-sensor model for neurotransmitter release in a central synapse. *Nature,* 450**,** 676-82.

TELGKAMP, P., PADGETT, D. E., LEDOUX, V. A., WOOLLEY, C. S. & RAMAN, I. M. 2004. Maintenance of high-frequency transmission at purkinje to cerebellar nuclear synapses by spillover from boutons with multiple release sites. *Neuron,* 41**,** 113-26.

TELGKAMP, P. & RAMAN, I. M. 2002. Depression of inhibitory synaptic transmission between Purkinje cells and neurons of the cerebellar nuclei. *J Neurosci,* 22**,** 8447-57.

TEUNE, T. M., VAN DER BURG, J., VAN DER MOER, J., VOOGD, J. & RUIGROK, T. J. 2000. Topography of cerebellar nuclear projections to the brain stem in the rat. *Prog Brain Res,* 124**,** 141-72.

THACH, W. T. 1970. Discharge of cerebellar neurons related to two maintained postures and two prompt movements. II. Purkinje cell output and input. *J Neurophysiol,* 33**,** 537-47.

THANAWALA, M. S. & REGEHR, W. G. 2013. Presynaptic calcium influx controls neurotransmitter release in part by regulating the effective size of the readily releasable pool. *J Neurosci,* 33**,** 4625-33.

THANAWALA, M. S. & REGEHR, W. G. 2016a. Determining Synaptic Parameters Using High-Frequency Activation. *J Neurosci Methods*.

THANAWALA, M. S. & REGEHR, W. G. 2016b. Determining synaptic parameters using high-frequency activation. *J Neurosci Methods,* 264**,** 136-152.

TROMMERSHAUSER, J., SCHNEGGENBURGER, R., ZIPPELIUS, A. & NEHER, E. 2003. Heterogeneous presynaptic release probabilities: functional relevance for short-term plasticity. *Biophys J,* 84**,** 1563-79.

TRUSSELL, L. O., ZHANG, S. & RAMAN, I. M. 1993. Desensitization of AMPA receptors upon multiquantal neurotransmitter release. *Neuron,* 10**,** 1185-96.

TSUJIMOTO, T., JEROMIN, A., SAITOH, N., RODER, J. C. & TAKAHASHI, T. 2002. Neuronal calcium sensor 1 and activity-dependent facilitation of P/Q-type calcium currents at presynaptic nerve terminals. *Science,* 295**,** 2276-9.

TURECEK, J., HAN, V. Z., CUZON CARLSON, V. C., GRANT, K. A. & WELSH, J. P. 2016a. Electrical Coupling and Synchronized Subthreshold Oscillations in the Inferior Olive of the Rhesus Macaque. *J Neurosci,* 36**,** 6497-502.

TURECEK, J., JACKMAN, S. L. & REGEHR, W. G. 2016b. Synaptic Specializations Support Frequency-Independent Purkinje Cell Output from the Cerebellar Cortex. *Cell Rep,* 17**,** 3256-3268.

TURECEK, J., JACKMAN, S. L. & REGEHR, W. G. 2017. Synaptotagmin 7 confers frequency invariance onto specialized depressing synapses. *Nature,* 551**,** 503-506.

TURECEK, J. & REGEHR, W. G. 2018. Synaptotagmin 7 Mediates Both Facilitation and Asynchronous Release at Granule Cell Synapses. *J Neurosci,* 38**,** 3240-3251.

URBANO, F. J., SIMPSON, J. I. & LLINAS, R. R. 2006. Somatomotor and oculomotor inferior olivary neurons have distinct electrophysiological phenotypes. *Proc Natl Acad Sci U S A,* 103**,** 16550-5.

UUSISAARI, M., OBATA, K. & KNOPFEL, T. 2007. Morphological and electrophysiological properties of GABAergic and non-GABAergic cells in the deep cerebellar nuclei. *J Neurophysiol,* 97**,** 901-11.

VAN DER KLOOT, W. & MOLGO, J. 1993. Facilitation and delayed release at about 0 degree C at the frog neuromuscular junction: effects of calcium chelators, calcium transport inhibitors, and okadaic acid. *J Neurophysiol,* 69**,** 717-29.

VAN OVERWALLE, F., BAETENS, K., MARIEN, P. & VANDEKERCKHOVE, M. 2014. Social cognition and the cerebellum: a meta-analysis of over 350 fMRI studies. *Neuroimage,* 86**,** 554-72.

VERHAGE, M., MAIA, A. S., PLOMP, J. J., BRUSSAARD, A. B., HEEROMA, J. H., VERMEER, H., TOONEN, R. F., HAMMER, R. E., VAN DEN BERG, T. K., MISSLER, M., GEUZE, H. J. & SUDHOF, T. C. 2000. Synaptic assembly of the brain in the absence of neurotransmitter secretion. *Science,* 287**,** 864-9.

VOOGD, J. & GLICKSTEIN, M. 1998. The anatomy of the cerebellum. *Trends Neurosci,* 21**,** 370-5.

VYLETA, N. P. & JONAS, P. 2014. Loose coupling between Ca2+ channels and release sensors at a plastic hippocampal synapse. *Science,* 343**,** 665-70.

WADICHE, J. I. & JAHR, C. E. 2001. Multivesicular release at climbing fiber-Purkinje cell synapses. *Neuron,* 32**,** 301-13.

WALTER, J. T. & KHODAKHAH, K. 2009. The advantages of linear information processing for cerebellar computation. *Proc Natl Acad Sci U S A,* 106**,** 4471-6.

WANG, L. Y. & KACZMAREK, L. K. 1998. High-frequency firing helps replenish the readily releasable pool of synaptic vesicles. *Nature,* 394**,** 384-8.

WANG, S. S., KLOTH, A. D. & BADURA, A. 2014. The cerebellum, sensitive periods, and autism. *Neuron,* 83**,** 518-32.

WEBER, J. P., TOFT-BERTELSEN, T. L., MOHRMANN, R., DELGADO-MARTINEZ, I. & SORENSEN, J. B. 2014. Synaptotagmin-7 is an asynchronous calcium sensor for synaptic transmission in neurons expressing SNAP-23. *PLoS One,* 9**,** e114033.

WEBER, T., ZEMELMAN, B. V., MCNEW, J. A., WESTERMANN, B., GMACHL, M., PARLATI, F., SOLLNER, T. H. & ROTHMAN, J. E. 1998. SNAREpins: minimal machinery for membrane fusion. *Cell,* 92**,** 759-72.

WEBSITE:. *© 2015 Allen Institute for Brain Science. Allen Brain Atlas [Internet]. Available from: http://www.brain-map.org.* [Online]. Website: . [Accessed].

WEN, H., LINHOFF, M. W., MCGINLEY, M. J., LI, G. L., CORSON, G. M., MANDEL, G. & BREHM, P. 2010. Distinct roles for two Synaptotagmin isoforms in synchronous and asynchronous transmitter release at zebrafish neuromuscular junction. *Proc Natl Acad Sci U S A,* 107**,** 13906-11.

WEN, H., MCGINLEY, M. J., MANDEL, G. & BREHM, P. 2016. Nonequivalent release sites govern synaptic depression. *Proc Natl Acad Sci U S A,* 113**,** E378-86.

WITTER, L. & DE ZEEUW, C. I. 2015. Regional functionality of the cerebellum. *Curr Opin Neurobiol,* 33**,** 150-5.

WITTER, L., RUDOLPH, S., PRESSLER, R. T., LAHLAF, S. I. & REGEHR, W. G. 2016. Purkinje Cell Collaterals Enable Output Signals from the Cerebellar Cortex to Feed Back to Purkinje Cells and Interneurons. *Neuron*.

WU, D., BACAJ, T., MORISHITA, W., GOSWAMI, D., ARENDT, K. L., XU, W., CHEN, L., MALENKA, R. C. & SUDHOF, T. C. 2017. Postsynaptic Synaptotagmins mediate AMPA receptor exocytosis during LTP. *Nature,* 544**,** 316-321.

WU, L. G. & BORST, J. G. 1999. The reduced release probability of releasable vesicles during recovery from short-term synaptic depression. *Neuron,* 23**,** 821-32.

XU-FRIEDMAN, M. A. & REGEHR, W. G. 1999. Presynaptic strontium dynamics and synaptic transmission. *Biophys J,* 76**,** 2029-42.

XU-FRIEDMAN, M. A. & REGEHR, W. G. 2000. Probing fundamental aspects of synaptic transmission with strontium. *J Neurosci,* 20**,** 4414-22.

XU-FRIEDMAN, M. A. & REGEHR, W. G. 2003. Ultrastructural contributions to desensitization at cerebellar mossy fiber to granule cell synapses. *J Neurosci,* 23**,** 2182-92.

XU-FRIEDMAN, M. A. & REGEHR, W. G. 2004. Structural contributions to short-term synaptic plasticity. *Physiol Rev,* 84**,** 69-85.

XU, J., MASHIMO, T. & SUDHOF, T. C. 2007. Synaptotagmin-1, -2, and -9: Ca(2+) sensors for fast release that specify distinct presynaptic properties in subsets of neurons. *Neuron,* 54**,** 567-81.

XU, J., PANG, Z. P., SHIN, O. H. & SUDHOF, T. C. 2009. Synaptotagmin-1 functions as a Ca2+ sensor for spontaneous release. *Nat Neurosci,* 12**,** 759-66.

YANG, H. & XU-FRIEDMAN, M. A. 2009. Impact of synaptic depression on spike timing at the endbulb of Held. *J Neurophysiol,* 102**,** 1699-710.

YANG, H. & XU-FRIEDMAN, M. A. 2010. Developmental mechanisms for suppressing the effects of delayed release at the endbulb of Held. *J Neurosci,* 30**,** 11466-75.

YANG, X., KAESER-WOO, Y. J., PANG, Z. P., XU, W. & SUDHOF, T. C. 2010. Complexin clamps asynchronous release by blocking a secondary Ca(2+) sensor via its accessory alpha helix. *Neuron,* 68**,** 907-20.

YAO, J., GAFFANEY, J. D., KWON, S. E. & CHAPMAN, E. R. 2011. Doc2 is a Ca2+ sensor required for asynchronous neurotransmitter release. *Cell,* 147**,** 666-77.

YOSHIHARA, M. & LITTLETON, J. T. 2002. Synaptotagmin I functions as a calcium sensor to synchronize neurotransmitter release. *Neuron,* 36**,** 897-908.

YU, Y., FU, Y. & WATSON, C. 2014. The inferior olive of the C57BL/6J mouse: a chemoarchitectonic study. *Anat Rec (Hoboken),* 297**,** 289-300.

ZENGEL, J. E. & MAGLEBY, K. L. 1980. Differential effects of Ba2+, Sr2+, and Ca2+ on stimulation-induced changes in transmitter release at the frog neuromuscular junction. *J Gen Physiol,* 76**,** 175-211.

ZHANG, W. & LINDEN, D. J. 2006. Long-term depression at the mossy fiber-deep cerebellar nucleus synapse. *J Neurosci,* 26**,** 6935-44.

ZHAO, J. P., PHILLIPS, M. A. & CONSTANTINE-PATON, M. 2006. Long-term potentiation in the juvenile superior colliculus requires simultaneous activation of NMDA receptors and L-type Ca2+ channels and reflects addition of newly functional synapses. *J Neurosci,* 26**,** 12647-55.

ZHAO, M., HOLLINGWORTH, S. & BAYLOR, S. M. 1996. Properties of tri- and tetracarboxylate Ca2+ indicators in frog skeletal muscle fibers. *Biophys J,* 70**,** 896-916.

ZHOU, H., LIN, Z., VOGES, K., JU, C., GAO, Z., BOSMAN, L. W., RUIGROK, T. J., HOEBEEK, F. E., DE ZEEUW, C. I. & SCHONEWILLE, M. 2014. Cerebellar modules operate at different frequencies. *Elife,* 3**,** e02536.

ZOLOTUKHIN, S., BYRNE, B. J., MASON, E., ZOLOTUKHIN, I., POTTER, M., CHESNUT, K., SUMMERFORD, C., SAMULSKI, R. J. & MUZYCZKA, N. 1999. Recombinant adeno-associated virus purification using novel methods improves infectious titer and yield. *Gene Ther,* 6**,** 973-85.

ZUCKER, R. S. & LARA-ESTRELLA, L. O. 1983. Post-tetanic decay of evoked and spontaneous transmitter release and a residual-calcium model of synaptic facilitation at crayfish neuromuscular junctions. *J Gen Physiol,* 81**,** 355-72.

ZUCKER, R. S. & REGEHR, W. G. 2002a. Short-term synaptic plasticity. *Annu Rev Physiol,* 64**,** 355-405.

ZUCKER, R. S. & REGEHR, W. G. 2002b. Short-term synaptic plasticity. *Annual Review of Physiology,* 64**,** 355-405.